

**Conditioning of clay soils  
for tunnelling machine screw conveyors**

**Andrew Stuart Merritt**



St John's College  
University of Cambridge

March 2004

A dissertation submitted for the  
degree of Doctor of Philosophy  
at the University of Cambridge

## **Declaration**

I hereby declare that expect where specific reference is made to the work of others, the content of this dissertation are original and have not been submitted in whole or in part for consideration for any other degree or qualification at this or any other university. This dissertation is entirely the result of my own work and includes nothing which is the outcome of work done in collaboration. This dissertation contains less than 65, 000 words and less than 150 figures.

A. S. Merritt

March 2004

# Conditioning of clay soils for tunnelling machine screw conveyors

## ABSTRACT

Earth pressure balance (EPB) tunnelling machines are commonly used for the construction of tunnels in soft soils ranging from coarse sands and gravels to stiff clays. These machines use the excavated soil in a pressurised head chamber to apply a support pressure to the tunnel face during excavation. A screw conveyor is used to discharge controlled volumes of soil from the machine, and to dissipate the pressure in the head chamber. By balancing the volume of soil flowing into and out of the machine, an earth pressure balance is established during excavation. The control of the excavation process and the EPB machine performance depend critically on the properties of the excavated soil. Conditioning of the soil by injecting foams, polymers, and other agents is usually required to modify the properties of the excavated soil to form a soft plastic paste. Effective soil conditioning significantly improves the machine performance and control of the soil flow through the screw conveyor. Although soil conditioning is commonly used in practice, effects of different conditioning treatments on soil properties and the machine performance are not clearly understood, and problems with EPB machine operations related to the soil properties are often encountered.

This thesis presents experimental investigations of soil conditioning for clays, and of the mechanics of a model EPB screw conveyor operating with clay soils.

Index tests were performed to investigate effects of foam and polymer conditioning treatments on the undrained strength of London Clay samples. The index tests allowed assessment of conditioning treatments for clay soils, and optimum ranges of treatments for London Clay are suggested.

An instrumented 1:10 scale model EPB screw conveyor was designed and commissioned. The soil flow rates, the pressure gradients and casing shear stresses along the conveyor, and the screw torque were measured during tests with varying soil properties and conveyor operating conditions. Tests were performed with consolidated kaolin and compacted conditioned natural clay soil samples.

During steady state conveyor operation with a constant soil flow rate, the casing shear stress and the total pressure gradient were constant along the conveyor, and the screw torque was constant. The total pressure gradient is influenced by conveyor operating conditions including the sample pressure, the discharge outlet restriction, the screw speed, and the screw pitch. Depending on the operating conditions and the soil strength, the total pressure can increase or decrease along the conveyor. The screw torque is proportional to the casing shear stress, and increased with the undrained strength of the soil. Conditioning natural clay soils with polymers and foams to form a soft plastic paste allowed controlled operation of the screw conveyor, with uniform soil flow rates and pressure gradients.

A theoretical model describing the screw conveyor operation is proposed. The model relates the total pressure gradient and the screw torque to the soil flow rate, the shear stresses acting in the conveyor, and the screw conveyor geometry. The model is expressed in dimensionless form to allow application to screw conveyors of varying scale. Close agreement between the predictions of the theoretical model and the measured pressure gradients and torques from the model screw conveyor tests was obtained, indicating the proposed model can accurately describe the conveyor operation.

**Keywords:** *Earth pressure balance machine, screw conveyor, clay, soil conditioning foam, polymer, model testing*

## Acknowledgements

There are many people who have contributed in different ways to this research and the enjoyment of my time in Cambridge over the last few years who I would like to acknowledge.

Firstly, I would like to express my sincere thanks to my supervisor, Professor Robert Mair, whose constant interest and enthusiasm for this research was a never ending source of inspiration and motivation. His technical knowledge and practical perspective have contributed in many ways and had a major influence on the direction of the work.

My thanks are also due to the other members of the academic staff and my colleagues in the Geotechnical Group at Cambridge, whose interest in the research, and their knowledge and experience of the geotechnical world and laboratory work have also contributed in many ways. They have also made many contributions outside of work, helping to make my time in Cambridge so enjoyable. Thanks are due to my friends and colleagues from around the world who found their way to the Geotechnical Group, particularly Xavier Borghi, Dave White, Andy Take, Lis Bowman, Subhamoy Bhattacharya, and Andrew Brennan, whom I shall miss spending time with but am sure will all go on to great things in the future.

I would also like to thank the Pipe Jacking Association, particularly Arthur Moss for his enthusiastic support of the research. The contribution to the work from the collaboration with Professor Guy Houlby and Miguel Pena from Oxford University, and Dr George Milligan from Geotechnical Consulting Group, has also been very beneficial.

Many people assisted with the details of the laboratory research I spent a lot of time doing. Clive Dalton from Cambridge Insitu was a great help with the design and manufacture of load cells. Alistair Ross, Dave Pittock, Peter Long, and their respective teams in the workshops and design office at the Engineering Department all played roles in the design and construction of my model screw conveyor, which would not have happened without their help. Chris Collison, Steve Chandler, and the other technicians at the Schofield Centre were also a great help with making and fixing various bits and pieces, and with details of getting things to work.

I would like to give my thanks to the Cambridge Commonwealth Trust and St John's College for making my coming to Cambridge possible through their scholarships. Cambridge University Engineering Department, Nishimatsu Construction Company, and the British Tunnelling Society also provided financial support to allow completion of my research, which is greatly appreciated.

Finally, but by no means least, I would like to thank my parents for their constant support, love and encouragement from the other side of the world. And one final thank you to Saskia, whose love has been a constant source of motivation and happiness from the very beginning.

# Table of contents

Declaration	.....i
Abstract	.....ii
Acknowledgements	.....iii
Table of contents	.....iv
List of figures	.....x
List of tables	...xvi
Notation	...xviii

## Chapter 1. Introduction

1.1 Earth pressure balance tunnelling machines	.....1
1.2 Soil conditioning for EPB machines	.....2
1.3 Scope and objectives of research	.....4
1.4 Outline of thesis	.....5

## Chapter 2. Literature review

2.1 Introduction	.....8
2.2 Soil conditioning agents	.....8
2.2.1 Bentonite slurries	.....8
2.2.2 Polymers	.....9
2.2.3 Foams	....11
2.2.4 Other conditioning agents	....14
2.3 Soil conditioning treatments	....15
2.3.1 Conditioning of granular soils	....15
2.3.2 Conditioning of clay soils	....18
2.3.3 Effects of soil conditioning on EPB tunnelling operations	....20
2.4 Laboratory testing of conditioned soils	....21
2.5 Practical applications of soil conditioning	....24

2.6	EPB machine screw conveyors	....27
2.6.1	Design and operation of EPB machine screw conveyors	....27
2.6.2	Studies of EPB machine screw conveyors	....28
2.6.3	Theoretical models of screw extruders and conveyors	....30
2.6.3.1	Darnell and Mol model of screw extruders	....31
2.6.3.2	Chung model of screw extruders	....31
2.6.3.3	Burbidge and Bridgwater screw extruder model	....32
2.6.3.4	Yoshikawa model of EPB screw conveyors	....33
2.6.3.5	Talmon and Bezuijen model of EPB screw conveyors	....35
2.7	Summary	....36

### **Chapter 3. Index testing of conditioned clay soils**

3.1	Introduction	....51
3.2	Soils tested	....52
3.2.1	E-grade kaolin	....52
3.2.2	London Clay samples	....53
3.3	Conditioning agents	....54
3.3.1	Polymer conditioning agents	....54
3.3.2	Foam agents	....55
3.4	Index testing apparatus and methods	....56
3.4.1	Foam generator	....56
3.4.2	Foam index tests	....57
3.4.3	Atterberg limit tests	....58
3.4.4	Conditioned London Clay index tests	....59
3.4.4.1	Sample preparation	....59
3.4.4.2	Large scale fall cone	....61
3.4.4.3	Shear vane tests	....62
3.5	Index properties of foams	....62
3.5.1	Comparison of foam agents	....63
3.5.2	Effects of foam generation parameters	....64
3.6	Plasticity and strength of reconstituted polymer conditioned clays	....65
3.6.1	Plasticity of polymer conditioned clays	....65

3.6.2	Remoulded strength of polymer conditioned clays	....66
3.7	Index testing of conditioned London Clay	....68
3.7.1	Polymer conditioning treatments	....68
3.7.2	Foam conditioning treatments	....69
3.7.3	Combined foam-polymer conditioning treatments	....72
3.7.4	Optimum conditioning treatments for London Clay	....74
3.8	Summary	....75

## **Chapter 4. Model EPB machine screw conveyor system**

4.1	Introduction	....97
4.2	Objectives of screw conveyor study	....97
4.3	Cambridge model EPB screw conveyor	....99
4.3.1	General arrangement	....99
4.3.2	Sample containers and consolidation system	...100
4.3.3	Conveyor casing	...101
4.3.4	Screw drive shaft	...102
4.3.5	Model screws	...104
4.3.6	Screw motor	...105
4.4	Screw conveyor system instrumentation	...106
4.4.1	Screw conveyor load cells	...106
4.4.1.1	Design of load cells	...106
4.4.1.2	Load cell calibration	...108
4.4.2	Pore water pressure transducers	...110
4.4.3	Drive shaft torque cell	...110
4.4.4	Jack pressure transducer	...111
4.4.5	Draw-wire transducer	...112
4.4.6	Data acquisition system	...112
4.5	Model screw conveyor tests	...113
4.5.1	Assembly and operation of the screw conveyor	...113
4.5.2	Design of screw conveyor tests	...114
4.6	Summary	...115

## **Chapter 5. Model screw conveyor tests with consolidated kaolin**

5.1	Introduction	...134
5.2	E-grade kaolin samples	...134
5.2.1	Sample preparation	...135
5.2.2	Consolidation of E-grade kaolin	...135
5.2.3	Undrained shear strength of E-grade kaolin	...138
5.3	Screw conveyor tests with kaolin samples	...140
5.4	Screw conveyor test data processing	...142
5.4.1	Data logging	...142
5.4.2	Data processing	...142
5.4.2.1	Sample pressure	...142
5.4.2.2	Sample height	...143
5.4.2.3	Screw torque	...143
5.4.2.4	Pore water pressures	...143
5.4.2.5	Load cell measurements	...143
5.4.2.6	Effective stress	...144
5.4.2.7	Pressure gradients	...145
5.5	Mechanics of screw conveyor operation	...145
5.5.1	Soil flow rate	...145
5.5.2	Total normal stresses	...147
5.5.3	Pore water pressures	...147
5.5.4	Casing shear stresses	...148
5.5.5	Screw torque	...149
5.5.6	Pressure gradients	...150
5.5.7	Mechanical operation of the model screw conveyor with clay soils	...151
5.6	Effects of screw conveyor operating conditions	...152
5.6.1	Sample strength	...152
5.6.2	Discharge condition	...154
5.6.3	Test pressure	...156
5.6.4	Screw pitch	...157
5.7	Interface shearing mechanisms in the model screw conveyor	...159
5.8	Summary	...160

## **Chapter 6. Model screw conveyor tests with conditioned clay soils**

6.1	Introduction	...186
6.2	Conditioned clay samples for screw conveyor tests	...187
6.2.1	Soil samples	...187
6.2.1.1	London Clay samples	...187
6.2.1.2	WRB/UP samples	...187
6.2.1.3	Index testing of conditioned WRB/UP soil	...188
6.2.2	Preparation of screw conveyor test samples	...190
6.2.3	Properties of screw conveyor test samples	...191
6.3	Screw conveyor tests with conditioned soil samples	...192
6.4	Screw conveyor tests with conditioned London Clay	...194
6.4.1	Soil flow rates	...194
6.4.2	Pressure gradients	...196
6.4.3	Casing shear stresses	...198
6.4.4	Screw torque	...199
6.5	Screw conveyor tests with conditioned WRB/UP soil	...200
6.5.1	Soil flow rates	...200
6.5.2	Pressure gradients	...200
6.5.3	Casing shear stresses	...202
6.5.4	Screw torque	...203
6.6	Effects of soil conditioning treatments on screw conveyor operation	...203
6.7	Summary	...205

## **Chapter 7. Theoretical model of screw conveyor operation**

7.1	Introduction	...229
7.2	Theoretical model of screw conveyor operation	...230
7.2.1	Screw conveyor geometry	...230
7.2.2	Flow of soil in the screw conveyor	...231
7.2.3	Forces acting on the soil	...234
7.2.4	Theoretical model of total pressure gradient	...236
7.2.5	Theoretical model of screw torque	...241

7.3	Total pressure gradients	...243
7.3.1	Theoretical pressure gradients	...243
7.3.1.1	Effect of shear stress ratio	...244
7.3.1.2	Effect of screw pitch	...245
7.3.1.3	Effect of soil strength	...245
7.3.2	Effects of conveyor operating conditions	...246
7.3.3	Comparison of experimental and theoretical pressure gradients	...247
7.3.3.1	Dimensionless pressure gradients	...247
7.3.3.2	Calculated pressure gradients	...250
7.4	Screw conveyor torque	...251
7.4.1	Theoretical screw torque	...251
7.4.2	Comparison of measured and theoretical screw torque	...252
7.5	Summary	...254

## **Chapter 8. Conclusions**

8.1	Introduction	...275
8.2	Conditioning treatments for clay soils	...275
8.3	Screw conveyor operation with clay soils	...277
8.4	Theoretical model of screw conveyor operation	...279
8.5	Further research	...281
	References	...284

## List of Figures

- Figure 1.1. Schematic of typical EPB tunnelling machine.
- Figure 1.2. 12 m diameter EPB tunnelling machine.
- Figure 2.1. Chemical structures of PHPA monomer and polymer molecules.
- Figure 2.2. Flocculation of particles by polymer molecules.
- Figure 2.3. Adsorption isotherms of anionic PHPA onto natural clayey soils and silica sands.
- Figure 2.4(a). Adsorption of cationic and anionic surfactants onto charged soil particle.
- Figure 2.4(b). Repulsion of soil particles by steric interactions of adsorbed surfactant molecules.
- Figure 2.5. Schematic diagram of aqueous foam structure at different scales.
- Figure 2.6. Foam generation plant on an EPB machine.
- Figure 2.7. Change of foam volume under pressure cycles.
- Figure 2.8. Application of EPB machines based on particle size distribution.
- Figure 2.9. General soil conditioning requirements based on particle size distributions.
- Figure 2.10(a). Recommended soil conditioning treatments.
- Figure 2.10(b). Recommended parameters for conditioning treatments.
- Figure 2.11. Selection chart for application of soil conditioning agents.
- Figure 2.12. Summary of conditioning treatments for different soils.
- Figure 2.13. Slump of various soils conditioned with foam.
- Figure 2.14. Reduction of mixing power with foam injection ratio.
- Figure 2.15. Model EPB machine apparatus.
- Figure 2.16. Compressibility of sand-foam mixtures.
- Figure 2.17. Effect of foam liquid injection on mining time in till soils.
- Figure 2.18. Screw conveyor discharge controls and compaction systems.
- Figure 2.19. Measured pore pressure distributions along model EPB screw conveyor.
- Figure 2.20. Measured total pressure distribution along EPB machine screw conveyor.
- Figure 2.21. Forces acting on solid plug element in screw extruder channel.
- Figure 2.22. Measured and calculated pressure gradients for EPB screw conveyor.
- Figure 2.23. Calculated pressure drop for screw conveyors with varying screw pitch.
- Figure 3.1. Grading curve of E-grade kaolin.
- Figure 3.2. Grading curves of London Clay samples.

- Figure 3.3. Plasticity chart for London Clay samples.
- Figure 3.4. Sieve for sampling of London Clay cuttings.
- Figure 3.5. Laboratory foam generator.
- Figure 3.6. Foam generator unit with plastic beads.
- Figure 3.7. Schematic of laboratory foam generator.
- Figure 3.8. Foam sampling tube and plunger.
- Figure 3.9. Large scale fall cone apparatus.
- Figure 3.10. Expansion ratio of various foam agents.
- Figure 3.11. Liquid drainage over time for various foam agents.
- Figure 3.12. Foam liquid drainage time index values.
- Figure 3.13. Foam expansion ratio with varying foam agent concentrations.
- Figure 3.14. Foam expansion ratio with varying air flow rates.
- Figure 3.15(a). Atterberg limits of E-grade kaolin reconstituted with MV polymer solutions.
- Figure 3.15(b). Atterberg limits of London Clay reconstituted with MV polymer solutions.
- Figure 3.16(a). Undrained strength of E-grade kaolin reconstituted with water and MV polymer.
- Figure 3.16(b). Undrained strength of London Clay reconstituted with water and MV polymer.
- Figure 3.17(a). Large scale fall cone penetration of polymer conditioned London Clay samples.
- Figure 3.17(b). Undrained strength of polymer conditioned London Clay samples from large scale fall cone tests.
- Figure 3.17(c). Vane shear strength of polymer conditioned London Clay samples.
- Figure 3.18. Undrained strength and moisture content of polymer conditioned London Clay samples.
- Figure 3.19. Undrained strength of polymer conditioned London Clay samples measured by vane shear and large scale fall cone tests.
- Figure 3.20. London Clay cuttings mixed with foam at varying injection ratios.
- Figure 3.21. Undrained strength of conditioned London Clay samples at varying foam injection ratios.
- Figure 3.22. Undrained strength of London Clay samples conditioned with foams and polymers at varying liquid injection ratios.
- Figure 3.23. Undrained strength and moisture content of London Clay samples conditioned with foam and polymer treatments.
- Figure 3.24. Undrained strength of conditioned London Clay samples at varying polymer and foam injection ratios.

- Figure 4.1. General arrangement of model EPB machine screw conveyor system.
- Figure 4.2(a). Overview of model EPB machine screw conveyor system.
- Figure 4.2(b). Model screw conveyor assembled for testing.
- Figure 4.3. Layout of model screw conveyor casing.
- Figure 4.4. Geometry and dimensions of unrestricted and restricted conveyor discharge outlets.
- Figure 4.5. Instrumented section of conveyor casing.
- Figure 4.6. Screw conveyor drive shaft assembly.
- Figure 4.7. Design drawings of drive shaft.
- Figure 4.8. Screw drive shaft with bearing and slip ring pieces.
- Figure 4.9. Assembled screw conveyor drive shaft and slip ring.
- Figure 4.10. Dimensions of model screws.
- Figure 4.11. Screw conveyor motor speed calibration.
- Figure 4.12. Load cell and housing components.
- Figure 4.13. Instrumented section of assembled screw conveyor.
- Figure 4.14. Load cell design drawings.
- Figure 4.15(a). Cambridge-type load cell for model screw conveyor.
- Figure 4.15(b). Assembled load cell unit.
- Figure 4.16. Load cell calibration.
- Figure 4.17. Example load cell calibration plots.
- Figure 4.18. Torque calibration for instrumented drive shaft.
- Figure 4.19. Drive shaft torque cell calibration.
- Figure 4.20. Arrangement of draw-wire transducer for sample height measurement.
- 
- Figure 5.1. Forces acting on soil sample in container.
- Figure 5.2. Consolidation of E-grade kaolin samples for screw conveyor tests.
- Figure 5.3(a). Measured and calculated undrained shear strength of E-grade kaolin samples at varying moisture contents.
- Figure 5.3(b). Measured and calculated undrained shear strength of E-grade kaolin samples at varying liquidity index.
- Figure 5.4. Undrained strength ratio of E-grade kaolin compared to values for various normally consolidated natural clays and silts.
- Figure 5.5. Typical load cell circuit outputs during screw conveyor operation.

- Figure 5.6. Total normal stress measured by loads cells at an instrumented section during conveyor operation.
- Figure 5.7. Piston pressure and sample height change during test 1.
- Figure 5.8. Average total normal stresses along conveyor during test 1.
- Figure 5.9. Pore water pressures along conveyor during test 1.
- Figure 5.10(a). Casing shear stress components parallel to screw axis during test 1.
- Figure 5.10(b). Casing shear stress components perpendicular to screw axis during test 1.
- Figure 5.10(c). Resultant casing shear stresses during test 1.
- Figure 5.11. Screw torque measured during test 1.
- Figure 5.12. Pressures measured at Section 3 during steady state operation in test 1.
- Figure 5.13(a). Total normal stresses at each section during steady state operation in test 1.
- Figure 5.13(b). Pore water pressures at each section during steady state operation in test 1.
- Figure 5.14. Pressure gradients along conveyor during steady state operation in test 1.
- Figure 5.15. Resultant casing shear stresses during steady state operation in test 1.
- Figure 5.16. Friction coefficients during steady state operation in test 1.
- Figure 5.17. Average resultant casing shear stresses and friction coefficients along conveyor during steady state operation in test 1.
- Figure 5.18. Average total normal stresses during test 2.
- Figure 5.19. Pressure gradients during test 2.
- Figure 5.20. Total pressure gradients during tests 1, 2 and 3 with kaolin samples of varying strength.
- Figure 5.21. Resultant casing shear stresses along conveyor during tests 1, 2 and 3 with kaolin samples of varying strength.
- Figure 5.22(a). Increase of screw torque with undrained shear strength of kaolin samples.
- Figure 5.22(b). Increase of screw torque with casing shear stress for kaolin samples.
- Figure 5.23. Total pressure gradients with varying discharge conditions in test 3.
- Figure 5.24. Plastic flow mechanism through square extrusion die with sliding on die face.
- Figure 5.25. Inferred discharge pressures for kaolin tests with restricted and unrestricted outlet conditions.
- Figure 5.26. Monitoring of screw conveyor test 4.
- Figure 5.27. Total normal stresses during test 4.
- Figure 5.28. Total pressure gradients with different piston pressures in test 4.
- Figure 5.29. Average resultant casing shear stresses with different piston pressures in test 4.
- Figure 5.30. Total pressure gradients with different piston pressures in test 5.

- Figure 5.31. Total pressure gradients with varied discharge conditions in test 6.
- Figure 5.32. Average friction coefficients along conveyor in tests with kaolin samples.
- Figure 6.1. Envelope of particle size distributions for WRB soil (Upper Mottled Clay).
- Figure 6.2. Envelope of particle size distributions for Upnor (UP) sand.
- Figure 6.3. Vane shear strength of WRB/UP soil conditioned with foam and polymer treatments.
- Figure 6.4. Vane shear strength of conditioned London Clay at varying moisture contents for screw conveyor and index test samples.
- Figure 6.5. Sample height and pressure during test 10 with varied screw speeds.
- Figure 6.6. Soil flow rates at different screw speeds in tests with conditioned soil samples.
- Figure 6.7. Conveyor discharge efficiency at different screw speeds in tests with conditioned soil samples.
- Figure 6.8. Conveyor discharge efficiency for conditioned London Clay samples of varying strength.
- Figure 6.9. Total normal stresses during test 9 at varying screw speeds.
- Figure 6.10. Pressure gradients during test 9 with screw rotating at 5 rpm.
- Figure 6.11(a). Total pressure gradients during test 9 with different screw speeds.
- Figure 6.11(b). Total pressure gradients during test 7 with different screw speeds.
- Figure 6.12. Total pressure gradients during tests with conditioned London Clay samples of varying strength.
- Figure 6.13(a). Total pressure gradients during test 13 with screw (1) at different speeds.
- Figure 6.13(b). Total pressure gradients during test 11 with screw (2) at different speeds.
- Figure 6.14. Resultant casing shear stresses during test 13.
- Figure 6.15. Average resultant shear stresses and friction coefficients along conveyor from tests with conditioned London Clay samples of varying strength.
- Figure 6.16. Comparison of casing shear stresses with undrained shear strength of conditioned London Clay samples.
- Figure 6.17. Screw torque measurements during test 10 with different screw speeds.
- Figure 6.18. Torque for varying sample strengths and screw speeds with conditioned soils.
- Figure 6.19. Increase of torque with casing shear stress for conditioned soil samples.
- Figure 6.20. Total normal stresses along conveyor during test 15 with conditioned WRB/UP soil.

- Figure 6.21. Total pressure gradients at different screw speeds during tests 15 and 16 with conditioned WRB/UP samples.
- Figure 6.22. Average casing shear stresses and friction coefficients along conveyor during tests with conditioned WRB/UP samples.
- Figure 7.1. Definition of screw conveyor geometry.
- Figure 7.2. Movement of soil plug along screw channel.
- Figure 7.3. Element of soil in the screw channel.
- Figure 7.4(a). Free body diagram of soil element in screw channel.
- Figure 7.4(b). Simplified free body diagram of soil element in screw channel.
- Figure 7.5(a). Effect of shear stress ratio and soil flow angle on dimensionless pressure gradient.
- Figure 7.5(b). Effect of shear stress ratio and soil flow rate on dimensionless pressure gradient.
- Figure 7.6(a). Effect of screw pitch and soil flow angle on dimensionless pressure gradient.
- Figure 7.6(b). Effect of screw pitch and soil flow rate dimensionless pressure gradient.
- Figure 7.7(a). Effect of soil strength and flow angle on total pressure gradient.
- Figure 7.7(b). Effect of soil strength and flow rate on total pressure gradient.
- Figure 7.8. Variation of  $\alpha$  ratio with undrained shear strength of clay soils from pile load tests.
- Figure 7.9(a). Measured and theoretical dimensionless pressure gradients and soil flow angles for screw (1) tests.
- Figure 7.9(b). Measured and theoretical dimensionless pressure gradients and soil flow rates for screw (1) tests.
- Figure 7.10(a). Measured and theoretical dimensionless pressure gradients and soil flow angles for screw (2) tests.
- Figure 7.10(b). Measured and theoretical dimensionless pressure gradients and soil flow rates for screw (2) tests.
- Figure 7.11. Measured and calculated total pressure gradients for test 3.
- Figure 7.12. Measured and calculated total pressure gradients for test 7.
- Figure 7.13. Theoretical screw torque for model conveyor with varying soil flow angles and casing shear stresses.
- Figure 7.14. Theoretical dimensionless torque for varying soil flow angles.
- Figure 7.15. Theoretical dimensionless torque and flow rate for varying screw pitch.
- Figure 7.16(a). Measured screw torque and casing shear stresses from model conveyor tests.
- Figure 7.16(b). Measured screw torque and undrained sample strengths from model conveyor tests.

- Figure 7.17(a). Comparison of measured and calculated torque based on casing shear stress.
- Figure 7.17(b). Comparison of measured and calculated torque based on undrained shear strength.
- Figure 7.18 Comparison of measured and theoretical dimensionless torque and soil flow angles.
- Figure 7.19 Comparison of measured and theoretical dimensionless torque and soil flow rates for different screw geometry.

## List of Tables

- Table 3.1. Chemical composition and physical properties of E-grade kaolin.
- Table 3.2. Engineering properties of E-grade kaolin.
- Table 3.3. Index properties and design parameters for London Clay samples.
- Table 3.4. Properties of polymer conditioning agents used in testing.
- Table 3.5. Properties of foam agents used in testing.
- Table 3.6. Laboratory shear vane.
- Table 3.7. Index properties of foam agents.
- Table 3.8. Atterberg limits of clays reconstituted with water and MV polymer.
- Table 3.9. London Clay samples conditioned with foams.
- Table 3.10. London Clay samples conditioned with combined foam-polymer solution treatments.
- Table 4.1. Dimensions of sample container and loading system.
- Table 4.2. Dimensions of screw conveyor casing and discharge outlet.
- Table 4.3. Dimensions of model screws.
- Table 4.4. Specification of screw conveyor motor.
- Table 4.5. Load cell specifications.
- Table 4.6. Load cell calibration procedures.
- Table 4.7. Calibration coefficients for screw conveyor instruments.
- Table 5.1. Properties of consolidated E-grade kaolin samples.

- Table 5.2. Cam-clay parameters for E-grade kaolin.
- Table 5.3. Model screw conveyor test conditions with consolidated E-grade kaolin samples.
- Table 5.4. Measurements from screw conveyor tests with consolidated kaolin samples.
- 
- Table 6.1. Index properties and design parameters of WRB soil (Upper mottled clay).
- Table 6.2. Index properties and design parameters of Upnor sand.
- Table 6.3. Index tests of conditioned WRB/UP soil.
- Table 6.4. Preparation of conditioned soil samples for screw conveyor tests.
- Table 6.5. Properties of conditioned soil samples for screw conveyor tests.
- Table 6.6. Summary of model screw conveyor tests with conditioned soil samples.
- Table 6.7. Measurements from screw conveyor tests with conditioned soil samples.
- 
- Table 7.1. Geometry of model screws.
- Table 7.2(a). Summary of screw conveyor test measurements for kaolin samples.
- Table 7.2(b). Summary of screw conveyor test measurements for conditioned soil samples.

# Nomenclature

## Roman symbols

### Geotechnical parameters

$d$	fall cone penetration
$e$	void ratio of soil
$G_s$	specific gravity of soil particles
$I_L$	liquidity index of soil
$I_p$	plasticity index of soil
$K_\alpha$	theoretical fall cone factor
$M$	Cam-clay frictional coefficient
$p'$	mean effective stress
$S_u$	undrained shear strength of soil
$v$	specific volume of soil
$w$	moisture content of soil
$w_l$	liquid limit of soil
$w_p$	plastic limit of soil
$W$	weight of fall cone

### Soil conditioning parameters

$c_f$	concentration of foam agent
FER	foam expansion ratio (ratio of volume of foam to volume of foam liquid at atmospheric pressure)
FIR	foam injection ratio (ratio of volume of foam at atmospheric pressure to volume of excavated soil)
FLIR	foam liquid injection ratio (ratio of volume of foam liquid to volume of excavated soil)
PIR	polymer injection ratio (ratio of volume of polymer solution to volume of excavated soil)
$t_{25}$	time for drainage of 25% of foam liquid volume
$t_{50}$	time for drainage of 50% of foam liquid volume

$V_f$	volume of foam (at atmospheric pressure)
$V_{fa}$	volume of foam agent
$V_{fs}$	volume of foam solution
$V_{fl}$	volume of foam liquid phase
$V_p$	volume of polymer solution
$V_s$	in-situ volume of excavated soil

### **Screw conveyor parameters**

$D_c$	internal diameter of screw conveyor casing
$D_d$	diameter of extrusion die
$D_f$	screw flight diameter
$D_o$	diameter of extrusion die barrel
$D_s$	diameter of screw shaft
$e$	screw flight thickness
$h$	screw channel depth
$l$	length along screw channel parallel to flights
$L$	length of screw conveyor
$L_d$	length of extrusion die
$L_o$	length of extrusion die barrel
$N$	rotational speed of screw
$P$	total pressure in screw conveyor die extrusion pressure
$\underline{P}$	dimensionless total pressure gradient
$Q$	volumetric soil flow rate
$\underline{Q}$	dimensionless volumetric soil flow rate
$r_a$	extrusion die area reduction
$t$	screw pitch
$T$	screw torque
$\underline{T}$	dimensionless screw torque
$w$	width of screw channel perpendicular to flights
$x$	axial length along screw conveyor

## Greek symbols

### Geotechnical parameters

$\Gamma_{\text{csl}}$	specific volume on critical state line at $p' = 1$ kPa
$\Gamma_{\text{iso}}$	specific volume on isotropic consolidation line at $p' = 1$ kPa
$\kappa$	slope of swelling line in $v - \ln p'$ space
$\lambda$	slope of critical state line or normal compression line in $v - \ln p'$ space
$\lambda^*$	slope of one-dimensional normal compression line
$\sigma_n'$	normal effective stress
$\sigma_v'$	vertical effective stress
$\tau$	shear stress

### Screw conveyor parameters

$\alpha$	ratio of shear stress on screw surfaces to shear stress on casing surface
$\phi_a$	average screw helix angle
$\phi_f$	screw flight helix angle
$\phi_s$	screw shaft helix angle
$\eta$	conveyor discharge efficiency
$\tau_{//}$	shear stress on screw conveyor casing parallel to screw axis
$\tau_{\perp}$	shear stress on screw conveyor casing perpendicular to screw axis
$\tau_c$	resultant shear stress acting on screw conveyor casing surface
$\tau_f$	shear stress acting on screw flight surface
$\tau_s$	shear stress acting on screw shaft surface
$\theta$	angle of soil flow at conveyor casing relative to perpendicular to screw axis

# Chapter 1

## Introduction

---

### 1.1 Earth pressure balance tunnelling machines

Earth pressure balance (EPB) machines are commonly used for the construction of tunnels in soft soils ranging from coarse sands and gravels to stiff clays. Figure 1.1 shows a schematic diagram of a typical EPB machine, and Figure 1.2 shows a large diameter EPB machine. These tunnelling machines range in size from about three metres to over 12 meters in diameter.

EPB machines are closed face machines, providing a support pressure to the tunnel face to stabilise the soil and reduce ground volume losses and movements during excavation. The tunnelling process involves a rotating cutterhead excavating the soil, which passes through openings into the head chamber as the shield is pushed forward by jacks. The excavated soil fills the chamber and acts as the support medium for the ground by transferring the thrust force from the shield jacks to the tunnel face. The screw conveyor removes the excavated soil from the pressurised head chamber. The screw conveyor plays an important role in the excavation process, controlling the volume of soil discharged from the machine, and providing a mechanism to dissipate the chamber pressure as the soil flows along the screw to the outlet.

Ideally, an EPB machine is operated to maintain a pressure in the chamber equal to or greater than the earth and groundwater pressures at the tunnel face. A stable support pressure is achieved by balancing the volume of soil entering the chamber with the volume discharged by the screw conveyor. This is controlled through the rotational speed of the cutterhead, the advance rate of the shield jacks, and the rotational speed of the screw conveyor. The control of the excavation process and the performance of the tunnelling machine depend critically on the properties of the excavated soil.

## **1.2 Soil conditioning for EPB machines**

Ideal ground conditions for EPB machines consist of soils with relatively high fines contents such as clayey silts or silty sands, with a consistency to form a low permeability, soft plastic paste when excavated. These properties allow the support pressure to be transferred uniformly to the tunnel face and controlled flow of the soil through the machine. However, natural soils rarely have these ideal properties, and conditioning of the soil is usually necessary to change its properties to suit the machine.

Soil conditioning for EPB machines involves injecting conditioning agents from the machine into the excavated soil. The objective is to modify the spoil properties to form a soft plastic paste of low permeability, leading to improvements in the machine performance and control of the excavation process in a wide range of soils. The specific treatments required to effectively condition different types of soil vary widely, and many factors influence the specification and performance of soil conditioning treatments.

Geotechnical factors including the particle size distribution, strength, permeability, water content, and plasticity influence the treatments required for effective conditioning of the soil. A range of materials are used as conditioning agents, including water, foams, polymers, dispersants, and bentonite slurries. Each agent has different properties, and varying effects on the properties of different soils. These conditioning agents can be used separately or in combination. Variables are associated with their application, such as the concentration, the injection ratio, and the expansion ratio for foams. Many commercial products are available as soil conditioning agents, with different types of foams, polymers, and dispersants for use in different ground conditions.

The performance of a conditioning treatment also depends on the injection system installed on an EPB machine. Conditioning agents are injected to the tunnel face from ports in the cutterhead to begin mixing with the soil as it is excavated. Further conditioning can be injected into the head chamber and the screw conveyor to mix with the soil inside the machine. Injection of conditioning agents at different points has varying effects on the machine operation. Thorough mixing with the excavated soil is necessary for effective conditioning, so the design of the EPB machine influences the success of the soil conditioning process.

Improvements to EPB machine operations resulting from effective soil conditioning include:

- Improved control of the chamber pressure supporting the tunnel face
- Controlled flow of soil through the machine
- Control of groundwater inflows
- Improved formation of a soil plug along the screw conveyor
- Reduced torque and power requirements for the machine
- Reduced wear of the cutterhead and screw conveyor
- Reduced clogging of the machine by sticky soils

Further improvements to the tunnelling process can result from effective soil conditioning, such as improved tunnelling advance rates, reduced shut down periods for machine maintenance, and reduced ground movements and effects on surrounding structures.

The properties of the excavated soil often cause problems during tunnelling with EPB machines. In coarse sands and gravels, the soil does not readily form a plastic paste, and control of the soil and ground water flow through the machine is difficult, particularly with high ground water pressures. In stiff, high plasticity clays, the excavated soil can recompact into a sticky mass and clog the machine. In these cases, controlling the soil flow through the screw conveyor can be problematic. If the soil is too 'liquid', or of very low strength, the flow through the screw conveyor and the dissipation of the chamber pressure cannot be controlled. If the strength of the soil is too high, the screw conveyor can become jammed and require a high torque for the soil to flow. Controlling the volume of soil discharged by the conveyor and the pressure dissipation along the screw is critical for controlling the chamber pressure supporting the tunnel face. Effective soil conditioning to form a soft plastic paste can reduce these problems by creating soil properties that allow improved control of the flow through the screw conveyor.

Soil conditioning has been commonly used in EPB tunnelling for some time, and its importance and potential benefits are well known. However, the many variables involved in specifying treatments for different soils has resulted in practical applications being based largely on trial and error. As a result, the conditioning treatments used in practice are not always effective, and related problems with the control of the excavation process and the machine operation are often encountered. Some research investigating soil conditioning in the laboratory and the field has been previously performed, and general guidelines for conditioning treatments for different soils

are available. Some test methods for assessing soil conditioning treatments exist, but these are not widely used in practice or for fundamental studies of conditioning for different soils. There is generally a limited understanding of the effects of conditioning treatments on the properties of different soils and EPB machine operations. Further research is needed to improve the fundamental understanding of soil conditioning, so that its application in practice can be improved to reduce the related problems encountered in EPB tunnelling projects.

### **1.3 Scope and objectives of research**

Despite the extensive use of soil conditioning in practice and the related problems that are often encountered on EPB tunnelling projects around the world, relatively little research investigating soil conditioning has been previously performed. Most of the research that has been carried out has investigated the properties of sands conditioned with foam, and the operation of EPB screw conveyors with these materials. Very little research into soil conditioning for clays has been previously reported.

The research presented in this thesis was performed as part of a project in collaboration with the University of Oxford, investigating soil conditioning and lubrication for tunnelling and pipe jacking. The scope of the research project includes laboratory investigations of soil conditioning for clays and sands, studies of model EPB screw conveyors operating with clays and sands, and field monitoring of EPB machines operating in a range of soils to investigate the effects of soil conditioning on the machine performance. Observation of the performance of several EPB machines operating on the Channel Tunnel Rail Link (CTRL) project currently under construction in London is being carried out for the field monitoring phase of the research.

This thesis presents laboratory investigations of soil conditioning for clays, and of a model EPB machine screw conveyor operating with clay soils. The effects of conditioning agents on the properties of clay soils, and effective conditioning treatments for stiff, high plasticity clays are not well defined. The mechanics of EPB screw conveyors and the effects of varying operating conditions and soil properties on the performance are not completely understood. The research presented in this thesis was performed to investigate these topics in the laboratory to advance the fundamental understanding and practical application of soil conditioning for EPB machines.

The specific objectives of the research presented in this thesis are summarised as follows:

- Review the current practice and previous research of soil conditioning for EPB machines
- Development of simple test methods suitable for assessing conditioning treatments for clays
- Investigate properties of soil conditioning foams
- Investigate the effects of foam and polymer conditioning treatments on clay soil properties
- Identify optimum conditioning treatments for London Clay
- Design and commission an instrumented model EPB screw conveyor system
- Investigate the mechanics of the model screw conveyor operating with clay soils
- Investigate the operation of the model screw conveyor with conditioned clay soils
- Develop a theoretical model describing the screw conveyor operation with clay soils

During the course of this research, some work related to lubrication for pipe jacking in clay soils was also performed. This research involved an investigation of the effects of various inhibiting agents used in pipe jacking lubricant fluids on the swelling behaviour of clay soils. This research is not presented in this thesis, but is described by Merritt and Mair (2001 a, b).

#### **1.4 Outline of thesis**

Chapter 1 introduces EPB tunnelling machines and the role of soil conditioning in their operation. The scope and objectives of the research presented in this thesis are summarised.

Chapter 2 is a review of literature relevant to this research. The review covers soil conditioning agents, their effects on soil properties and EPB tunnelling operations, laboratory testing of conditioned soils, and some case studies of soil conditioning in practice. Previous studies of EPB screw conveyors and theoretical models describing screw extruders and conveyors are reviewed.

Chapter 3 presents testing performed to investigate properties of foams and conditioned clay soils. The observed effects of various foam and polymer conditioning treatments on the undrained shear strength of London Clay samples are discussed, and optimum conditioning treatments for this soil are suggested.

Chapter 4 describes the instrumented model EPB screw conveyor system designed and commissioned for this research. Design details of the system components and instrumentation are described. The screw conveyor operation and test procedures are summarised.

Chapter 5 reports a series of model screw conveyor tests performed with consolidated kaolin samples. The mechanics of the screw conveyor operation with clay soils observed in the tests are described, and the effects of varying conveyor operating conditions are discussed.

Chapter 6 reports a series of model screw conveyor tests performed with conditioned natural clay soil samples. The preparation and properties of the samples are described, and the screw conveyor operation observed in the tests with varying sample conditioning treatments and conveyor operating conditions are discussed.

Chapter 7 presents an analysis of the screw conveyor operation. A theoretical model is proposed to describe the conveyor operation and allow calculation of the pressure gradients and the screw torque. The predicted effects of different variables on the conveyor operation are discussed, and the results of the model screw conveyor tests are compared with the theoretical model.

Chapter 8 summarises the conclusions from this research investigating soil conditioning for clay soils and the operation of EPB screw conveyors with clay soils. Some suggestions for further research of these topics are given.

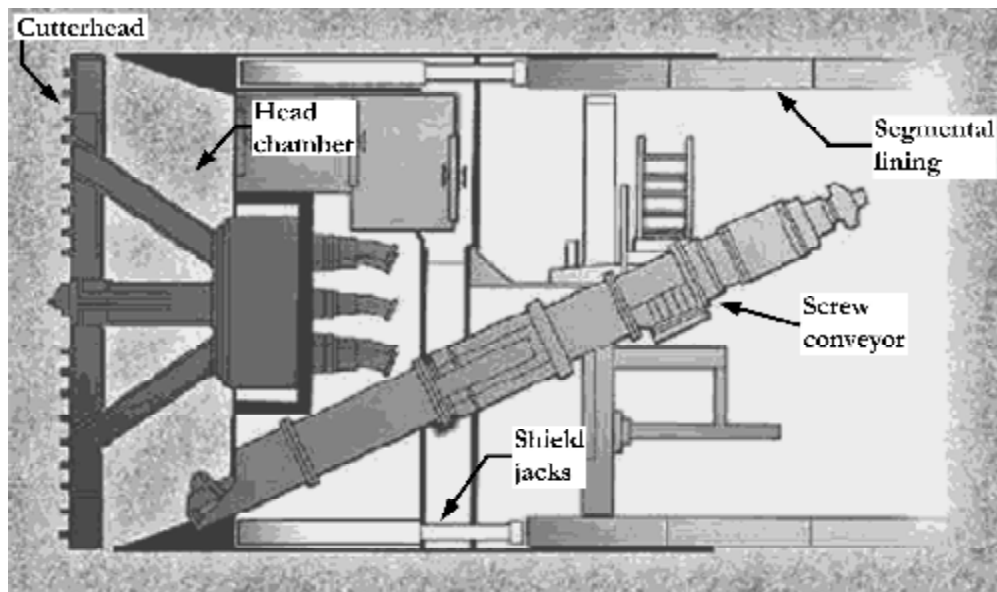


Figure 1.1 Schematic of typical EPB tunnelling machine.



Figure 1.2. 12 m diameter EPB tunnelling machine.  
(from Herrenknecht AG)

# Chapter 2

## Literature Review

---

### 2.1 Introduction

This chapter summarises the current practice of soil conditioning for EPB tunnelling, and reviews literature reporting work relevant to the research presented in this thesis. The properties of some conditioning agents, their application and effects on soil properties are discussed. Typical conditioning treatments for granular and clay soils, and effects of soil conditioning on EPB tunnelling machine performance are reviewed. Laboratory test methods and investigations of conditioned soil properties are discussed, and some case studies of applications of soil conditioning in practice are reviewed. The design and operation of EPB machine screw conveyors, laboratory and field studies of their operation, and theoretical models describing the mechanics of screw conveyors are discussed.

### 2.2 Soil conditioning agents

A wide range of materials are used as soil conditioning agents, and many commercial products based on these are available. The most common conditioning agents are foams, polymers and bentonite slurries, although others such as water, dispersants and oils also have applications. Each type of conditioning agent has different properties and effects on soil properties, as discussed below.

#### 2.2.1 Bentonite slurries

The properties of bentonite slurries and applications for soil conditioning in EPB machines are discussed by a number of authors, including Maidl *et al.* (1996), Williamson *et al.* (1999), Milligan (2000, 2001), and EFNARC (2001). Bentonite slurries are dispersions of montmorillonite clays in

water. The slurry properties depend on the type of montmorillonite, the chemistry of the water, and the slurry proportions. Slurries are prepared by mixing bentonite in water with a high shear mixer, to fully disperse and hydrate the clay particles. The density and viscosity of bentonite slurries require control and monitoring during tunnelling, with the required slurry properties depending on the soil being excavated. Additives such as polymers and dispersants can be added to modify the slurry properties.

Bentonite slurries were among the first soil conditioning agents used with EPB machines. For excavation of coarse granular soils, bentonite slurries can be injected from the cutterhead to form a low permeability filter cake in the soil at the tunnel face, improving control of ground water inflows and support of the face. The addition of bentonite increases the fines content and forms a soil paste with improved plastic flow properties and reduced permeability. The bentonite slurry also provides lubrication between the soil grains and the machine surfaces, leading to lower cutterhead and screw conveyor torques, and reduced machine wear. Bentonite slurries are often used in combination with polymers and foam to condition soils. They are also sometimes used to fill the machine head chamber to support the tunnel face during prolonged shut down periods, or in the case of a sudden chamber pressure loss during tunnelling (e.g. Williamson *et al.*, 1999).

### **2.2.2 Polymers**

Polymers are macromolecules consisting of large numbers of repeating smaller molecules (monomers) chemically bonded into long chains. Polymerisation of a single type of monomer produces a homopolymer, while polymerisation of two or more different monomers produces a copolymer. The properties of polymers vary widely, depending on their chemical composition and structure. The size of polymer molecules (characterised by the molecular weight), branches or groups attached to the polymer chain, cross-linking between chains, and intermolecular forces all influence the physical properties of polymers (e.g. Bailar *et al.*, 1989).

A range of polymers are used as soil conditioning agents in EPB tunnelling. Natural polymers such as starches and guar, modified natural polymers including carboxymethylcellulose (CMC) and polyanionic cellulose (PAC), and synthetic polymers, particularly derivatives of polyacrylamides, have been used for various functions during tunnelling with EPB machines (Milligan, 2000).

Partially hydrolysed polyacrylamides (PHPA) are among the most commonly used polymers as soil conditioning agents. Their chemical properties and interactions with charged particles (such as clay minerals) are discussed by Moss (1978) and Moody (1992, 1995). PHPA is a linear copolymer of anionic acrylate and non-ionic acrylamide monomers, with chemical structures as shown in Figure 2.1. The molecular charge and weight can be varied to create polyacrylamide polymers with different properties. PHPAs with anionic (negative), non-ionic (neutral), or cationic (positive) charges can be produced, which affects their interactions with soil particles. The molecular weight can be varied over several orders of magnitude, influencing the viscosity of the polymer in solution and their action as dispersants or flocculants. The anionic charge of the PHPA molecule depends on the ratio of the acrylamide and acrylate monomers combined in the polymerisation reaction. The molecular charge can also be varied by partial hydrolysis of polyacrylamide, in which OH groups are substituted for some of the NH<sub>2</sub> groups. PHPAs used as soil conditioning agents are typically 30% anionic, with molecular weights of the order 10<sup>6</sup> g/mol. The molecules have a linear structure, resulting in high water solubility of PHPAs with a large molecular weight. To produce the polymer particle sizes necessary to achieve these properties (smaller than 2 µm), PHPA polymers are often produced as dispersions in oils.

PHPA polymers with high molecular weights (greater than 10<sup>6</sup> g/mol) can act as flocculants for clay soils through a bridging mechanism. Anionic polymers adsorb onto the surface of clay particles through electrostatic attractions to positively charged sites on the particle edges, and by other chemical bonding mechanisms. The polymer chains extend from the particle surface to create bridges between particles and form a flocculated clay structure, as illustrated in Figure 2.2. A number of chemical factors influence the interactions between polymers and clay particles, such as the polymer molecular weight and charge, and the pH and ionic strength of the solution, which affect the shape of the polymer molecule and the surface charge of the clay particles in solution.

Studies of the adsorption of polyacrylamide polymers onto different clay minerals and natural soils, and the influence of various chemical factors, are reported by Schamp and Huylebroeck (1973), Lee *et al.* (1991), and Malik and Letey (1991). Figure 2.3 shows adsorption isotherms measured by Malik and Letey (1991) for 21% anionic PHPA adsorbing onto soils containing varying clay, silt and sand fractions, and silica sands with varying gradings. The polymer adsorbed onto all types of soil, with increasing amounts adsorbed at higher polymer concentrations. Similar amounts of polymer were adsorbed by the natural soil samples prepared with similar aggregate

sizes and containing varying clay fractions composed of montmorillonite, mica, vermiculite and kaolinite clay minerals. The amount of polymer adsorbed onto the silica sands was higher for the finer size fractions due to the increased surface area. These measurements indicate that polymer adsorption occurs on the external surface of aggregates of soil particles, and depends on the surface area available for the polymer molecules.

Modified natural polymers such as CMC and PAC are also used in tunnelling with EPB machines. These polymers are often used as additives to improve the properties of bentonite slurries and foams, with examples of these functions discussed by Williamson *et. al* (1999) and Milligan (2000). Applications of these and various other polymers, such as starches, guar and xanthan, for soil conditioning are discussed further by Lyon (1999a, b).

The use of polymers as conditioning agents has several effects on soil properties that lead to improvements for EPB machine operations. The functions of polymers as water absorbing and soil structuring agents to bind the excavated soil into a plastic paste are discussed by Babendererde (1998), Langmaack (2000), and Leinala *et. al* (2002). Jefferis (1995) discusses the flocculating action of PHPA polymer solutions on excavated soils, forming a paste with increased plasticity able to absorb large amounts of water. Polymers are thought to coat the surface of stiff clay cuttings to provide lubrication and reduce the stickiness of these soils. Polymers can be injected as water based solutions, or as additives to foam solutions and bentonite slurries, where they are used to improve the properties of these agents and form a combined conditioning treatment. The improved structure and plasticity of soils conditioned with polymers, and their lubrication effects, can improve control of the flow of soil through an EPB machine, with lower cutterhead and screw conveyor torques, and with reduced wear and clogging of the machine.

### **2.2.3 Foams**

Foam is a dispersion of air bubbles in a liquid phase comprising of a water based surfactant solution. The properties of surfactants and foams, their interactions with soils, and their effects as conditioning agents are discussed by authors including Maidl *et. al* (1996), Langmaack (2000), Milligan (2000) and Leinala *et. al* (2002). Surfactants are surface active agents, which are molecules with chemical structures based on a hydrophobic chain and a hydrophilic end group which can have anionic, cationic, non-ionic or amphoteric charge properties. The surfactant chemistry affects the surface tension of the solution, their interactions with soils, and the properties of the foam. Surfactants can adsorb onto charged soil particles through electrostatic

attractions and chemical bonding mechanisms, and cause steric interactions and repulsive forces to disperse fine-grained soils, as illustrated in Figure 2.4. The adsorption of surfactants onto steel surfaces of a tunnelling machine is also thought to reduce the adhesion of clay soils.

Surfactants solutions are used to produce foam, where they adsorb at the air-liquid interface to reduce the surface tension and stabilise the thin liquid films between air bubbles in the foam. The structure of aqueous foam at different scales is shown schematically in Figure 2.5. Most foam agents for soil conditioning are based on anionic surfactants, and various agents are available with properties designed for conditioning different types of soil. Polymer additives such as CMC and PHPA are often added to the solution to act as foam stabilisers. Foams have the advantage of introducing surfactants to the soil without adding a large liquid volume, and injection with compressed air enhances mixing of the foam through the excavated soil.

The generation of foam in an EPB machine requires substantial plant and integration with the control systems of the machine. Maidl *et. al.* (1996) and Williamson *et. al.* (1999) describe the typical foam generation and injection plant and control systems on an EPB machine. A schematic of the foam plant for an EPB machine is shown in Figure 2.6. The foam solution is pumped through a pressurised line to the foam generator unit, which is also supplied with a compressed air line. The foam solution and compressed air flow through the generator unit, which causes turbulent mixing of the two phases and produces foam from the outlet. Usually, each foam injection port has a generator unit, located close by so that foam is injected to the soil soon after generation. The generator design and operation influences the properties of the foam produced, as the material inside the generator unit, and the air and liquid flow rates and pressures, affect the foam bubble sizes and expansion ratio.

The properties of foams depend on the solution chemistry, the relative air and liquid phase volumes (the foam expansion ratio, FER), and the foam bubble sizes. The solution concentration influences the amount of surfactant available to treat the soil, and the stability of the foam. The foam expansion ratio determines the amount of liquid and compressed air contained in a volume of foam. Foams are meta-stable, and their structure and properties degrade over time. The difference in density between the air and liquid phase results in drainage of liquid from the bubbles, and the liquid films between bubbles can rupture and cause coalescence of adjacent bubbles. The diffusion of gas between bubbles also causes the foam structure to change over time. Foam stability can be increased by generating a small and uniform bubble size, and by

polymer additives to increase the viscosity of the liquid phase and slow down drainage of the foam. It has been suggested that uniformly sized foam bubbles with diameters less than 1 mm are desirable for foam stability (Cash and Vine-Lott, 1996). Langmaack (2000) states that foam generators for tunnelling machines typically form air bubbles ranging in size from 0.5 to 2 mm.

As foams for soil conditioning are typically composed of about 90% air (at an FER of 10), their volume change with pressure conforms approximately to ideal gas laws. Quebaud *et al.* (1998) present measurements of foam volume changes with pressure which, as shown in Figure 2.7, agree with theoretical volume changes calculated from gas laws. The ideal gas law pressure-volume relationship ( $PV = \text{constant}$ ) is expressed in terms of the foam expansion ratio as:

$$FER = \frac{P_a}{P} \times (FER_a - 1) + 1 \quad \text{Eqn 2.1}$$

where  $FER_a$  is the foam expansion ratio at the atmospheric pressure  $P_a$  and  $FER$  is the expansion ratio at the absolute pressure  $P$ . As shown in Figure 2.7, the application of several pressure cycles causes an approximately elastic response of the foam volume change.

Conditioning with foam has several effects on soil properties that lead to improvements in EPB machine performance, as discussed by authors including Maidl *et al.* (1996), Babendererde (1998), Quebaud *et al.* (1998), Leinala *et al.* (1999, 2000, 2002) and Milligan (2000). When mixed with granular soils, foam gives the soil a plastic consistency, with the air bubbles reducing the density and the friction between grains, and providing lubrication of machine surfaces. These spoil properties lead to lower cutterhead and screw conveyor torques, and reduced wear of the machine. The compressibility of the spoil is increased by the foam, which improves control of the chamber pressure as the bubbles can expand or compress to compensate for pressure fluctuations when the excavation and discharge rates are not balanced. Foam also reduces the permeability of the soil to improve control of ground water inflows.

Foam is also used for conditioning clay soils to improve the spoil properties and the tunnelling machine performance. The surfactants in the foam liquid can coat clay cuttings to inhibit adsorption of water. Foam is also thought to disperse the cuttings to reduce recompaction and stickiness of the soil and adhesion to the machine surfaces. These improvements to clay soil properties lead to reduced driving torques and reduced clogging of the machine. Foams are also

used in combination with other agents such as polymers, bentonite slurry, and dispersants to condition different types of soil, as discussed later.

The stability of a foam-soil mixture is important so that the properties of the conditioned soil persist over time. The foam mixed in the soil should remain stable during the time taken for it to pass through the head chamber and screw conveyor. Rapid breakdown of the foam or degradation during delays or shut-down periods can result in loss of the face support pressure or the soil plug in the screw conveyor, and loss of workability of the spoil in the machine (Milligan, 2000). The stability of foam mixed with soil is different to that of the foam alone, and some foam-soil mixtures can remain stable for a considerable time. Williamson *et al.* (1999) report slump tests showing that sand conditioned with foam remained stable for up to seven hours, and Babendererde (1998) reported no significant loss of foam volume mixed with limestone after three days. Bezuijen *et al.* (1999) measured the vane shear strength of sand-water-foam mixtures prepared under pressurised conditions, showing that the mixture remained stable with a similar strength over four days, considerably longer than the stability of the foam alone.

#### **2.2.4 Other conditioning agents**

As well as the commonly used conditioning agents discussed above, a number of other materials find applications in certain ground conditions.

Water can be used to condition soils with in-situ properties close to ideal for EPB tunnelling, such as soft clays, silts and fine sands with low permeability. If conditioning of these soils is necessary, water can be added to soften the soil into a paste of pulpy to soft consistency, with  $I_c$  in the range 0.4 to 0.75, where the consistency index,  $I_c = (w_l - w) / I_p$  (Maidl *et al.*, 1996).

Dispersants are used to condition stiff clay soils, injected as additives in the foam liquid or as water based solutions. Langmaack (2000) discusses some properties of dispersing agents, which are polymer molecules with a high charge density, such as polycarboxylic acids (eg. MBT, 2002). These agents adsorb onto the soil particle surface and create a steric barrier to disperse and de-structure clay soils, reducing their stickiness and tendency to clog the tunnelling machine.

Various types of oil, such as jute and palm oil, have been suggested as conditioning agents for lubrication of the cutterhead (Lyon, 1999b). These agents can be injected as emulsions in water,

typically at concentrations of 3 to 10%, or in combination with polymers, bentonite slurries or foams. For environmental reasons, natural biodegradable oils are most suitable.

## **2.3 Soil conditioning treatments**

There are many variables involved in the application of soil conditioning. Geotechnical factors, the selection of conditioning agents and their application, and the design of the tunnelling machine all influence the performance of conditioning treatments. The application of soil conditioning for granular soils and clays, and the improvements to EPB machine performance are discussed below.

### **2.3.1 Conditioning of granular soils**

Excavation of granular soils with EPB machines can encounter problems, particularly in high permeability coarse sands and gravels with low fines contents and high groundwater pressures. A support pressure is required to stabilise the tunnel face in granular soils, and effective soil conditioning is required to form a low permeability, plastic soil paste suitable for EPB tunnelling. Granular soils can also be very abrasive, causing excessive wear of the cutterhead and screw conveyor. Conditioning treatments to improve the properties of granular soils are discussed below.

The conditioning requirements for EPB machines operating in granular soils with different gradings are discussed by Maidl *et al.* (1996). As shown in Figure 2.8, soils with particle size distributions in regions defined by three curves have different conditioning requirements. It is suggested that EPB machines can be used in soils with grading curves above line (1) containing a minimum of 30% fines, as these soils form a low permeability plastic paste. Depending on the soil composition, conditioning with water, bentonite, polymers or foams can be employed. The application of EPB machines and the conditioning treatments required for soils with grading curves below line (1) depends on the permeability and groundwater pressure. High density bentonite slurry or combined foam-polymer conditioning treatments are suggested for soils with grading curves below line (2). EPB machines are not recommended for use in soils beneath line (3), as conditioning agents are ineffective in such coarse, high permeability soils.

Jancsecz *et al.* (1999) also consider the conditioning requirements for different soils based on the particle size distribution, as shown in Figure 2.9. Soils containing less than approximately 30%

gravel can be excavated by EPB machines with conditioning treatments suitable for coarse, frictional soils. Soils containing higher fractions of gravel and coarse sand are not considered suitable for EPB tunnelling as they cannot be conditioned effectively, and excavation with a slurry shield is recommended. Well graded soils containing sands and significant silt fractions are well suited to EPB tunnelling, requiring only low rates of conditioning. These criteria are generally similar to those suggested by Maidl *et. al.* (1996).

Conditioning treatments for granular soils based on the particle size distribution are also discussed by Kusakabe *et. al.* (1997) and Williamson *et. al.* (1999). An empirical equation based on the soil grading is suggested to estimate the density of bentonite slurry required to increase the fines content to effectively condition the soil:

$$D = a \times (30 - p_{0.075}) \times 2.0 + (40 - p_{0.25}) \times 0.5 + (60 - p_{2.0}) \times 0.2 \quad \text{Eqn 2.2}$$

In this equation,  $D$  is the slurry density (%),  $p_{0.075}$ ,  $p_{0.25}$ , and  $p_{2.0}$  are the percentages of soil passing through 0.075 mm, 0.25 mm and 2.0 mm sieves, and  $a$  is a parameter based on the uniformity coefficient of the soil grading. For coarser soils, a higher slurry density is required for effective conditioning. This equation provides a basis for designing bentonite slurry conditioning treatments for granular soils. However, for specific applications, adjustments of the calculated densities are usually required based on the observed properties of the slurry and the conditioned soil.

Conditioning of granular soils with bentonite slurry has the disadvantage of adding significant amounts of liquid to the soil, which can cause problems for disposal of the spoil. Foams are now the most commonly used conditioning agents, and have the advantage of improving soil properties while adding only a small liquid volume to the soil. Typically 90% of the foam volume is air, which dissipates over time and returns the soil close to its original consistency after excavation. An empirical equation to estimate the foam injection ratio (FIR) required to condition granular soils, based on the particle size distribution, is suggested by Kusakabe *et. al.* (1997) and Williamson *et. al.* (1999):

$$FIR = \frac{a}{2} \times \left[ (60 - 4(p_{0.075})^{0.8}) + (80 - 3.3(p_{0.42})^{0.8}) + (90 - 2.7(p_{2.0})^{0.8}) \right] \quad \text{Eqn 2.3}$$

The parameters in this equation are similar to those defined above for equation 2.2. Higher FIRs are predicted by equation 2.3 for conditioning soils with a coarser grading. A minimum FIR of 20% is suggested when a lower value is calculated from equation 2.3. This equation provides a basis for designing foam conditioning treatments for granular soils, but the calculated FIRs require adjustment based on the observed properties of the conditioned soil. Also, several factors that influence the conditioned soil properties are not considered, such as the foam solution concentration and composition, the expansion ratio, the soil water content, permeability and consistency, and the head chamber pressure in the EPB machine.

Other approaches for determining foam injection ratios have also been suggested. Bezuijen *et al.* (1999) suggest that the foam injection ratio should be such that the porosity of conditioned sand in the pressurised head chamber is increased above the maximum porosity of the sand alone. Cash and Vine-Lott (1996) suggest that the volume of foam injected should be approximately equal to the void content of the excavated soil, after accounting for bulking of the soil and the chamber pressure.

The EFNARC (2001) specification provides some guidance for conditioning treatments for different soils. The type of foam and other additives required are recommended based on the composition of the soil, as shown in Figure 2.10(a). Relative quantities of conditioning agents are suggested, as well as general ranges of parameter values for conditioning treatments, as summarised in Figure 2.10(b). For sands, conditioning with foam type B or type C is recommended at increased concentrations and very high injection ratios. The general properties of the foam types are described in Figure 2.10. Foam stabilisers and soil stabiliser additives are suggested at increased quantities to reduce segregation of the soil. For clayey and sandy gravels, high to very high foam concentrations and injection ratios are recommended, with very high quantities of foam and soil stabilisers. According to these recommendations, as the soil becomes coarser, the foam solution composition is designed to increase the foam stability and structuring effects on the soil, and larger volumes of foam are injected. These recommendations reflect the increasing difficulty in forming a homogenous plastic soil paste from coarser grained soils.

The suppliers of conditioning agents provide recommendations for their application. Foam agents with different chemical compositions and properties are available, as well as various polymers and dispersants, for application in different ground conditions. The choice of particular conditioning agents is initially based on the soil type and permeability, as illustrated for one

supplier's products in Figure 2.11 (MBT, 2001). For coarse to fine sands, conditioning with various foam agents (SLF10, SLF 20) and polymers (SLF P1, SLF P2) is recommended. Typical values of parameters for conditioning treatments are also suggested by suppliers. Recommended foam injection ratios usually range from approximately 30% to 60%, with expansion ratios of 7 to 11. Recommended concentrations are also given for the conditioning agents, usually ranging from 2 to 6% for various foam agents, and from 0.2 to 1% for polymers. The injection ratios and concentrations typically recommended by suppliers are similar to the ranges suggested by the EFNARC specification (e.g. MBT, 2001; Lamberti, 2002).

### 2.3.2 Conditioning of clay soils

EPB machines are well suited for excavation of soils with significant fines contents, as only low rates of conditioning are required to form a spoil with suitable properties. These soils typically have low permeability, improving control of groundwater and sealing of the screw conveyor. However, problems are often encountered with EPB machines operating in clay soils. During excavation of high plasticity clays, the soil cuttings tend to recompact and adhere to the machine, clogging the cutterhead and chamber, causing high cutterhead torques, low advance rates, and maintenance periods to clear blockages. For low plasticity clays, the strength and liquidity change rapidly with small changes in moisture content, causing difficulties controlling the spoil properties and the excavation process. Conditioning treatments for clay soils to improve the properties for EPB tunnelling are discussed below.

Maidl *et. al* (1996) suggest that stiff soils with particle size distributions above curve (1) in Figure 2.8 should be conditioned to form a soft plastic paste with consistency index in the range 0.4 to 0.75, corresponding to an undrained shear strength ranging from about 10 to 25 kPa (Milligan, 2000). As shown in Figure 2.9, Jancsecz *et. al* (1999) suggest that soils in this region of the grading chart require conditioning mainly due to the adhesiveness of the soil. Milligan (2000) discusses the problems of conditioning these soils with water. Low plasticity clays are sensitive to changes of the moisture content. For stiff high plasticity clays with low permeability, excessive mixing with large quantities of water is required to soften the soil cuttings, which tend to recompact and clog the machine. It is suggested that the best approach to conditioning stiff clays is by injecting foam or polymers that coat the clay cuttings and inhibit adsorption of water, forming a mixture of discrete cuttings that can pass through the machine without recompacting. Foam has the advantage of introducing a small liquid volume, with the surfactants dispersing the clay and the bubbles forming a compressible matrix to improve control of the chamber pressure.

The foam injection ratio required to condition stiff clays is suggested to be about 30%, although this is only based on limited evidence (Milligan, 2000). This figure is also suggested by Williamson *et. al* (1999), as a minimum foam injection ratio to reduce adhesion of cohesive soils.

To determine the suitability of EPB tunnelling and soil conditioning requirements, Steiner (1996) suggests that the Atterberg limits, natural water content and liquidity index of a soil should be considered as well as the grain size distribution. Analysis of some case histories showed that EPB machines could easily excavate clays with the liquidity index in the range 0.25 to 0.60, and that for successful operations, soils should be located above the A-line on a plasticity chart and have a liquid limit greater than 30%, either naturally or after conditioning. On some projects, the Atterberg limits of silts were increased by injecting 5 to 10% bentonite slurry by volume, forming low plasticity clays less sensitive to changes in water content.

The EFNARC (2001) specification provides some recommendations for conditioning soils containing clay, as summarised in Figure 2.10(a). For clays and sandy clay-silt soils, conditioning with low quantities of foam type A at low concentration, and with low or increased quantities of dispersing agents is recommended. The conditioning agents suggested for soils with high clay contents have high dispersing and coating capacity, aimed at reducing adhesion and clogging problems. For sand-clayey silt soils, conditioning with increased quantities of foam type B with some foam stabiliser and dispersing agents is recommended. For soils containing smaller amounts of clay, the conditioning treatments tend towards those recommended for granular soils, with higher foam injection ratios and increased foam stability.

Some suppliers produce conditioning agents with properties specifically designed for use in clay soils, and provide some guidance for their application. As shown in Figure 2.11 for one supplier's products, particular foams (SLF20, SLF30) and polymers (SLF P1, SLF P2) are recommended for conditioning clay soils. Dispersants (Rheosoil 211, X212) are also recommended for conditioning intact clay soils of low permeability, to reduce their stickiness. Typical concentrations and injection ratios for the application of these agents are also recommended by the supplier.

As discussed above, conditioning treatments are often based initially on the soil composition and particle size distribution, which influence their behaviour during excavation. A summary of conditioning treatments for different soils is given by Milligan (2001), as shown in Figure 2.12. Factors such as the permeability, Atterberg limits, and water content also influence the

conditioning treatments for a soil. Various foams and polymers are used to condition a wide range soils, with other agents such as bentonite slurries and dispersants used in certain soils. Some empirical equations have been suggested to estimate conditioner injection ratios, and ranges of typical values for conditioning treatment parameters have been established through practical applications. However, due to the many influencing factors involved, optimum conditioning treatments for different soils remain difficult to specify.

### **2.3.3 Effects of soil conditioning on EPB tunnelling operations**

Effective soil conditioning leads to significant improvements in EPB machine performance. The lubrication effects of foam air bubbles, surfactant foam liquids, and polymers at machine-soil interfaces contribute to lower cutterhead and screw conveyor torques, and reduce wear of the machine. The use of dispersants for clay soils is aimed at reducing their stickiness that causes high driving torques and clogs the machine. Reduced wear and clogging of the machine can reduce the shutdown periods required for maintenance during tunnelling.

The excavation process is improved by effective conditioning, allowing controlled flow of the soil from the cutterhead through to the screw conveyor discharge outlet. A homogeneous plastic soil paste, with compressibility from foam bubbles dispersed through the soil, allows a more uniform and stable pressure in the head chamber, which improves control of the earth pressure balance. Reduced permeability of the spoil improves control of groundwater inflows into the machine in permeable soils. Improvements to EPB machine operations resulting from soil conditioning are discussed by a number of authors, including Maidl *et. al* (1996), Quebaud *et. al* (1998), Langmaack (2000), Leinala *et. al* (1999, 2000, 2002), and Milligan (2000).

Improvements to the EPB machine performance resulting from soil conditioning also lead to improvements in the broader tunnelling process. Reduced machine driving parameters allow faster tunnelling advance rates. Increased advance rates resulting from soil conditioning are reported by Wallis (1996) and Leinala *et. al* (2000). Improved control of the flow of soil through the machine and of the face support pressure improves control of ground volume losses and settlements induced by tunnelling. Shirlaw *et. al* (2002) discuss relationships between volume losses and face pressures during EPB tunnelling in a range of soils in Singapore. Large local volume losses occurred when an adequate face pressure could not be maintained due to ineffective conditioning of a high permeability granular soil, and a soil plug could not be formed in the screw conveyor to seal against high groundwater pressures. Conditioning treatments used

in different ground conditions and their effects on EPB tunnelling operations reported in some case studies are discussed in Section 2.5.

## **2.4 Laboratory testing of conditioned soils**

Various laboratory tests can be performed to investigate the effects of conditioning treatments on soil properties, and to identify optimum treatments for specific soils. Some simple index tests have been used to measure conditioned soil properties. More advanced geotechnical and model tests also have been performed on conditioned soils under conditions representative of an EPB machine, as discussed below.

Some standard test methods for measuring properties of foams and conditioned soils are proposed in the EFNARC (2001) specification. The foam expansion ratio can be measured through the density of a foam sample, and the stability by the time for the liquid to drain from the foam, allowing comparison of basic properties of foams at atmospheric pressure. A test of the stability of foams mixed with sand is proposed by measuring the volume of the mixture over time. Test methods are proposed to measure properties of conditioned soils, including mixing tests, cone penetrometer tests, slump tests, shear box tests, and vane shear tests. Tests such as these are also discussed by Milligan (2000), and have been used in several studies to measure properties of conditioned soils.

Slump tests, similar to those for testing concrete, are often used to measure the consistency of conditioned soils. Quebaud *et al.* (1998) reports slump tests of sands conditioned with foams, and suggests that a slump of 12 cm represents the optimum consistency of spoil for EPB machines. The foam injection ratio (FIR) required to achieve this optimum slump with the sands tested ranged from 10% to 35%, depending on the foam concentration and expansion ratio, and the soil water content. Leinala *et al.* (2000, 2002) also report slump tests of various soils conditioned with foam, and suggest that a slump of 5 cm represents an optimum for EPB machines. Figure 2.13 shows that the slump of different soils increases with the FIR, with the expansion ratio constant and similar initial soil moisture contents. The FIR required for a given slump depends on the soil composition, and increases as the clay fraction of the soil increases. FIRs greater than 300% were tested for the hard till. Soils conditioned with foam have a similar slump at lower moisture contents than soils mixed with water, due to the fluidising effects of the

foam. Slump tests performed on granular soils conditioned with foams are also reported by Jancsecz *et. al.* (1999), Williamson *et. al.* (1999) and Langmaack (2000).

The cone penetrometer test is another index test used to measure effects of conditioning agents on soil properties (Jancsecz *et. al.* 1999; Langmaack, 2000). The measured cone penetration is described as indicating the 'fluidity' of a conditioned soil, but fundamentally this measurement is related to the sample undrained shear strength. Cone penetrometer tests were performed on sandy clay and gravely sand conditioned with foams and polymers. The cone penetration increased with the FIR, indicating a reduction of undrained strength. Conditioning the same soils with polymers resulted in lower cone penetrations than for foams, which did not increase with increasing water content due to the structuring and water-binding effects of the polymers. Langmaack (2000) also reports cone penetration tests to measure the effects of dispersing agents on clay soils.

Various test methods have been used to measure the adhesion and friction characteristics of conditioned soils on steel surfaces, parameters relevant to the power requirements, clogging and wear of an EPB machine. Quebaud *et. al.* (1998) describes a simple interface shear test for the lubricating effects of foam, measuring the friction angle when sand slipped on a sloping stainless steel plate. The interface friction angle was reduced by 10 to 15° when the sand was conditioned with foam.

Langmaack (2000) describes an adhesion test in which the displacement of a steel plate slipping vertically on the surface of a clay sample is measured over time. Different conditioning agents are introduced to the clay-steel interface to measure their influence on the adhesion. Stickiness and adhesion of clays in tunnelling machines was also investigated in the research project Eupalinos 2000 (Laquerbe, 2002). Laboratory tests were performed to investigate the adhesion of clays to steel surfaces through tensile tests, interface shear tests and compression tests, which lead to a proposed method for characterising the stickiness of a soil. Stickiness was found not to be an intrinsic property of a soil, but dependent on factors including the moisture content, interface properties and shear rates. Although it is recognised as a significant problem for tunnelling in clay soils, the mechanisms involved and test methods for measuring the influence of conditioning agents on the stickiness of clays and adhesion to steel surfaces are not well defined.

Mixing tests performed on conditioned soils have been reported by several authors, to investigate the effects of conditioning on power requirements for EPB machines. Quebaud *et al.* (1998) measured reductions in power of up to 60% for mixing sand as the FIR was increased, as shown in Figure 2.14. The soil water content influences the effects of conditioning with foam, particularly at low injection ratios. Williamson *et al.* (1999) report a 72% reduction in the torque required to mix sand with a hydraulic mixer after conditioning with foam, although no details of injection ratios or water contents are given. Mixing tests on sand-water-foam mixtures performed in more advanced apparatus designed to model the rotating cutterhead of an EPB machine, shown in Figure 2.15, are reported by Bezuijen *et al.* (1999, 2001). The chamber was pressurised to 350 kPa, with foam injected from the rotor as it penetrates into the sand. The measured rotor torque increased when the porosity of the conditioned sand was lower. Experiments with foam-conditioned sands using the model EPB screw conveyor apparatus also shown in Figure 2.15 are reported by Bezuijen *et al.* (1999, 2001), as discussed in Section 2.6.

The effects of conditioning agents on various geotechnical properties of soils have been investigated by several authors. Bezuijen *et al.* (1999) measured the compressibility of sand-water-foam mixtures during the mixing tests described above. Houlsby and Psomas (2001) performed compression tests in a Rowe cell on sands conditioned with foams, bentonite and polymers. The initial void ratios of the foam-sand mixtures depended on the FIR, and were much higher than the maximum possible for the sand alone. As shown in Figure 2.16, the foam-sand mixtures were highly compressible, and were stable at void ratios greater than the maximum for the sand at total pressures over 200 kPa. Bentonite and polymers mixed with the sand at low dosage rates had less influence on the compressibility, although high bentonite dosage rates produced mixtures with high initial void ratios.

Houlsby and Psomas (2001) also report shear box tests performed on foam-sand mixtures. The measured friction angles were much lower than for the sands alone, and decreased with increasing void ratios. The reduced friction angles were attributed to the void ratios being much higher than possible for the sand alone, with the injection of foam resulting in negative values of the relative density. However, recent tests reported by Pena (2003) have shown that although foam-sand mixtures have reduced shear strengths compared to the sand alone, this results from high pore water pressures in the mixture causing low effective stresses between the sand grains.

The effects of foam on the permeability of sands have also been reported by several authors, with Quebaud *et. al.* (1998), Bezuijen *et. al.* (1999), and Williamson *et. al.* (1999) all measuring significant reductions in permeability for sand conditioned with foam. Langmaack (2000) also reports reductions in the permeability of soils conditioned with foams, polymers and bentonite.

Tests performed with the various methods discussed above have shown that conditioning agents have a number of effects on soil properties beneficial to EPB machine operations, such as reducing the undrained shear strength, internal and interface friction, permeability, and increasing the compressibility. However, most of the tests reported have investigated the effects of foam on granular soil properties, and relatively little has been reported on testing of conditioned clay soils. Tests modelling the EPB excavation process and screw conveyor operation with conditioned soils have also been reported, as discussed in Section 2.6.

## **2.5 Practical applications of soil conditioning**

Much of the knowledge regarding the effects of conditioning treatments on soil properties and EPB machine performance has developed from experience with practical applications. A number of case studies of soil conditioning on EPB tunnelling projects in various ground conditions have been reported, some of which are discussed here.

The application of soil conditioning during EPB tunnelling on the Jubilee Line Extension project in London is discussed by Wallis (1996). Problems were encountered with tunnelling in London Clay and the clay strata of the Woolwich and Reading Beds. The clays balled up during excavation and recompacted in the head chamber, preventing flow into the screw conveyor. Clogging of the machines by these stiff, high plasticity clays resulted in low advance rates, high cutterhead torques, and shutdown periods to manually clear the chamber. Bentonite slurries and polymers were initially injected to condition the clays, but these agents were not effective as they could not mix into the soil after the cuttings had recompacted. Foam was injected and was a more effective conditioning agent for these soils. The foam coated the clay cuttings, which prevented recompaction and allowed the soil to flow through the chamber and screw conveyor. After field trials, the most appropriate treatment for these clays was with a foam agent concentration of 5%, and an expansion ratio of 10 to 15. The foam solution consumption was dependent on the composition of the ground and the TBM advance rate, and was generally 50 to 100 L/m<sup>3</sup> of excavated soil, corresponding to FIRs of 50 to 150%. Conditioning of the soils with

foam resulted in reductions in the cutterhead and screw conveyor torque of about 20%, and the advance rates were significantly increased.

The effects of foam soil conditioning on the performance of EPB machines tunnelling through glacial tills, silty sands and clays in Toronto were analysed by Leinala *et al.* (1999, 2000), and are also discussed by Boone *et al.* (2002). A foam agent concentration of about 0.6% was used with an expansion ratio of 4 to 10, with wide variations in the FIR for different soils. A minimum FIR of 10% was specified to protect the machines from wear. However, an average FIR of 72% was used, and values were often greater than 120%, with peaks up to 200%, in the hard till soils. Statistical analysis of data recorded from the machines was performed to examine the influence of several variables on the excavation times, including the foam liquid and air injection rates. The air and liquid components of the foam had varying effects on excavation times in different soils. As shown in Figure 2.17 for the glacial tills, increasing foam liquid injection rates lead to higher TBM penetration rates and shorter excavation times, due to the fluidising effect of the foam liquid on these soils. An optimum foam liquid injection ratio of approximately 120 L/min was found to maximise the TBM penetration rate in this soil. For the granular and cohesive soils, increasing the foam air injection rate had more influence on reducing the excavation times than the foam liquid component. It was concluded that conditioning with foam significantly improved the EPB machine performance and advance rates, by improving the flow of excavated material through the machine and control of the chamber pressure and ground surface settlements. Results of the statistical analysis indicated that the foam expansion and injection ratios should be adjusted to optimise the effects of foam in different soils.

The soil conditioning used during EPB tunnelling in Seattle through mixed ground consisting of clays, silts, sands and gravels under the water table is described by Webb and Breeds (1997). The machine was fitted with flood doors in the cutterhead and pressure relief gates to allow operation in open or semi-EPB modes, with conditioner injection ports in the cutterhead and chamber. A coagulating polymer was injected at solution concentrations of 0.5 to 2% to bind the soil, with higher concentrations used for soils with lower silt and clay contents. Higher polymer concentrations of 4 to 10% were used to seal the tunnel face and prevent ground water inflows during cutterhead maintenance. Foam was sometimes injected to prevent sticking of clays, and also in combination with a bentonite-polymer slurry to condition gravels that were too coarse for the foam alone. The effective soil conditioning allowed excavation without operating the machine in full-EPB mode using a screw conveyor to control the ground.

Williamson *et al.* (1999) discuss the application of soil conditioning on a project in San Diego for EPB tunnelling through silts, sands and gravels with head chamber pressures up to 7 bars. Details of the foam and bentonite mixing and injection plant installed on the machine are discussed. The tunnelling machine was fitted with injection ports on the cutterhead and head chamber, and along the 47 metre, two-stage screw conveyor designed to control the high excavation pressures. Foam stabilised with a CMC polymer was predominantly used to condition the soils, with an expansion ratio of 8, and FIRs of 25 to 35%. An automatic foam injection system was used to control the air and liquid flow rates to produce a specified FIR based on the machine operating parameters. During excavation of coarse gravels under high water pressures, bentonite slurry thickened with a PHPA polymer was also injected at a ratio of 45%, as the foam alone could not effectively condition these soils.

The use of polymer stabilised foam for conditioning sands and gravels with low fines contents in Milan are discussed by Peron and Marcheselli (1994). The foam solution contained 1.5% surfactant and 0.7% CMC polymer, with the foam generated at an expansion ratio of 5 to 8. FIRs for the granular soils were estimated with equation 2.3, and the actual values used were in the range 50 to 85%, with 5% water also injected in the soils above the water table. Lower FIRs of 50 to 60% were used for soils below the water table, and the slump of the conditioned soil was maintained between 5 and 10 cm with these treatments.

Jancsecz *et al.* (1999) present results of laboratory tests performed to investigate conditioning of clays, silts, sands and gravels from a project in Turkey, and discuss the conditioning used during tunnelling and the effects on the EPB machine performance. Foam and bentonite slurry were injected to condition the soils. The injection ratios were adjusted to condition the different soils to improve the spoil consistency, leading to reduced cutterhead torque and wear, and stabilisation of the face support pressure to reduce ground settlements. In soft, silty soils at water contents greater than their liquid limit, high advance rates were achieved without the use of any soil conditioning.

These case studies demonstrate that foams, polymers, and bentonite slurry can be used to effectively condition a range of soils and improve the performance of EPB machines. The conditioning treatments used on the different projects varied significantly to suit the specific soils and ground conditions encountered. Further practical experience with soil conditioning will

improve the knowledge of effective treatments for different soils and lead to improvements in the application in practice.

## **2.6 EPB machine screw conveyors**

The screw conveyor of an EPB machine plays a critical role in the excavation process, and effective soil conditioning is required for controlled operation. The main topic of the research presented in this thesis involves investigations of the operation of a model EPB screw conveyor. The design and operation of EPB machine screw conveyors, and some previous studies of their operation in laboratory experiments and field trials are discussed below. Theoretical models developed for EPB screw conveyors and screw extruders are also discussed.

### **2.6.1 Design and operation of EPB machine screw conveyors**

The screw conveyor of an EPB machine consists of an auger rotating inside a cylindrical casing, with the start of the screw extending into the head chamber and a discharge outlet at the end of the casing, as shown in Figure 1.1. The screw conveyor has the function of removing a controlled volume of soil from the chamber, ideally equal to the volume excavated by the cutterhead to balance the soil flow into and out of the machine. This process balances the earth pressure in the head chamber supporting the tunnel face. A pressure gradient exists along the screw to dissipate the chamber pressure to atmospheric at the discharge outlet. The discharge of spoil from the conveyor, and the chamber pressure balance, is controlled by the rotational speed of the screw and the opening of the outlet. Screw conveyors are instrumented to monitor the torque, the rotational speed, and the pressure along the screw during operation. For controlled flow of spoil through the conveyor, effective conditioning of the soil is usually necessary to create a soft, plastic paste of low permeability. If the spoil is too stiff, the screw can clog and require a high torque to convey the material. If the spoil is too liquid or of high permeability, a soil plug can not be formed in the screw to seal against the ground water pressure and dissipate the chamber pressure. This can lead to loss of control of the soil flow and the face support pressure.

The design of screw conveyors for EPB machines is discussed in Maidl *et al.* (1996). A typical conveyor has a central shaft screw, with a gate valve controlling the opening of the discharge outlet. Ports are often included in the conveyor casing for injecting conditioning agents into the screw, which is thought to reduce the torque and improve the formation of a soil plug. Locating the screw conveyor towards the bottom of the head chamber, with two to three flights extending

into the chamber improves the flow of spoil into the conveyor. For central shaft screws, the maximum soil cutting size that can fit in the conveyor is about 40% of the screw channel depth. Ribbon screws without a central shaft can be used to allow larger cuttings and boulders to be transported through the conveyor. To improve sealing of the screw conveyor and formation of a soil plug by mechanical methods, various discharge outlet controls and compaction systems can be used, as shown in Figure 2.18. Gate valves, rotary valve systems and solid material piston pumps can be installed to provide a mechanical seal and control the discharge of spoil from the outlet. Two-stage conveyors, with the second screw rotating at a lower speed, and rotating casing sections can be used to increase compaction of the spoil to form a plug in the screw. These more complex screw conveyor designs are usually employed on machines operating under high ground water pressures, with some examples described by Wallis (1990, 1994) and Williamson *et al.* (1999).

### **2.6.2 Studies of EPB machine screw conveyors**

The operation and mechanics of EPB machine screw conveyors have been studied in laboratory scale experiments and from field measurements. Bezuijen and Schaminee (2000, 2001) report laboratory tests modelling the EPB excavation process with sand-water-foam mixtures. A model EPB machine, shown on the right in Figure 2.15, formed sand-water-foam mixtures in a pressurised chamber with a cutterhead injecting foam as it drilled into the sand. The foam-conditioned sand was extracted from the mixing chamber behind the cutterhead by a vertical screw conveyor. The volume of foam injected and the amount of pore water replaced by the foam were controlled during drilling to control the porosity of the sand-water-foam mixture. The apparatus was operated by controlling the cutterhead advance rate and the screw conveyor rotational speed and discharge opening. Stable drilling conditions were reached with a constant pressure in the mixing chamber and a stable pressure drop along the screw conveyor. The model EPB machine was instrumented to measure the pressure in the mixing chamber, the pore water pressures along the screw conveyor, and the torque to rotate the cutterhead and screw conveyor.

During some of the tests, the drilling process was unstable due to a low pressure drop over the screw, indicating uncontrolled flow of the soil through the conveyor. The drilling process was improved by replacing a higher proportion of the pore water in the sand with foam, resulting in a larger pressure drop over the screw. Replacing more of the pore water resulted in a higher shear strength of the sand-water-foam mixture, leading to higher shear stresses in the screw and a larger pressure drop over the conveyor. When a stable drilling process was maintained, the chamber

pressure remained constant and dissipated along the vertical screw with approximately constant pressure gradients, as shown in Figures 2.19(a) and (b). The constant pressure gradients indicate that the shear stresses between the spoil and the steel surfaces of the conveyor are approximately constant along the screw.

In test 204 (Figure 2.19a), the valve at the discharge outlet was not completely open. The 100 kPa chamber pressure in this test was not completely dissipated over the screw conveyor, due to the pressure required to discharge the spoil through the restricted outlet. In test 302 (Figure 2.19b) the outlet valve was fully open, and the 100 kPa chamber pressure completely dissipated along the conveyor to atmospheric pressure at the unrestricted outlet. During stable drilling periods, the cutterhead and screw conveyor rotational speeds and torques were approximately constant, indicating a constant spoil flow rate through the model EPB machine when stable pressure gradients were measured along the screw. In test 206, an additive was injected into the conveyor at a point past 400 mm along the conveyor, which was said to increase the cohesion and adhesion of the spoil in the screw. As shown in Figure 2.19(c), past the point of additive injection the pressure increased along the conveyor due to the effects of the additive on the spoil properties. The outlet was restricted by the valve and the spoil had a higher viscosity due to the additive, causing an increase of the pressure required to discharge the spoil. The increase of the discharge pressure resulted in the pressure gradient changing along the screw, from initially dissipating pressure to generating pressure as a result of the changes in the spoil properties and the shear stresses acting in the conveyor. The results from these tests demonstrate that the conveyor outlet restriction and the spoil properties influence the pressure change over the screw conveyor.

In tests performed with different sands, the drilling process was more stable with fine sand than with medium sand, due to different properties of the sand-water-foam mixtures. From tests with different foams, similar pressure drops were measured along the screw conveyor, indicating that the type of foam had little influence on the excavation process in the model EPB machine. The porosity of the sand-water-foam mixture significantly influenced the drilling process. When the mixture porosity was less than the maximum porosity of the sand, the cutterhead torque increased significantly, due to the higher strength of the mixture. When the mixture had a very high porosity, the pressure drop over the screw conveyor was reduced and the drilling process became unstable. This resulted from the reduced shear strength of the spoil and reduced shear stresses acting in the screw conveyor, leading to uncontrolled flow through the conveyor. These results indicate that the injection of large amounts of foam to a granular soil to produce a fluid

mixture with a very high porosity can cause loss of control of the flow and pressure dissipation along the conveyor.

Field measurements of spoil properties and screw conveyor operations during EPB tunnelling on the Botlek tunnel in Holland are reported by Talmon and Bezuijen (2002). Samples of foam-conditioned sand were taken from the TBM chamber, and for most samples, the measured porosity was higher than the maximum porosity of the sand. The vane shear strength of the spoil in the chamber was also measured, with values in the range 5 to 30 kPa. The total pressures along the screw conveyor were also measured during operation. Chamber pressures of typically 300 kPa were balanced by the screw conveyor. A pressure drop of about 100 kPa was observed at the entrance of the screw, and a further drop of about 150 kPa was measured along the length of the conveyor. Regulation of the spoil flow by controlling the opening of the gate valve at the discharge outlet influenced the pressure at the end of the conveyor. The total pressures measured at five points along the screw conveyor indicate approximately constant pressure dissipation gradients, as shown in Figure 2.20.

The field measurements were analysed using the theoretical model of the screw conveyor discussed in Section 2.6.3. This analysis showed that the internal friction of the spoil and the interface friction against steel surfaces affect different functions of the screw conveyor. It is suggested that the internal friction controls the pressure drop at the entrance of the conveyor and at the discharge outlet, and the interface friction controls the pressure dissipation along the screw. Although differences were found in the functioning of the laboratory model and full scale screw conveyors, mainly due to differences in the spoil properties, similar mechanics were observed with constant pressure gradients and control of the discharge outlet influencing the operation of both screw conveyors.

### **2.6.3 Theoretical models of screw extruders and conveyors**

Several theoretical models have been developed to describe the mechanics of EPB machine screw conveyors and screw extruders, as discussed below. Screw extruders for polymer materials and pastes operate by similar mechanics as EPB machine screw conveyors, and the theoretical models describing both systems are similar.

### **2.6.3.1 Darnell and Mol model of screw extruders**

Darnell and Mol (1956) developed a theoretical model for solids conveying in a screw extruder for polymers. The polymer material was treated as an elastic solid plug, in contact with all surfaces of the screw channel. The forces acting on the material plug as the screw rotates cause it to flow along the screw channel. The direction of the plug movement relative to the casing is variable, depending on the forces acting on the plug, as shown in Figure 2.21.

From the motion of the plug in the screw channel, an equation was derived relating the conveying rate to the screw geometry and speed, and the direction of plug movement. Another equation defining the direction of plug movement was derived from the static equilibrium condition of the forces acting on the plug when it is about to move. Figure 2.21 shows the forces acting on the solid plug considered in the analysis, including the forces from shear stresses acting on the surfaces of the screw channel, the normal force from the screw flight pushing on the plug, and the force from the pressure change along the screw channel. The shear stresses acting on the plug were defined in terms of friction coefficients and the normal force acting on the screw channel surfaces. The normal forces were related to the pressure in the screw channel, assumed to be equal in all directions. Assuming that the friction coefficients on the screw and casing surfaces are equal, an equation was derived defining the direction of plug movement in terms of the screw geometry, the friction coefficient, and the pressure change along the screw.

The theoretical model derived was used to investigate factors influencing the conveying rate. The angle of plug movement and conveying rate are increased for a screw with a deep channel and small helix angle. A low friction coefficient on the screw surfaces and a high friction coefficient on the barrel surface increase the angle of plug movement and the conveying rate. The model based on friction coefficients and normal forces predicts a non-linear change of pressure along the screw, as the shear stresses vary along the screw due to the change of the normal force. The pressure gradient along a screw extruder was not investigated in depth by Darnell and Mol, but the predictions of this theoretical model do not agree with the behaviour observed by others.

### **2.6.3.2 Chung model of screw extruders**

Chung (1970) also developed a theoretical model of solids conveying in screw extruders for polymers. Chung's model was based on the model of Darnell and Mol (1956), but assumed viscous shear stresses driving the flow of the material in the screw. The polymer was treated as a solid plug surrounded by a molten polymer film in contact with all surfaces of the screw channel.

Viscous shear stresses develop in the polymer film when the plug moves relative to the screw and casing surfaces. As in the Darnell and Mol model, the angle of plug movement relative to the casing is determined by the forces acting on the plug in the screw channel. The forces considered in Chung's model were the same as those shown in Figure 2.21. However, Chung assumed the shear stresses acting on the surfaces of the screw channel were constant along the conveyor, rather than being determined by the normal force and friction coefficient. A relationship defining the conveying rate in terms of the screw geometry and speed, and the angle of plug movement was first derived. The balance of forces acting on the plug in the equilibrium condition during steady state flow was used to derive a relationship defining the angle of plug movement relative to the casing. Chung's analysis leads to an expression relating the pressure gradient along the screw to the screw geometry, the shear stresses acting on the screw channel surfaces, and the angle of plug movement. For a given screw geometry, the pressure gradient is variable, depending on the shear stresses acting on the casing and screw surfaces, and the direction of plug movement, which determines the direction of the shear stress acting on the casing surface.

Chung's theoretical model assuming constant shear stresses acting on the screw and casing surfaces predicts a constant pressure gradient along the screw. This is because the shear stresses are not proportional to the pressure in the screw channel, as in Darnell and Mol's model which predicted a non-linear pressure gradient. The constant pressure gradient predicted by Chung's model agrees with the behaviour observed in experiments with screw extruders and conveyors.

Chung also derives a theoretical equation for the torque required to rotate the screw. Based on the equilibrium of the moments about the screw axis resulting from the perpendicular components of the forces acting on the plug, the torque is related to the screw geometry, the shear stresses, and the angle of plug movement. The torque is proportional to the surface area of the plug in contact with the casing, and the shear stress acting on the casing surface.

### **2.6.3.3 Burbidge and Bridgwater screw extruder model**

Burbidge and Bridgwater (1995) develop a theoretical model describing the pressure gradient along a screw extruder for paste materials. Again, the analysis takes a similar approach to that of Darnell and Mol (1956), but the model is developed considering paste rheology with velocity dependent shear stresses acting on the screw channel surfaces. Based on the motion of an element of paste in the screw channel, an expression for the angle of movement relative to the casing is derived in terms of a dimensionless flow rate and the screw geometry. The equilibrium

of the forces acting on the paste in the screw channel during steady state flow is used to derive an equation for the pressure gradient along the screw extruder. The forces due to the shear stresses acting on the surfaces of the screw channel, and due to the pressure gradient along the channel are considered in the analysis. The theoretical pressure gradient is expressed in dimensionless form, and related to dimensionless groups representing the screw geometry, the flow rate, and the shear stresses acting on the screw channel surfaces. This theoretical model based on the shear stresses acting on the screw channel surfaces predicts a constant pressure gradient along the extruder, similar to the model of Chung (1970).

Burbidge and Bridgwater (1995) use the theoretical model to evaluate the effects of varying the screw helix angle, the screw channel depth, the shear stresses, and the flow rate on the angle of material flow and the dimensionless pressure gradient. Laboratory experiments were performed with a small screw extruder operating with a paste material. The total pressure acting on the casing was measured at four points along the extruder to determine the pressure gradients during operation. Experiments were performed with the extruder operating with varying flow rates, screw speeds, screw pitches and channel depths, and with varying paste properties. The theoretical model was able to accurately predict the pressure gradients measured for the different operating conditions and paste properties.

#### **2.6.3.4 Yoshikawa model of EPB screw conveyors**

Yoshikawa (1996a) presents two theoretical models for EPB screw conveyors to calculate the pressure gradients for granular and plastic materials. A frictional model was derived for granular materials based on the screw extruder model of Darnell and Mol (1956). The forces acting on the soil plug in contact with the surfaces of the screw channel were defined by friction coefficients and the normal forces acting on the surfaces. This model predicts an exponential decrease of pressure along the screw conveyor, as the shear stresses varied along the conveyor as the pressure and normal forces changed.

A model was also developed for a plastic material in an EPB machine screw conveyor, based on the analysis of a screw extruder by Chung (1970). The shear stresses acting on the surfaces of the soil plug in contact with the screw channel were constant along the conveyor in this model. The soil was treated as a Bingham fluid, with the shear stress at the relevant shear velocity (depending on the screw speed) determined from a relationship with the slump of the soil. Based on the equilibrium of the forces acting on the soil in the screw channel, equation 2.4 is derived relating

the pressure change over the conveyor to the screw geometry, the shear stresses acting on the screw channel surfaces, and the direction of soil movement:

$$P_L = P_0 - \frac{L}{H} \left[ C_1 \tau_c \left( \frac{\cos \phi_f}{\cos \phi_a} \sin \theta - C_1 \frac{\cos \phi_f}{\sin \phi_a} \cos \theta \right) + C_2 \tau_s \left( \frac{\sin \phi_s \cos \phi_s}{\cos \phi_a} + C_2 \frac{\cos^2 \phi_s}{\sin \phi_a} \right) + \frac{(\tau_f + \tau_{fp})H}{(t-e) \sin \phi_a \cos \phi_a} + H \rho g \sin \beta \right]$$

Eqn. 2.4

where:  $P_L$  = pressure at length L (kPa)

L = length of conveyor (m)

$\tau_c$  = casing shear stress (kPa)

$\tau_f$  = trailing flight shear stress (kPa)

$\theta$  = direction of soil flow

e = screw flight thickness (m)

$\phi_a$  = average screw helix angle

$\rho$  = soil bulk density (kg/m<sup>3</sup>)

$C_1, C_2$  = ratios describing screw geometry

$P_0$  = pressure at start of conveyor (kPa)

H = screw channel depth (m)

$\tau_s$  = shaft shear stress (kPa)

$\tau_{fp}$  = pushing flight shear stress (kPa)

t = screw pitch (m)

$\phi_f$  = screw flight helix angle

$\phi_s$  = screw helix angle at shaft diameter

$\beta$  = inclination of screw conveyor

This model predicts a constant pressure gradient along the conveyor for a given screw geometry, direction of soil flow, and shear stresses acting on the screw channel surfaces. The static pressure drop due to the inclination of the conveyor is also included. The terms of equation 2.4 represent the effects of the shear stress acting on the casing surface, the screw shaft, and the screw flights on the pressure drop along the conveyor.

The pressure gradients calculated by the two theoretical models presented by Yoshikawa were compared with measurements from experiments with a full-scale EPB screw conveyor, as shown in Figure 2.22. Approximately constant pressure gradients were measured along the conveyor in most of the tests. Pressure gradients calculated from equation 2.4 for the different experimental conditions are shown as curves (a) to (e). The non-linear pressure gradient calculated from the frictional model is shown as curve (f). The constant pressure gradients predicted by the model for a plastic material with constant shear stresses acting along the conveyor agree well with the measurements. The non-linear gradient predicted by the frictional model does not match the pressure gradients observed in these tests or those discussed in Section 2.6.2.

Yoshikawa (1996b, c) also investigated effects of the screw geometry and design, operating conditions, and injection of conditioning agents on the pressure drop. Modelling the screw conveyor operation for a plastic soil with equation 2.4, and with a similar equation derived for a ribbon screw, the pressure drop along screws of different pitch was calculated for a range of discharge efficiencies (defining the angle of soil flow), as shown in Figure 2.23. The pressure drop over the screw increases with the discharge efficiency (or the angle of soil flow), and with a reducing screw pitch. Experiments performed with a full-scale screw conveyor showed that injecting a conditioning agent to reduce the fluidity and increase the shear stress of the spoil in the conveyor resulted in a larger pressure drop.

### 2.6.3.5 Talmon and Bezuijen model of EPB screw conveyors

Talmon and Bezuijen (2002) present a theoretical model for EPB machine screw conveyors. The model relates the spoil discharge rate and pressure gradient to the screw conveyor geometry and operating conditions and the rheological properties of the spoil. The spoil was modelled as a homogeneous plastic paste, and the interface shear stresses were assumed to be uniformly distributed over the screw channel surfaces. The direction of spoil flow relative to the casing, and the direction of the casing shear stress are variable depending on the conveyor operating conditions. The theoretical model defines a relationship for the pressure change over the screw conveyor as follows:

$$\Delta p = \frac{4L}{D - \frac{D_r^2}{D}} \left( \frac{1}{\pi} \left( 1 - \frac{D_r}{D} + \frac{1 - (D_r/D)^3}{3 \tan^2 \phi_f} \right) \tau_f + \frac{\tan \theta}{|\tan \theta|} \frac{\tan \phi_f \tan \theta - 1}{\tan \phi_f \sqrt{\tan^2 \theta + 1}} \tau_c + \frac{D_r}{D} \sqrt{1 + \left( \frac{\pi D_r}{t} \right)^2} \tau_s \right)$$

Eqn 2.5

where:  $\Delta p$  = pressure drop (kPa)

$L$  = conveyor length (m)

$D$  = conveyor diameter (m)

$D_r$  = screw shaft diameter (m)

$t$  = screw pitch (m)

$\phi_f$  = screw flight helix angle

$\theta$  = angle of soil flow at casing surface

$\tau_f, \tau_c, \tau_s$  = shear stresses on screw flight, casing surface and screw shaft

For a given screw geometry and assuming that all shear stresses are equal, Talmon and Bezuijen (2002) calculate a dimensionless pressure drop over the conveyor as a function of a

dimensionless flow rate. Depending on the operating conditions and the flow rate, the pressure drop can be either positive or negative, indicating that the screw conveyor can operate to either generate or dissipate pressure. The effect of reducing the shear stress on the casing surface (by injecting conditioning agents into the screw) on the pressure change was investigated using equation 2.5. Injection of conditioning agents to lubricate the conveyor casing can, in theory, significantly influence the pressure drop over the screw.

The theoretical model was compared with measurements from the laboratory model and full-scale screw conveyors discussed in Section 2.6.2. From the spoil flow rates and operating conditions measured in the laboratory tests, the dimensionless flow rate was calculated, allowing prediction of the dimensionless pressure drop over the conveyor. The dissipation of pressure predicted by the theoretical model agreed with the test measurements. The shear stresses acting in the model conveyor were back calculated from the measured and theoretical pressure changes. The back calculated shear stresses in the model screw conveyor were about a factor of two smaller than the measured vane shear strength. Some field measurements of the EPB machine screw conveyor operation were compared with theoretical model by a similar approach. The direction of the theoretical pressure drop did not always agree with the measured pressure changes, and the back calculated shear stresses were an order of magnitude smaller than the measured vane shear strength of the spoil. These results suggest differences in the operation of the laboratory scale and full scale screw conveyors, in terms of the magnitude of the shear stresses relative to the internal shear strength of the spoil. However, estimating the spoil flow rate from the field measurements can be inaccurate, and variations in the spoil properties or conveyor operation could also influence the theoretical analysis of the full-scale screw conveyor.

## **2.7 Summary**

This chapter has provided a review of the literature relevant to the research presented in this thesis.

Soil conditioning agents were discussed in Section 2.2. The properties of bentonite slurries, polymers, and surfactant foams were reviewed. Their applications as conditioning agents and effects on soil properties to improve EPB machine performance were discussed. Other soil conditioning agents including water, dispersants, and oils are also mentioned.

Section 2.3 discussed conditioning treatments for granular and clay soils, and the improvements to EPB tunnelling operations. The excavation characteristics and conditioning requirements of different types of soil, and the design of conditioning treatments based on various soil properties was discussed. Conditioning agents used for granular and clay soils, empirical methods for estimating injection ratios, and typical ranges of conditioning treatment parameters for different soils were summarised. Improvements to EPB machine performance and tunnelling operations resulting from soil conditioning were also discussed.

Various test methods used to measure properties of conditioned soils were reviewed. Slump tests and cone penetrometer tests have often been used as index tests to measure the consistency of conditioned soils, and various tests have been used to measure the adhesion and friction of soils on steel surfaces. The properties of sand-foam mixtures have been investigated by several researchers, performing tests to measure the compressibility, shear strength, and permeability. Mixing tests to represent EPB machine excavations have also been performed to measure the effects of conditioning sands with foam. These tests have shown that conditioning treatments have significant effects on the geotechnical properties of soils, which lead to improvements in EPB machine operations.

Some case studies of soil conditioning applications on EPB tunnelling projects were reviewed. The conditioning agents used and typical application rates for the different ground conditions were summarised. The performance of the conditioning treatments and the effects on soil properties and the machine operations were discussed. Bentonite slurries, foams, and polymers have been successfully used to condition soils ranging from coarse sands and gravels, to stiff high plasticity clays. The specific conditioning treatments vary depending on the particular ground conditions encountered. Effective applications of soil conditioning lead to significant improvements of EPB machine operations in a range of soil types, with reduced machine driving parameters, increased tunnelling advance rates, and improved control of the excavation process.

Section 2.6 outlined EPB machine screw conveyor designs, and their operation to control the excavation process. Laboratory model tests and field measurements performed to investigate the operation and pressure changes along screw conveyors operating with foam conditioned sands were discussed. Some theoretical models describing the mechanics of screw extruders and EPB screw conveyors were discussed. These models allow prediction of the conveying rates and pressure gradients along screw conveyors, based on the screw geometry and the interactions

between the material and the screw. The effects of screw geometry and material properties on the conveying rate and pressure change over the screw have been investigated through the theoretical models, and the predicted behaviour was compared with measurements from laboratory tests and field trials. The theoretical models based on constant shear stresses acting along the conveyor predict constant pressure gradients, as observed in model scale and full scale EPB machine screw conveyors.

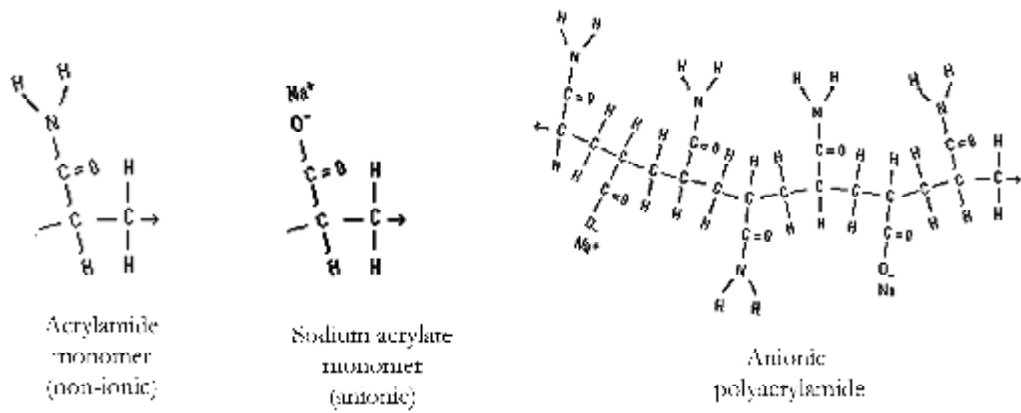


Figure 2.1. Chemical structures of PHPA monomer and polymer molecules.

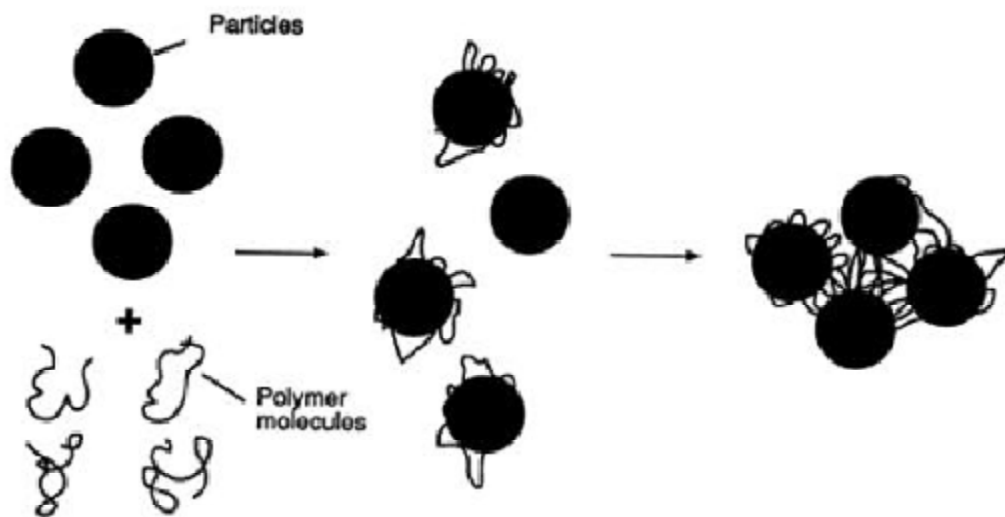


Figure 2.2. Flocculation of particles by polymer molecules.  
(after Moody, 1992)

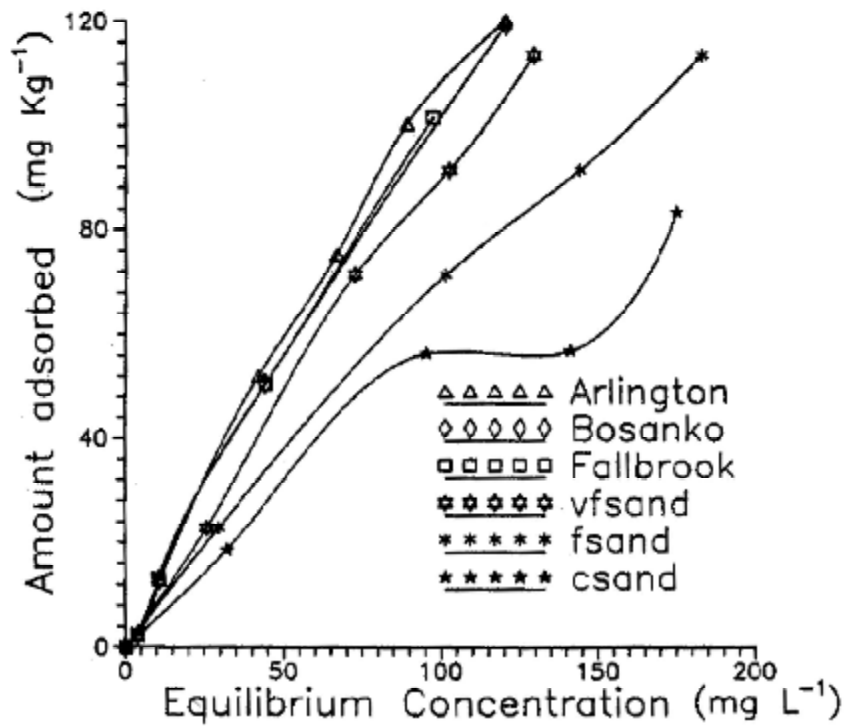


Figure 2.3. Adsorption isotherms of anionic PHPA onto natural clayey soils and silica sands.  
(after Malik and Letey, 1991)

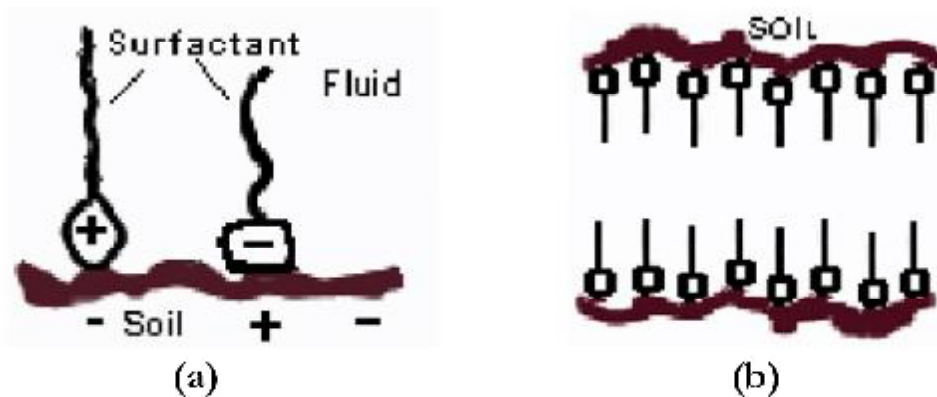


Figure 2.4. (a) Adsorption of cationic and anionic surfactants onto charged soil particle.  
(b) Repulsion of soil particles by steric interactions of adsorbed surfactant molecules.  
(after Leinala *et al.*, 2002)

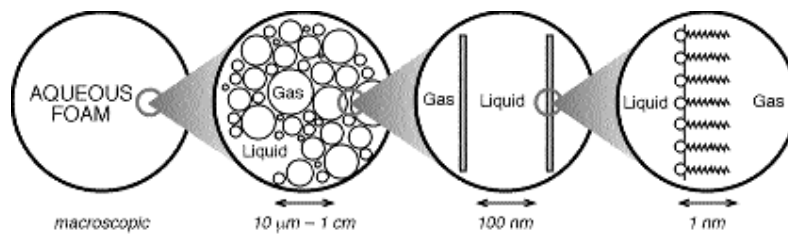


Figure 2.5. Schematic diagram of aqueous foam structure at different scales.  
(after Durian, 1994)

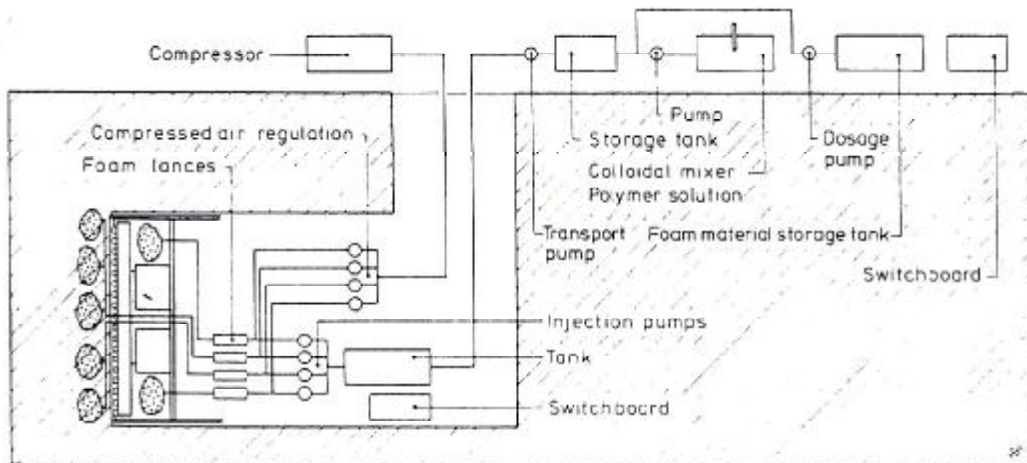


Figure 2.6. Foam generation plant on an EPB machine.  
(after Maidl *et. al.*, 1996)

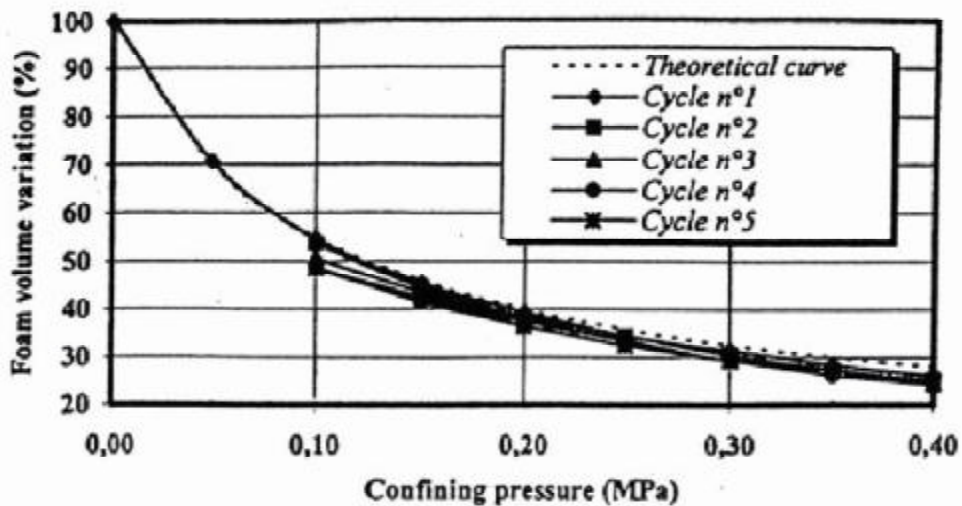


Figure 2.7. Change of foam volume under pressure cycles.  
(after Quebaud *et. al.*, 1998)

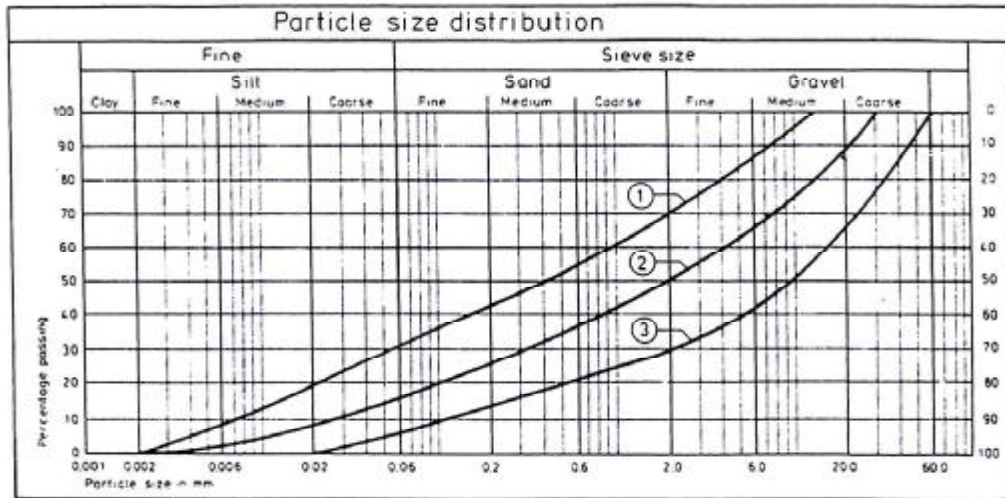


Figure 2.8. Application of EPB machines based on particle size distribution.  
(after Maidl *et. al.*, 1996)

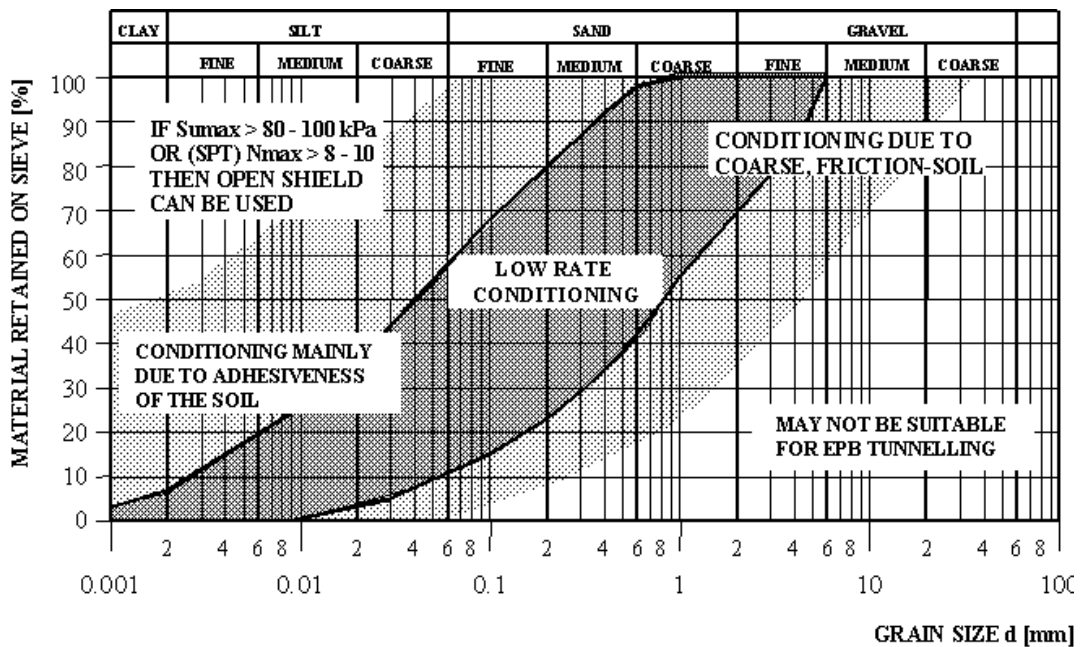


Figure 2.9. General soil conditioning requirements based on particle size distributions.  
(after Jancsecz *et. al.*, 1999)

Soil	EFNARC Foam types			Foam injection		Other additives		
	A	B	C	c <sub>F</sub>	FIR	Dispersing agents	Foam stabilisers	Soil stabilisers
Clay				+	+	++	-	-
Sandy clay-silt				+	+	+	-	-
Sand – clayey silt				+	++	o	+	-
Sand				++	+++	-	++	++
Clayey gravels				++	++	-	+++	+
Sandy gravels				+++	+++	-	+++	+++

EFNARC foam types:

**Type A** – high dispersing capacity (breaking clay bonds) and/or good coating capacity (reduce swelling effects)

**Type B** – general purpose, with medium stability

**Type C** – high stability and anti segregation properties to develop and maintain a cohesive soil as impermeable as possible

c<sub>F</sub> – foam agent concentration

FIR – foam injection ratio

Conditioning agent quantities:

- generally not necessary

o not generally necessary, but sometimes useful

+ useful in low quantities

++ useful in increased quantities

+++ strongly recommended in increased quantities

NB other soil conditions may exist which affect the suitability of different foam types

Figure 2.10(a). Recommended soil conditioning treatments (after EFNARC, 2001).

Parameter	General value range	Typical values	Notes
Foam solution concentration (c <sub>F</sub> )	0.5 – 5.0%	approx. 3%	Depends on amount of water injected and on soil water content; also on activity and stability of foam
Foam expansion ratio, FER	5 – 30	approx. 10	Higher FER (drier foam) recommended for higher soil water content; lower FER for lower soil water content
Foam injection ratio, FIR	10 – 80%	30 – 60%	Laboratory testing to determine optimum FIR; depends on soil water content and water injected
Polymer concentration	0.1 – 5.0%	-	Add to foam solution to improve stability or adjust soil consistency; can also inject directly to soil undiluted
Stabiliser concentration	0.1 – 5.0%	-	Added to foam solution to improve stability; also to prevent segregation of soil

Figure 2.10(b). Recommended parameters for conditioning treatments (after EFNARC, 2001).

Permeability (m/s)	10 <sup>-1</sup>	10 <sup>-2</sup>	10 <sup>-3</sup>	10 <sup>-4</sup>	10 <sup>-5</sup>	10 <sup>-6</sup>	10 <sup>-7</sup>	10 <sup>-8</sup>	10 <sup>-9</sup>
Typical ground conditions	Coarse gravels Mixed ground		Coarse to fine sands			Silty sands to silty clays		Intact clays	
Suggested soil conditioning foam	Conditions probably more suited to slurry machines		MEYCO Fix SLF 10 or MEYCO Fix SLF 20 + polymer						
			MEYCO Fix SLF 20						
					MEYCO Fix SLF 30				
Complementary polymer	Modify slurry with MEYCO Fix SLF P1 or P2		MEYCO Fix SLF P1 and/or MEYCO Fix SLF P2						
Other products								Rheosoil 211, X212	

Figure 2.11. Selection chart for application of soil conditioning agents.  
(after MBT, 2001)

Soil type	Mining characteristics	Treatment	
Plastic clays	Tend to reconstitute with little loss of strength in machine chamber.	High dosage of foam at head to keep excavated material as separate pieces.	
Laminated, silty or sandy clays	Break up better, but still tend to re-constitute, slightly abrasive, form plug.	Possibly none other than water to reduce shear strength to acceptable value; in stiffer clays, medium dosage of foam at head. Possibly add lubricant to foam to reduce abrasion.	
Clayey sands and gravels.	Flow easily, may form plug if fines content in excess of 10%; highly abrasive.	Add lubricant polymer at head to reduce wear; add water-absorbing polymer if required to form plug in screw and control water inflow.	
Silty fine sands	Do not flow, do not form plug, allow ground water inflow, highly abrasive	Foam with polymer additive to stiffen foam and provide lubrication; approximate dosage rates for polymer:-	0.1%
Sand/gravel			0.25%
Gravel and cobbles			1 - 3%
Cobbles and boulders	Tend to congregate in clumps in head and/or jam screw.	Large dosages of additive to keep cobbles separate in head and provide water control and lubrication.	

Figure 2.12. Summary of conditioning treatments for different soils.  
(after Milligan, 2000).

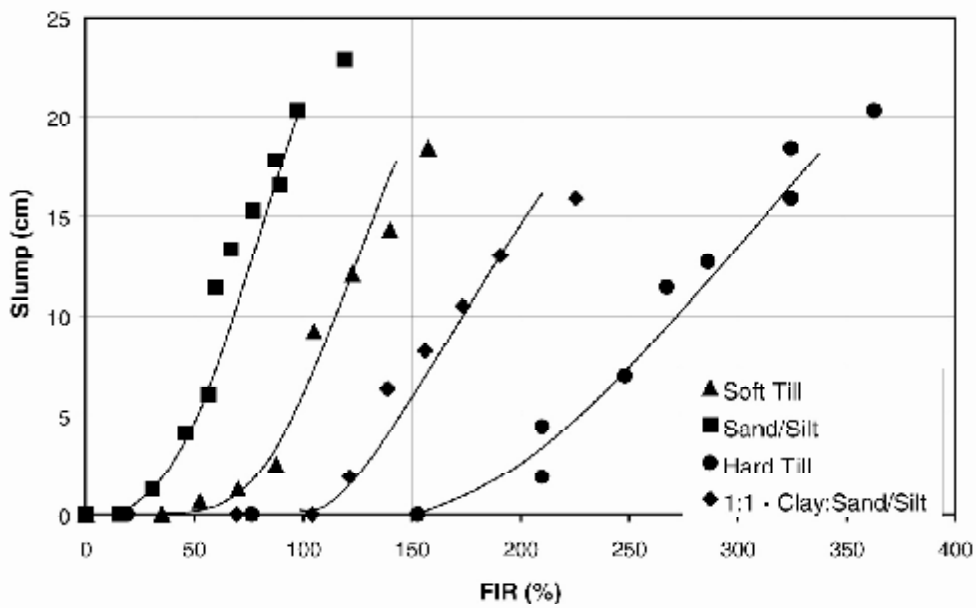


Figure 2.13. Slump of various soils conditioned with foam.  
(after Leinala *et al.*, 2000)

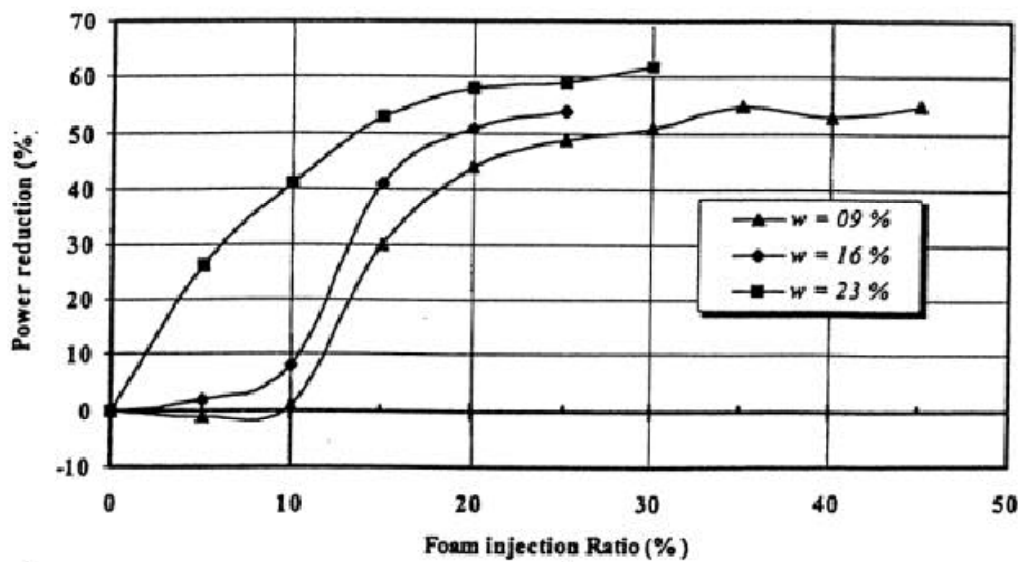


Figure 2.14. Reduction of mixing power with foam injection ratio.  
(after Quebaud *et al.*, 1998)

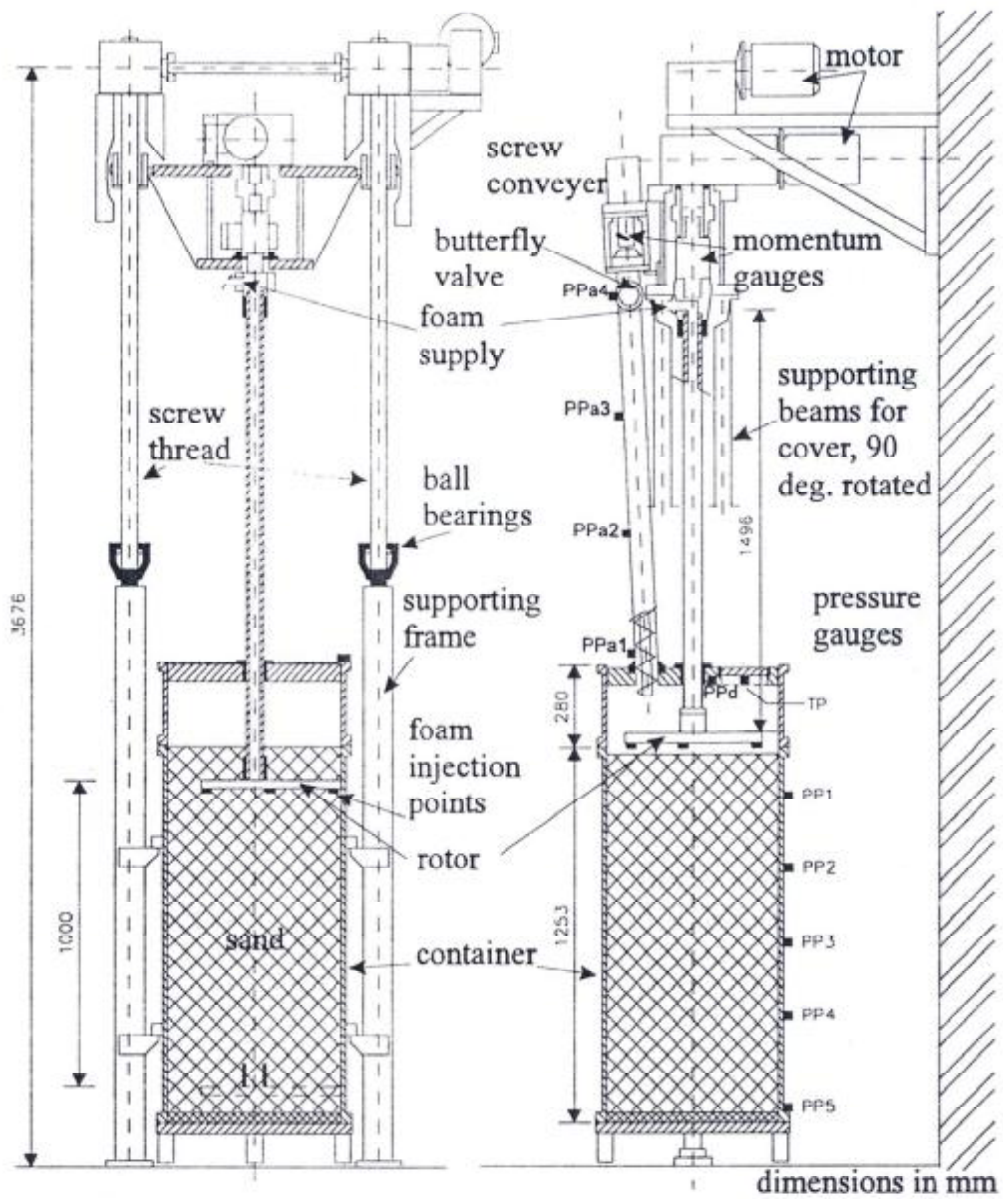


Figure 2.15. Model EPB machine apparatus.  
(after Bezuijen and Schaminee, 2001)

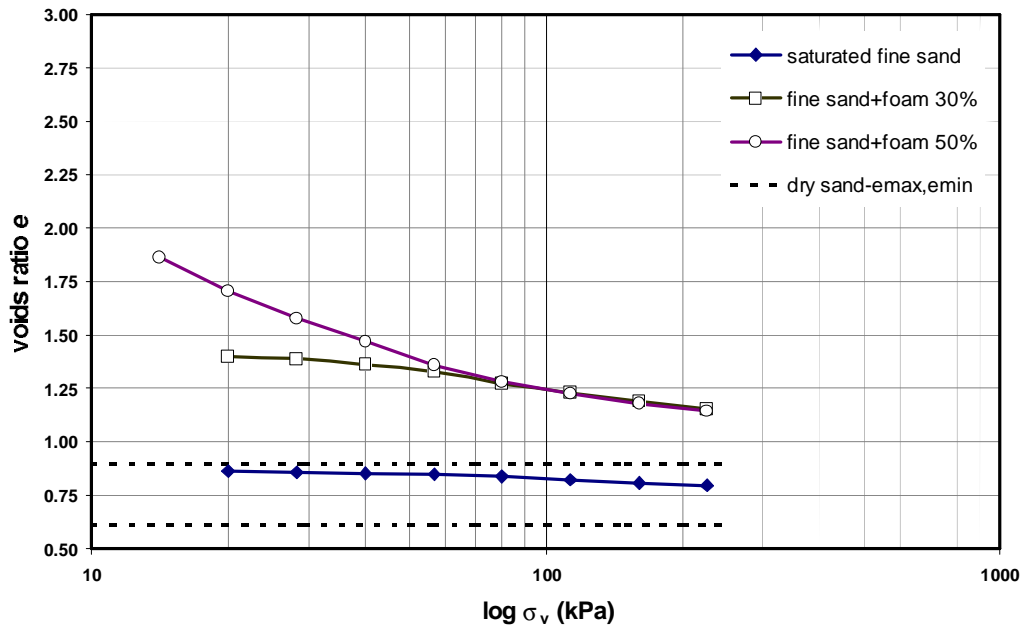


Figure 2.16. Compressibility of sand-foam mixtures.  
(after Houlsby and Psomas, 2001)

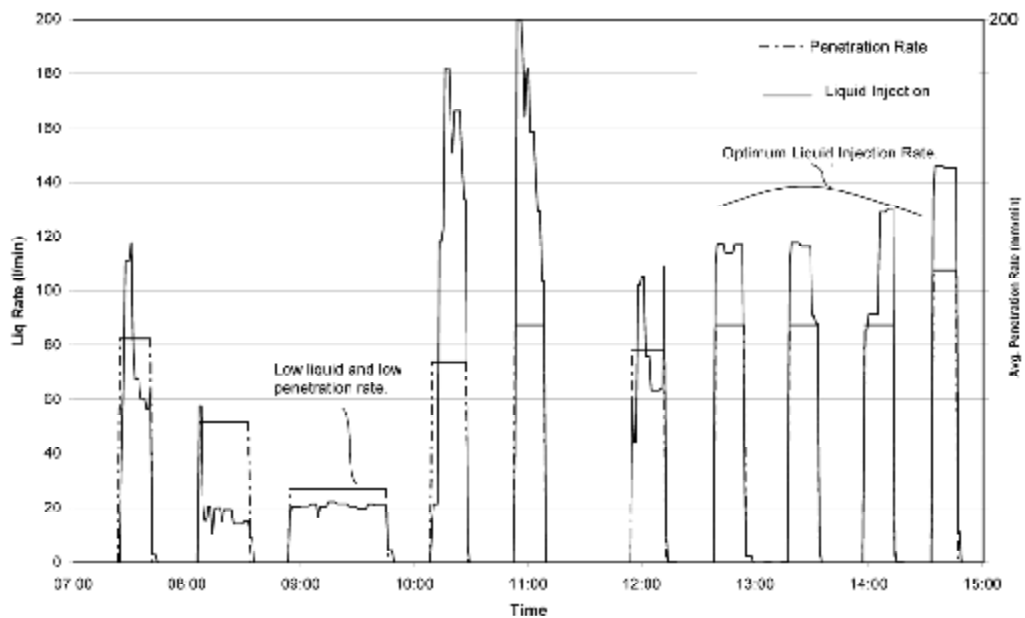


Figure 2.17. Effect of foam liquid injection on mining time in till soils.  
(after Leinala *et al.*, 1999)

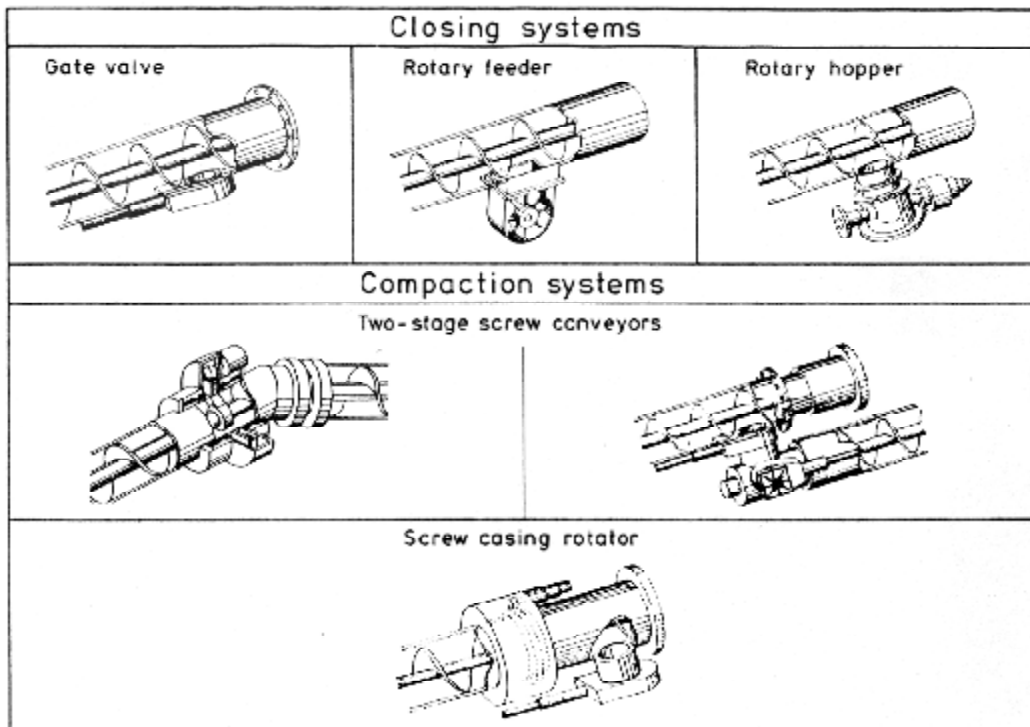


Figure 2.18. Screw conveyor discharge controls and compaction systems.  
(after Maidl *et al.*, 1996)

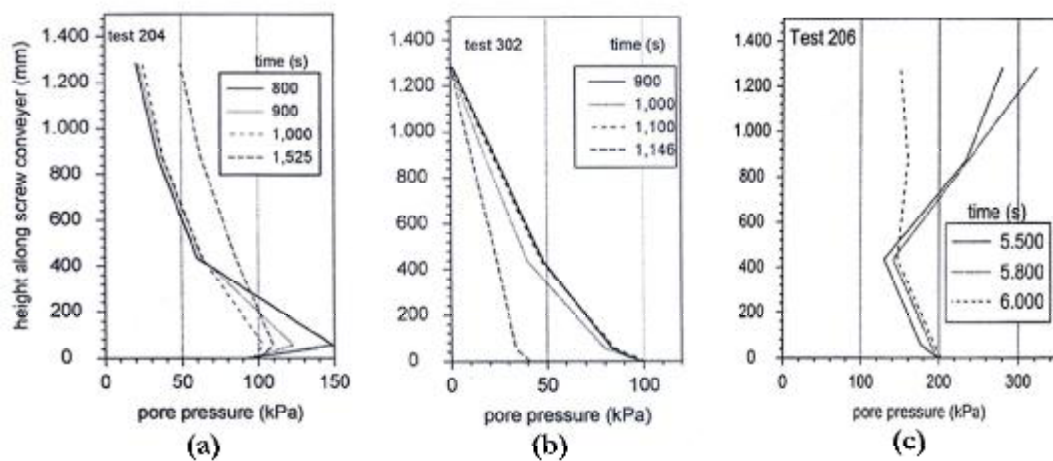


Figure 2.19. Measured pore pressure distributions along model EPB screw conveyor.  
(after Bezuijen and Schaminee, 2001)

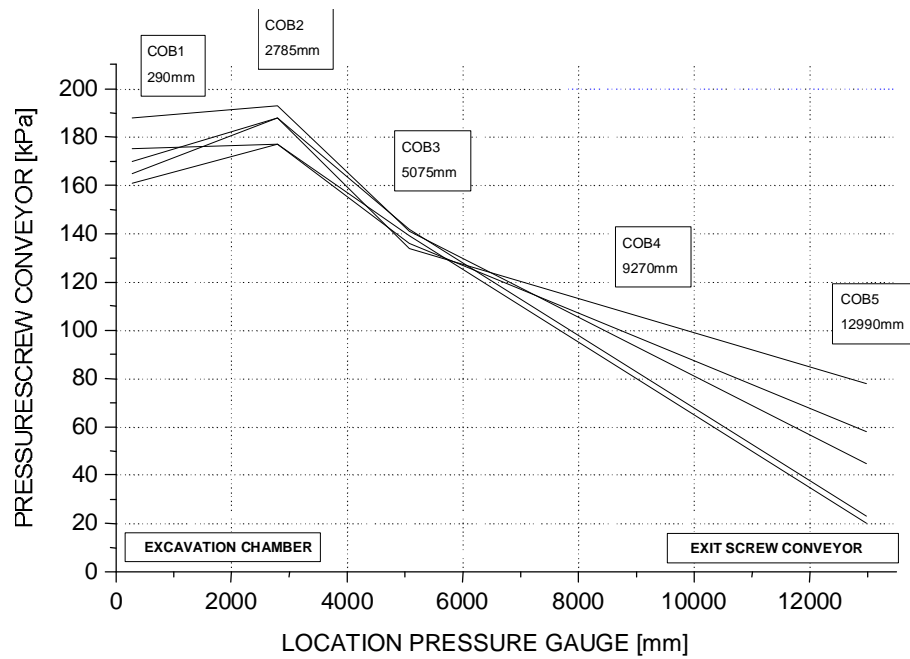


Figure 2.20. Measured total pressure distribution along EPB machine screw conveyor.  
(after Talmon and Bezuijen, 2002)

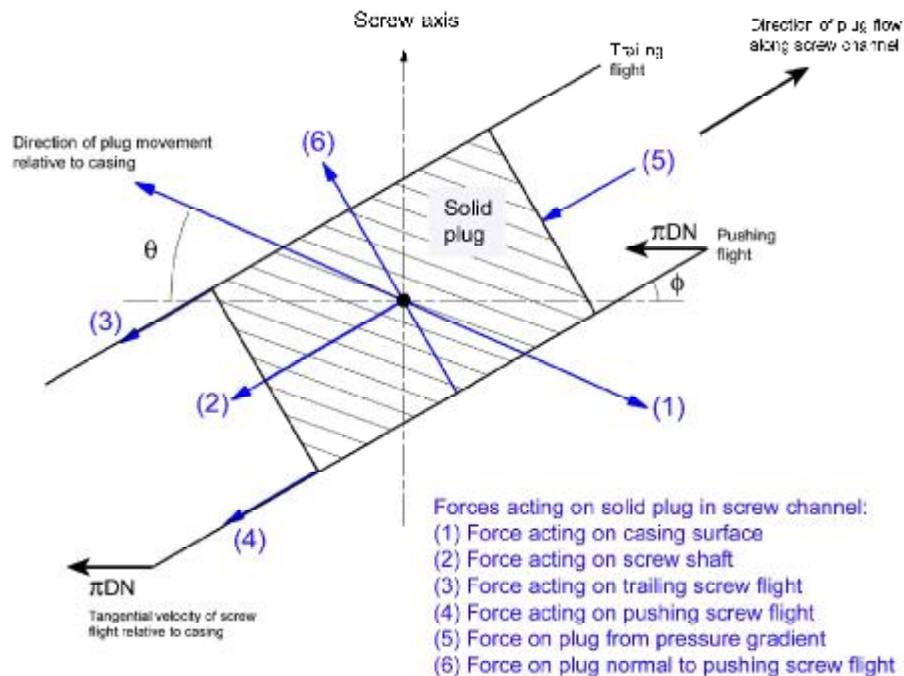


Figure 2.21. Forces acting on solid plug element in screw extruder channel.  
(after Darnell and Mol, 1956; Chung, 1970)

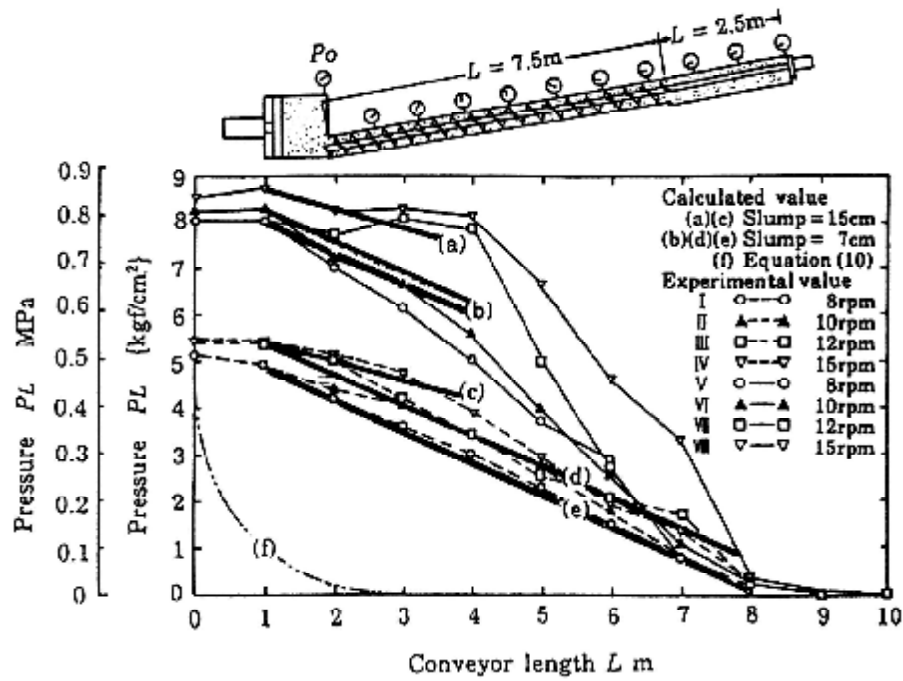


Figure 2.22. Measured and calculated pressure gradients for EPB screw conveyor. (after Yoshikawa, 1996a).

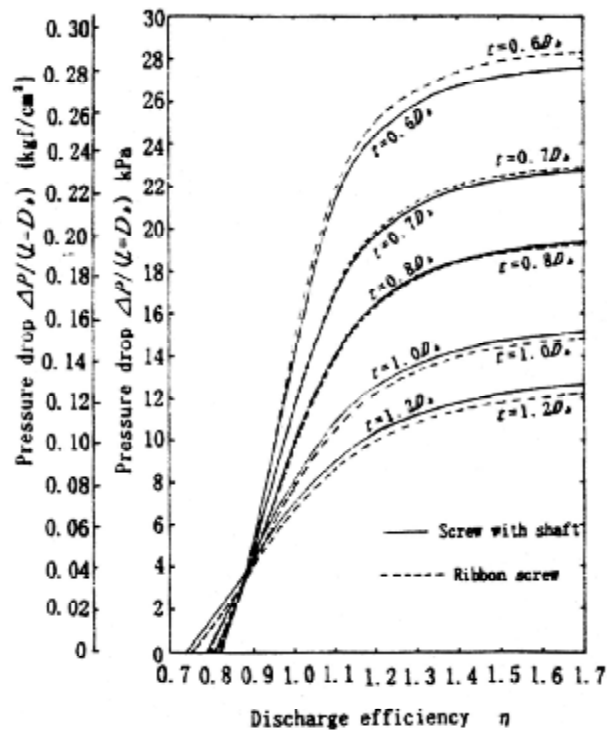


Figure 2.23. Calculated pressure drop for screw conveyors with varying screw pitch. (after Yoshikawa, 1996b).

# Chapter 3

## Index testing of conditioned clay soils

---

### 3.1 Introduction

Conditioning treatments for a particular soil can be difficult to specify due to the number of agents available and variables involved in their application. Properties of different conditioning agents and the effects of different treatments on soil properties have not often been studied fundamentally. Suitable agents and general ranges of parameters for conditioning different types of soil have been established through practical experience, and various laboratory tests have been used to measure conditioned soil properties. Index tests are useful for comparing the effects of different conditioning treatments on soil properties and to determine effective treatments. However, most of the research reported in the literature has investigated properties of sands conditioned with foam, and conditioning of clay soils has received relatively little attention.

This chapter reports index tests performed to compare the properties of various foams and the effects of different conditioning treatments on some basic properties of clay soils. The expansion ratio and stability of foams produced from various agents, and effects of generation variables on foam properties were measured in a series of foam index tests. The effects of polymer conditioning agents on the plasticity and undrained strength of some remoulded clays were measured by Atterberg limit tests. The effects of various polymer and foam conditioning treatments on the undrained strength of London Clay samples were measured in series of index tests using a large-scale fall cone and shear vane apparatus. This chapter first summarises the properties of the clay soils and the polymer and foam conditioning agents used in the index testing. The experimental apparatus, sample preparation, and test methods used for the different index tests are then described. Results from the foam index tests and the conditioned clay soil

index tests are presented, leading to some conclusions regarding the properties of the foams and effective conditioning treatments for London Clay.

## **3.2 Soils tested**

Index tests investigating properties of conditioned clay soils were performed with E-grade kaolin and London Clay samples. These two clays were also used for model EPB screw conveyor tests discussed in Chapters 5 and 6. The sampling and properties of the test soils are discussed below.

### **3.2.1 E-grade kaolin**

Kaolin clays have been used extensively in geotechnical research at Cambridge, for studies of fundamental soil mechanics and physical model tests. These clays have the advantages of being available as processed powders, produced to a controlled quality from high purity kaolinite with consistent physical and engineering properties. Spestone and speswhite kaolin clays were used by many researchers at Cambridge until about 1990, and more recently E-grade kaolin has been used as a model clay soil for geotechnical research. E-grade is a coarse variety of processed kaolin clay, with a high permeability of the order  $10^{-6}$  m/s (Barker, 1998), allowing rapid consolidation of clay samples. The chemical composition and some physical properties of E-grade kaolin as specified by the supplier are shown in Table 3.1, and the grading curve is shown in Figure 3.1.

The engineering properties of spestone and speswhite kaolin have been studied extensively in the research performed with these clays, as discussed by authors including Mair (1979), Al-Tabbaa (1987), Elmes (1985), Barker (1998). However, the properties of E-grade kaolin have not been investigated in such detail. Elmes (1985) was the first to study of the properties of E-grade kaolin at Cambridge, performing Atterberg limit tests, and oedometer and triaxial tests. The engineering properties of E-grade kaolin measured by Elmes are summarised in Table 3.2. Based on the Atterberg limits, E-grade kaolin can be classified as a clayey silt of medium to high plasticity.

The properties of E-grade kaolin reported by Elmes (1985) have since been used by several other researchers at Cambridge using this clay (e.g. Evans (1994), Potter (1996), Barker (1998)). Various relationships describing the compressibility and permeability of E-grade kaolin in terms of the effective stress and void ratio have been proposed by these workers.

### 3.2.2 London Clay samples

London Clay was used in this research as a source of stiff, high plasticity clay to investigate conditioning treatments and the EPB excavation process in this type of soil. The engineering properties of London Clay are well known, and this soil is often encountered during tunnelling in London so investigations of effective conditioning treatments are of practical interest.

Unweathered London Clay is typically a very stiff, very closely fissured, grey or grey-brown clay of very low to medium compressibility and high to very high plasticity (Withers *et al.*, 2001). Water bearing silt and sand laminations occur in London Clay, and weathering close to the top of the strata causes higher moisture contents and a firm to stiff consistency. Towards the base of the strata, London Clay becomes dominated by silt and sand layers, and is often clayey, silty sand in this zone. Withers *et al.* (2001) presents ranges of index properties, undrained shear strength and stiffness measurements, and engineering design parameters for London Clay suggested for use on the Jubilee Line Extension project.

The samples of London Clay used in this research were obtained from the Corsica Street shaft excavation for the CTRL project. At this location, the London Clay lies at depths of 3.4 to 32.2 m, with the upper few metres of weathered material underlain by the unweathered London Clay that was sampled. During the geotechnical investigation for the CTRL project, a borehole was drilled at this site and laboratory and in-situ tests were performed on the London Clay, as described in CTRL (1997). The index properties and design parameters for London Clay determined in this investigation are shown in Table 3.3, and are generally similar to those suggested by Withers *et al.* (2001). Grading curves and Atterberg limits of London Clay measured in the classification tests are shown in Figures 3.2 and 3.3. The London Clay sampled was of high to very high plasticity, and natural moisture contents were generally near or below the plastic limit, corresponding to the stiff to very stiff consistency of the clay. The description of the clay from the borehole log indicates an undrained shear strength of at least 40 kPa at the top of the strata, increasing with depth to over 150 kPa. The design parameters shown in Table 3.3 for the increase of strength and stiffness of London Clay with depth were based on results of undrained triaxial tests and pressuremeter tests.

The London Clay samples were obtained for index tests investigating conditioning treatments for this soil, and for model EPB screw conveyor tests with conditioned London Clay. For these tests it was desired to prepare samples representative of excavated London Clay cuttings mixed with

conditioning agents, as produced by an EPB machine. To allow index testing of samples of relatively small volume, and because of the reduced scale of the model EPB screw conveyor, the discrete cuttings of London Clay were required to have a maximum dimension less than approximately 25 mm. To meet these requirements, London Clay was mechanically excavated from the ground during construction of the Corsica Street shaft, and the cuttings were passed through a large sieve with a mesh size of approximately 25 mm, constructed for this sampling process and shown in Figure 3.4. During the mechanical excavation and handling of the London Clay before sieving, the clay cuttings tended to break up and no special efforts were required to pass sufficient volumes of the cuttings through the sieve. After sieving, the clay cuttings were collected into plastic bags and sealed to retain the natural moisture content of the soil. Approximately three tonnes of sieved London Clay cuttings were obtained by this process for the testing reported in this thesis.

### **3.3 Conditioning Agents**

A number of foam and polymer conditioning agents were used in this research, for foam index tests and for preparation of conditioned soil samples for index testing and model screw conveyor tests. The conditioning agents were commercial products obtained from various suppliers, and as they are proprietary products, full details of their chemical compositions are not available. The conditioning agents tested and their properties as stated by the suppliers are summarised below.

#### **3.3.1 Polymer conditioning agents**

Three polymer conditioning agents from different suppliers were used in the laboratory testing of conditioned clay soils, detailed in Table 3.4. Drillam MV is a high molecular weight anionic PHPA polymer, described as having a stabilising effect on soils and encapsulating active clays to inhibit water adsorption (Lamberti, 2002). PHPA polymers for soil conditioning are discussed in Section 2.2.2. TFA34 is also an anionic PHPA polymer product with similar composition and properties as MV. This polymer is described as having applications to viscosify conditioned soils, and reduce sticking of soils to steel surfaces (Condat, 1998). SLF P1 is a polymer product based on polyalkylene oxides, which have properties as bridging flocculants similar to PHPA polymers (Moody, 1995). This polymer is recommended for use in fine sands, silts and clays with high water contents, and has powerful structuring and viscosifying effects by binding soil and water to improve the spoil consistency and provide lubrication (MBT, 2002). These polymers are all in a

liquid form for easier use in practice, and are recommended for use at concentrations of 0.1 to 1.0%, injected into excavated soil as water based solutions or as additives in foam solutions.

The environmental effects of conditioning agents are an important issue for application in practice, as they are released into the soil around the machine underground, and spoil removed from the tunnel becomes contaminated with conditioning agents. To minimise adverse environmental effects and problems with disposal of conditioned spoil, environmentally friendly conditioning agents are required. The three polymers used in this research are non-toxic, and although they do not readily biodegrade, their application is generally not restricted by environmental regulations. An environmental risk assessment of one supplier's polymer and foam conditioning agents found generally very low risks associated with their use (MBT, 2001).

### **3.3.2 Foam agents**

Seven foam agents from four suppliers were used in the foam index tests. Two of the foam agents were used for preparation of conditioned soil samples for the index tests and model screw conveyor tests. The properties of the foam agents used are shown in Table 3.5. These foam agents are all solutions based on anionic surfactants or glycols, with some including polymer additives. Full details of the chemical compositions are not available, but the various foam agents have different compositions designed to achieve different foam properties for conditioning various types of soil.

Foamex TR is recommended for use in all types of soil, and is said to reduce sticking of clays to the machine and provide lubrication to reduce the internal and interface friction of the soil (Lamberti, 2002). Foamex EC has similar applications and effects on soil properties, and this agent includes a polymer additive to increase the stability and lubrication properties of the foam. Condat F4 is recommended for use in all ground conditions, with the concentration and foam expansion ratio varied to condition different soils (Condat, 1998). Condat F4/L is a foam agent designed for use in impermeable soils containing clay, with a low expansion ratio to improve lubrication of the spoil. Condat F4/TM was formulated for use in saturated permeable ground, and is described as having a drying effect on the soil to reduce the permeability and ground water inflows, and has enhanced lubrication properties. MBT SLF30 is recommended for use in silty soils and clays with the application parameters varied depending on the soil, and is compatible with polymer additives to stabilise the foam or modify the spoil properties. These foam agents

are all non-toxic, biodegradable and have minimal effects on the environment, so there are generally no restrictions on their use for environmental reasons.

### 3.4 Index Testing Apparatus and Methods

The index tests performed on foams and conditioned clay soils involved several pieces of laboratory apparatus, as described here. The sample preparation and test methods for the various index tests are also described.

#### 3.4.1 Foam generator

A laboratory foam generator was used to produce foam for the index tests of different agents and for preparing conditioned soil samples. The foam generator was designed and manufactured by Spoilmaster Ltd, UK. The design was similar to a foam generator for an EPB machine, scaled down to produce smaller volumes of foam for laboratory testing, with similar properties to the foam produced by a full-scale generator. Figure 3.5 shows the laboratory foam generator.

Foam is produced from a water based solution of a foam agent, prepared at a specific concentration by diluting the foam agent in water. The foam concentration ( $c_f$ ) is given by:

$$c_f (\%) = \frac{V_{fa}}{V_{fs}} \times 100 \quad \text{Eqn. 3.1}$$

where  $V_{fa}$  is the volume of foam agent, and  $V_{fs}$  is the volume of the foam solution. The foam solution is prepared in a tank connected to the liquid line of the foam generator. The foam generator is also supplied by an air compressor, and the flows in the separate liquid and air lines are adjusted with pressure regulators and control valves. Pressure gauges at various points and flow meters in the liquid and air lines monitor the foam generator operation. The flow lines carry the foam solution and compressed air to the foam generator unit, a steel tube packed with small plastic beads, as shown in Figure 3.6. Turbulent flow of the foam solution and air through the generator unit mixes the two components and forms the foam bubbles. The foam produced by the generator is discharged from the outlet tube.

The operation of the laboratory foam generator is described here with reference to the schematic diagram shown in Figure 3.7. The foam solution is pumped from the supply tank to fill the

accumulator vessel by opening the tank outlet valve (1) and starting the liquid pump by opening the compressed air supply with valve (2), keeping valve (3) closed. A regulator (4) controls the air pressure supplied to the liquid pump. Once the accumulator vessel is filled with foam solution, valve (3) is opened and flow control valve (5) is used to adjust the flow through the liquid flow meter to the foam generator unit inlet. The pressure in the air flow line is controlled with a regulator (6) and measured by a pressure gauge (7). Valve (8) is opened to allow the air to flow through the control valve (9) and the air flow meter to the generator unit inlet. The pressurised air and foam solution then flow through the generator unit to produce the foam. Pressure gauges (10, 11) measure the pressure in the liquid and air lines at the exit of the flow meters, and the pressure at the foam generator outlet (12). Valves (13) and (14) remain closed during operation.

The design of the foam generator allows the liquid and air flow rates and pressures to be adjusted and monitored separately to control the properties of the foam produced. For the testing discussed here, the foam generator was usually operated with an air line pressure of 1.5 to 2.5 bar (at gauge (7)), and a liquid line air pressure supply of 3 bar (at gauge (4)). The flow rates were typically 150 L/h for the liquid line, and 1.5 to 3.5 Nm<sup>3</sup>/h for the air line (the unit Nm<sup>3</sup> represents the air volume at atmospheric pressure). With these generator settings, the foams produced were generally of suitable quality for testing.

### **3.4.2 Foam index tests**

Foam index tests were performed to measure the properties of foams generated from different agents, and to investigate effects of generation variables on foam properties. The expansion ratio and liquid drainage time of foam samples were measured based on the methods described in the Ministry of Defence Standard (1998). The tests are performed with foam samples collected in a cylindrical steel container of 1600 ml volume, with a conical base and drainage outlet through a perspex stopcock. Foams were produced with the generator and a sample was collected to fill the container after the generator was running for about 10 seconds to establish stable operation. The weight of the container filled with the foam sample is measured. From the weight of the empty sample container, the weight of the foam liquid contained in the sample immediately after generation is calculated. This is equal to the initial volume of the liquid in the foam sample, assuming a solution density of 1.0 g/cm<sup>3</sup>. The foam expansion ratio (FER), representing the ratio of the foam volume at atmospheric pressure to the liquid volume in the sample, is calculated from the test measurements:

$$FER = \frac{V_f}{V_{f1}} = \frac{1600}{(W_{cf} - W_c)} \quad \text{Eqn. 3.2}$$

where:  $V_f$  is the volume of foam ( $V_f = 1600$  ml for these samples)  
 $V_{f1}$  is the initial volume of foam liquid in sample (ml)  
 $W_{(cf)}$  is the weight of sample container filled with foam (g)  
 $W_c$  is the weight of empty sample container (g)

The liquid drainage time of the foam is measured by placing the sample container in a stand, with a 50 ml graduated cylinder beneath the outlet. The liquid draining from the foam is regulated with the stopcock and collected in the graduated cylinder. The volume of liquid is recorded over time to define the foam liquid drainage rate. The time for drainage of certain proportions of the initial liquid volume, such as the 25% ( $t_{25}$ ) and 50% ( $t_{50}$ ) drainage times, are measured as an index for the stability of the foam. Results from the foam index tests are presented in Section 3.5.

### 3.4.3 Atterberg limit tests

Atterberg limit tests were performed to investigate the effects of PHPA polymer on the plasticity of clay soils. These test methods were according to British Standard 1377 (1975). The plastic limit was measured by rolling soil threads and the liquid limit by cone penetrometer tests, using a standard penetrometer with a fall cone angle of  $30^\circ$  and mass of 80g. Tests were performed on reconstituted samples of E-grade kaolin and London Clay. E-grade kaolin is supplied as a powder, and London Clay powder was produced from the clay cutting samples. London Clay cutting samples were oven-dried, ground into a powder, and passed through a  $425 \mu\text{m}$  sieve to produce a clay powder. The dry clay powders were mixed with water and polymer solutions to form reconstituted clay samples at moisture contents between the plastic and liquid limits. The samples were sealed for at least 24 hours before testing to allow hydration of the clay and homogenisation of the samples.

For the liquid limit tests, the liquidity of the clay-polymer samples was increased by adding the polymer solution, rather than water as for a usual test. The undrained shear strength of the samples at varying liquidity was measured with a shear vane following each cone penetration measurement. The laboratory shear vane described in Section 3.4.4.3 was used for these tests. These tests provided measurements of the Atterberg limits and the undrained strength at varying

moisture contents over the plastic range of the clays reconstituted with water and PHPA polymer solutions at different concentrations.

### 3.4.4 Conditioned London Clay index tests

Index tests were performed to measure the effects of different conditioning treatments on the undrained shear strength of London Clay cutting samples. A large-scale fall cone apparatus was constructed for these tests, and shear vane tests were also performed to measure the sample strength. The sample preparation methods and apparatus used for these index tests are described below, and the test results are discussed in Section 3.7.

#### 3.4.4.1 Sample preparation

Samples of London Clay cuttings conditioned with various treatments were prepared to represent the state of excavated, conditioned London Clay as produced by an EPB machine. The samples were prepared using the polymer and foam conditioning agents described in Section 3.3, with varying concentrations and injection ratios, and different foam expansion ratios.

The polymer and foam solutions were prepared to accurate concentrations by diluting measured volumes of the conditioning agents in measured volumes of water. The conditioning agents used were all liquids and readily dissolved in water to form a uniform solution when mixed during the dilution. Foam was produced with the generator as described in Section 3.4.1, with the foam concentration and generator settings adjusted to achieve target foam expansion ratios for the samples. Foam from the generator was collected in a foam sampling tube with a maximum volume of 5.5 L, using a graduated plunger to measure the foam volume in the tube, as shown in Figure 3.8. The volume of foam required was collected in the sampling tube, and the plunger was used to discharge the foam from the tube.

The conditioned London Clay samples were prepared with specific polymer and foam injection ratios (PIR and FIR), which represent the volume of the conditioning agents relative to the in-situ volume of the excavated soil in the sample:

$$PIR(\%) = (V_p / V_s) \times 100 \quad \text{Eqn. 3.3}$$

$$FIR(\%) = (V_f / V_s) \times 100 \quad \text{Eqn. 3.4}$$

where:  $V_p$  is the volume of polymer solution (L)  
 $V_f$  is the volume of foam at atmospheric pressure (L)  
 $V_s$  is the in-situ volume of excavated soil (L)

Measured volumes of the polymer solutions and foams were mixed with a weighed mass of soil cuttings to create conditioned clay samples with accurately known injection ratios. A bulk unit weight of  $20 \text{ kN/m}^3$  was assumed for the London Clay, used to relate the mass of the clay cuttings in a sample to the in-situ volume of the soil, and allowing calculation of the conditioning agent volumes required for specific injection ratios. Test samples were typically prepared from approximately 20 kg of London Clay cuttings, representing a 10 L in-situ soil volume. The polymer and foam volumes required for specific injection ratios were calculated from equations 3.3 and 3.4.

The clay cuttings, at natural moisture content, were mixed with the measured quantities of polymer solutions and foams in a small concrete mixer. A uniform conditioned soil mixture was typically formed after mixing for 30 to 60 seconds. The conditioned soil sample was then transferred to a container and compacted by hand, avoiding entrapment of air voids. A circular steel bin with a top diameter of 300 mm and a base diameter of 220 mm, and height of 280 mm was used as a sample container. This container had sufficient volume for the conditioned soil samples prepared, and the dimensions were large enough to avoid any influence of boundary effects during the strength testing. Large-scale fall cone tests and shear vane tests were then performed to measure the undrained shear strength of the samples.

With the sample preparation methods employed, foam is injected into the soil cuttings at atmospheric pressure and in unconfined conditions. This differs from the confined, pressurised conditions under which foam is injected into the excavated soil in an EPB machine. The sample mixing is likely to be more effective than the mixing process in an EPB machine, but for comparison of different samples, complete mixing to achieve uniform conditioned soil samples is necessary. Although not ideally representative of the conditions pertaining to the application of conditioning agents in an EPB machine, the sample preparation methods are adequate for the simple index tests performed to measure the effects of different conditioning treatments on the undrained strength of clay soils.

### 3.4.4.2 Large scale fall cone

The fall cone test measurement is based on the undrained shear strength of a clay soil, and has been previously used for testing conditioned soil samples, as discussed in Section 2.4. The test involves measuring the penetration of a cone of known mass and dimensions into a sample when released at the sample surface. The measured cone penetration can be used as an index to compare different samples, and the undrained shear strength can also be deduced.

The conditioned London Clay samples were prepared from the clay cuttings, sieved for a maximum size of approximately 25 mm. To minimise the scale effects of the size of the clay cuttings relative to the testing apparatus, and to measure the strength of the bulk sample, a large scale fall cone was used to achieve a high penetration into the samples. The fall cone apparatus used for these index tests, shown in Figure 3.9, consisted of a steel cone piece with a circular shaft sliding through a Teflon guide mounted in a frame supporting the fall cone. The weight of the fall cone was adjusted by filling the hollow cone piece with lead shot and placing weights on top of the cone. A steel pin through the shaft was used to hold the fall cone in place, and the height was adjusted with screw threads on the frame so that the tip of the cone was level with the surface of the sample. The fall cone is released by pulling the pin out of the shaft, and the penetration into the sample is measured from the vertical displacement of the top of the sliding shaft. A steel ruler was used to measure the cone penetration to an accuracy of  $\pm 1$  mm, which was in the range 35 to 170 mm for the 20 kg fall cone mass used with the range of sample strengths tested.

The dimensions and mass of the large scale fall cone were determined based on the expected range of sample strengths and target cone penetration values. The fall cone had a base diameter of 180 mm and a cone angle of  $60^\circ$ , and a mass of 20 kg. The  $60^\circ$  cone angle was used as this angle gives good agreement between theoretical and experimental values of the fall cone factor, and the surface roughness of the cone has less influence, as discussed by Koumoto and Houlsby (2001). The undrained shear strength of the conditioned clay samples was calculated from the fall cone factor and the measured penetration according to equation 3.5, from Wood (1985):

$$S_u = \frac{K_\alpha W}{d^2} \quad \text{Eqn. 3.5}$$

where:  $S_u$  is the undrained shear strength (kPa)  
 $K_\alpha$  is the theoretical cone factor ( $K_\alpha = 0.30$  for 60° cone)  
 $W$  is the weight of fall cone (N)  
 $d$  is the fall cone penetration (mm)

The value of  $K_\alpha = 0.30$  for a 60° cone was calculated by Koumoto and Houlsby (2001) from theoretical analysis of the fall cone test. They obtained good agreement between the undrained shear strength calculated by equation 3.5 and the vane shear strengths measured for various clays at different water contents, indicating that the undrained strength of a sample can be estimated accurately using this equation.

### 3.4.4.3 Shear vane tests

Following the fall cone tests, the undrained shear strength of the conditioned clay samples was measured directly using a laboratory shear vane. A hand shear vane manufactured by Pilcon was used for these measurements. This device consists of a handle with a calibrated torque spring and two shear vanes of different dimensions to measure different ranges of sample strengths, detailed in Table 3.6. The large vane was used for most of the samples tested as their strength was less than 30 kPa, and the dimensions of the vane are larger relative to clay cutting sizes in the samples. The tests were performed by inserting the vane vertically into the sample away from any boundaries and rotating the vane until the peak shear strength is reached, indicated directly on the calibrated dial on the handle. At least four vane tests were performed on each sample to calculate an average vane shear strength for comparison with the value from the fall cone test.

After the strength testing, specimens of the conditioned London Clay samples were taken for measurement of the moisture content. The results from these index tests provide measurements of the undrained shear strength and moisture content of the samples for comparison of the effects of the various conditioning treatments, discussed in Section 3.7.

## 3.5 Index properties of foams

Properties of foams produced from various agents and the influence of foam generation variables were investigated through a series of index tests as described in Section 3.4.2. The results of the foam index tests performed are discussed below.

### 3.5.1 Comparison of foam agents

Index tests were performed to compare the properties of foams generated from the seven foam agents described in Section 3.3.2. The samples for these tests were all produced using the same generator settings so that variations in foam properties were due only to the different properties of the foam agents. The specific generator settings were determined using the T-7 foam agent at a concentration of 2.0% as a reference, with the liquid and air flow rates and pressures adjusted to generate foam with an expansion ratio of approximately 20. The 'standard' foam generator settings determined on this basis were an air pressure of 1.5 bar, an air flow rate of 2.1 Nm<sup>3</sup>/h, and a liquid flow rate of 150 L/hr.

The foam expansion ratio (FER) and liquid drainage over time was measured for samples produced from each foam agent at various concentrations with the standard generator settings. The foams tested and the measured index properties are shown in Table 3.7. The foam liquid volume in the samples immediately after generation was calculated from the mass of liquid, assuming a density of 1.0 g/cm<sup>3</sup>. From the foam agent densities stated in Table 3.5 and the test concentrations, the maximum actual foam solution density was 1.0045 g/cm<sup>3</sup> (for F4 at  $c_f=5.0\%$ ), so the error introduced by using the assumed density is negligible. From the initial liquid volume in a sample, the FER is calculated by equation 3.2, and the proportion of the initial liquid remaining at a time after commencing drainage is calculated using the volume of liquid measured in the graduated cylinder.

The FER measured for the various agents at different concentrations are shown in Figure 3.10. The expansion ratio of the foams generated from the different agents with the standard conditions varied from 6.5 to 27.7. The measured FER values were within the recommended ranges for each foam agent, shown in Table 3.5. The FER increased with concentration for each foam agent, but they produced foams with different expansion ratios over different ranges of concentration. These measurements indicate that the different foam agents have varying activities with regard to foam generation, with some agents producing a high FER at low concentrations, and others a low FER at high concentrations. This is believed to result from the varying effects of the foam agents on the surface tension of the solutions. The specific chemical compositions of the foam agents, containing different surfactants at varying concentrations as well as other additives, determines their influence on the surface tension of the solutions.

The drainage of foam liquid over time, expressed as the percentage of the initial liquid volume remaining in the sample, is shown for some foam samples in Figure 3.11. From these measurements, the times for drainage of 25% ( $t_{25}$ ) and 50% ( $t_{50}$ ) of the initial foam liquid can be determined to compare different samples. The  $t_{25}$  and  $t_{50}$  values measured for each foam sample are listed in Table 3.7, and shown in Figure 3.12 for the samples generated with standard conditions. The liquid drainage times of the foams generated from the SLF30, TR, EC and T-7 foam agents were all similar and relatively low, with 50% drainage occurring less than 10 minutes after generation. For these agents, the drainage times were not significantly influenced by the concentration or expansion ratio over the ranges tested. Foam agent EC contains a polymer additive to improve the foam stability, but this effect was not apparent in these tests as this foam drained rapidly compared to the others. Foam agents F4 and F4TM produced foams of significantly higher stability, with 50% drainage of the F4 foam taking up to one hour. The stability of these foams was significantly influenced by the concentration, with the initial time period before drainage commenced, and the  $t_{25}$  and  $t_{50}$  values, all increasing with concentration.

### 3.5.2 Effects of foam generation parameters

Index tests were also performed to investigate the effects of some generation variables on foam properties. The foam agents were tested with different concentrations, as discussed above, and samples were also produced with varying air flow rates in the generator. The foam index properties measured for the samples generated under different conditions are shown in Table 3.7.

The increase of FER with concentration observed for samples produced with standard generator settings was discussed in Section 3.5.1. These measurements are plotted in Figure 3.13, with additional data from samples generated with higher air flow rates. For a given air flow rate the FER increases with concentration, at different rates for the various foam agents. An increase in the concentration of a foam agent reduces the surface tension of the solution, and as less energy is then required to generate the foam, a higher expansion ratio results. The varying effects of the different foam agents on the surface tension of the solution result in the different rates of increase of FER with concentration.

The effect of the air flow rate on the expansion ratio of foams at different concentrations is shown in Figure 3.14. The FER increased with the air flow rate used to generate the foams for all concentrations tested. For a given air pressure, a higher flow rate introduces a greater volume of

air into the foam, and increases the energy available for mixing the air and liquid in the generator unit, producing a higher FER.

While the index test results are specific to the foam generator and test conditions used, the measurements illustrate that the properties of foams generated from different agents vary. The observed differences in the FER and foam stability result from the specific chemical composition of the different foam agents, but as these are not known in detail more definite conclusions cannot be drawn. For a given agent, the expansion ratio of the foam produced can be varied by adjusting the solution concentration and the foam generator parameters. Some index tests performed using a foam generator unit with different dimensions showed that the design of the generator also influences the properties of the foam produced. For soil conditioning applications, the expansion ratio of the foam injected into the excavated soil can be changed through the generation variables to suit the soil encountered during tunnelling.

### **3.6 Plasticity and strength of reconstituted polymer conditioned clays**

The effects of PHPA polymer (Drillam MV) on the plasticity and undrained strength of reconstituted E-grade kaolin and London Clay samples were measured through Atterberg limit and shear vane tests, as described in Section 3.4.3. The results of these tests are presented here.

#### **3.6.1 Plasticity of polymer conditioned clays**

Atterberg limit tests were performed on E-grade kaolin and London Clay samples reconstituted with water and MV polymer solutions at 0.25% and 0.50% concentrations. The liquid limit was determined as the soil moisture content corresponding to a cone penetration of 20 mm, and the plastic limit as the moisture content at which the soil threads crumble. The Atterberg limits measured for these samples are shown in Table 3.8.

The Atterberg limits measured for the soils reconstituted with water agree with those reported previously for these clays, shown in Tables 3.2 and 3.3. When reconstituted with MV polymer solutions, the liquid limit increased significantly with the polymer concentration, with small increases also measured in the plastic limit. These changes resulted in the plasticity index of the clays also increasing significantly with the polymer concentration. Figures 3.15(a) and (b) show the Atterberg limits of the E-grade kaolin and London Clay samples at different polymer concentrations, with the samples reconstituted with water shown as a concentration of 0%.

The effects of the polymer on the liquid limit and plasticity of the clays result from the PHPA polymer molecules adsorbing onto the clay particles and binding the soil and water together through their flocculating action, as discussed in Section 2.2.2. With increasing polymer concentrations, the liquid limit (and plasticity index) increase as greater amounts of the polymer are introduced to the soil at the higher moisture contents approaching the liquid state. This increases the flocculating action and water absorbing capacity of the clay-polymer samples. Similar effects on the plasticity were observed for the two clays tested with different mineralogy, as the polymer adsorbs onto the different clay minerals and soil particles present in these samples. Lambe (1953) presents similar results showing the liquid limit of natural clay and silt soils increasing with the amount of an aggregating polymer (partially hydrolysed polyacrylonitrile) present in the soil, due to the increased water holding capacity of the aggregated soil structure.

### 3.6.2 Remoulded strength of polymer conditioned clays

During the liquid limit tests, the undrained strength of the reconstituted clay samples with varying moisture contents was measured directly by shear vane tests, and also through the fall cone penetration. The strengths calculated from the cone penetrations according to equation 3.5 (assuming  $K_\alpha = 0.85$  for the 30° cone used) agreed well with the vane shear strengths. The liquid limit and plasticity index of the clay-polymer samples were much greater than for the clay-water samples, as the polymer allowed the samples to have much higher moisture contents before reaching the liquid state. To compare the strengths of the clays reconstituted with the different solutions, the sample moisture contents ( $w$ ) were normalised by calculating the liquidity index ( $I_L$ ) based on the liquid limit ( $w_l$ ) and plastic limit ( $w_p$ ) of the clays with water:

$$I_L = \frac{w - w_p}{w_l - w_p} \quad \text{Eqn 3.6}$$

Figures 3.16(a) and (b) show the strengths of the E-grade kaolin and London Clay samples reconstituted with water and MV polymer solutions, plotted against the liquidity index calculated based on the Atterberg limits of the clays with water. Also shown is a range of strengths for various natural clays reconstituted at different liquidities, reported by Mitchell (1993). For E-grade kaolin and London Clay with water, the strengths at varying liquidities are within the expected range of values. At a given liquidity index (based on the Atterberg limits with water), the clay-polymer samples had higher strengths than the clay-water samples, and the strength increased with the polymer concentration. In other words, for a given strength, the moisture

content of the clay-polymer samples was higher than the clay-water samples. At lower values of the liquidity index in Figure 3.16, the strengths of the clay-polymer samples were within the range expected for clays with water. With increasing liquidity the polymer had a greater influence, and the strength of the clay-polymer samples was significantly higher than that of the clays with water, and the range of strengths for other clays.

If the liquidity index is calculated based on the Atterberg limits of the clays with the polymer solutions, the curves shown in Figure 3.16 become similar, and indicate a similar variation of strength with liquidity index for the different samples. However, presenting the data in this way does not illustrate the effects of the small concentrations of polymer on the strength of the clay at different moisture contents.

The strength of fine-grained soils at the liquid limit, corresponding to  $I_L = 1.0$ , is usually in the range 1.7 to 2.0 kPa (Wood, 1990; Mitchell, 1993). As shown in Figures 3.16(a) and (b), the strengths of E-grade kaolin and London Clay with water at  $I_L = 1.0$  are close to the expected value. To reach a similar strength, the clay-polymer samples have much higher moisture contents, increasing with the polymer concentration. Based on the Atterberg limits of the clay-water samples, the liquidity index of the E-grade-polymer samples for a strength of 2 kPa was 2.3 and 3.1 for polymer concentrations of 0.25 and 0.50%. These values of  $I_L$  represent moisture contents of 78 and 95% for the clay-polymer samples, compared to a moisture content of about 53% for E-grade with water at the same strength. Similarly, for the London Clay-polymer samples, the liquidity index for a strength of 2 kPa was 1.4 and 2.0 for polymer concentrations of 0.25 and 0.50%. These values of  $I_L$  represent moisture contents of 87 and 113% for the clay-polymer samples, compared to a moisture content of about 66% for London Clay with water at the same strength. The higher moisture contents required for the clay-polymer samples to reach a strength of 2 kPa correspond to the increases in the liquid limits when small concentrations of polymer are introduced.

These test results illustrate the effects of PHPA polymer on the Atterberg limits and undrained strength of reconstituted clays. The flocculating action of the polymer binds the clay, increasing the liquid limit and plasticity, and increasing the strength of the soil at a given moisture content, depending on the amount of polymer introduced. For soil conditioning applications, increasing the plasticity and water holding capacity of a soil is beneficial as it reduces the sensitivity of the strength to changes in the water content, which is particularly an issue for low plasticity clay soils.

### **3.7 Index testing of conditioned London Clay**

To investigate conditioning treatments for London Clay, index tests were performed to measure the undrained strength of conditioned soil samples as described in Section 3.4.4. The results of the tests performed on London Clay cutting samples conditioned with polymer, foam and combined foam and polymer treatments are discussed below.

#### **3.7.1 Polymer conditioning treatments**

A series of index tests was performed to investigate conditioning of London Clay with polymer solutions. Samples were prepared by mixing clay cuttings with solutions of MV, TFA34 and SLF P1 polymers, each at two concentrations and with polymer injection ratios (PIR) ranging from 10 to 60%. Large scale fall cone and shear vane tests were performed to measure the undrained strength of the samples.

During the sample mixing, the clay cuttings absorbed the polymer solutions and were bound together to form a paste, with the strength and consistency depending on the polymer concentration and injection ratio. The measured fall cone penetrations and the undrained strengths calculated by equation 3.5 are shown plotted against the PIR for the different polymer solutions in Figures 3.17(a) and (b) respectively, and the average vane shear strengths are shown in Figure 3.17(c). The cone penetration increased with the PIR for all polymer solutions, as the sample strength reduced. At a PIR of 10%, the clay cuttings formed pastes of relatively high strengths, with little difference between the various polymer solutions. With a PIR of 20 to 40%, the strength of the samples ranged from approximately 5 to 25 kPa, corresponding to the range suggested as suitable for EPB machines (Milligan, 2000). The sample strengths reduced further with higher PIRs, but the relatively small reductions in strength for injection ratios greater than 40% result in inefficient conditioning treatments.

The samples conditioned with MV and TFA34, both based on PHPA polymers, had similar strengths for PIRs greater than 20%. The samples conditioned with high injection ratios of SLF P1, a polymer based on polyalkylene oxides, had higher strengths due to the powerful structuring action that this polymer has to bind soils and water (MBT, 2002). The polymer concentration only had a small influence over the ranges tested, with samples conditioned with higher concentrations having slightly higher strengths.

The average of the strengths measured by the fall cone and shear vane tests are plotted against the moisture content of the polymer conditioned samples in Figure 3.18. Also shown is a curve representing the remoulded shear strength of London Clay, from the index tests on samples reconstituted with water discussed in Section 3.6. The polymer solutions softened the clay cuttings similarly to water, but slightly increased the strengths relative to those for London Clay with water. These results illustrate the effects of the polymers binding the clay and water to form a higher strength paste, with more pronounced effects at higher injection ratios.

The undrained strength of the polymer conditioned samples measured by the fall cone and shear vane tests are compared in Figure 3.19. The correlation coefficient  $R^2 = 0.96$  indicates good agreement between the measurements. The strengths measured by the two test methods were approximately equal, particularly for strengths less than 25 kPa as these soft samples were more uniform and the large shear vane could be used. The large scale fall cone probably gives a more reliable measurement of the bulk sample strength as the instrument is large relative to the size of the clay cuttings, and the measurements with the shear vane may be more susceptible to non uniformities in the samples.

### **3.7.2 Foam conditioning treatments**

Index tests were performed to investigate foam conditioning treatments for London Clay. Samples were prepared using foams generated from TR and EC foam agents with varying foam expansion ratios and injection ratios, as summarised in Table 3.9. The foam agent concentrations and air flow rates were adjusted to achieve target FER values for the samples. Measured volumes of the foams were mixed with the clay cuttings at injection ratios required to achieve sample strengths in the range suitable for EPB machines.

When foam was mixed with London Clay cuttings at injection ratios of 30 to 60% as typically recommended, the foam rapidly broke down as the foam liquid was absorbed by the soil. The clay cuttings were slightly wetted by the small amount of foam liquid added at these injection ratios (about 2.5% of the clay soil mass, with a FIR of 50% and FER of 10), and the samples were not effectively conditioned or suitable for testing. With increasing injection ratios the foam continued to break down during mixing as the soil absorbed more foam liquid, gradually softening the clay and binding the cuttings into a paste as the moisture content increased. Injection ratios greater than 200% were required before the clay cuttings absorbed enough liquid so that some of the foam bubbles persisted in the conditioned soil and a paste of consistency and

strength suitable for testing was formed. Some photographs of the London Clay cuttings mixed with foam at various injection ratios are shown in Figure 3.20.

The effect of foam coating stiff clays to form a mixture of discrete cuttings in a stable foam matrix as described by some authors (e.g. Milligan, 2000; Wallis, 1996) was not observed in these tests. Rather, the clay absorbed the foam liquid, causing the foam to rapidly break down and softening the cuttings to form a paste when sufficient foam was injected. The increased surface area of the small clay cuttings used for the samples, sieved for a maximum size of about 25 mm, allows the foam liquid to be absorbed more rapidly by the clay than for larger cuttings as produced by an EPB machine. This scale effect of the clay cuttings is expected to cause some differences in the behaviour of the test samples compared to clay-foam mixtures formed in an EPB machine. The samples were mixed at atmospheric pressure in unconfined conditions, so effects of the compressed air in the foam on the properties of the conditioned soil were also not captured. Although the index test methods are not ideal, the results demonstrate significant differences in the performance of foams for conditioning clay soils, compared to that with granular soils as discussed in Section 2.2.3.

The vane shear strength of London Clay cuttings mixed with foams at injection ratios sufficiently high to effectively condition the soil are shown in Figure 3.21. For the TR and EC foams with an FER of about 20, FIRs in the range 500 to 600% were required for sample strengths below 25 kPa. Similar strengths were measured for the samples conditioned with both foam agents at similar FIRs and FERs. For the samples conditioned with EC foam with an FER of 10, strengths below 25 kPa were achieved at FIRs in the range 200 to 300%. By reducing the foam concentration, the FER of the EC foam was reduced from 19 to 10, increasing the foam liquid volume by a factor of about two. The FIR required for a given sample strength was reduced by approximately one half with the lower FER, in proportion to the amount of foam liquid injected. Figure 3.22 shows the strength of the foam conditioned samples plotted against the conditioner liquid injection ratio, represented by the foam liquid injection ratio (FLIR) for the foam conditioned samples:

$$FLIR(\%) = \frac{V_{fl}}{V_s} = \frac{V_f}{V_s \times FER} = \frac{FIR}{FER} \quad \text{Eqn. 3.7}$$

For the foam conditioning treatments, the sample strengths were approximately equal when similar volumes of foam liquid were injected to the clay. The foam conditioned samples were of similar strength to the polymer conditioned samples at equivalent liquid injection ratios. The strengths of the samples are plotted against the conditioned soil moisture content in Figure 3.23, also with the reference curve for remoulded London Clay. The samples conditioned with foam had approximately the same strength as remoulded London Clay at the same moisture content, again indicating that the effect of the foam on the strength of the samples resulted principally from the foam liquid softening the clay.

These results demonstrate that the amount of foam liquid injected to the London Clay cuttings, controlled by the FIR and FER, determined the strength of the samples. The EC foam contains a polymer additive and was prepared at higher concentrations than the TR foam, but did not show improved performance. The polymer in the liquid phase of the EC foam is present at a low concentration, so only small amounts are injected to the soil. For both foams, the liquid was absorbed and the foam broke down when mixed with the clay samples, rather than forming a stable clay-foam mixture. The surfactant and polymer molecules contained in the liquid phase of foams adsorb onto soil particles, which removes the molecules from the liquid phase and prevents them from stabilising the foam air bubbles. The absorption of foam liquid by clay soils is also expected to occur in an EPB machine and cause some of the foam to break down, although probably to a lesser extent due to the larger size of the clay cuttings. The London Clay cuttings used in the samples had a high capacity to absorb the foam liquid, due to the high surface area and the high plasticity of the clay. As a result, the chemical composition of the foam liquid did not influence the performance of the foams with the clay, and the amount of foam liquid injected was the dominant factor controlling the strength of the samples.

Field data and laboratory tests have shown that foam can effectively condition granular soils at the injection ratios typically recommended. However, the FIRs required to effectively condition the London Clay cuttings in the index tests were significantly higher than those typically recommended. As discussed in Section 2.3.2, the EFNARC (2001) specification recommends small quantities of foam for conditioning clay soils, with typical FIRs of 30 to 60% and FER of about 10. These values are similar to those suggested by product suppliers. For the test samples conditioned with foam of FER = 10, FIRs greater than 200% were required for a strength below 25 kPa, as is suitable for EPB machines.

There is further evidence from the laboratory and the field in support of the index test results indicating that FIRs considerably higher than usually recommended are required to condition clays. As shown in Figure 2.13 and discussed in Section 2.4, slump tests reported by Leinala *et al.* (2000) showed that the FIR required to condition soils increased with the clay content. Injection ratios of 150 to 300% (with FER = 6) were required to condition the mixed clay-sand and hard till soils to achieve a suitable consistency for EPB machines. As discussed in Section 2.5, Wallis (1996) reported that FIRs of up to 150%, with a FER of 10 to 15, were used to condition London Clay during EPB tunnelling on the Jubilee Line Extension Project. Leinala *et al.* (2000) and Boone *et al.* (2002) report that FIRs up to 200%, with a FER of 4 to 10, were required to condition stiff clay and till soils during EPB tunnelling in Toronto.

### 3.7.3 Combined foam-polymer conditioning treatments

Foams and polymers are often used in combination, with the polymer contained in the foam liquid phase or injected as a solution separately to the foam. Index tests of London Clay conditioned with EC foam including a polymer additive were discussed in Section 3.7.2. A series of index tests was also performed to investigate conditioning of London Clay with combined foam and polymer solution treatments. Samples were prepared using TR foam at 0.5% concentration for a FER of about 12, in combination with MV polymer solutions at 0.2% concentration. The foam and polymer solutions were mixed with London Clay cuttings at varying injection ratios for both agents as summarised in Table 3.10, to form conditioned soil samples with strengths in the range suitable for EPB machines.

The vane shear strength of the samples conditioned with the combined foam and polymer solution treatments are shown in Figures 3.21 and 3.22. For these treatments, the conditioner liquid injection ratio was calculated from the foam liquid injection ratio (by equation 3.7) plus the polymer injection ratio. The performance of the foam was significantly improved when used in combination with polymer solutions, with FIRs of 50 to 150% required to effectively condition the London Clay. The polymer solutions reduced the amount of foam liquid absorbed by the clay, improving the stability of the foam mixed with the soil at lower FIRs. With higher PIRs, lower FIRs were required for a given sample strength. The effect of increasing the FIR was reduced at higher PIRs, as the polymer solution had more influence on the sample strength than the foam.

The sample strengths are shown plotted against the PIR for different FIRs in Figure 3.24. Conditioning with the combined treatments reduced the strength compared to samples conditioned with polymer solutions only, and increasing the FIR reduced the PIR required for a given strength. A higher FIR also reduced the effect that an increase in PIR had on the strength, as the foam had more influence at high injection ratios. The results show that the strength of the conditioned soil depends on the combination of PIR and FIR, with an increase of the amount of one conditioning agent reducing the amount of the other required for a given strength.

Depending on the combination of the PIR and FIR, varying amounts of foam remained in the samples after mixing, but this gradually broke down as the polymer solutions slowed the absorption of the foam liquid by the clay. For the lower values of FIR at each PIR tested, most of the foam broke down as the clay absorbed the foam and polymer liquid, with the cuttings softening and binding into a paste with only some foam air bubbles remaining. As shown in Figure 3.22, these samples were of similar strength to those conditioned with MV polymer solutions at similar liquid injection ratios, although with slightly lower strengths due to the foam that remained in the samples.

For the higher values of FIR at each PIR tested, significant amounts of foam remained in the conditioned soil and dispersed the clay to form a mixture of discrete cuttings in foam, while the foam remained stable. The foam prevented the clay cuttings from recompacting into a paste and resulted in sample strengths of less than 5 kPa. As shown in Figure 3.22, the strengths of these samples were significantly lower than those conditioned with other foam and polymer treatments at similar liquid injection ratios, due to the large amounts of foam present in the mixture dispersing the clay cuttings.

Similar effects are also shown in Figure 3.23. The samples conditioned with combined foam and polymer solution treatments have significantly lower strengths than remoulded London Clay with water at the same moisture content, due to the foam dispersing the clay cuttings and reducing the strength. However, the foam in these samples gradually broke down as the foam liquid was absorbed by the clay over time, causing the cuttings to soften and form a paste with the strength depending on the amount of liquid injected and the conditioned soil moisture content.

#### **3.7.4. Optimum conditioning treatments for London Clay**

The index test methods used are not ideally representative of the field conditions, as simplifications were necessary for laboratory testing. The clay cutting samples had a reduced size and increased surface area compared to the cuttings produced by an EPB machine, which influences some effects of the conditioning agents. The samples were mixed at atmospheric pressure in unconfined conditions, so effects of the compressed air in foams on the sample properties were not captured. The samples were also mixed more effectively than is likely to occur in an EPB machine, which will cause differences between the conditioned soil mixtures in the laboratory tests and in the field. However, the tests allowed evaluation of the performance of various conditioning treatments and the effects of different variables on the conditioned soil properties. The simplicity of the index tests allows their use in the laboratory or on site for estimating optimum treatments for different soils.

Based on the results of the index tests presented in Figures 3.17 to 3.24, optimum ranges of conditioning treatments for London Clay can be suggested.

Polymer solutions were effective conditioning treatments, forming a paste with strengths in the range 5 to 25 kPa at polymer injection ratios of 20 to 40%, with the strength reducing as the injection ratio increased.

Foams were only effective for conditioning London Clay at injection ratios considerably higher than typically recommended. The amount of foam liquid injected influenced the sample strength, and reducing the FER allowed effective conditioning at a lower FIR. With a FER of about 10 as typically recommended, FIRs greater than 200% were required to effectively condition the London Clay. Although higher than usual, these FIRs are similar to others reported for conditioning clay soils in laboratory tests and during EPB tunnelling. The FIR required for effective conditioning depends on the amount of water or liquid conditioning agents present in the mixture, which can reduce the required FIR. The foam liquid composition or concentration did not have a significant influence on the strength or stability of the conditioned London Clay samples.

Combined foam and polymer solution treatments were the most efficient, producing effectively conditioned samples with the lowest liquid injection ratios. The polymer solutions improved the performance of the foams mixed with the London Clay, and the sample strengths depended on

the combination of the FIR and PIR used. For PIRs in the range 10 to 30%, FIRs of 30 to 150% (with a FER of about 12) were required to effectively condition the London Clay, with lower FIRs required at higher PIRs and vice versa. The samples conditioned with these treatments reached low strengths with the lowest liquid injection ratios and moisture contents.

While foams could effectively condition London Clay at high injection ratios, or at lower injection ratios in combination with a polymer solution, the clay-foam mixtures had poor stability. Absorption of the foam liquid by the clay caused the foam to break down and the properties of the conditioned soil to deteriorate. Some effects of foam conditioning treatments depend on the presence of air bubbles dispersed through the soil, so the stability of the foam is important to control the conditioned soil properties during the excavation process. For samples conditioned with foam only, the liquid absorption was rapid and the foam broke down within minutes after mixing. The stability of the foam was improved by combined use with a polymer solution, but the foam mixed in the London Clay remained stable for a maximum of about 15 minutes, depending on the specific conditioning treatment.

These observations are influenced by the increased surface area of the clay cutting samples, and clay-foam mixtures in an EPB machine are likely to be more stable due to the larger cuttings. However, the observed performance is very different to that of mixtures of foam with sand that have been reported to remain stable for several hours or days, with significantly lower injection ratios (see Section 2.3.1). For high plasticity clays, the stability of the foam might be improved by increasing the concentration so a greater amount of surfactant is present to stabilise the air bubbles. This was not observed in the tests, as the reduced size of the clay cuttings increased their capacity to absorb liquid. For combined conditioning treatments, a higher polymer solution concentration could have a similar effect by reducing the rate of liquid absorption by the clay.

### **3.8 Summary**

This chapter has summarised the properties of the E-grade kaolin and London Clay samples, and the foam and polymer conditioning agents used in the research. The experimental apparatus and index test methods used for investigations of the properties of foams and effects of conditioning treatments on properties of clay soils were described. The main conclusions from the results of the index testing performed are summarised below.

The foam index tests showed that the expansion ratio and stability of foams generated from different agents vary, due to differences in the chemical composition of the foam agents. The properties of the foam produced from an agent can be varied through the solution concentration and the foam generator operation. Increasing the foam agent concentration, or the air flow rate in the generator, increased the expansion ratio of the foam produced.

Index tests measuring the effects of PHPA polymer on the Atterberg limits and undrained strength of reconstituted E-grade kaolin and London Clay samples showed that the polymer significantly increased the liquid limit and plasticity of the clays. This has the effect of increasing the undrained strength of the clay-polymer mixture relative to that of the clay-water mixture at the same moisture content. The effects on the clay plasticity and undrained strength increase with the polymer concentration. The effects result from the flocculating action of the PHPA polymer binding the soil particles together and increasing the water absorbing capacity of the mixture.

The large scale fall cone and shear vane tests were effective methods for measuring the strength of conditioned clay soils and evaluating the performance of foam and polymer conditioning treatments. The test methods are suitable for laboratory or site applications for identifying effective conditioning treatments for different clay soils.

The index tests performed with London Clay cutting samples showed that polymer solutions were effective conditioning agents for this soil, forming a soft paste from the clay. Foam injection ratios higher than usually recommended were required to effectively condition London Clay, and the sample strength was influenced by the amount of foam liquid injected to the soil. The stability of foam mixed with clay was poor compared to that with sand, as the foam liquid was absorbed by the clay and caused the foam to rapidly break down. Combined conditioning treatments with foam and polymer solutions were the most effective, improving the stability of the foam which dispersed the clay cuttings and resulted in low sample strengths at low liquid injection ratios. The properties of the conditioned soil depend on the combination of foam and polymer injection ratios. Based on the results of the index tests, optimum ranges for foam and polymer conditioning treatments for London Clay were suggested. These are expected to be similar for other stiff high plasticity clay soils.

<b>Chemical Composition</b>	
SiO <sub>2</sub>	48.20%
Al <sub>2</sub> O <sub>3</sub>	36.79%
Alkalis	2.01%
Fe <sub>2</sub> O <sub>3</sub>	0.68%
<b>Physical properties</b>	
Clay fraction (< 2 μm)	25%
Specific gravity	2.60
Surface area	8 m <sup>2</sup> /g

Table 3.1. Chemical composition and physical properties of E-grade kaolin.  
(after Richard Baker Harrison Group, 1994)

Plastic limit (%)	30
Liquid limit (%)	51
Plasticity index (%)	21
Cam-clay compression index, $\lambda$	0.12
Cam-clay swelling index, $\kappa$	0.02
Specific volume at $p'=1$ kPa for isotropic consolidation, $\Gamma_{iso}$	2.65
Cam-clay frictional coefficient, $M$	1.05
$c_v$ (normal consolidation) (mm <sup>2</sup> /s)	1.0
$c_v$ (isotropic rebound) (mm <sup>2</sup> /s)	5.0

Table 3.2. Engineering properties of E-grade kaolin.  
(after Elmes, 1985)

<b>Index properties</b>	<b>Typical range</b>	<b>Average value</b>
Bulk unit weight ( $\text{kN/m}^3$ )	17.5 – 20.5	19.5
Liquid limit (%)	45 – 85	75
Plastic limit (%)	20 – 36	28
Plasticity index (%)	30 – 60	45
Natural moisture content (%)	20 – 31	-
<b>Design parameters</b>	<b>Suggested values</b>	
Constant volume angle of friction, $\phi_{cv}$ (°)	21	
Undrained shear strength (kPa)	$30 + 6z$ (with $z$ = depth below ground level (m))	
Shear modulus (at depth, $z$ ) (MPa)	$330 \times c_u$	

Table 3.3. Index properties and design parameters for London Clay samples.  
(from CTRL, 1997)

<b>Supplier</b>	<b>Polymer product</b>	<b>Chemical description</b>	<b>Density (<math>\text{g/cm}^3</math>)</b>	<b>pH</b>	<b>Recommended dosage rates</b>
LAMBERTI S.p.A Italy	Drillam MV	Anionic polyacrylamide in liquid emulsion	1.05	6.0 – 8.0 (at 0.5% conc.)	0.2 – 0.5% (conc. in water or foam solution)
Condat Lubrifiants France	TFA 34	Anionic polyacrylamide in liquid emulsion	1.15	7.5 (at 1% conc.)	0.1 – 1.0% (conc. in water)
MBT International Switzerland	SLF P1	Water soluble liquid poly(alkylene oxide)	0.9 – 1.1	6.5 – 7.5	0.3 – 3.0% (conc. in foam solution) 0.2 – 2.0 $\text{kg/m}^3$ (volume of soil excavated)

Table 3.4. Properties of polymer conditioning agents used in testing.  
(from supplier product information).

Supplier	Foam agent	Chemical description	Density (g/cm <sup>3</sup> )	pH	Recommended concentration (%)	Recommended FER range
LAMBERTI S.p.A Italy	Foamex TR	Liquid based on anionic surfactants (alkylethoxysulphate sodium salt)	1.05 – 1.06	6.0 – 8.0 (at 1% conc.)	0.5 – 2.0	5 - 20
LAMBERTI S.p.A Italy	Foamex EC	Liquid based on anionic surfactants (sulphoric ester) with natural polymer	1.04	6.0 – 8.0 (at 1% conc.)	2.0 – 4.0	5 - 20
CONDAT Lubrifiants, France	CLB F4	Liquid based on alkylether sodium sulphate (anionic surfactant)	1.09	7.1 (at 5% conc.)	2.0 – 8.0	6 - 32
CONDAT Lubrifiants, France	CLB F4 L	Glycol based foaming agent	1.03	7.1 (at 5% conc.)	2.0 – 8.0	6 - 15
CONDAT Lubrifiants, France	CLB F4 TM	Glycol based foaming agent	1.05	7.3 (at 5% conc.)	2.0 – 8.0	6 - 15
MBT International, Switzerland	SLF30	Aqueous solution of anionic surfactant	1.02 – 1.06	6.5 – 7.5	2.0 – 6.0	7 - 12
KAO Corporation, Japan	T-7	Liquid solution of poly(oxyethylene) sulfo(alkyl) sodium salt	<i>No details given</i>	8.0	0.5 – 2.0	12 - 20

Table 3.5. Properties of foam agents used in testing.  
(from supplier's product information).

Large shear vane	
Vane length (mm)	50
Vane width (mm)	33
Shear strength range (kPa)	0 – 28
Small shear vane	
Vane length (mm)	29
Vane width (mm)	19
Shear strength range (kPa)	0 – 120

Table 3.6. Laboratory shear vane.

Foam agent	Concentration (%)	Air flow rate (Nm <sup>3</sup> /h)	FER	t <sub>25</sub> (h:m:s)	t <sub>50</sub> (h:m:s)
F4	1.5	2.1	17.9	0:14:44	0:29:20
		3.5	26.3	0:20:30	0:38:15
	2.0	2.1	21.1	0:21:10	0:42:00
		3.5	27.2	0:24:12	0:44:30
	5.0	2.1	27.7	0:33:30	1:02:00
F4 TM	2.5	2.1	7.7	0:04:45	0:11:30
		5.2	10.8	0:12:30	0:25:30
	5.0	2.1	9.5	0:13:10	0:26:30
		3.5	12.9	0:17:45	0:33:54
		5.2	15.6	0:16:48	0:31:55
F4 L	5.0	2.1	6.5	-	-
		5.2	9.0	0:07:10	0:14:50
SLF30	3.0	2.1	13.9	0:04:32	0:06:45
		5.2	21.3	0:05:48	0:08:05
TR	1.0	2.1	12.8	0:04:04	0:06:10
		3.5	16.8	0:05:54	0:08:36
	3.5	2.1	16.4	0:05:38	0:08:06
		2.1	15.6	0:05:38	0:07:59
		3.5	23.7	0:07:00	0:09:35
EC	2.5	2.1	9.9	0:03:01	0:05:04
		3.5	11.0	0:04:10	0:06:27
	4.0	2.1	13.8	0:04:55	0:07:10
T-7	1.0	2.1	16.4	0:05:10	0:07:55
	2.0	1.5	15.5	0:04:06	0:06:05
		2.1	22.9	0:04:55	0:07:10

Table 3.7. Index properties of foam agents.

Sample	Liquid limit w <sub>l</sub> (%)	Plastic limit w <sub>p</sub> (%)	Plasticity index I <sub>p</sub> (%)
E-grade + water	51	30	21
E-grade + 0.25% MV	74	34	40
E-grade + 0.50% MV	92	37	55
London Clay + water	70	27	43
London Clay + 0.25% MV	89	32	57
London Clay + 0.50% MV	121	35	86

Table 3.8. Atterberg limits of clays reconstituted with water and MV polymer.

Foam agent	Foam agent concentration (%)	Foam expansion ratio	Foam injection ratio (%)	Foam liquid injection ratio (%)
TR	1.5	20	300	15.0
			500	25.0
			600	30.0
EC	4.0	19	300	15.8
			500	26.3
			600	31.8
EC	2.5	10	100	10.0
			200	20.0
			300	30.0

Table 3.9. London Clay samples conditioned with foams.

Polymer injection ratio (%)	Foam injection ratio (%)	Foam expansion ratio	Foam liquid injection ratio (%)	Conditioner liquid injection ratio (%)
10	100	12.7	7.7	17.7
	120	12.7	9.2	19.2
	150	12.7	11.5	21.5
20	50	12.7	3.9	23.9
	100	12.7	7.9	27.9
	120	12.7	9.5	29.5
	150	12.7	11.8	31.8
30	30	12.7	2.4	32.4
	50	17.5	2.9	32.9
	80	12.7	6.3	36.3
	100	17.5	5.7	35.7
40	50	12.7	3.8	43.8

Table 3.10. London Clay samples conditioned with combined foam-polymer solution treatments.

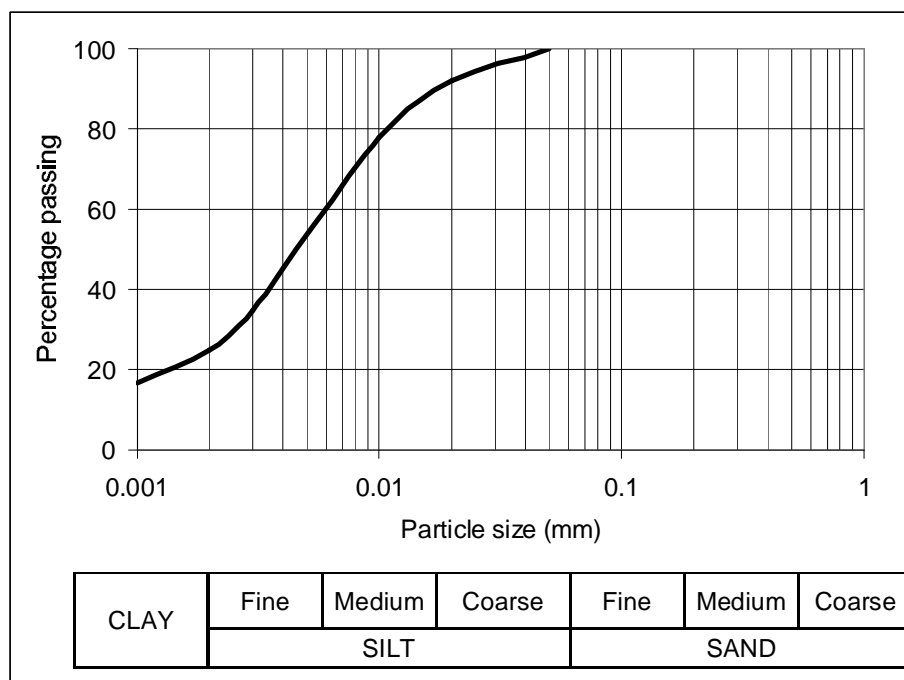


Figure 3.1. Grading curve of E-grade kaolin.

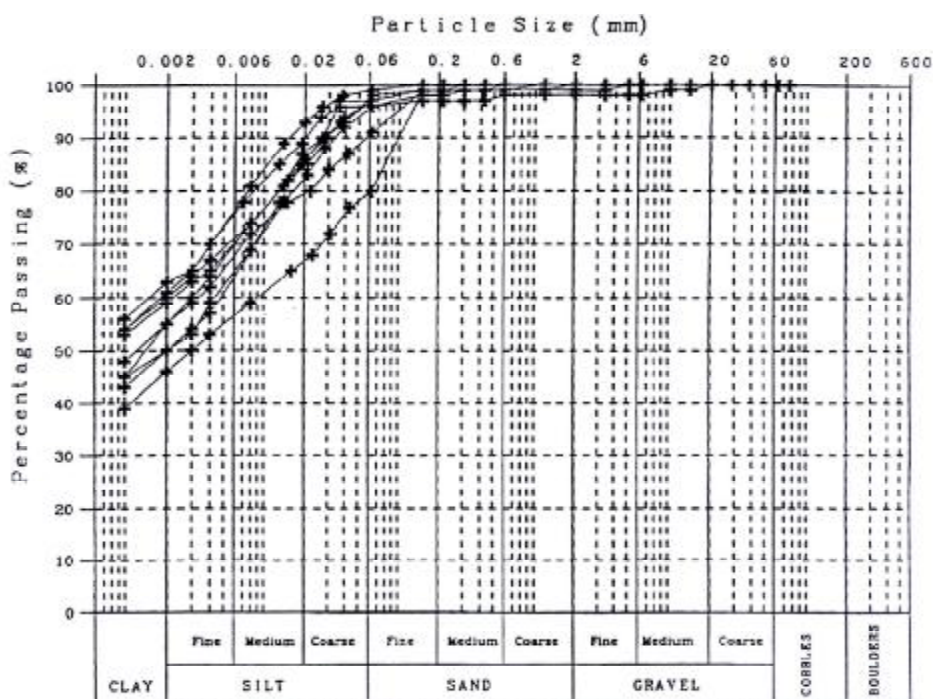


Figure 3.2. Grading curves of London Clay samples from Corsica Street shaft.  
(after CTRL, 1997)

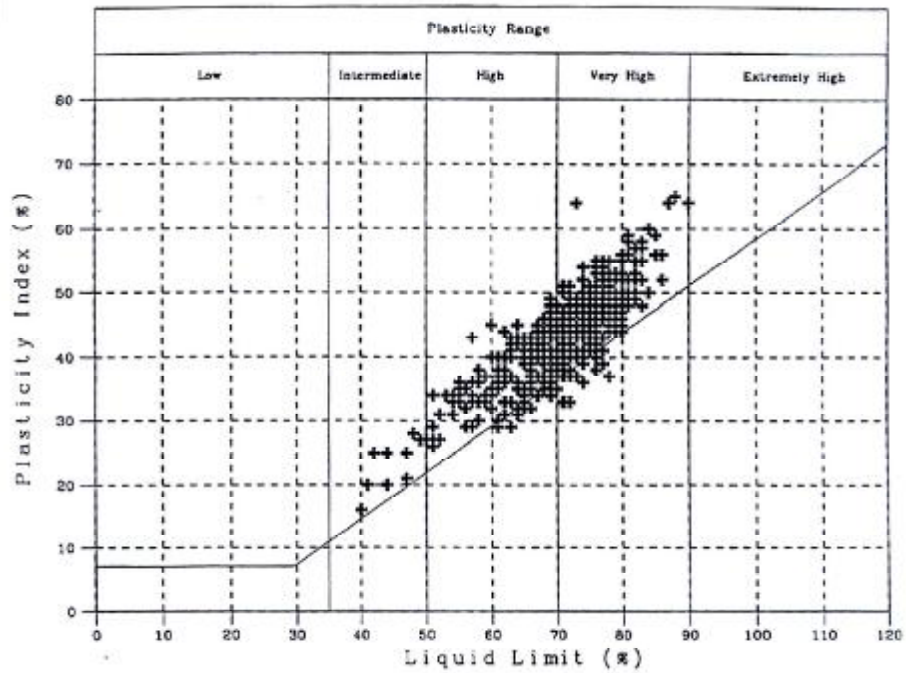


Figure 3.3. Plasticity chart for London Clay samples.  
(after CTRL, 1997)



Figure 3.4. Sieve for sampling of London Clay cuttings (mesh size approx. 25 mm).



Figure 3.5. Laboratory foam generator.



Figure 3.6. Foam generator unit with plastic beads.

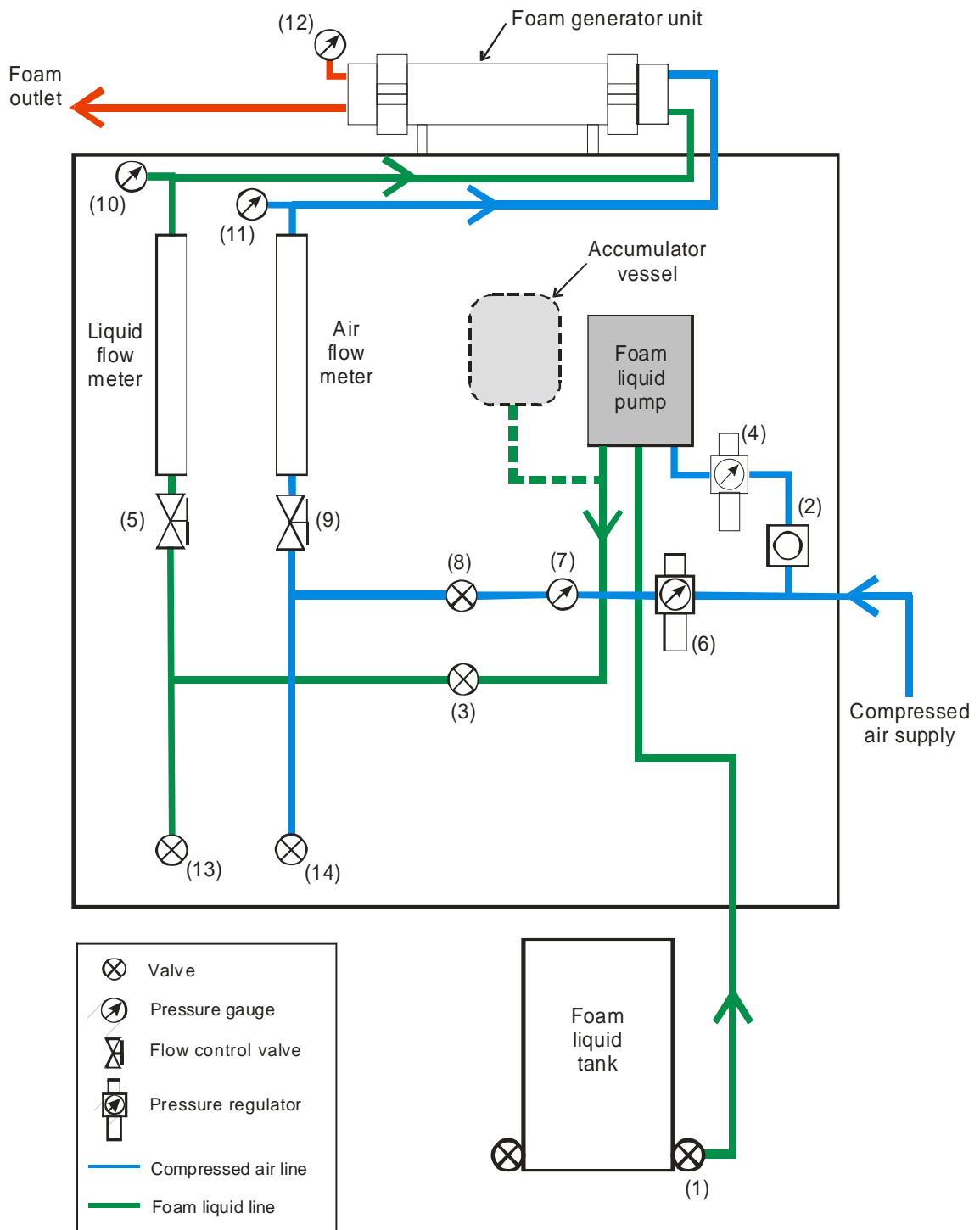


Figure 3.7. Schematic of laboratory foam generator.  
(see text for number references)



Figure 3.8. Foam sampling tube and plunger.



Figure 3.9. Large scale fall cone apparatus.

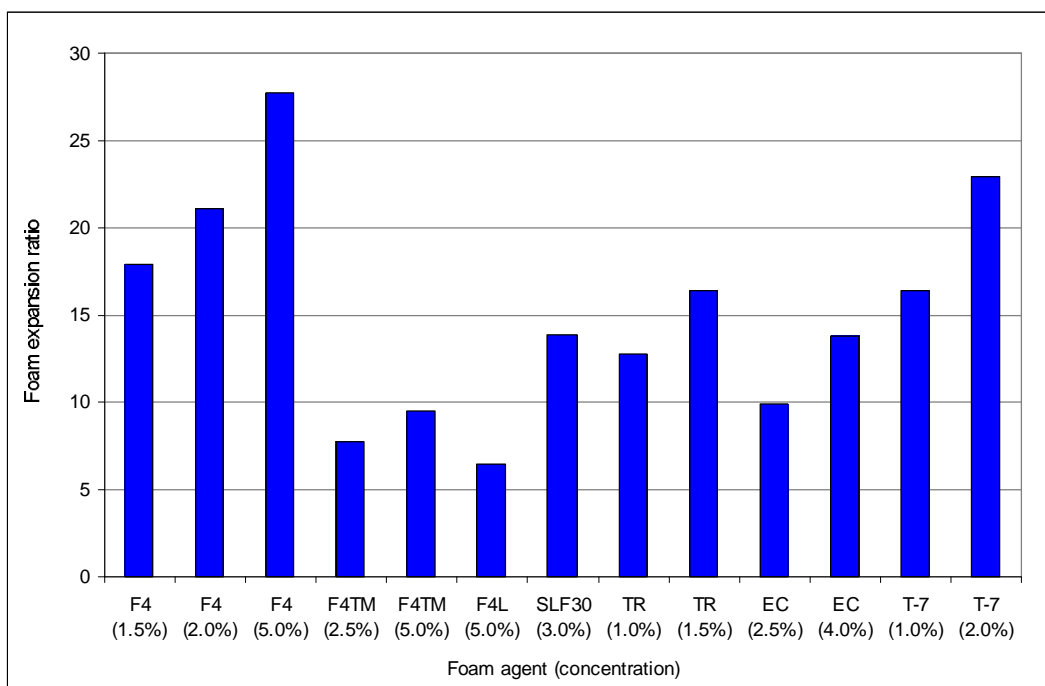


Figure 3.10. Expansion ratio of various foam agents.

(all samples produced with standard generator settings: air flow rate 2.1 Nm<sup>3</sup>/h, air pressure 1.5 bar, liquid flow rate 150 L/h)

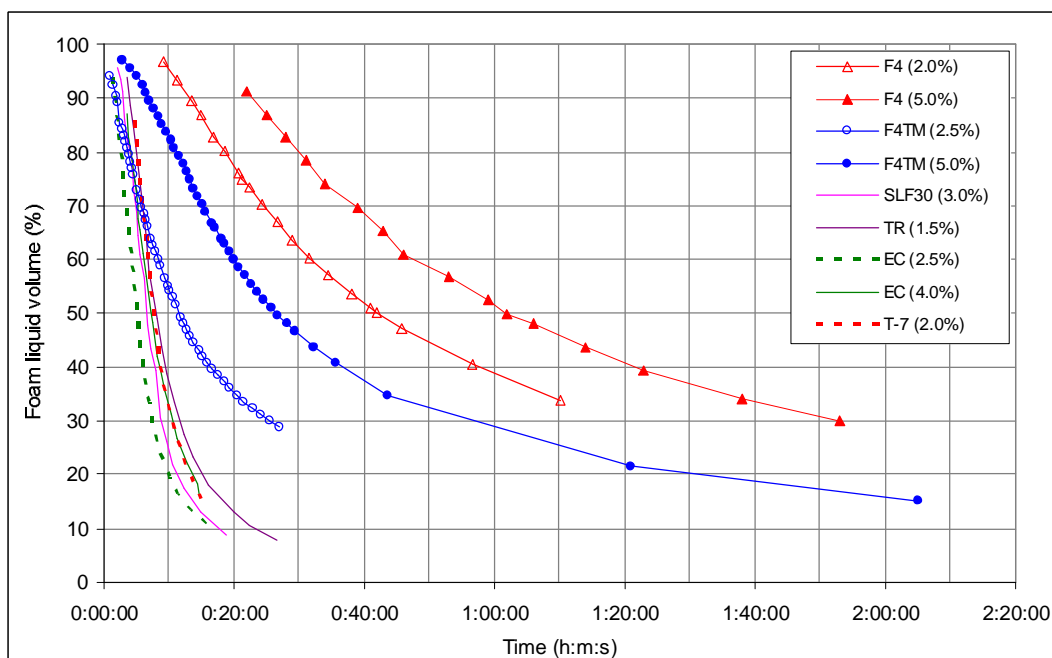


Figure 3.11. Liquid drainage over time for various foam agents.

(all samples produced with standard generator settings: air flow rate 2.1 Nm<sup>3</sup>/h, air pressure 1.5 bar, liquid flow rate 150 L/h)

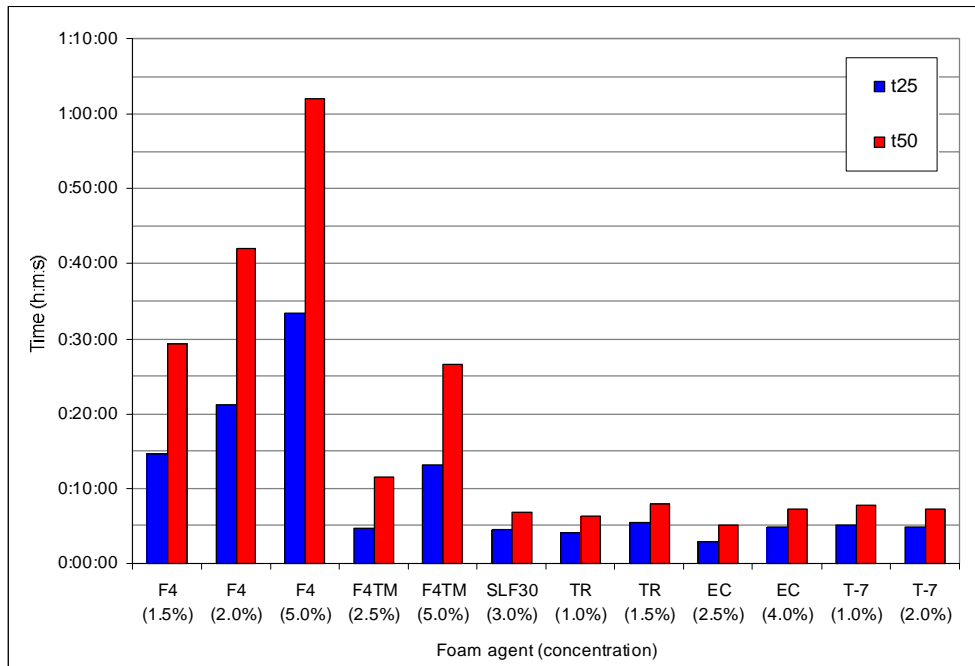


Figure 3.12. Foam liquid drainage time index values.

(all samples produced with standard generator settings: air flow rate 2.1 Nm<sup>3</sup>/h, air pressure 1.5 bar, liquid flow rate 150 L/h)

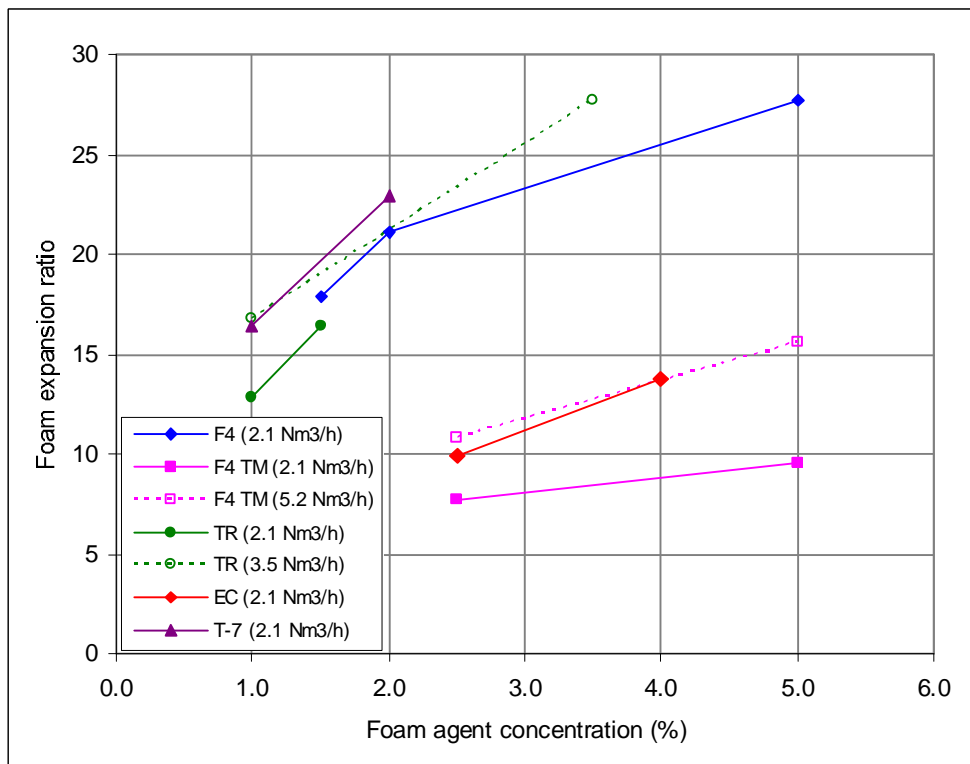


Figure 3.13. Foam expansion ratio with varying foam agent concentrations.

(all samples produced with air pressure 1.5 bar, liquid flow rate 150 L/h; air flow rate in legend)

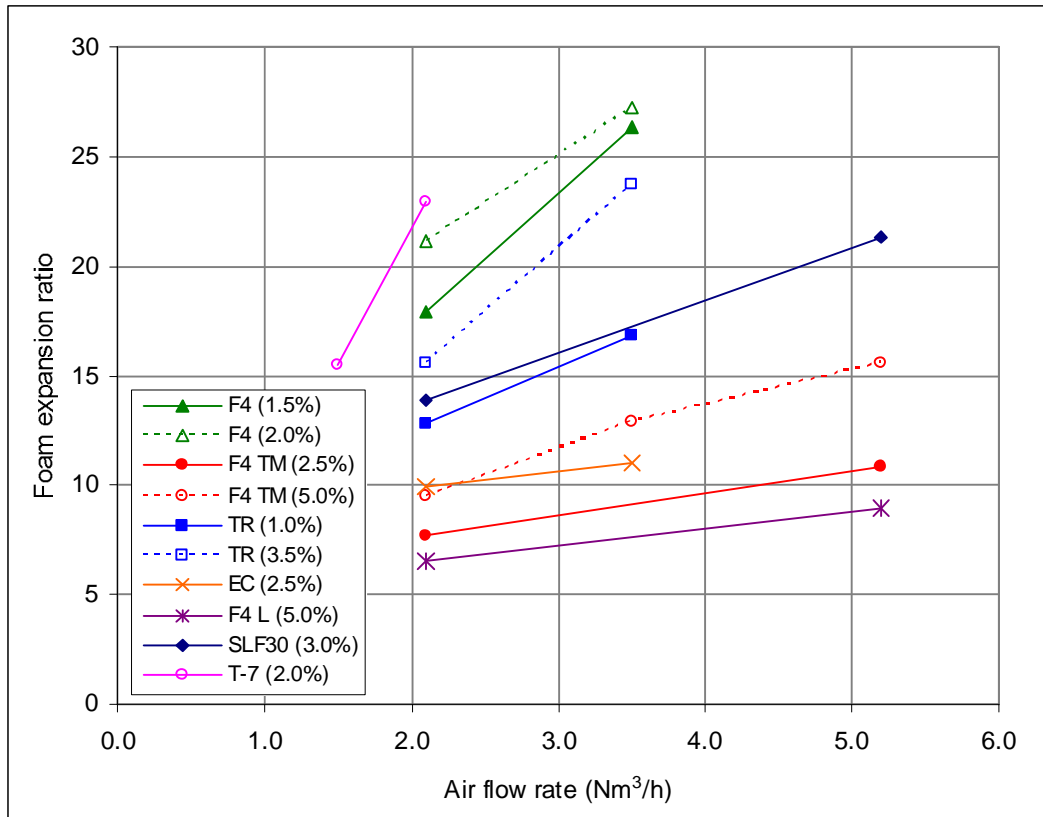


Figure 3.14. Foam expansion ratio with varying air flow rates.

(all samples produced with air pressure 1.5 bar, liquid flow rate 150 L/h; foam agent concentrations in legend).

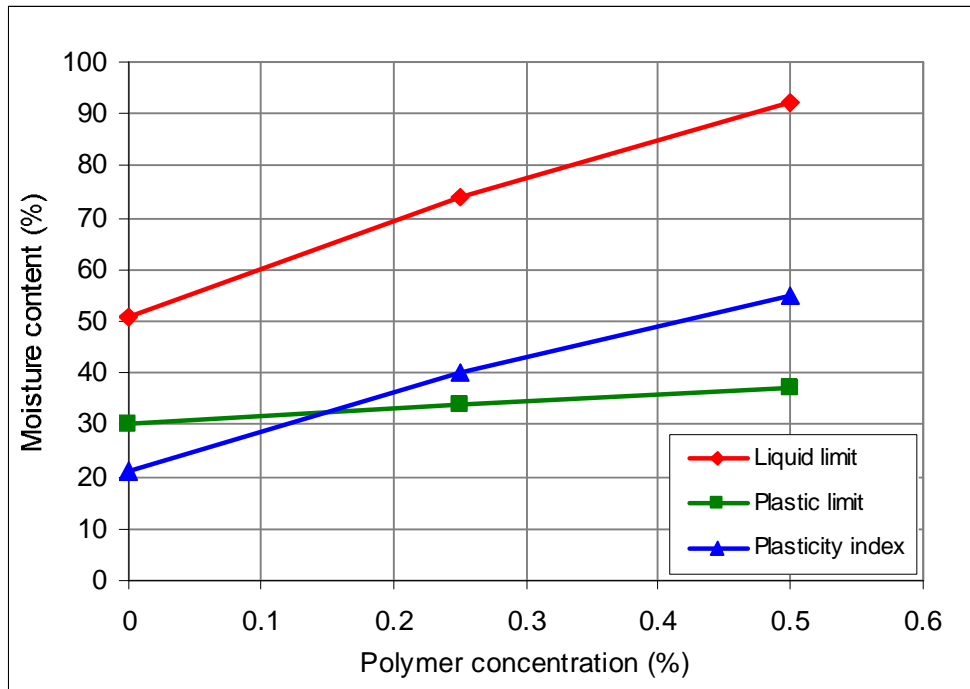


Figure 3.15(a). Atterberg limits of E-grade kaolin reconstituted with MV polymer solutions.

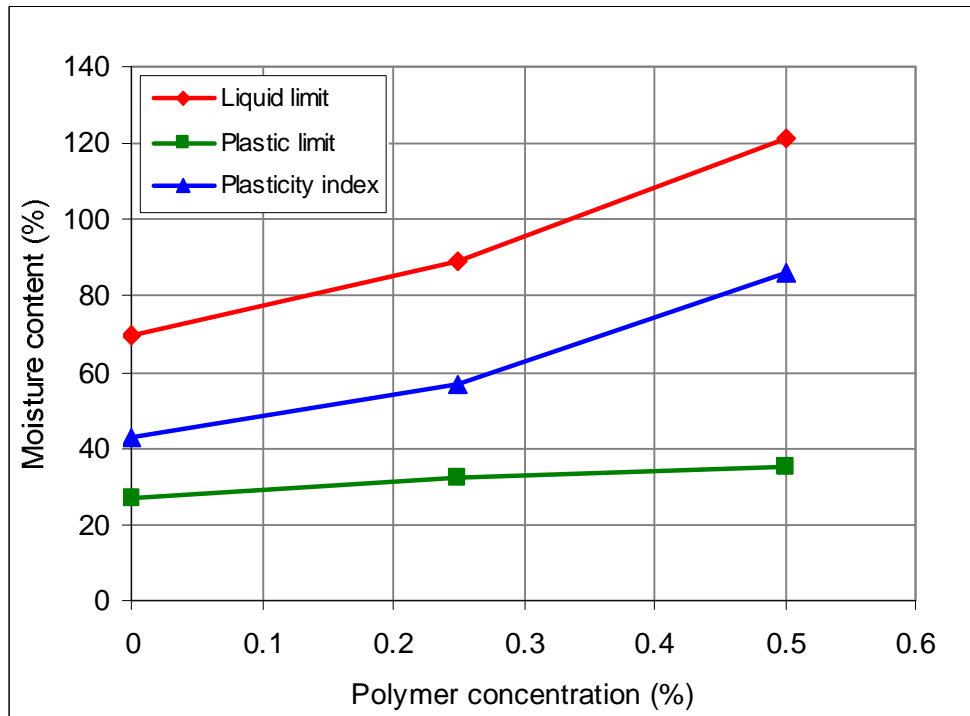


Figure 3.15(b). Atterberg limits of London Clay reconstituted with MV polymer solutions.

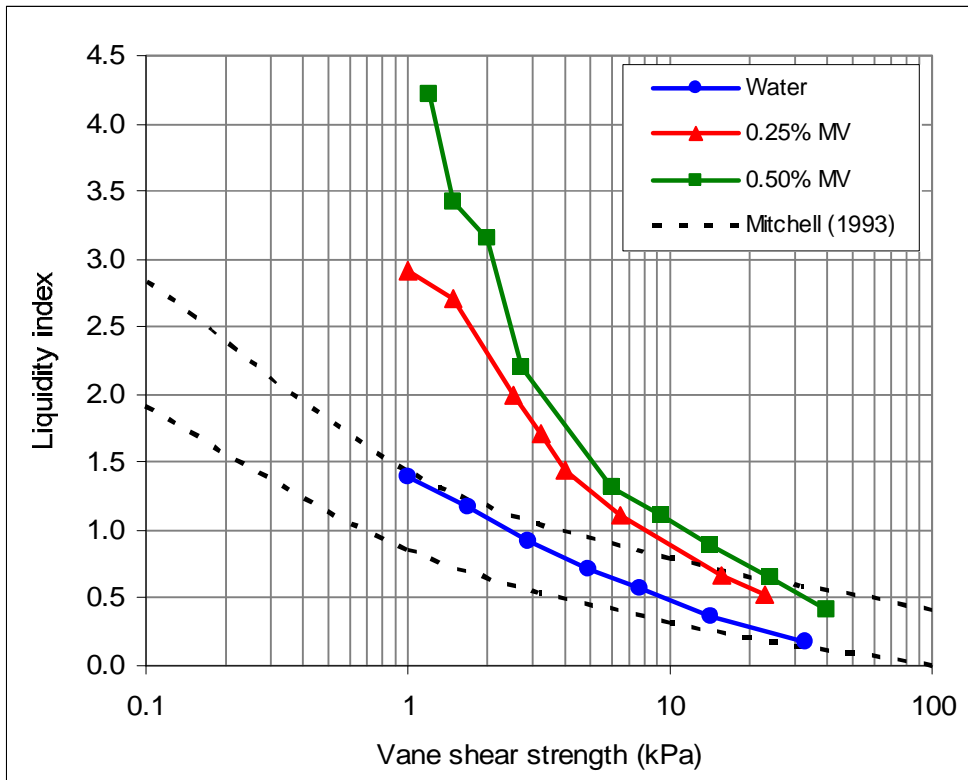


Figure 3.16(a). Undrained strength of E-grade kaolin reconstituted with water and MV polymer.

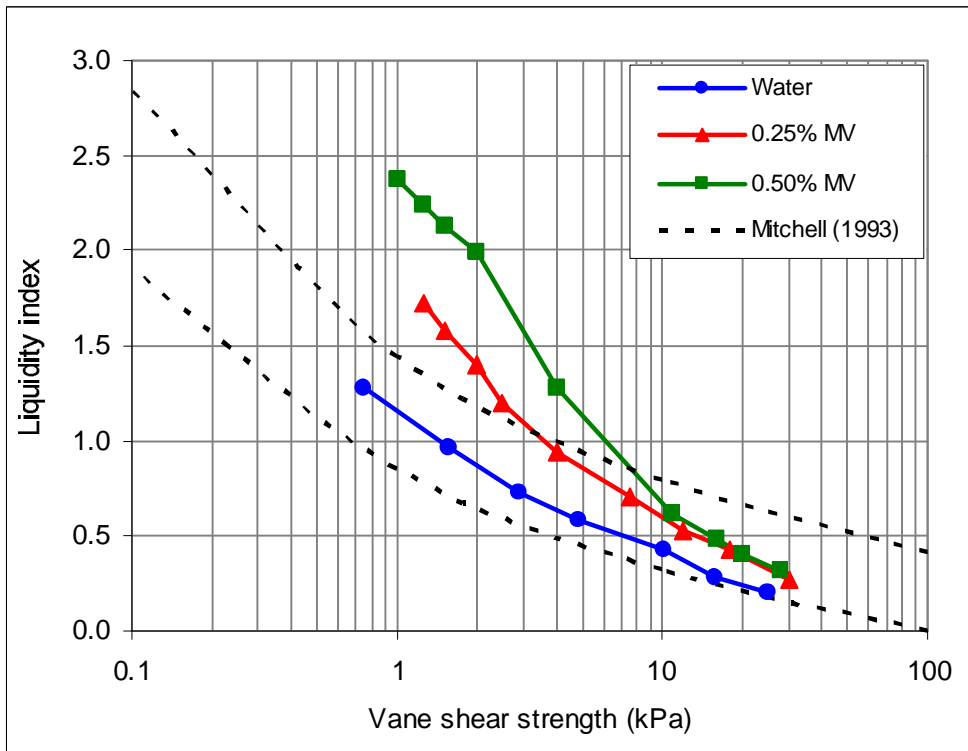


Figure 3.16(b). Undrained strength of London Clay reconstituted with water and MV polymer.

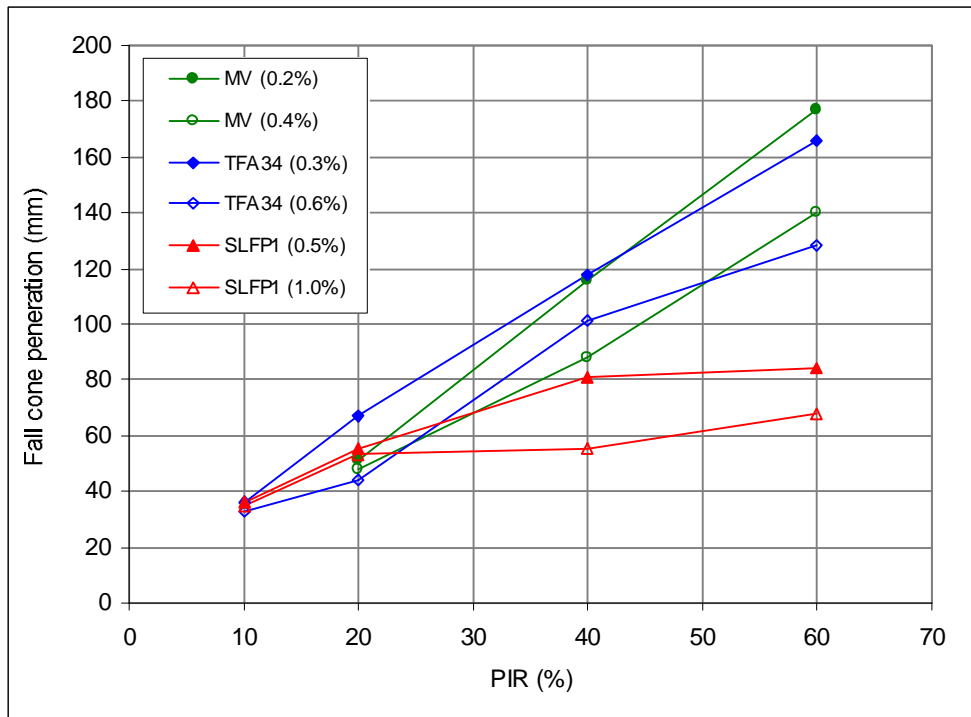


Figure 3.17(a). Large scale fall cone penetration of polymer conditioned London Clay samples.

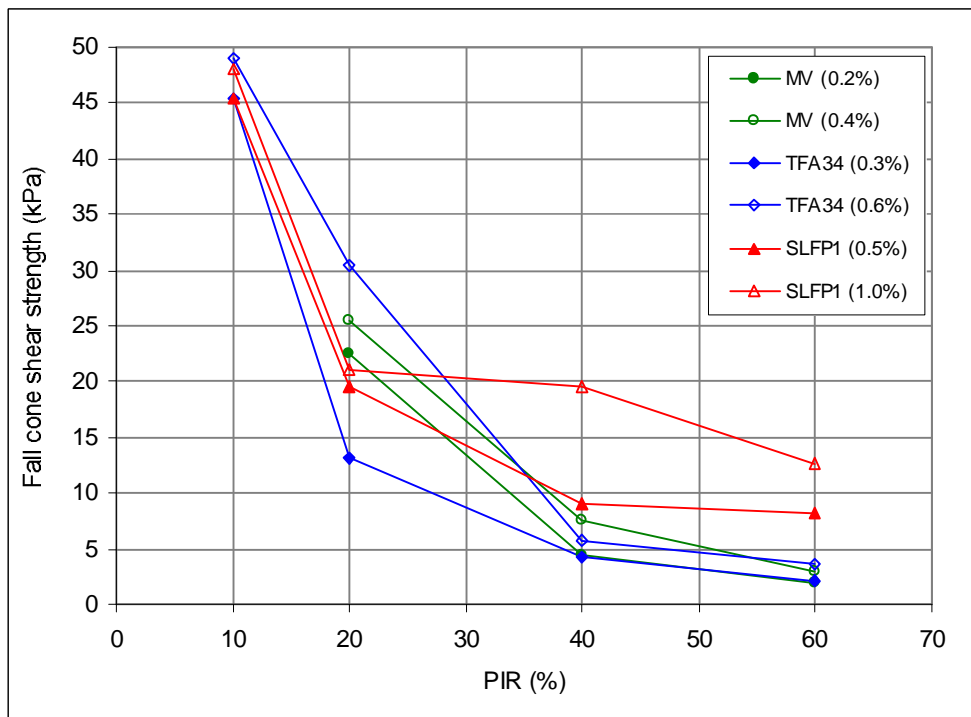


Figure 3.17(b). Undrained strength of polymer conditioned London Clay samples from large scale fall cone tests.

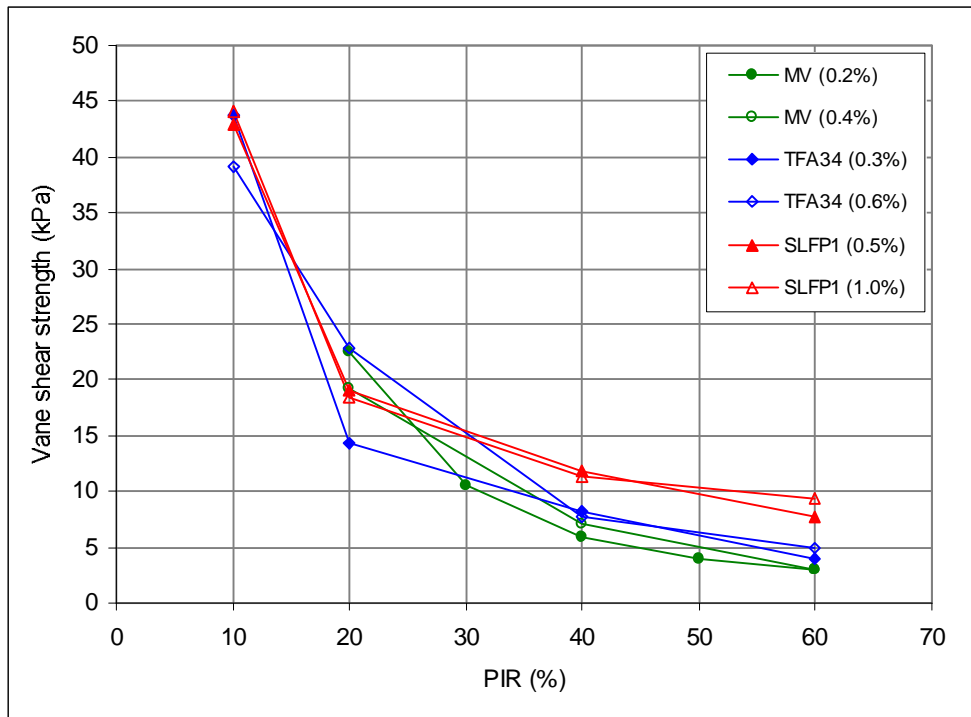


Figure 3.17(c). Vane shear strength of polymer conditioned London Clay samples.

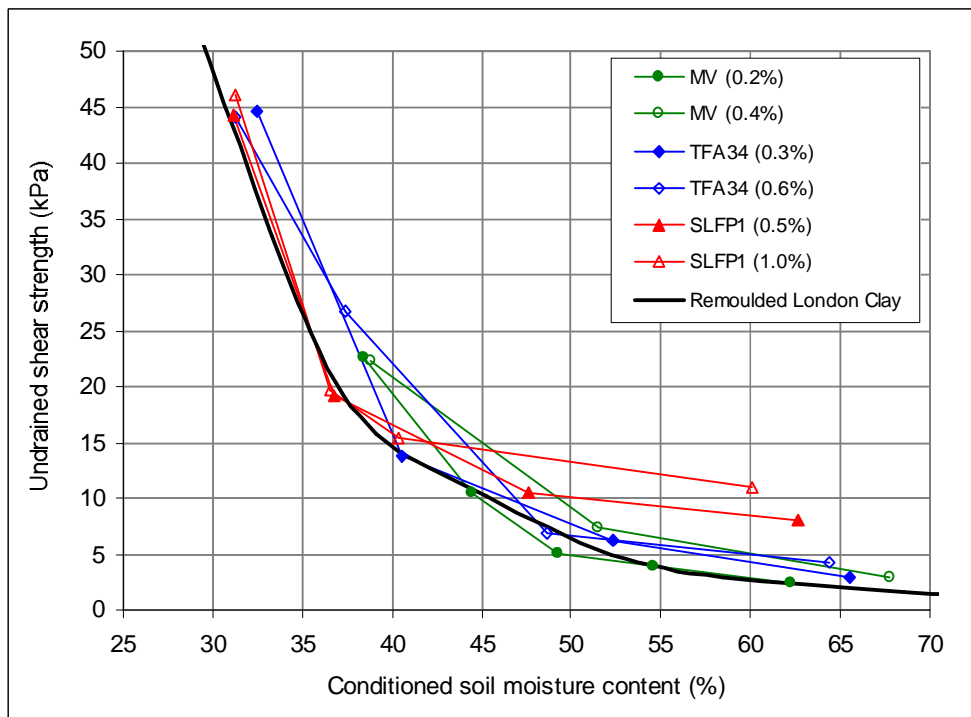


Figure 3.18. Undrained strength and moisture content of polymer conditioned London Clay samples.

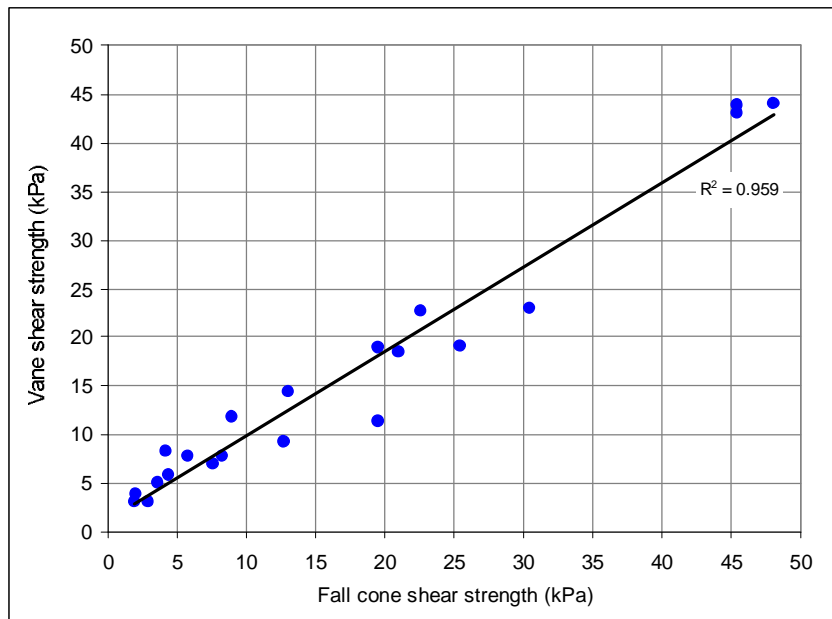


Figure 3.19. Undrained strength of polymer conditioned London Clay samples measured by vane shear and large scale fall cone tests.



(a) FIR = 0%



(b) FIR = 100%



(c) FIR = 200%



(d) FIR = 350%

Figure 3.20. London Clay cuttings mixed with foam at varying injection ratios.

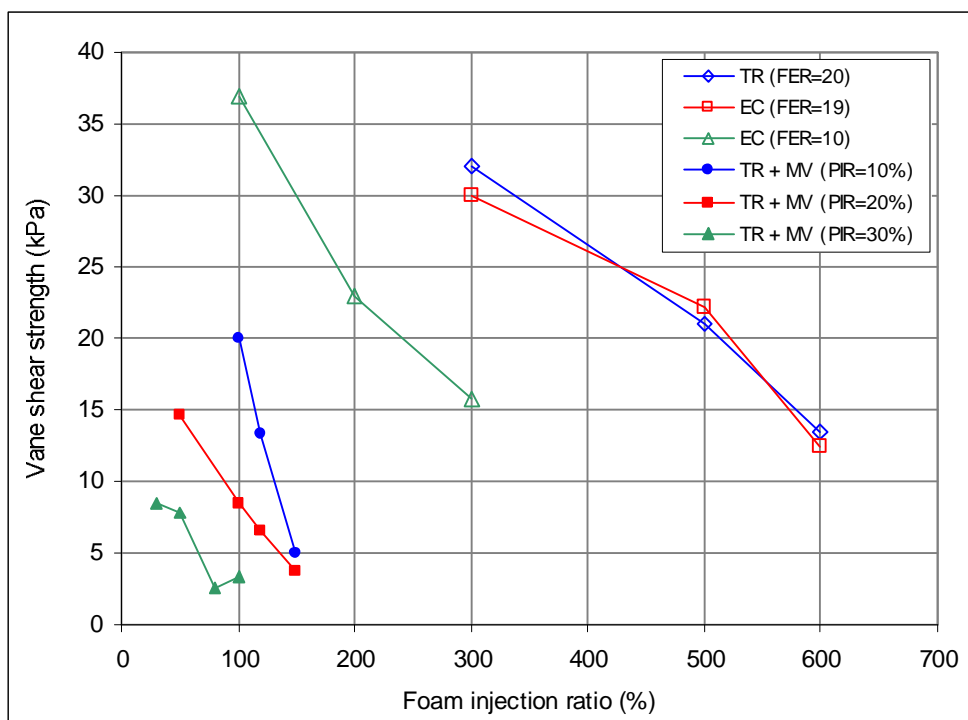


Figure 3.21. Undrained strength of conditioned London Clay samples at varying foam injection ratios.

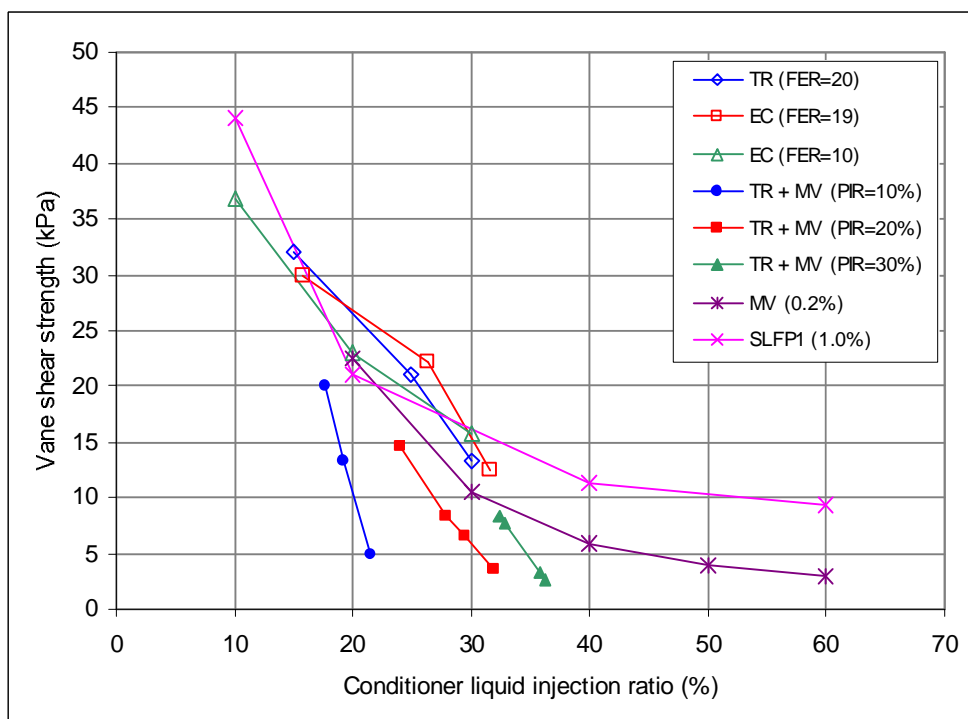


Figure 3.22. Undrained strength of London Clay samples conditioned with foams and polymers at varying liquid injection ratios.

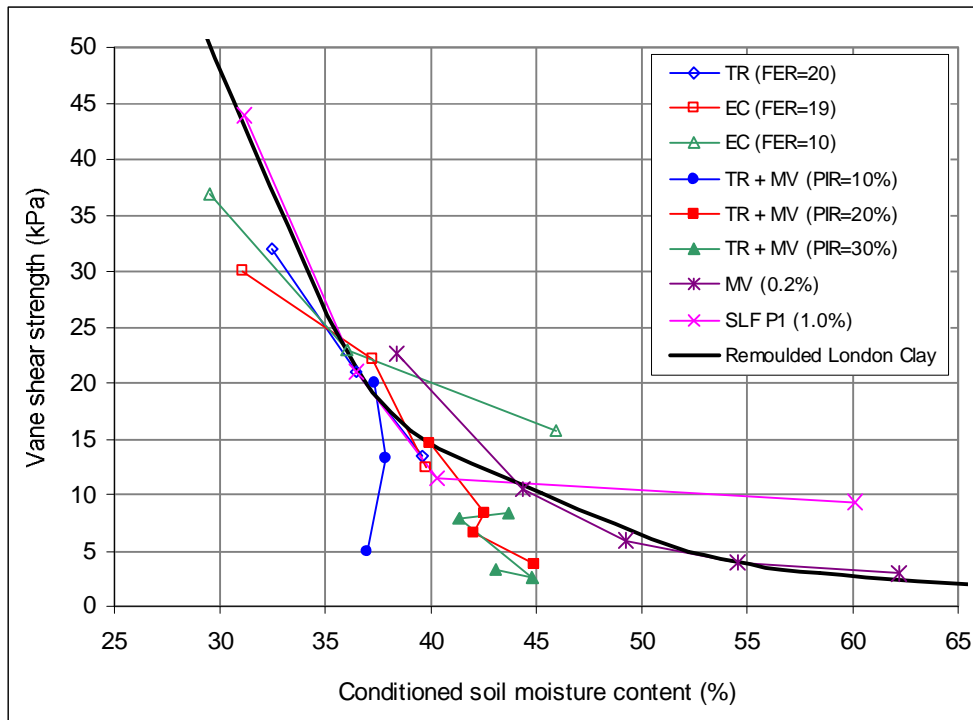


Figure 3.23. Undrained strength and moisture content of London Clay samples conditioned with foam and polymer treatments.

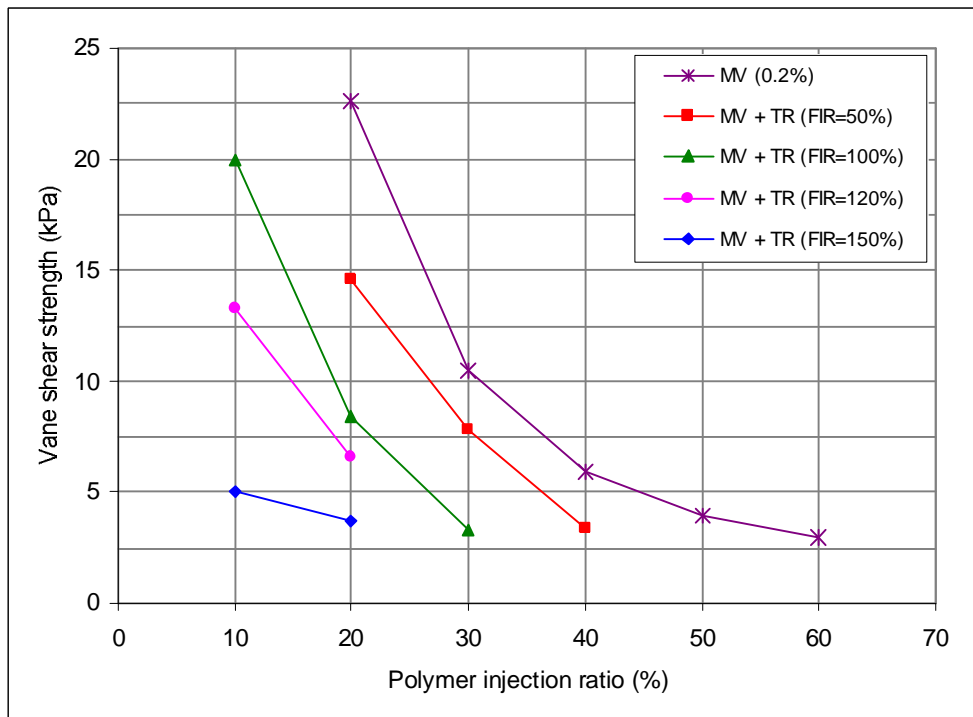


Figure 3.24. Undrained strength of conditioned London Clay samples at varying polymer and foam injection ratios.

# Chapter 4

## Model EPB machine screw conveyor system

---

### 4.1 Introduction

The main topic of the research presented in this thesis involved an investigation of EPB machine screw conveyor operations with clay soils. A novel instrumented model EPB screw conveyor system was designed and commissioned for laboratory experiments. This chapter outlines the motivation for creating the model screw conveyor, and the objectives of the tests. The design of the various components of the apparatus, including the sample containers and consolidation system, the conveyor casing tube, screw drive shaft and motor, and the model screws, are described. The various instruments installed on the system to monitor the screw conveyor operation, and the data logging system, are also described. The assembly and operation of the model screw conveyor for testing are outlined.

### 4.2 Objectives of screw conveyor study

The screw conveyor of an EPB machine has a critical role in the excavation process, and the performance depends on the soil properties and the conveyor operation. Control of the soil flow rate and the pressure dissipation along the screw conveyor are critical for control of the EPB excavation process. The design of screw conveyors for EPB machines is largely empirical, and although they are used successfully in many machines, the mechanics of operation and effects of various factors on the operation are not completely understood. The soil properties, screw conveyor geometry, screw speed and discharge outlet control influence the operation of the conveyor. The relationships between these factors and the conveyor operation in terms of the soil flow rate, pressure gradients, and screw torque have not been clearly established. An improved understanding of EPB screw conveyor mechanics could lead to improved conveyor

design and operation, and provide guidance for soil conditioning treatments to achieve soil properties that improve the conveyor performance.

Field studies of screw conveyor operations are not often performed during EPB tunnelling projects. Such studies have difficulties with variable soil conditions and characterisation of the soil properties, and the instrumentation typically installed is only sufficient for basic monitoring of the conveyor. Laboratory experiments with reduced scale model screw conveyors allow investigations under controlled conditions with uniform samples of known properties, and with more extensive instrumentation to monitor the conveyor operation. Some studies of EPB screw conveyors in the field and with laboratory model conveyors were discussed in Section 2.6. Theoretical models describing the mechanics of screw extruders and EPB screw conveyors have been developed, also discussed in Section 2.6. However, much of the previous research of EPB screw conveyors has studied the operation with sand conditioned with foam. Screw conveyor operations with clay soils and effects of different conditioning treatments on the performance have received little attention. Also, relatively little experimental data has been obtained to compare with the predictions of theoretical models describing screw conveyor operations.

The model screw conveyor commissioned for this research represents an approximate 1:10 scale of a full scale EPB machine screw conveyor. The system includes extensive instrumentation and allows variable operating conditions for experiments investigating the mechanics of the screw conveyor operation. The instrumentation includes Cambridge type load cells to measure normal stresses and shear stresses acting on the conveyor casing, pore water pressure transducers in the casing, a torque cell on the screw drive shaft, and instruments to monitor the sample pressure and the soil flow rate in the conveyor. The model conveyor can be operated with variable sample pressures, screw speeds, and discharge outlet conditions, and screws of different geometry can be installed. Experiments were performed with consolidated kaolin samples to investigate effects of varying operating conditions on the conveyor performance. Tests were also performed with compacted conditioned natural clay soils, prepared with different conditioning treatments to investigate effects on the conveyor performance.

### **4.3 Cambridge model EPB screw conveyor**

The general arrangement and operation of the model EPB screw conveyor system is described below. The design of the various components of the system is described in the following sections, and details of the instrumentation are given in Section 4.4.

#### **4.3.1 General arrangement**

The model screw conveyor system consists of a sample container mounted in a load frame, with the screw conveyor connected horizontally to a flange near the base of the container. The conveyor is supported by a frame and consists of a cylindrical casing tube with the screw rotating inside, driven through a drive shaft by a variable speed electric motor. The screw is a separate component of the system, allowing screws of different geometry to be installed in the conveyor. When assembled, the sample container is pressurised by a vertical load applied through a piston and jack in the load frame, and the screw extends from the conveyor casing into the soil in the container. During operation, the screw extracts soil from the container and carries it along the conveyor to the discharge outlet. The discharge outlet has a removable reduction valve to create restricted or unrestricted discharge conditions. The general arrangement of the screw conveyor is shown in Figure 4.1, and photographs of the system assembled for a test are shown Figure 4.2.

Some general dimensions of the system are shown in Figure 4.1. The model screw conveyor was designed to represent an approximate 1:10 scale of a typical EPB machine screw conveyor. Medium to large diameter EPB machines typically have a screw conveyor with a length in the range of about 8 to 12 meters, and a diameter of about 0.8 to 1.2 meters. Based on these typical full scale dimensions, the model screw conveyor was designed with an internal diameter of 108 mm and a length of 1050 mm when connected to the container flange.

The screw conveyor casing is instrumented at four sections along the length, as shown in Figure 4.3. Two load cells and a pore water pressure transducer are mounted in the casing at each section. The eight Cambridge type load cells measure the total normal stress and shear stress acting on the internal surface of the casing. Two load cells are installed at each section to measure the shear stress components parallel and perpendicular to the screw axis. The screw drive shaft is instrumented for direct measurement of the torque provided by the motor to rotate the screw. The pressure applied to the soil in the container is monitored. The sample volume change is measured through the displacement of the piston, which lowers into the container as the soil is

extracted by the screw. The instrumentation scheme provides detailed measurements of the screw conveyor operation through the total pressures and pore water pressures acting on the casing, the casing shear stresses, the effective stresses, the screw torque, and the soil flow rate through the conveyor. These measurements provide data for investigations of the screw conveyor mechanics with the different soil samples and conveyor operating conditions.

### **4.3.2 Sample containers and consolidation system**

The sample container consists of two cylindrical steel tubs, which bolt together at flanges as shown in Figure 4.1. The assembled container bolts to a steel base plate, and is mounted in a load frame. The lower section of the container has a circular hole in the wall, with a flange for connection of the screw conveyor. When the conveyor is assembled, the screw extends through the hole into the container, and the soil enters the conveyor through this connection. Rubber o-rings are included in the bolted flange connections to seal the assembled containers and conveyor casing. The soil samples are pressurised in the container through a piston, with a vertical load applied by a jack mounted in the load frame. During the conveyor operation, the piston lowers into the container as the soil is extracted by the screw, with the jack extending to maintain the pressure on the sample.

Dimensions of the containers and piston are shown in Table 4.1. The container dimensions were designed based on the expected conveyor discharge rates, so that samples of sufficient volume could be prepared for the tests. The ratio of the total container volume to the screw conveyor channel volume is approximately 18, although during the tests the sample volume passing through the conveyor was about 6 to 10 times the conveyor volume. The connection flange has the same internal diameter as the conveyor casing. The piston diameter was designed to give a small clearance to the container walls, and the depth of the piston was designed to prevent it from jamming as it lowered into the container during the test. To minimise friction, an o-ring seal was not used between the piston and container. The containers were constructed from steel tube sections, and machined to the final dimensions with a tolerance of 0.1 mm. The container and piston pieces were manufactured by PLC Hunwick Ltd, Halstead, UK.

The jack used to apply the load to the piston and pressurise the sample was connected to a nitrogen gas cylinder, which had a maximum pressure of 2500 psi. With this system, the maximum pressure that could be applied to the sample was approximately 250 kPa, including a 5 kPa pressure from the mass of the piston. The pressure supplied to the jack was controlled with

a regulator in the gas line, and was monitored with a dial gauge accurate to 5 psi, and also with a pressure transducer connected to the jack.

The container and loading system was used as the consolidation apparatus for kaolin samples, discussed in Chapter 5. A blanking plate was bolted to the conveyor connection flange during consolidation. The base plate of the container includes drainage holes, and drainage is also provided at the top of the sample through the clearance between the piston and the container walls, allowing two-way drainage during consolidation. A drainage layer consisting of filter paper, a porous vyon sheet, and wire mesh was used at the top and bottom of the kaolin slurry, to allow uniform drainage of water from the sample.

### **4.3.3 Conveyor casing**

The screw conveyor casing was produced from a steel tube, machined to meet the requirements of the conveyor design. Flanges were welded to the ends of the casing tube, for connections to the container flange and the screw drive shaft assembly. A circular hole was bored through the casing tube at one end for the discharge outlet. A short section of tube was welded around the hole in the casing, with a thread to allow connection of a valve to the discharge outlet. At each of the four instrumented sections along the conveyor, the casing has two ports for mounting load cells and a hole for inserting a pore water pressure transducer. A drawing of the conveyor casing layout is shown in Figure 4.3, and the dimensions are shown in Table 4.2.

The steel tube used for the conveyor casing was supplied by M/K Wheeler Ltd, UK. Machining of the tube was performed in the workshops at Cambridge University Engineering Department. The casing was made from a high quality cold finished steel tube, with a minimum yield stress of 360 MPa and closely controlled tolerances on the dimensions. The tube was supplied with the internal diameter honed to a tolerance of 0.1 mm and the straightness of the tube was within 1:1000. With the 9.5 mm wall thickness, the conveyor casing can withstand internal pressures well in excess of those expected during the tests. The casing tube has a length of 1000 mm, and when connected to the container flange the total length of the conveyor from the internal wall of the container to the end of the casing is 1050 mm.

The discharge outlet diameter is approximately equal to the pitch of the screw initially used with the conveyor. The 85 mm internal diameter allowed connection of standard size fittings used to connect the reduction valve to the discharge outlet. With this design, two discharge conditions

can be created at the end of the conveyor. Without the valve connected, the outlet was 'unrestricted', with the soil discharging through the 85 mm diameter tube of 55 mm length welded to the casing. A ball valve with 50 mm internal diameter can be connected to the discharge outlet through a reduction fitting screwed into the outlet. The discharge outlet and conveyor casing can be sealed by closing the valve. With the valve open, a 'restricted' discharge condition was created with the soil flowing through the casing outlet and the reduction piece and valve with a diameter of 50 mm and length of 115 mm. The geometry and dimensions of the unrestricted and restricted discharge conditions are shown in Figure 4.4.

A drawing of the instrumented section of the conveyor casing is shown in Figure 4.5. The two ports for mounting the load cells are located in the lower half of the casing, with centres at 45° to the vertical axis. This location was chosen to ensure contact between the soil and the load cells if the conveyor was not completely full during operation. The ports were welded to the casing tube and machined to the final dimensions required for a close fit of the load cell housings, and to the height required so the active face of the load cells is coincident with the internal surface of the conveyor casing. The surface of the ports includes tapped holes for the screws connecting the load cell housings to the conveyor casing, and an o-ring groove to seal these connections. The instrumented sections also include a tapped hole through the casing on the centreline of the section to insert a pore water pressure transducer. The four instrumented sections were spaced evenly along the casing at centres of 225 mm, with the first section located as close as possible to the start of the conveyor, and the fourth section as close as possible to the discharge outlet. The locations of the instrumented sections along the conveyor are shown in Figure 4.3.

#### **4.3.4 Screw drive shaft**

The screw drive shaft is assembled with a number of pieces that fit together between the conveyor casing and the motor to make the mechanical connections to transfer the torque driving the screw. The drive shaft assembly consists of two steel plates bolted to the end flange of the conveyor casing which house the shaft seals and bearing, the drive shaft piece, and a flexible coupling connecting the drive shaft to the output shaft of the motor. An adaptor piece fits into the shaft of the screw and through the conveyor end plate into the drive shaft tube, with a shear pin connecting the two pieces. A drawing of the assembled drive shaft is shown in Figure 4.6, and the components are described further below. The components of the drive shaft were machined from mild steel in the workshops at Cambridge University Engineering Department.

The drive shaft piece was machined from a cold finished steel tube section with a yield stress of 390 MPa, supplied by M/K Wheeler Ltd. The steel tube supplied had an internal diameter (I.D.) of 25.4 mm and wall thickness 7.9 mm, with tolerances of  $\pm 0.2$  mm and a straightness within 1:1000. Drawings of the drive shaft are shown in Figure 4.7, and a photograph of the shaft with the bearing and slip ring pieces (described later) is shown in Figure 4.8. A shoulder was welded around one end of the drive shaft, and at this section the tube was machined to an outer diameter (O.D.) of 40.0 mm for mounting the shaft bearing. Another section of the drive shaft was machined to an O.D. of 29.0 mm to give a wall thickness of 1.8 mm. This section was instrumented with strain gauges for measurement of the torque transferred through the shaft as described in Section 4.4. A length of the other end of the drive shaft was machined into a hexagonal section to fit into the coupling connecting to the motor shaft.

The bearing for the drive shaft was a double row angular contact bearing, with an I.D. of 40 mm and O.D. of 80 mm, fitted with rubber seals for protection from contamination. The bearing was manufactured by SKF and supplied by BSL Ltd, UK. A double row angular contact bearing was used as these can accommodate axial loads in both directions, as expected during operation of the screw conveyor. The choice of the bearing was dictated by the internal diameter required to fit onto the drive shaft tube, and the load ratings for bearings of this size were greater than the estimated radial and axial loads transferred through the screw conveyor shaft. The bearing was mounted against the shoulder at one end of the drive shaft, and held in place by a circlip in a groove around the shaft behind the bearing.

The drive shaft assembly includes two steel plates bolted to the end flange of the conveyor. The first plate acts as a blanking plate at the end of the conveyor, with a circular hole through the centre to allow the connection between the screw shaft inside the casing and the drive shaft. The end plate houses a rubber lip seal and two o-rings around the central hole, which form seals around the screw shaft adapter piece where it leaves the conveyor casing. The second plate in the assembly has a cut-out section to house the shaft bearing mounted on the drive shaft. As shown in Figure 4.6, the end plates bolted to the conveyor casing flange support the drive shaft and bearing, and locate the drive shaft so the centreline is coincident with the axis of the conveyor casing. This aligns the assembled drive shaft with the shaft of the screw inside the conveyor.

The connection between the assembled drive shaft and the screw shaft inside the conveyor is made through a shaft adaptor piece. The screw shafts are made from hexagonal bore steel tubes,

and the drive shaft tube has a circular cross section. The shaft adaptor piece was machined with a hexagonal section at one end to fit into the screw shaft, and a circular section at the other end to fit into the drive shaft tube. The adapter piece was fixed into the screw shaft by a steel pin, and the circular section of the piece passed through the hole in the conveyor end plate and into the drive shaft tube. The rubber seals in the end plate provide a seal around the shaft at this point to seal the conveyor casing.

The connection between the drive shaft and the shaft adaptor piece was made with a transverse shear pin through the two pieces. Hardened steel dowel pins, supplied by Ondrives Ltd UK, were used as shear pins. Shear pins of 6.0 mm diameter were used, which had a quoted double shear strength of 56 kN and were expected to fail at a torque of about 1400 Nm, allowing a factor of safety for the strength of the pins. This maximum shear pin capacity exceeds the torque available from the motor, and these pins performed successfully during the tests, although some failures occurred at lower than expected torques.

The screw drive shaft is connected to the output shaft of the motor through a flexible coupling. The coupling used was supplied by Ondrives Ltd UK. The coupling comprises two cast iron hubs connected with a flexible polyurethane piece, which compensates for small axial, radial and angular misalignments in the drive shaft assembly. One hub of the coupling was bored with a hexagonal section to fit the end of the drive shaft, and the other hub was bored to match the keyway on the shaft of the motor.

The assembled drive shaft provides the mechanical connection between the screw shaft and the motor. The torque is transferred from the motor through the flexible coupling to the drive shaft, which rotates in the shaft bearing. The shear pin connection between the drive shaft and the shaft adaptor piece transfers the torque to the screw shaft to drive the screw inside the conveyor casing. The assembled drive shaft with the end plates, bearing, flexible coupling and slip ring is shown in Figure 4.9.

#### **4.3.5 Model screws**

Two screws were designed and manufactured for the model conveyor. The two screws have similar dimensions but were designed with a different pitch of the screw flights for experiments investigating effects of screw geometry on the conveyor operation. The pitch of the screw influences the soil flow rate and pressure gradient along the conveyor, as discussed in Section 2.6

and shown in Figure 2.23. Screws used in extruders typically have helix angles in the range  $\phi_f = 15 - 25^\circ$ , corresponding to pitch ( $t$ ) to diameter ( $D_f$ ) ratios of  $t/D_f = 0.84 - 1.46$ , with  $\tan \phi_f = t/\pi D_f$  (Darnell and Mol, 1956; Goodson, 1959; Burbidge and Bridgwater, 1995). Based on details of EPB tunnelling machine screw conveyors reported in some case studies, the screw geometry is typically in a similar range to that for extruders (e.g. Peron and Marcheselli, 1994; Maidl *et al.*, 1996; Talmon and Bezuijen, 2002). The two screws for the model conveyor were designed with geometries based on this typical range. The specific dimensions were chosen to suit the length and diameter of the model conveyor, and to give a significant difference in the pitch to measure the effects on the conveyor operation.

The screws were manufactured to the specified designs by Universal Augers Ltd, UK. The screws have a central shaft of a hexagonal bore mild steel tube, with the screw flights made from mild steel welded to the shaft. The flight surfaces were hard faced to reduce wear of the screws during testing. The dimensions of the two screws were within a small range of the design values, and are shown in Table 4.3 and Figure 4.10. The 1200 mm length of the screws was designed to leave a 150 mm length, equivalent to one to two screw flights, extending into the sample container when assembled. The screw shaft was a standard section available from the supplier, with suitable dimensions for the drive shaft connection and the screw channel depth in the conveyor casing. The outer diameter of the screw flights was designed to provide a nominal 3 mm clearance between the flights and the conveyor casing, so the screw would fit inside the casing allowing for tolerances on the dimensions. The shorter pitch screw (No. 1) has a total of 15 flights along the shaft, and the longer pitch screw (No. 2) a total of nine flights. The average pitch and flight helix angles for the model screws are shown in Table 4.3, and are similar to the typical range of screw geometries discussed above.

#### **4.3.6 Screw motor**

The model screw conveyor is driven by a variable speed electric motor and gearbox mounted on the conveyor frame and connected to the screw drive shaft through the coupling, as shown in Figure 4.1. The motor was selected based on design requirements of a maximum torque of about 600 Nm, with an output speed range of about 5 to 30 rpm. This range of screw speeds corresponds to those typically used for full scale EPB machine screw conveyors.

The combined electric motor and gearbox used was a Varmeca model three phase induction motor integrally mounted with a parallel gearbox, supplied by Leroy Somer Ltd, UK. The

specifications of the motor and gearbox are shown in Table 4.4. The electric motor has a power of 2.2 kW and a rated torque of 9.4 Nm. With the reduction gearbox ratio of 62.3, the motor provides an output torque of 585 Nm over a speed range of 5 to 35 rpm. The speed of the motor is controlled by an inverter unit, with a dial gauge used to adjust the motor speed to settings in the range 15 to 100%. The rated torque is available over the full speed range, with a maximum 3% variation of the motor speed resulting from fluctuations in the output torque. The maximum overload torque is approximately 1050 Nm for motor speed settings of 15 to 60%, reducing to approximately 875 Nm for speed settings from 60 to 100%. A second output shaft extension was provided at the back of the motor to allow rotation of the drive shaft and screw by hand. An RFI filter was included in the inverter unit to reduce interference with the screw conveyor instruments, generated by the inverter controlling the frequency of the power supply to control the motor speed.

A calibration was performed with the motor running under no load to relate the speed control dial gauge setting to the rotational speed of the output shaft. The calibration shown in Figure 4.11 is linear in the forward and reverse directions over the full range of motor speeds for dial gauge settings of 20 to 100%. The 20% speed setting corresponds to the minimum speed of the motor and gives an output speed of 5 rpm through the reduction gearbox. Below this setting the speed of the motor could not be accurately controlled due to the low operating speed required of the motor. For the screw conveyor tests, the minimum screw speed of 5 rpm was therefore used with the dial gauge at the 20% setting, with higher screw speeds of 15 and 25 rpm achieved with the dial gauge set at 45% and 70% respectively.

## **4.4 Screw conveyor system instrumentation**

The model screw conveyor system is extensively instrumented to monitor the operation during experiments. The general arrangement of the instrumentation was described earlier, and details of the design and calibration of the various instruments and the data logging system are discussed in the following sections.

### **4.4.1 Screw conveyor load cells**

#### **4.4.1.1 Design of load cells**

The Cambridge-type load cells installed in the model screw conveyor were designed based on similar instruments previously used in geotechnical research at Cambridge. The design and some

other applications of this type of load cell are described by Bransby (1973) and Bond (1989). In the screw conveyor, eight load cells were used to measure the total normal stress and shear stress acting at points on the surface of the conveyor casing. The load cells and their housings were specifically designed for the model screw conveyor, and were manufactured by Cambridge Insitu Ltd, UK.

The instruments consist of four main components, namely the load cell, a housing frame, a load platen, and a cover plate. An exploded view of these components is shown in Figure 4.12. These pieces are assembled and mount into the ports at the instrumented sections of the conveyor casing, as shown in Figure 4.13. The platen acts as the active face of the load cell, and is fixed to the housing frame through a hot-bonded rubber seal around the edges of the platen. The load cell fits inside the frame, with two screws fixing the top of the load cell to the platen. The cover plate fits over the base of the frame, with screws fixing it to the base of the load cell and the frame, and with a central outlet hole for the load cell cable. The assembled load cell units are fixed in the ports on the conveyor casing with six screws. The load cells were designed so the platen is coincident with the internal surface of the conveyor, so the normal and shear stresses acting on the casing are applied to the platen and transferred to the load cells. The load cells and housing pieces were machined from HE15 aluminium alloy.

The load cells measure the normal and shear stresses applied to the platen through strain-gauged webs oriented in vertical and horizontal directions. A pair of vertical webs at each end of the load cell measure the normal stress, and four horizontal webs measure the shear stress in the direction parallel to these webs. Some design drawings of the load cells are shown in Figure 4.14 and some details of the load cell specification are given in Table 4.5. The normal and shear web sizes were designed to prevent failure in compression or by buckling under the design loads, as described by Bransby (1973). The shear web size was also determined by the minimum dimensions required to mount the strain gauges, and the limits of the machining used to manufacture the load cells. The design load capacities were based on the maximum stresses expected during the screw conveyor tests, increased by a factor of about three to prevent damaging the instruments, and assuming a maximum allowable stress of 140 MPa for the webs. With the web dimensions shown in Table 4.5, the load cells have a maximum load capacity equivalent to about 1420 kPa normal stress applied in combination with the maximum shear stress of 600 kPa. Although these capacities were significantly higher than the stresses applied during the tests, the sensitivity of the load cells was high enough for accurate measurements.

A total of 24 strain gauges are included on the normal and shear stress webs of each load cell, wired into three separate circuits to measure the applied loads. At each end of the load cell, the strain gauges on the two vertical webs are wired with dummy strain gauges to form a half active Wheatstone bridge. The output from each of these circuits is proportional to the load carried by the webs at each end of the transducer. The total normal force acting on the platen is measured as the sum of the forces in the normal stress webs. The moment applied to the load cell from an eccentric normal force is measured through the difference in the forces carried by the two pairs of vertical webs. The strain gauges on the shear webs are wired into a fully active Wheatstone bridge, with the output proportional to the shear force acting on the platen in the direction parallel to the shear webs. The three strain gauge circuits are wired to a nine core cable carrying the common power supply and the output from each circuit to the data logging system.

The two load cells at each instrumented section of the conveyor were oriented in different directions to measure the shear stress components parallel and perpendicular to the screw axis. The orientation of the load cell in the housing frame is changed through the alignment of the screw holes in the platen and cover plate for the connections to the load cell. These pieces were manufactured with the screw hole positions to have four load cells aligned in each direction along the conveyor. The top surfaces of the platen and housing frame were machined to a radius of 54.0 mm to match the internal diameter of the conveyor, and the dimensions of the frame piece were accurately machined to give a close fit into the mounting ports in the casing. The load cell housing is sealed to prevent entrance of water by the hot-bonded rubber between the platen and the frame, and silicon sealant was used to seal the screws connecting the load cell to the platen. Figure 4.15 shows photographs of the load cell and the assembled load cell housing unit.

#### **4.4.1.2 Load cell calibration**

The calibration of the load cells is performed by applying known load increments to the transducer assembled in the housing, and recording the outputs from each strain gauge circuit to determine the calibration coefficients. Calibration of a load cell requires application of normal load cycles, shear load cycles, and normal loads at varying eccentricity. A calibration rig was designed to apply these loads to the transducer, as shown in Figure 4.16. The instruments were assembled with screws extending from the load cell and platen to connect an adapter piece and loading plate. The adapter piece had a convex surface to fit into the curved platen, and was rotated to fit the load cells with different shear load orientations. The assembled load cell and loading plate was bolted to a base plate and mounted on the calibration bench. Normal loads

were applied by weights hanging from the loading plate on a frame with a knife-edge blade. Grooves machined across the top of the loading plate allowed for different positions of the knife-edge blade to apply normal loads to the transducer at varying eccentricities. Horizontal shear loads were applied by weights hanging from cables running over pulleys and connected to the loading plate through a frame as shown in Figure 4.16. Careful assembly of the load cells in the housings and the calibration rig, ensuring that all components were aligned correctly, was necessary to achieve consistent values for the calibration coefficients.

The strain gauges on the load cells are wired to make each circuit directly sensitive to loads applied in the direction of the web orientations, but each circuit also has a small cross-sensitivity to loads applied in the opposite direction. The output of each of the three circuits is proportional to the normal load, shear load and moment applied to the platen, resulting in a matrix of nine calibration coefficients relating the applied loads to the change in the circuit outputs:

$$\begin{bmatrix} V_B - V_{B0} \\ V_C - V_{C0} \\ V_A - V_{A0} \end{bmatrix} = \begin{bmatrix} a_{11} & a_{12} & a_{13} \\ a_{21} & a_{22} & a_{23} \\ a_{31} & a_{32} & a_{33} \end{bmatrix} \begin{bmatrix} N \\ S \\ M \end{bmatrix}$$

Eqn 4.1

where:  $V_B, V_C$  are the outputs from the normal force circuits  
 $V_A$  is the output from the shear force circuit  
 $V_{0B}, V_{0C}, V_{0A}$  are the zero offsets of the circuits  
 $a_{11}, a_{12}, \dots, a_{33}$  are the calibration coefficients  
 $N, S, M$  are the normal load, shear load and moment applied to the platen

Once the calibration coefficients are determined, the matrix is inverted to calculate the applied loads from the measured circuit outputs.

Each load cell was calibrated by applying the load cycles summarised in Table 4.6. Several calibration runs were performed with each load cell to obtain consistent values for the calibration coefficients. The output from each circuit was recorded for each load increment, and the calibration coefficients determined from the slopes of regression lines fitted to plots of the output voltages against the applied loads. Figure 4.17 shows an example set of calibration plots for a load cell. The coefficients  $a_{11}$  and  $a_{21}$  represent the direct sensitivity of the vertical webs to

normal load, with a typical value of  $1.05 \mu\text{V}/\text{V}/\text{N}$  measured for these loads cells. The coefficient  $a_{32}$  represents the direct sensitivity of the shear webs to the applied shear load, with a typical value of  $3.95 \mu\text{V}/\text{V}/\text{N}$ . The coefficients  $a_{13}$ ,  $a_{23}$  and  $a_{33}$  represent the sensitivity of the normal and shear webs to the moment applied by an eccentric normal load. The coefficients  $a_{12}$ ,  $a_{22}$  and  $a_{31}$  represent the cross-sensitivities of the circuits to loads applied in the direction opposite to the orientation of the webs.

#### 4.4.2 Pore water pressure transducers

Pressure transducers were installed at each instrumented section to measure the pore water pressure in the soil at the interface with the casing. Druck PDCR 810 pressure transducers with a seven bar range were used for these instruments. A brass cap with a porous ceramic stone glued into a recess in the top was screwed onto the transducer so it functioned as a pore water pressure transducer. The cavity above the diaphragm of the pressure transducer was filled with de-aired water, and the cap was screwed onto the transducer after it was boiled in water to de-air the porous ceramic. The connection between the transducer and the cap was sealed with PTFE tape and a Dowty washer, and the assembled transducer was stored underwater to keep the porous ceramic saturated. This assembly created a reservoir of water above the transducer diaphragm, with the saturated porous ceramic allowing flow of pore water from the soil into the reservoir to measure the pore water pressure. The pressure transducers assembled with the caps were screwed into tapped holes in the conveyor casing so the top of the cap was level with the internal surface of the casing during the tests.

The transducers were calibrated under air pressure controlled with a regulator and measured by a dial gauge. The transducers have a linear response over the full pressure range, and the calibration coefficients determined from regression lines fitted to the calibration data are shown in Table 4.7. The pore pressure transducers successfully measured the positive pore water pressures in the soil during the tests.

#### 4.4.3 Drive shaft torque cell

The screw drive shaft was instrumented for direct measurement of the torque supplied by the motor to rotate the screw. As shown in Figure 4.7, a section of the drive shaft was machined to an outer diameter of 29.0 mm for a wall thickness of 1.8 mm. The thin section of the drive shaft was designed for a maximum torque of 600 Nm before approaching the yield stress, giving a maximum normal strain in the shaft of about  $2000 \mu\epsilon$ . This resulted in a measurable strain in the

shaft over the range of torque expected during the tests. Four strain gauges were mounted around the circumference of the thin section, oriented at 45° to the shaft axis to measure the normal strain in the shaft. The strain gauges are wired into a Wheatstone bridge and to an amplifier mounted on the screw shaft. A slip ring was mounted on the drive shaft to provide the electrical connections between the power supply and data acquisition system, and the strain gauge circuit and amplifier rotating with the shaft.

The components of the instrumented drive shaft are shown in Figure 4.8, and the assembled drive shaft with the slip ring and amplifier are shown in Figure 4.9. The slip ring was constructed from a plastic sleeve with four brass rings that fits over the drive shaft, with an outer plastic tube mounted on ball bearings. The inner sleeve rotates with the drive shaft, and spring loaded carbon brushes run over the brass slip rings and connect to the electrical terminals in the stationary outer tube. Two of the slip ring connections carry the power supply to the amplifier and strain gauge circuit, one slip ring carries the amplified output signal to the data acquisition system, and the fourth slip ring connects the electrical components to a common earth. The 100x amplifier was included in the circuit to increase the strain gauge output signal before it passed through the slip ring. This improved the quality of the output to the data acquisition system by increasing the signal relative to the noise on the signal from the slip ring.

The instrumented drive shaft was calibrated by applying torque loads to the shaft assembled in the conveyor, and recording the output voltages from the strain gauge circuit through the amplifier and slip ring. Known torque loads were applied by weights hanging from a horizontal lever arm connected to the shaft through a split collar clamp, as shown in Figure 4.18. Weights were added to the hanger to apply incremental torque loads to the shaft, covering the range of torque measured during the tests. The output voltage varied linearly with the applied torque at the same rate in both rotational directions, as shown in Figure 4.19. The calibration coefficient for the torque cell was determined from the regression line fitted to the data points, and the value obtained from several calibration cycles is shown in Table 4.7.

#### **4.4.4 Jack pressure transducer**

The jack mounted in the load frame was used to pressurise the soil samples during the tests. The gas pressure supplied to the jack was controlled with a regulator, and a dial gauge indicated the pressure. An electronic pressure transducer was also connected to the line to monitor the gas pressure. A Druck PMP 1400 pressure transducer with a 250 bar range was used for this

instrument, to measure the pressure over the 172 bar (2500 psi) range available from the nitrogen cylinder. These pressure transducers have a linear response, with the typical accuracy quoted by the manufacturer as  $\pm 0.15\%$ .

The transducer was calibrated using the nitrogen cylinder and regulator to apply pressure increments to the jack, indicated by the dial gauge to an accuracy of 5 psi. The transducer output was recorded at each pressure and the calibration coefficient shown in Table 4.7 was determined from the slope of the regression line fitted to the data points. The pressure applied to the soil sample was calculated from the output of the jack pressure transducer, using the calibration coefficient and the ratio of the jack bore and piston areas.

#### **4.4.5 Draw-wire transducer**

The position of the piston in the container was monitored during the tests to indicate the height of the soil sample. This measurement was used to control the tests, with different stages of the experiments and the final stop point of the test based on the height of the sample. A draw-wire transducer was used to measure the piston position. The instrument has a measuring range of 1000 mm, with the output voltage linearly proportional to the extension of the cable. The draw-wire transducer was mounted on the load frame above the sample container, with the cable connected vertically to the piston beneath it by a clamp, as shown in Figure 4.20. The cable extended as the piston lowered into the container during the conveyor operation, with the transducer output indicating the sample height. The measured change of sample height over time was also used to calculate the volumetric soil flow rate through the screw conveyor.

The draw-wire transducer was calibrated by mounting the instrument on a bench and using a meter rule to measure the extension of the cable. The cable was connected to a steel block which was moved along the ruler to various positions and measured to an accuracy of one millimetre. The transducer output was recorded at various cable extensions. The output of the transducer was linear, and the calibration coefficient is shown in Table 4.7.

#### **4.4.6 Data acquisition system**

The instruments installed on the model screw conveyor were connected to a data logging system to record the measurements during experiments. The instruments were plugged into channels on two junction boxes, which connected to a computer logging the data. The power supply for the instruments is provided through the junction boxes, and the instrument output signals are

amplified and filtered in the junction boxes. The torque cell and amplifier on the drive shaft had a separate power supply to the other instruments, and the output signal was amplified before the slip ring and the connection to the junction box as described earlier. Each load cell has three output signals from the strain gauge circuits, and the cables are split into three connections to different channels on the junction boxes. With this arrangement, a total of 31 instrument connections were made to the two junction boxes and logged by the computer.

The junction boxes were connected through 55-way cables to the data logging computer. The data logging program DASyLab was used to record the instrument outputs from each channel through an analogue to digital data card installed in the computer. This data acquisition system was used for calibration of the instruments, using the same electronic connections as in the experiments. During the tests, the output voltage from each instrument channel was logged at a rate of 5 Hz, which was sufficient to accurately monitor the operation of the screw conveyor.

## **4.5 Model screw conveyor tests**

Screw conveyor tests were performed with different soil samples and varying operating conditions. The assembly and operation of the screw conveyor system, and the design of the tests performed are described below.

### **4.5.1 Assembly and operation of the screw conveyor**

Soil samples were prepared in the containers by consolidation of kaolin slurries and by compacting conditioned natural clay soil samples, as described in Chapters 5 and 6. The sample containers were assembled with a blanking plate covering the conveyor connection flange, and with the piston on top of the soil sample. The assembled containers were mounted in the load frame and the jack extended onto the piston. The draw-wire transducer cable was connected to the piston, and the initial position of the piston was measured to determine the initial sample height for the test.

The screw conveyor was assembled by first bolting the end plate and bearing housing plate with the drive shaft to the casing flange. The drive shaft was then connected to the motor shaft through the coupling. The load cells assembled in their housings were mounted into the ports along the conveyor, with the two load cells at each section oriented in different directions. The conveyor casing was sealed at the end plate connection and the load cell ports with rubber o-

rings. The bolt holes in the conveyor casing flange were aligned for the connection to the container flange, and the casing fixed in place by tightening the brackets supporting the conveyor in the frame. Prior to a test, the pore pressure transducers were screwed part way into the casing, and water was poured into the conveyor to maintain saturation of the porous ceramic filters. At the start of a test, these transducers were screwed into the full depth so the caps were level with the internal casing surface. The final stage of the conveyor assembly was inserting the screw into the casing with the drive shaft adapter piece fitting through the end plate and into the drive shaft tube. The shear pin connection was made through the drive shaft pieces and the screw conveyor was ready for operation.

The conveyor was connected to the container by first reducing the pressure in the jack to atmospheric and removing the blanking plate from the connection flange. The conveyor was aligned with the container flange and the motor turned on to drill the length of screw extending from the casing into the sample. The motor was turned off once the screw was at the final position, and the container and conveyor flanges were bolted together. The screw conveyor system was then fully assembled and ready for testing.

Tests were performed with varying pressures applied to the samples, with varying screw speeds, and with different discharge conditions. The sample pressure was applied for a few minutes before starting the screw to commence the test. The speed of the screw was varied with the dial gauge speed controller on the motor. The conveyor discharge condition was varied by connecting or removing the reduction piece and valve that screw onto the discharge outlet.

As described below, the different stages of the tests at which the conveyor operating conditions were varied were based on the height of the sample in the container. The screw was stopped to end the test after sufficient soil had been extracted such that the piston approached the level of the screw inside the container. The instrument outputs were logged continuously to monitor the operation of the screw conveyor throughout the tests.

#### **4.5.2 Design of screw conveyor tests**

The screw conveyor tests were performed in two or three stages with varied operating conditions. The tests were controlled based on the height of the sample in the container, as indicated by the draw-wire transducer connected to the piston.

The total sample height available for a test is determined by the initial sample height and the position of the screw inside the container. When the screw conveyor is assembled, the top of the screw flight corresponds to a height of 225 mm above the base of the container. This represents the minimum sample height for termination of the test, so that the piston does not come into contact with the screw inside the container.

The total sample height available is divided into sections so approximately equal volumes of soil pass through the conveyor during the different stages of a test. Based on the draw-wire transducer output corresponding to the initial sample height, the outputs at the sample heights for the different test stages, and for the end point of the test, are calculated using the draw-wire transducer calibration factor shown in Table 4.7. During a test, the draw-wire transducer output is monitored, and changes to the conveyor operating conditions are made at the calculated outputs corresponding to the different stages.

## **4.6 Summary**

This chapter has described a model EPB screw conveyor system designed and commissioned for investigations of the conveyor operation and effects of soil conditioning treatments on the performance. The model was designed to an approximate 1:10 scale of a full-scale EPB machine screw conveyor, to perform experiments under controlled conditions with different soil samples and conveyor operating conditions. Extensive instrumentation was included on the conveyor to monitor its operation during the tests.

The general arrangement and operation of the screw conveyor system and the instrumentation scheme was described. The sample containers and loading system used to consolidate clay samples and pressurise the samples during tests was described. The design of the conveyor casing tube with variable discharge outlet conditions and instrumented sections was described, as well as the various components of the conveyor drive shaft. Two model screws were constructed for the conveyor, with similar geometries except for a different pitch of the screw flights for tests investigating the influence of the screw pitch on the conveyor operation. The variable speed electric motor used to drive the screw conveyor was described.

The design and assembly of the Cambridge-type load cells and their housing components to mount into the conveyor with different load cell orientations was described. Some specifications

of these transducers and their load capacities were also detailed. The calibration rig designed for the load cells and the procedures followed to determine the calibration coefficients were described. The drive shaft was instrumented to measure the torque to rotate the screw during the tests. The design of this instrument and the associated electronic components was described, as well as the calibration apparatus and procedures. The screw conveyor includes pore water pressure transducers at each instrumented section, and transducers to monitor the sample pressure and height. The instrumentation scheme allows detailed measurements of the conveyor operation through the total pressure and pore water pressure gradients along the conveyor, the casing shear stresses along the conveyor, the screw torque, and the soil flow rates through the conveyor.

Some design drawings and specifications detailing components of the model screw conveyor and the instrumentation were presented. The response of some of the instruments was illustrated, and the calibration coefficients determined for the various instruments used in the analysis of the test data were summarised. The data acquisition system used to monitor the instruments during the tests was described. The assembly of the screw conveyor system and instruments for a test, and the control of the conveyor operating conditions were summarised. The design and monitoring of the different stages of the tests was also described.

The model screw conveyor system operated successfully throughout the 16 tests performed in this research, using various clay soil samples and investigating the effects of differing operating conditions. The instrumentation provided detailed measurements of the conveyor operation throughout the tests, as presented in the following chapters.

<b>System Component</b>	<b>Dimension</b>
Container internal diameter (mm)	420.0
Top container height (mm)	400.0
Bottom container height (mm)	600.0
Container volume (L)	138.5
Conveyor connection flange internal diameter (mm)	108.0
Conveyor connection flange length (mm)	50.0
Piston diameter (mm)	419.0
Piston depth (mm)	150.0
Jack bore (mm)	50
Jack stroke (mm)	750

Table 4.1. Dimensions of sample container and loading system.

<b>Casing tube component</b>	<b>Dimension</b>
Conveyor casing length (mm)	1000
Assembled conveyor length (mm)	1050
Casing outer diameter (mm)	127.0
Casing internal diameter (mm)	108.0
Discharge outlet internal diameter (mm)	85
Discharge outlet length (mm)	55
Discharge valve internal diameter (mm)	50
Discharge valve length (mm)	115

Table 4.2. Dimensions of screw conveyor casing and discharge outlet.

Screw dimension (mm)	Screw 1	Screw 2	Range (mm)
Total screw length	1200	1200	±2.0
Screw shaft diameter, $D_s$	43.0	43.0	±0.5
Screw flight diameter, $D_f$	102.0	102.0	±1.0
Radial flight-casing clearance	3.0	3.0	±1.0
Screw channel depth, $h$	29.5	29.5	±1.0
Channel depth in casing, $h_c$	32.5	32.5	±0.5
Screw flight thickness, $e$	5.0	5.0	±1.0
Number of pitches	15	9	-
Screw pitch (range)	76 – 80	125 – 135	-
Screw pitch (average), $t$	80	133	-
Pitch to diameter ratio, $t/D_f$	0.78	1.33	-
Flight helix angle, $\phi_f$ (°)	13.9	22.9	-

Table 4.3. Dimensions of model screws.

Power supply	400 V at 50 Hz
Rated motor power (kW)	2.2
Rated motor torque (Nm) (speed settings 15 – 100%)	9.4
Reduction gearbox ratio	62.3
Output speed range (rpm)	5 – 35
Rated output torque (Nm) (speed settings 15 – 100%)	585
Maximum overload torque (Nm) (speed settings 15 – 60%)	1050 (constant over this speed range)
Maximum overload torque (Nm) (speed settings 60 – 100%)	1050 – 875 (linear reduction with speed over this range)

Table 4.4. Specification of screw conveyor motor.

<b>Load cell dimensions</b>	
External dimensions (w x l x h, mm)	30.0 x 30.0 x 24.0
Normal stress web dimensions (w x t x h, mm)	3.0 x 1.0 x 8.0
Shear web dimensions (w x t x l, mm)	2.0 x 0.55 x 6.0
Load platen plan dimensions (w x l, mm)	32.0 x 32.0
<b>Load cell capacities</b>	
Maximum normal stress on platen (kPa) (with $\tau = 0$ kPa)	1640
Maximum shear stress on platen (kPa)	600
Maximum combined normal and shear stresses on platen (kPa)	$\sigma_n = 1420, \tau = 600$
<b>HE15 aluminium alloy material properties</b>	
Yield stress, $\sigma_y$ (MPa)	220
Maximum allowable stress, $2/3\sigma_y$ (MPa)	140
Young's modulus (MPa)	70000

Table 4.5. Load cell specifications.

Calibration stage	Applied loads	Normal load (kg)	Normal stress (kPa)	Shear load (kg)	Shear stress (kPa)	Normal load eccentricity (mm)	Applied moment (Nm)
Normal stress calibration	Normal load cycles applied at zero eccentricity No shear load applied	0 to 125	0 to 1240	0	0	0	0
Moment calibration	Constant normal load applied at varying eccentricity No shear load applied	50	512	0	0	-14.0 to +14.0	-7.34 to +7.34
Shear stress calibration	Constant normal load applied at zero eccentricity Shear load cycles applied in both directions	30	287	0 to 55	-480 to +480	0	0

Table 4.6. Load cell calibration procedures.

<b>Instrument</b>	<b>Calibration coefficient</b>	<b>Unit</b>
Pore pressure transducer 1	0.001424	V / kPa
Pore pressure transducer 2	0.001423	V / kPa
Pore pressure transducer 3	0.001415	V / kPa
Pore pressure transducer 4	0.001418	V / kPa
Jack pressure transducer	0.000196	V / kPa
Draw-wire transducer	-0.00885	V / mm
Torque cell	-0.00330	V / Nm
Load cells (typical direct sensitivity to normal load)	1.05	$\mu\text{V}/\text{V}/\text{N}$
Load cells (typical direct sensitivity to shear load)	3.95	$\mu\text{V}/\text{V}/\text{N}$

Table 4.7. Calibration coefficients for screw conveyor instruments.

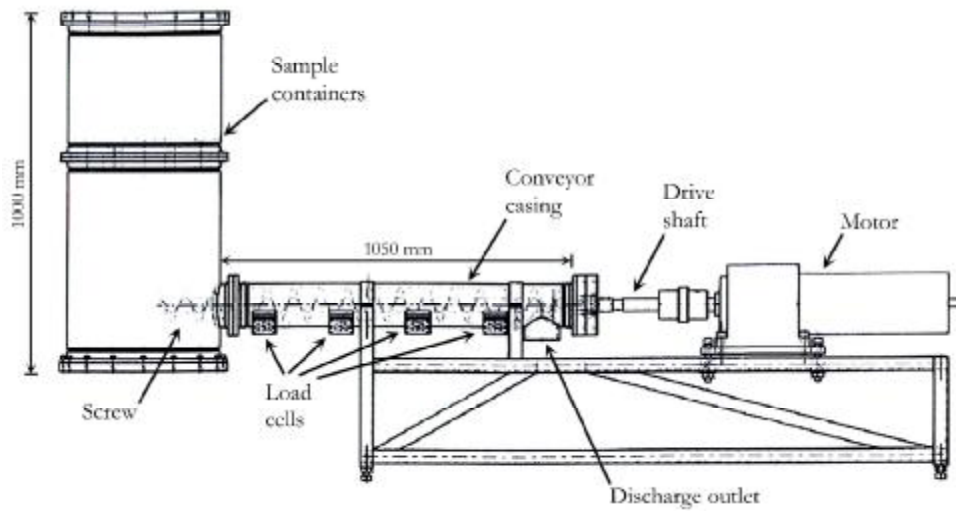


Figure 4.1. General arrangement of model EPB machine screw conveyor system.



Figure 4.2(a). Overview of model EPB machine screw conveyor system.



Figure 4.2(b). Model screw conveyor assembled for testing.

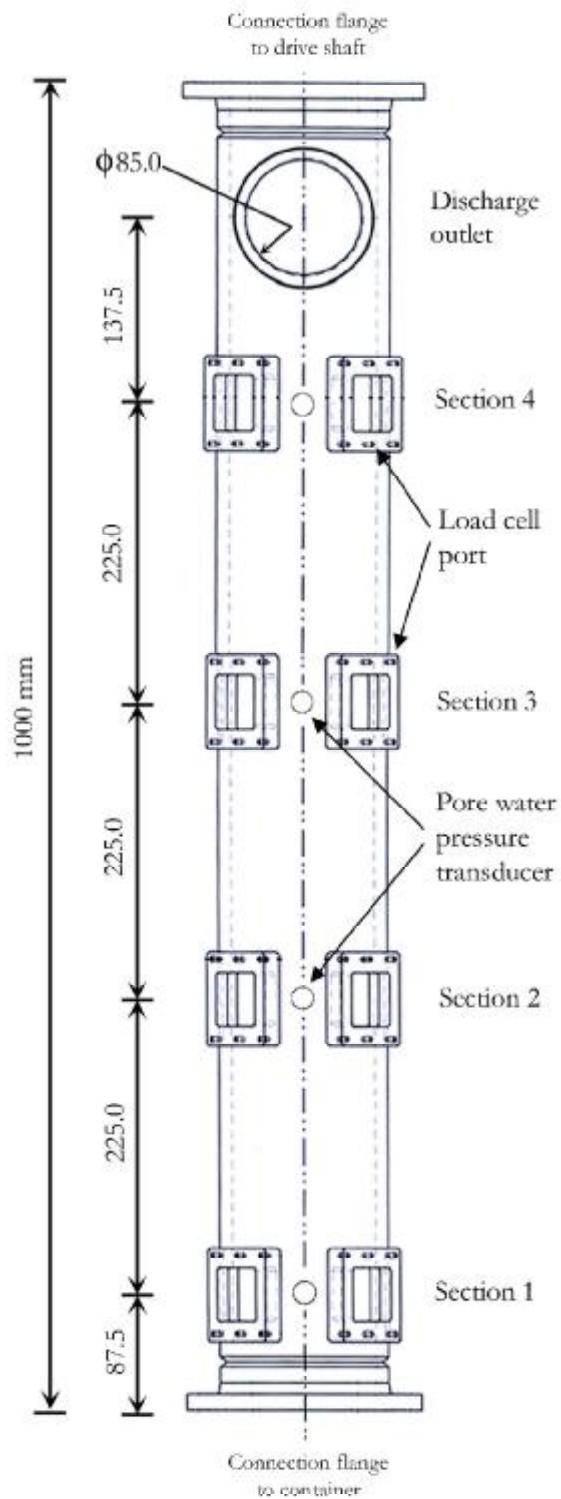


Figure 4.3. Layout of model screw conveyor casing.

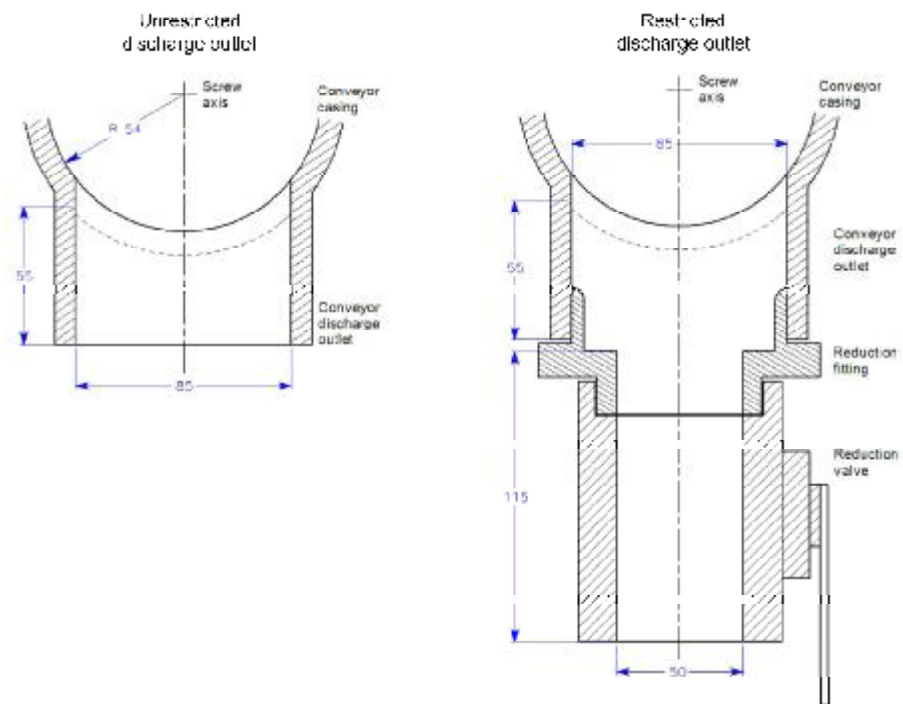


Figure 4.4. Geometry and dimensions of unrestricted and restricted conveyor discharge outlets.

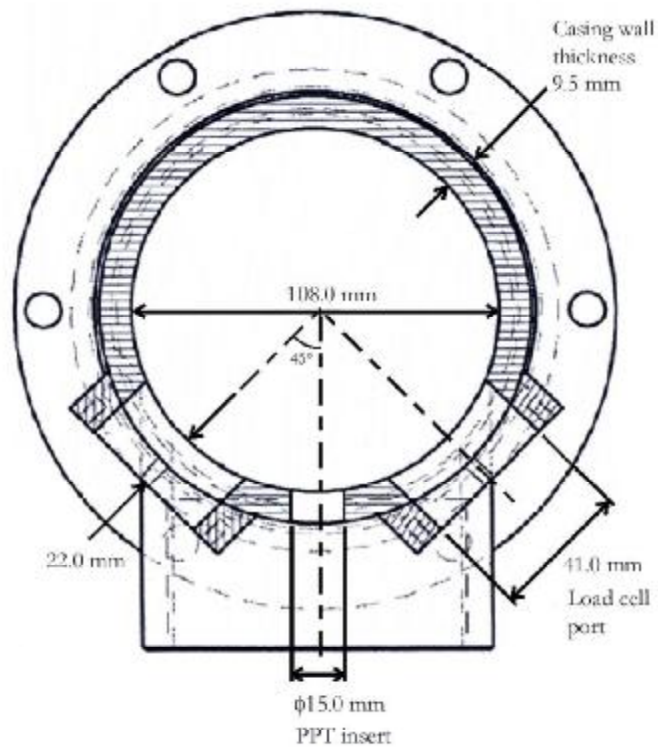


Figure 4.5. Instrumented section of conveyor casing.

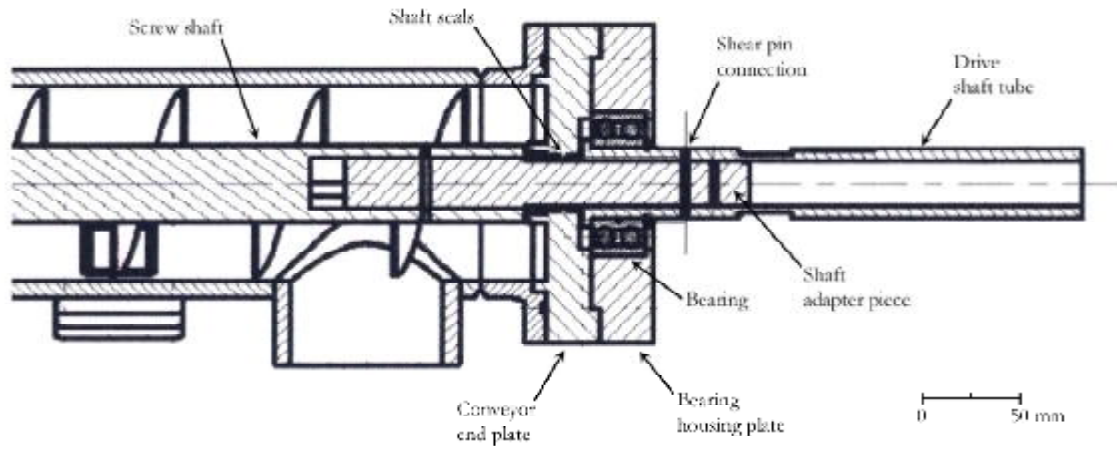


Figure 4.6. Screw conveyor drive shaft assembly.

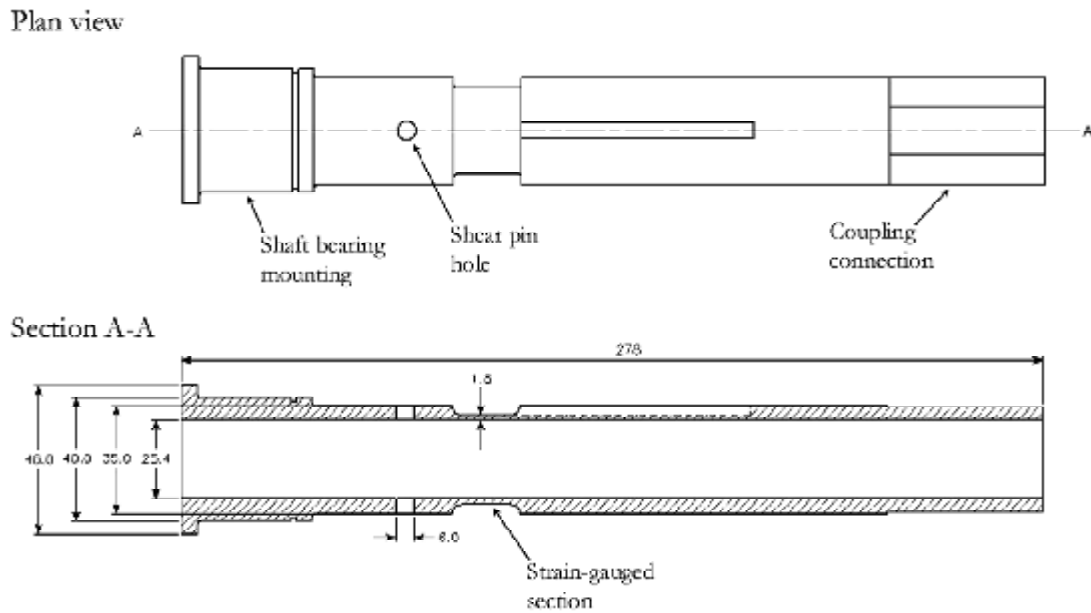


Figure 4.7. Design drawings of drive shaft.



Figure 4.8. Screw drive shaft with bearing and slip ring pieces.

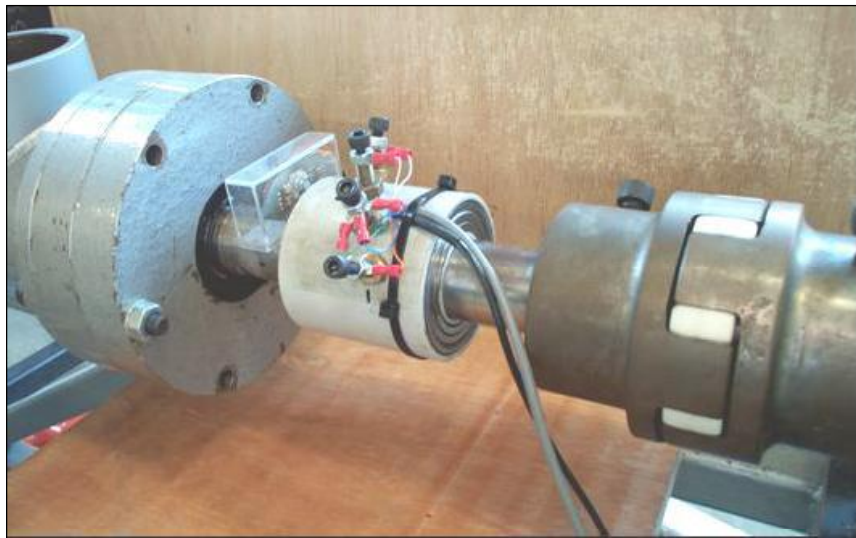


Figure 4.9. Assembled screw conveyor drive shaft and slip ring.

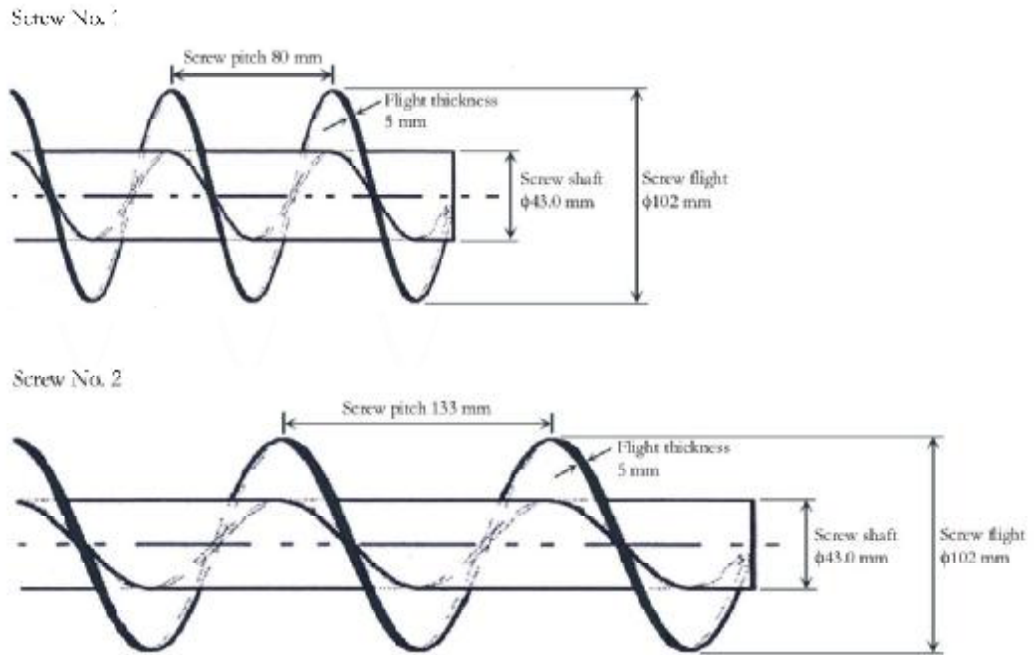


Figure 4.10. Dimensions of model screws.

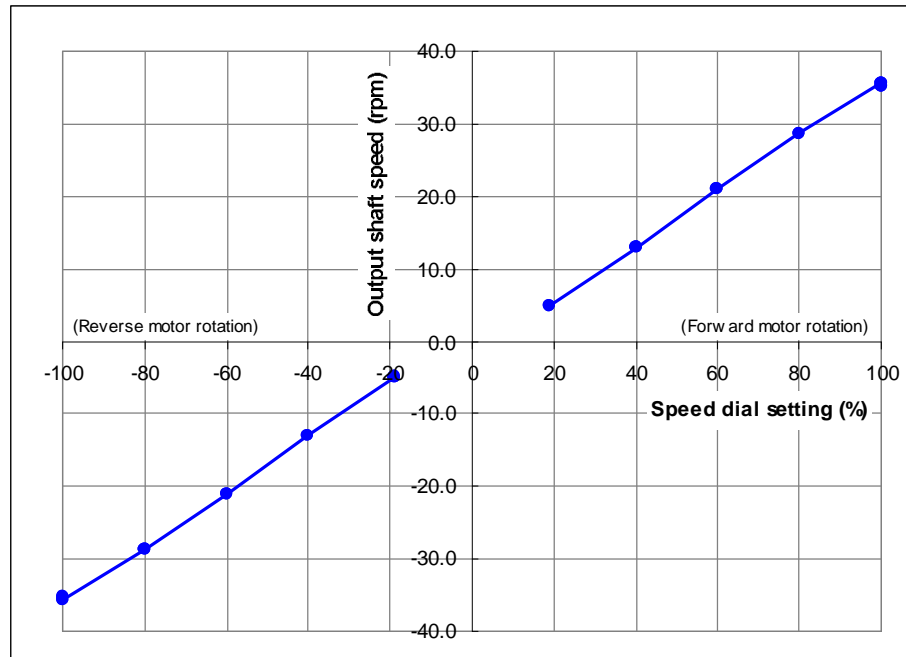


Figure 4.11. Screw conveyor motor speed calibration.

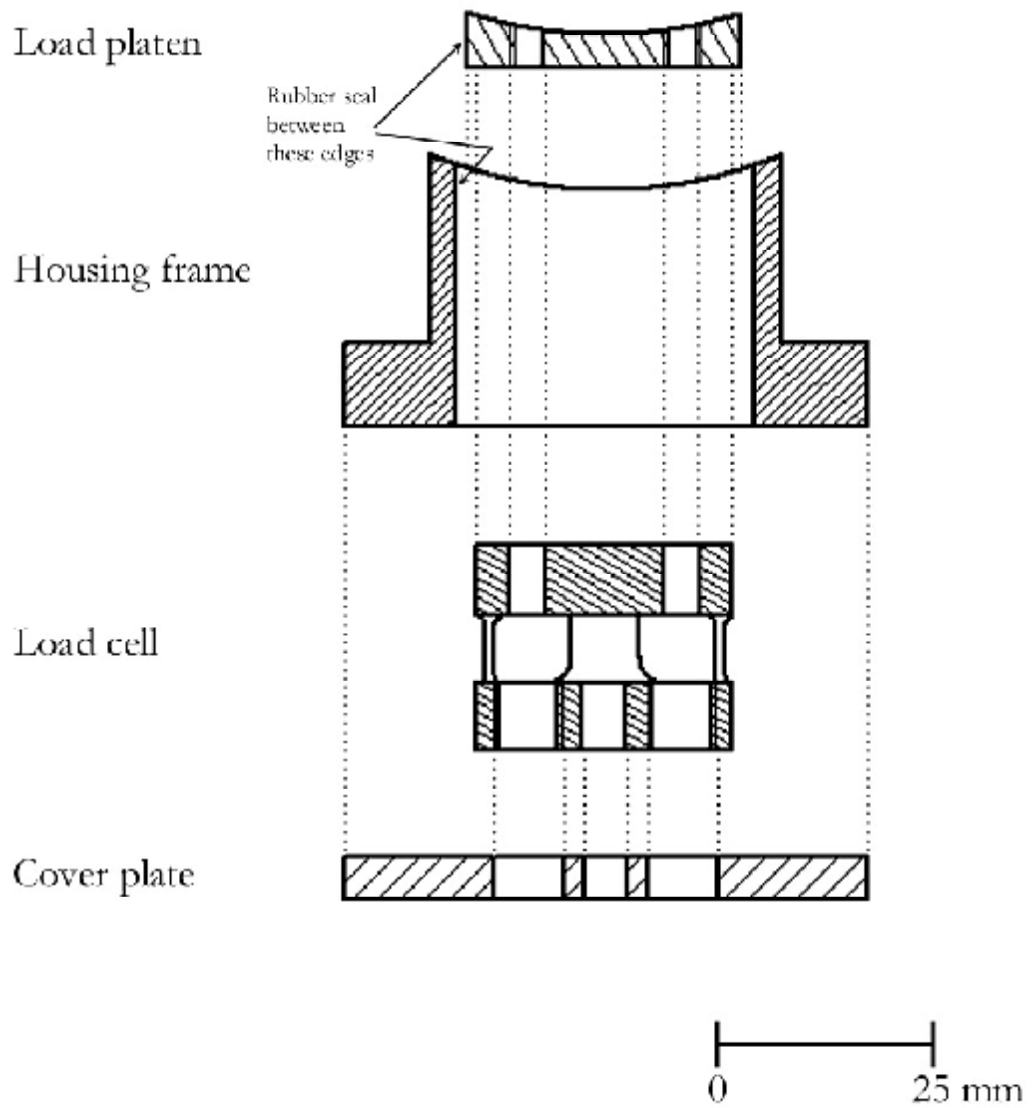


Figure 4.12. Load cell and housing components.

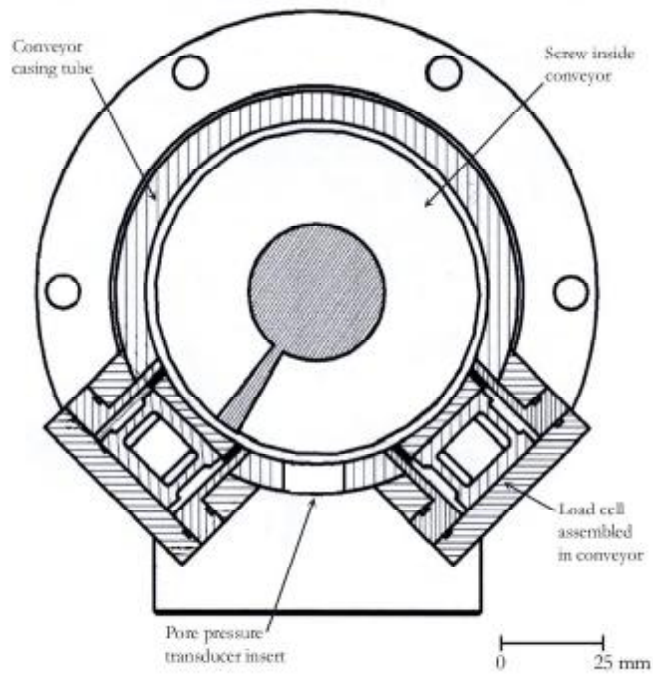


Figure 4.13. Instrumented section of assembled screw conveyor.

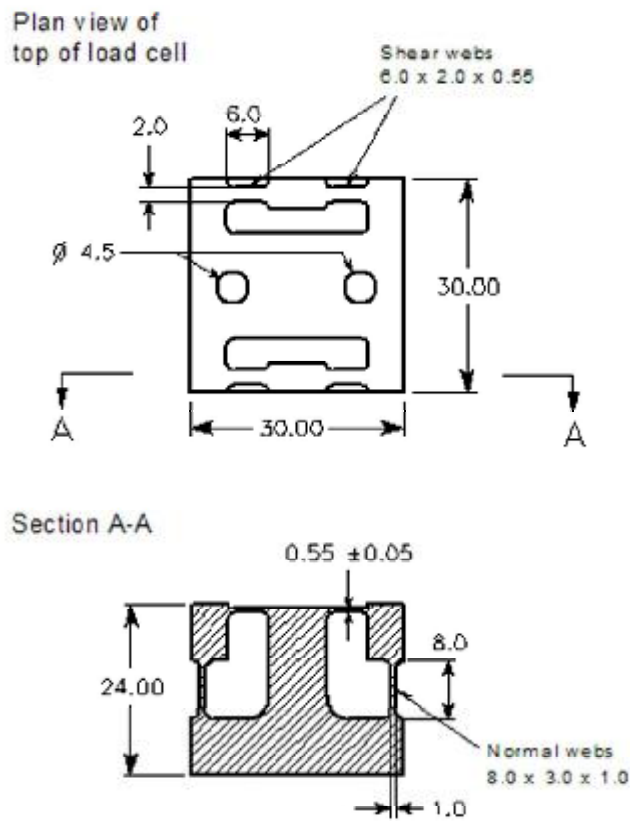


Figure 4.14. Load cell design drawings.

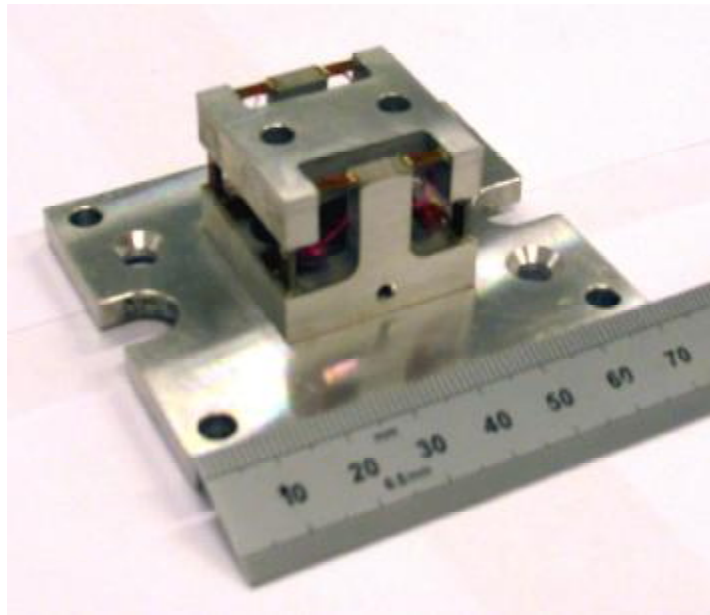


Figure 4.15(a). Cambridge-type load cell for model screw conveyor.

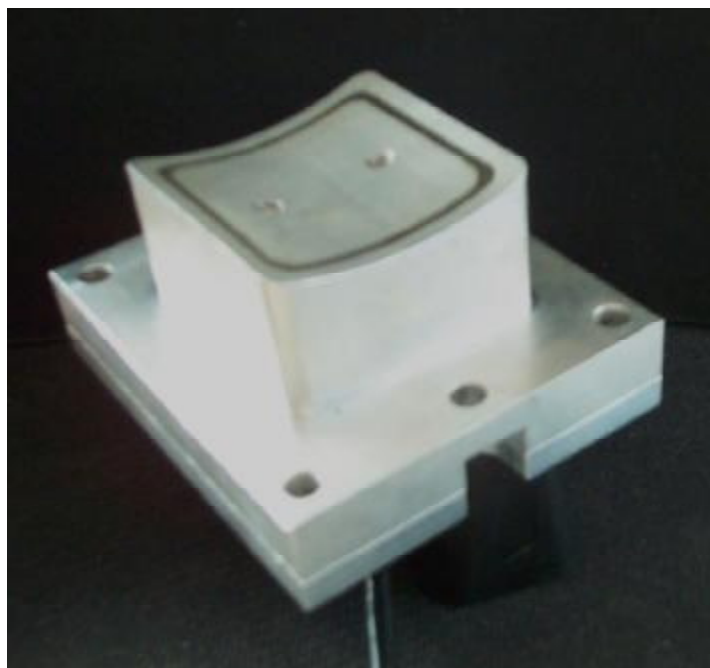


Figure 4.15(b). Assembled load cell unit.

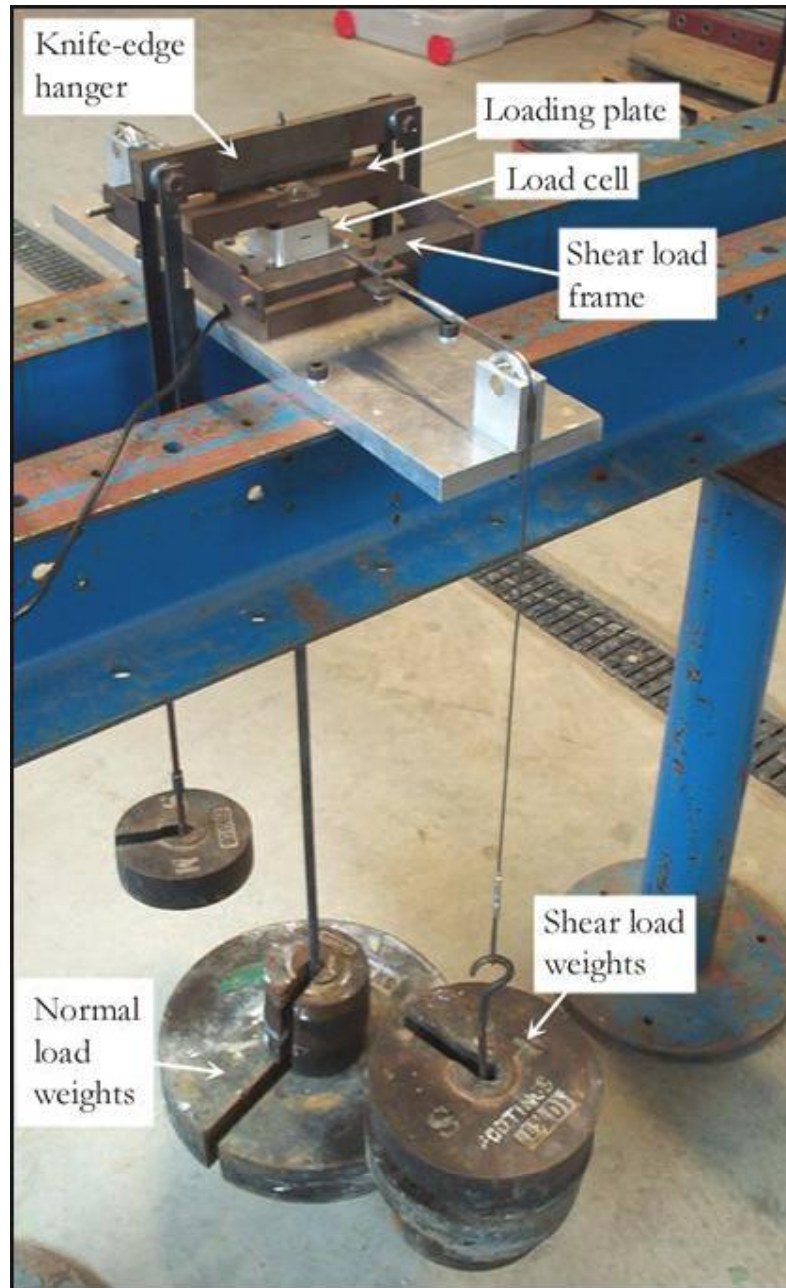
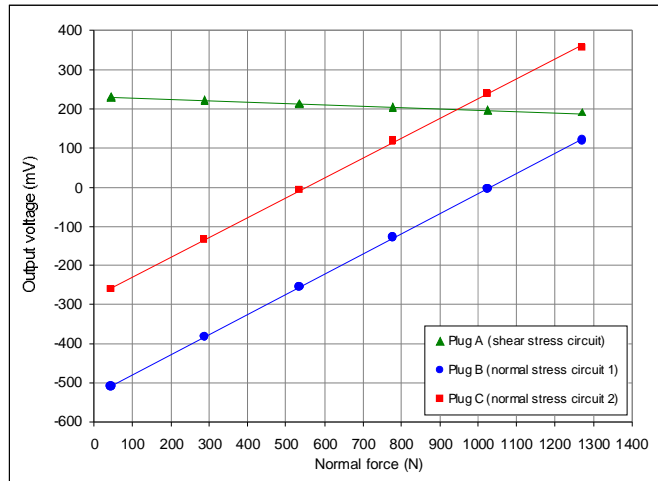
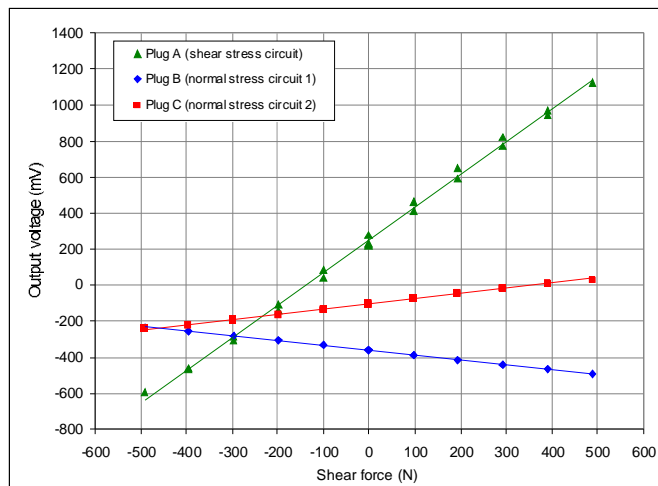


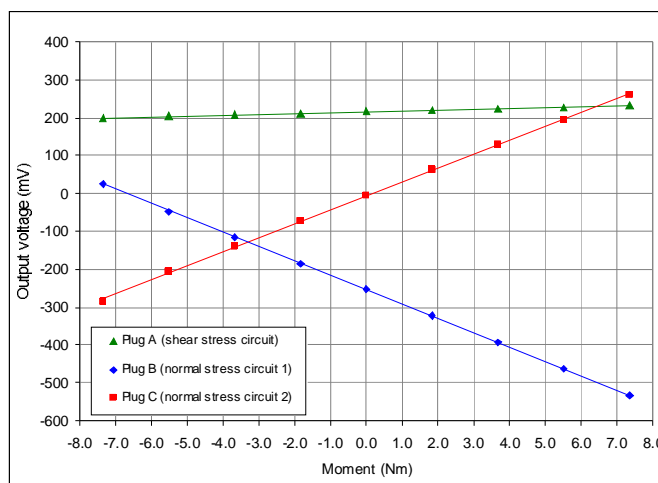
Figure 4.16. Load cell calibration.



(a) Normal load calibration.



(b) Shear load calibration.



(c) Moment calibration.

Figure 4.17. Example load cell calibration plots.

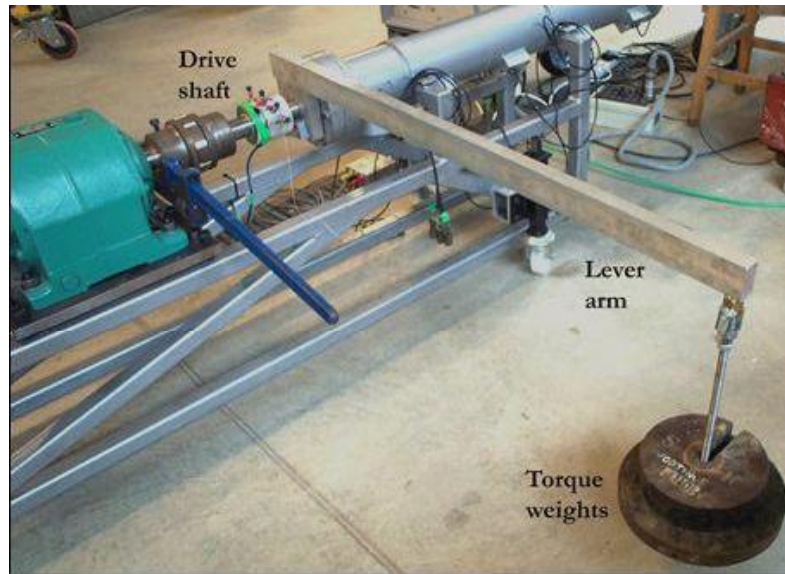


Figure 4.18. Torque calibration for instrumented drive shaft.

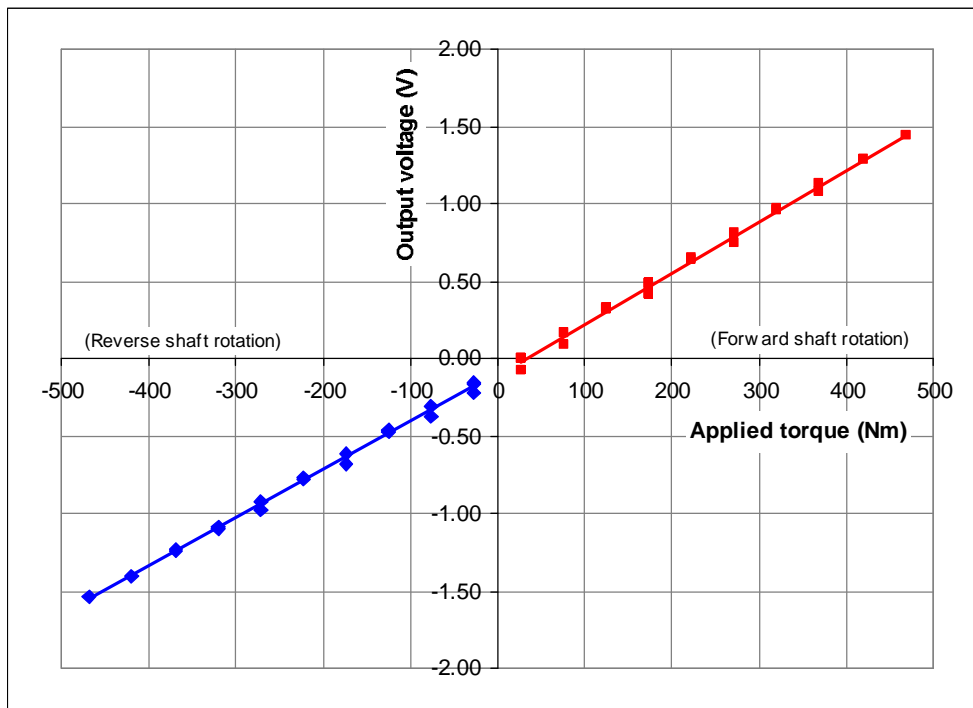


Figure 4.19. Drive shaft torque cell calibration.

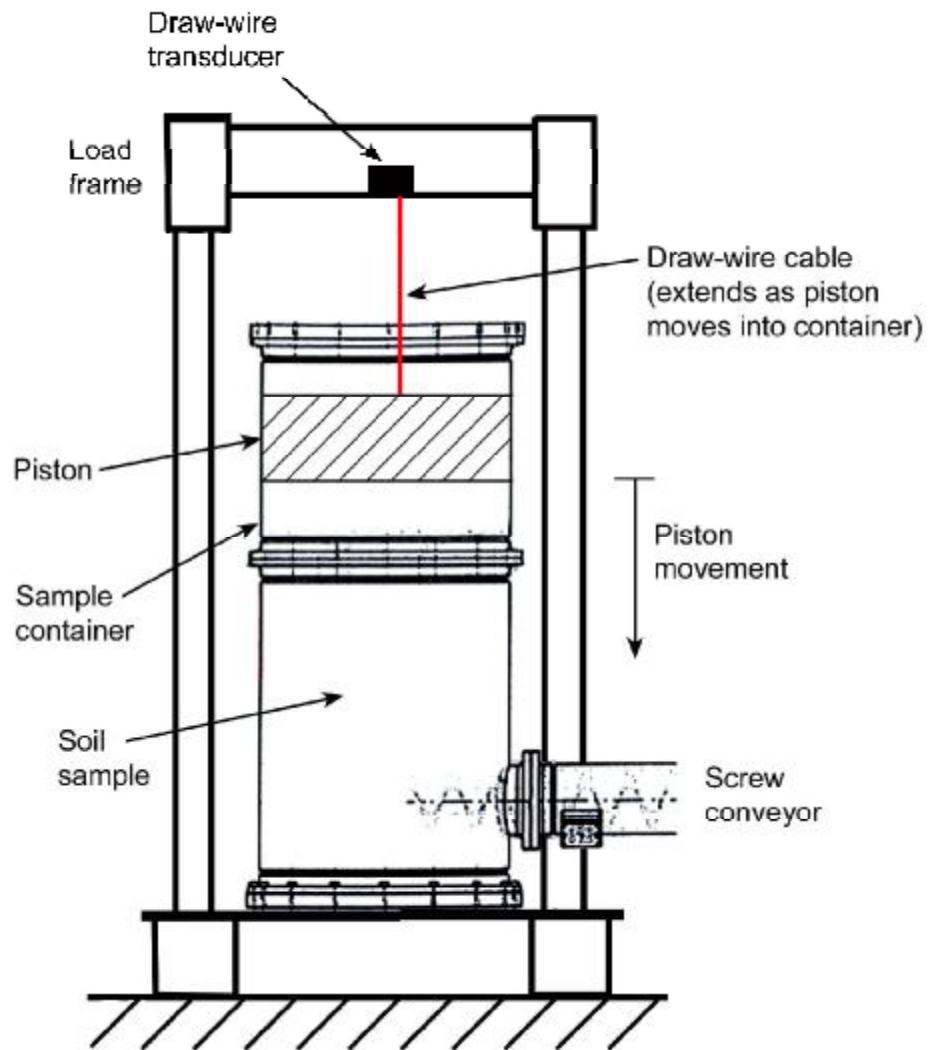


Figure 4.20. Arrangement of draw-wire transducer for sample height measurement.

# Chapter 5

## Model screw conveyor tests with consolidated kaolin

---

### 5.1 Introduction

This chapter reports a series of model screw conveyor tests performed with consolidated kaolin samples. Six tests were performed to investigate the mechanics of the screw conveyor operation with samples of varying strength under different test conditions. The E-grade sample preparation and the measured consolidation and strength properties are first presented and compared with theoretically predicted behaviour. The conveyor operating conditions for the tests are then described. The analysis of the measurements from the instruments during the screw conveyor tests are detailed. Detailed measurements from a test are presented to illustrate the mechanics of the screw conveyor operation with clay soils. Results from the various tests illustrating effects of the sample strength, the conveyor discharge condition, the applied sample pressure, and the screw pitch on the conveyor operation are then presented. The mechanisms of interface shearing observed in the screw conveyor tests are also discussed.

### 5.2 E-grade kaolin samples

The preparation and monitoring of the E-grade kaolin samples for the screw conveyor tests are described below. The sample volume changes measured during consolidation are presented. The characterisation of the test samples is described, and the measured strengths are compared with theoretical predictions and typical strengths for other normally consolidated clays.

### **5.2.1 Sample preparation**

E-grade kaolin samples were prepared in the container of the screw conveyor system by one-dimensional consolidation from a slurry to different vertical stresses, forming samples of varying strength. The slurry was prepared by mixing E-grade kaolin powder with de-ionised water at an initial moisture content of approximately 100%, equal to twice the liquid limit of the clay. For a slurry volume approximately equal to the maximum container volume of 138.5 L, 100 kg of dry kaolin powder was mixed with 100 L of water. The clay powder and water was mixed under a vacuum for at least four hours to obtain a uniform, fully saturated slurry. After mixing, the slurry was transferred to the sample container, with grease applied to the walls to reduce friction during consolidation and the screw conveyor tests. Drainage was provided at the top and bottom of the samples, as described in Section 4.3.2.

The containers were filled with slurry to an initial height of approximately 950 mm. The slurry was allowed to consolidate under self-weight before the piston was assembled in the container. The weight of the piston applied a 5.1 kPa pressure to the sample, acting as the first pressure increment for consolidation. The sample containers with the piston were mounted in the load frame, and further pressure increments applied through the piston and jack. A backpressure was not applied to the sample, so the effective vertical stress at equilibrium was equal to the total vertical stress applied to the sample. The samples were consolidated in increments to maximum vertical stresses of 50, 100 and 200 kPa.

During consolidation, the pressure applied to the sample was controlled by a regulator in the gas pressure line supplying the jack, monitored by a dial gauge. The sample height was monitored by measuring the position of the piston in the container. Each pressure increment was applied until the sample height remained approximately constant over time, indicating that primary consolidation was complete. The maximum consolidation pressure for the samples was applied for at least 48 hours prior to performing the screw conveyor test to ensure full equilibrium was reached. Monitoring of the sample height at each pressure provided data to determine the consolidation parameters for the large scale E-grade kaolin slurries, as discussed below.

### **5.2.2 Consolidation of E-grade kaolin**

E-grade kaolin has often been used at Cambridge as a model clay soil; however, little data describing the consolidation of large scale slurry samples has been previously reported. As discussed in Section 3.2.1 and summarised in Table 3.2, Elmes (1985) determined some

engineering properties of E-grade kaolin from an oedometer test and triaxial tests. It was reported that the one-dimensional Cam-clay compressibility parameter,  $\lambda^*$ , was nearly constant over the stress range  $\sigma'_v = 27$  kPa to  $\sigma'_v = 537$  kPa, with an average value of  $\lambda^* = 0.124$ . From the triaxial tests, isotropic consolidation of E-grade kaolin samples (with initial moisture content of 44.2%) to a mean effective stress of  $p' = 510$  kPa also showed constant compressibility over this pressure range, with an average value of  $\lambda = 0.13$ . Based on Elmes' test results, Potter (1996) expressed the one-dimensional compressibility of E-grade kaolin in terms of the vertical effective stress,  $\sigma'_v$ , and the void ratio,  $e$  as:

$$e = 1.754 - 0.124 \ln \sigma'_v \quad \text{Eqn 5.1}$$

For the screw conveyor tests, six large scale E-grade kaolin samples were consolidated in the container with maximum applied piston pressures of 50, 100 or 200 kPa. The container has a large height to diameter ratio, and the friction acting between the sample and the container walls significantly reduces the vertical stress acting on the sample during consolidation. To determine the effective vertical stress acting on the sample for a given piston pressure, a force balance on an element of the sample is considered as shown in Figure 5.1. The applied piston pressure at the top of the sample ( $\sigma'_p$ ) is reduced by the shear stresses ( $\tau$ ) acting on the walls of the container, to a lower stress ( $\sigma'_o$ ) at the base of the container. The shear stresses acting on the greased walls of the container are assumed to be 10% of the vertical effective stress acting on the sample ( $\sigma'$ ), so  $\tau = 0.1\sigma'$ . Considering an element of the sample of thickness  $dz$ , balancing the forces from the vertical effective stress and the wall shear stress leads to:

$$\frac{\pi D^2}{4} d\sigma' = 0.1\sigma' \pi D dz \quad \text{Eqn 5.2}$$

Equation 5.2 can be rearranged and integrated over the height ( $H$ ) of the sample between the limits of  $\sigma'_p$  and  $\sigma'_o$ , leading to:

$$\frac{\sigma'_o}{\sigma'_p} = \exp\left[-0.4 \frac{H}{D}\right] \quad \text{Eqn 5.3}$$

Equation 5.3 relates the pressure at the base of a sample of height  $H$ , ( $\sigma'_o$ ), to the applied piston pressure, ( $\sigma'_p$ ), assuming the wall shear stress is 10% of the vertical effective stress acting on the sample. Using this equation, the vertical effective stresses acting on the kaolin samples during consolidation are calculated from the applied piston pressures in the interpretation of the consolidation data.

For each sample, the final moisture content and the measured height changes during consolidation were used to determine the sample void ratio at the end of each pressure increment. The vertical effective stress acting on the sample at the end of each increment was calculated using equation 5.3, based on the applied piston pressures and the sample heights. The values in Table 5.1 show that the final vertical effective stresses acting on the samples, ( $\sigma'_v = \sigma'_o$ ), were approximately 60% of the maximum applied piston pressures ( $\sigma'_p$ ), due to the reduction caused by wall friction in the container. The measurements from the sample consolidation provide data of the one-dimensional compressibility of large scale E-grade kaolin samples over the applied stress range. The properties of the consolidated E-grade samples are summarised in Table 5.1. For the maximum consolidation pressures used, the final sample heights ( $H$ ) were 56 to 60% of the initial slurry height ( $H_o$ ), and the final moisture contents ranged from 42.4 to 48.4%.

The volume changes of the E-grade kaolin samples during consolidation are shown in Figure 5.2, plotting the void ratio against the vertical effective stress acting on the sample, reduced for the effects of the wall friction. Equation 5.1 proposed by Potter (1996) to describe the one-dimensional consolidation of E-grade kaolin is also shown on Figure 5.2. The large scale slurry samples had high void ratios at  $\sigma'_v = 1$  kPa due to the high initial moisture contents. The initial void ratios back-calculated from the measured sample volume changes were similar to those based on the initial moisture contents, shown in Table 5.1. At vertical effective stresses greater than 25 kPa, the consolidated samples approached the one-dimensional compression line represented by equation 5.1. This compression line indicates a lower void ratio at  $\sigma'_v = 1$  kPa than measured, as it was derived from consolidation of samples at higher stress levels than achieved for the large scale kaolin samples. As has been found by other researchers at Cambridge (e.g. Springman, 1993), the one-dimensional compression index,  $\lambda^*$ , for these kaolin samples was non-linear, with higher values at lower vertical effective stresses. The  $\lambda^*$  values measured for the final consolidation increments for each sample are shown in Table 5.1. As the maximum vertical

effective stress applied to the samples increased, the measured  $\lambda^*$  values approach the value determined by Elmes (1985) at higher stress levels.

### 5.2.3 Undrained shear strength of E-grade kaolin

After the screw conveyor tests were performed, the undrained shear strength of the E-grade kaolin samples was measured using the laboratory shear vane described in Section 3.4.4.3. A number of shear vane tests were performed on the soil remaining in the sample container when disassembled after the test, and on samples of the soil that had passed through the screw conveyor ('spoil' samples). The ranges of strengths measured for each consolidated sample in the containers and for the spoil are shown in Table 5.1. Soil specimens were taken from the container and the spoil to measure the moisture content of the consolidated samples, with the average values shown in Table 5.1.

The average vane shear strengths measured for the E-grade kaolin samples are shown plotted against the soil moisture content in Figure 5.3(a). The sample strengths are plotted against the corresponding liquidity indices on semi-logarithmic axes in Figure 5.3(b), showing the expected linear relationship between these parameters. The strengths measured for the soil in the container were consistently higher than the strength of the spoil samples. The moisture content of the soil samples taken from the container and from the spoil was equal. The difference in the strengths suggests some sensitivity of the E-grade kaolin, with the lower strength of the spoil relative to the 'undisturbed' soil in the container resulting from remoulding of the soil due to shearing as it passes along the screw conveyor and through the discharge outlet.

The vane shear strengths of the E-grade kaolin samples are compared to the undrained shear strength calculated theoretically for different moisture contents, and the corresponding liquidity indices, in Figure 5.3. Based on the equations defining the critical state line for clays, a relationship between the undrained shear strength,  $S_u$  and specific volume,  $v$ , can be derived (e.g. Wood, 1990):

$$S_u = \frac{M}{2} \exp\left(\frac{\Gamma_{csl} - v}{\lambda}\right) \quad \text{Eqn 5.4}$$

where:  $M$  is the Cam-clay frictional coefficient  
 $\Gamma_{csl}$  is the specific volume on critical state line at  $p'=1$  kPa  
 $\lambda$  is the slope of critical state line in  $v-\ln p'$  space

The values of the Cam-clay parameters for E-grade kaolin reported by Elmes (1985) are shown in Table 5.2. Elmes determined a value of  $\Gamma_{iso} = 2.65$ , representing the specific volume on the isotropic consolidation line at  $p' = 1$  kPa. The value  $\Gamma_{csl} = 2.55$  was calculated using Elmes' parameter values according to:

$$\Gamma_{csl} = \Gamma_{iso} - \lambda + \kappa \quad \text{Eqn 5.5}$$

The undrained shear strength of saturated clay at different moisture contents is calculated by equation 5.4 using the relationship between the specific volume  $v$ , the moisture content  $w$ , and specific gravity ( $G_s$ ) of the soil particles:

$$v = (1 + e) = 1 + G_s w \quad \text{Eqn 5.6}$$

The parameters in Table 5.2 were used to calculate the undrained shear strength at moisture contents of  $w = 40 - 50\%$ , as shown in Figure 5.3(a). The calculated undrained strengths at the corresponding liquidity indices based on the liquid and plastic limits for the soil are shown in Figure 5.3(b). The strengths of the consolidated samples calculated from the moisture contents are also shown in Table 5.1. The measured vane shear strengths compare well with the theoretical undrained strengths. The agreement between these measurements and calculations indicates that the parameters in Table 5.2 accurately describe the properties of E-grade kaolin, and the vane shear tests accurately measured the undrained strength of the samples.

The values of the ratio of undrained shear strength to vertical effective stress,  $S_u/\sigma_v'$ , for the consolidated E-grade samples are shown in Table 5.1. The  $\sigma_v'$  values are the final consolidation pressures, accounting for the effects of wall friction in the container. Based on the average vane shear strengths measured for the 'undisturbed' soil in the container, the  $S_u/\sigma_v'$  values ranged from 0.17 – 0.24, with an average value of  $S_u/\sigma_v' = 0.20$ . With the lower average strengths measured for the remoulded spoil samples,  $S_u/\sigma_v'$  ranged from 0.12 – 0.17, with an average value of 0.14.

The  $S_u/\sigma_v'$  values determined for the 'undisturbed' E-grade kaolin samples compare well with the typical range of values for normally consolidated clays.

There is significant scatter in reported values of  $S_u/\sigma_v'$  for normally consolidated clays of varying plasticity, however, the empirical relationship proposed by Skempton (1957) shown as equation 5.7 provides a reasonable fit to data collected for various soils (Wood, 1990).

$$\frac{S_u}{\sigma_v'} = 0.11 + 0.37I_p \quad \text{Eqn 5.7}$$

For E-grade kaolin with a plasticity index  $I_p = 21\%$ , this relationship predicts a value of  $S_u/\sigma_v' = 0.19$ , in good agreement with the average value of 0.20 determined for the 'undisturbed' kaolin samples. Figure 5.4 shows data of  $S_u/\sigma_v'$  compiled from field shear vane tests on normally consolidated soft clays and silts of varying plasticity, from Terzaghi *et al.* (1996). Also shown is a typical relationship proposed by Bjerrum (1973). The values of  $S_u/\sigma_v'$  determined for the 'undisturbed' E-grade kaolin samples are plotted in Figure 5.4, showing good agreement with the range of values for other normally consolidated soils of similar plasticity.

The undrained shear strengths of the normally consolidated E-grade kaolin samples measured with the shear vane compared well with theoretical values based on the sample moisture contents and the Cam-clay parameters for this soil. Based on the vertical effective stresses adjusted for wall friction effects in the container during consolidation, the  $S_u/\sigma_v'$  values for the E-grade kaolin samples agree well the typical range of values for normally consolidated clays. Based on the data obtained from these large scale samples, the parameters shown in Table 5.2 are considered to be accurate for describing the strength and compressibility of E-grade kaolin.

### 5.3 Screw conveyor tests with kaolin samples

Consolidated E-grade kaolin samples were prepared to form uniform, saturated clay samples with consistent properties for the model screw conveyor tests. The measured properties of these samples are discussed above and summarised in Table 5.1. The maximum consolidation pressures were varied to form samples of different strength. The tests were performed with different

operating conditions to investigate effects of the discharge condition, the sample pressure, and the screw pitch on the conveyor operation.

The preparation of the model screw conveyor system for a test is described in Section 4.5. Immediately prior to the test, the sample pressure was applied with the container drainage valve closed to pressurise the sample under undrained conditions. The different stages of the tests when operating conditions were varied were based on the sample height, as described in Section 4.5. The height of the kaolin samples after consolidation ranged from approximately 530 to 580 mm, so the sample height available for the tests was 305 to 355 mm. With this sample volume, tests could be performed in two stages. The sample properties and test conditions for the kaolin tests are summarised in Table 5.3.

The test 1 sample was consolidated to  $\sigma'_{v\max} = 100$  kPa, with a 200 kPa pressure applied during the test. The conveyor discharge outlet was restricted by the reduction valve, and screw (1) (with a pitch of 80 mm) was used, with a nominal screw speed of 5 rpm.

Test 2 was performed with the same conditions as test 1, but with the sample consolidated to  $\sigma'_{v\max} = 200$  kPa for a higher undrained strength.

The test 3 sample was consolidated to  $\sigma'_{v\max} = 50$  kPa for a lower undrained strength than in tests 1 and 2. A 200 kPa pressure was applied during the test, with a nominal screw speed of 5 rpm. The reduction valve was installed on the outlet for the first stage, and removed for the second stage to investigate effects of the different discharge conditions.

The test 4 sample was consolidated to  $\sigma'_{v\max} = 100$  kPa, for a similar strength as in test 1. The nominal screw speed was 5 rpm, and the discharge outlet was unrestricted. A sample pressure of 100 kPa was applied for the first stage, and increased to 200 kPa for the second stage. This test was performed to investigate effects of the sample pressure on the conveyor operation.

Test 5 was performed with the same conditions as test 4, but using screw (2) (with a longer pitch of 133 mm). This test measured the effect of the screw pitch on the conveyor operation with sample pressures of 100 and 200 kPa applied during the different stages.

Test 6 was also performed using screw (2) and with the sample consolidated to  $\sigma_{v\max}' = 100$  kPa. A pressure of 200 kPa was applied, and the nominal screw speed was 5 rpm. The test was carried out in two stages with different discharge conditions as in test 3.

The objective of the tests with consolidated kaolin samples was to investigate the mechanics of the model screw conveyor operation under different conditions with uniform soft clay samples. These tests provided data of the effects of the sample strength, discharge condition, sample pressure, and screw pitch on the conveyor operation.

## 5.4 Screw conveyor test data processing

The processing of the data logged during the tests to calculate the parameters measured by the instruments monitoring the screw conveyor operation is described here.

### 5.4.1 Data logging

The data acquisition system used to log the outputs of the instruments on the screw conveyor system was described in Section 4.4.6. A total of 31 channels were logged at a rate of 5 Hz throughout the tests. During the data processing, a five-point moving average was applied to the raw data to reduce noise in the output signals recorded. The parameters measured by the instruments were calculated from the averaged data.

During preparation of the screw conveyor system for a test, the zero offsets of the instrument outputs were recorded. This was carried out with the load cells and the torque cell assembled in the conveyor, and with the pore pressure transducers and jack pressure transducer at atmospheric pressure.

### 5.4.2 Data processing

#### 5.4.2.1 Sample pressure

The pressure applied to the sample throughout a test was calculated from the jack pressure transducer output, measuring the pressure in the gas supply line to the jack. The calibration coefficient in Table 4.7 was used. The total vertical pressure applied to the sample was calculated from the gas pressure, using the ratio of the jack bore and piston areas from the dimensions shown in Table 4.1. The pressure on the sample from the mass of the piston was also included.

As shown later, the sample pressure was constant throughout the tests with the jack extending as the piston lowered into the container as the screw conveyor extracted the soil.

#### **5.4.2.2 Sample height**

The height of the soil sample in the container was measured by the draw-wire transducer (DWT) fixed to the piston. The initial sample height was determined from the initial position of the piston, measured with a ruler to the nearest millimetre. The changes in sample height were calculated from the DWT output, using the calibration coefficient in Table 4.7.

As shown later, the sample height decreased at a constant rate during the conveyor operation. From the change of sample height over time, the rate of change of the sample volume is calculated to measure the volumetric flow rate of the soil through the screw conveyor.

#### **5.4.2.3 Screw conveyor torque**

The torque to rotate the screw was measured by the strain-gauge torque cell on the drive shaft. Using the calibration coefficient in Table 4.7, the torque in the screw drive shaft was calculated from the torque cell output recorded during the conveyor operation.

#### **5.4.2.4 Pore water pressures**

The pore water pressure at the soil-casing interface was measured at the instrumented sections along the conveyor by the pore pressure transducers described in Section 4.4.2. The pore water pressures were calculated from the recorded outputs using the calibration coefficients for these instruments shown in Table 4.7.

#### **5.4.2.5 Load cell measurements**

The load cells measuring the total normal stress and shear stress acting on the conveyor casing were described in Section 4.4.1. The typical response of a load cell during a test is shown in Figure 5.5. The outputs of the two strain gauge circuits measuring the normal force at each end of the instrument were similar, indicating the normal stress was uniform over the active face.

The normal force, shear force and moment on the active face are calculated from the outputs of the three circuits using the inverse of the matrix of calibration coefficients:

$$\begin{pmatrix} N \\ S \\ M \end{pmatrix} = [A]^{-1} \begin{Bmatrix} V_B - V_{B0} \\ V_C - V_{C0} \\ V_A - V_{A0} \end{Bmatrix} \quad \text{Eqn 5.8}$$

where:  $N, S, M$  are the normal force, shear force and moment  
 $[A]^{-1}$  is the inverse of the matrix of calibration coefficients  
 $V_B, V_C$  are the outputs from the normal force circuits  
 $V_A$  is the output from the shear force circuit  
 $V_{B0}, V_{C0}, V_{A0}$  are the zero offsets of the circuits

Assuming the normal and shear stresses are uniformly distributed over the active face, the stresses are calculated from the measured forces and the plan area of the platen, using the dimensions in Table 4.5.

The average total normal stress and resultant shear stress acting on the casing were calculated from the measurements of the two load cells at each instrumented section. As shown in Figure 5.6, the normal stresses measured by the two load cells were approximately equal, resulting in a similar average normal stress. The similar measurements of the two load cells with different orientations indicate a uniform distribution of total normal stress over the internal surface of the casing. The resultant shear stress was calculated from the components measured simultaneously by the load cells oriented parallel and perpendicular to the screw axis:

$$\tau_c = \sqrt{(\tau_{//}^2 + \tau_{\perp}^2)} \quad \text{Eqn. 5.9}$$

where:  $\tau_c$  is the resultant shear stress acting on the casing (kPa)  
 $\tau_{//}$  is the shear stress component parallel to screw axis (kPa)  
 $\tau_{\perp}$  is the shear stress component perpendicular to screw axis (kPa)

#### 5.4.2.6 Effective stress

The effective normal stress in the soil at the interface with the casing was calculated as the difference between the average total normal stress and the pore water pressure measured at each instrumented section.

#### **5.4.2.7 Pressure gradients**

The instrumentation scheme was designed to measure the pressure gradients along the length of the conveyor. From the total normal stress, pore water pressure and effective stress measured at the instrumented sections, the pressure changes along the conveyor can be determined.

The screw conveyor reached a steady state operating condition once the conveyor was filled and discharging soil at a constant rate. During steady state operation, the total normal stress, pore water pressure, and effective stress at each instrumented section was approximately constant over time. The pressures measured at each section were averaged over time and plotted against the positions of the instrumented sections to construct the gradients of total stress, pore water pressure and effective stress along the conveyor.

The shear stresses measured at the instrumented sections reached approximately stable values during steady state operation. The values of the resultant shear stress at each section were averaged over time, and plotted against the position of the instrumented section to show the changes of the shear stress along the conveyor.

Gradients of the total stress, pore water pressure, effective stress and resultant shear stress along the conveyor during the tests with various soil samples and operating conditions are presented with the discussions of the test results.

### **5.5 Mechanics of screw conveyor operation**

The following section presents results from test 1, with the test conditions as summarised in Table 5.3. Detailed measurements from this test are presented to illustrate the mechanical operation of the screw conveyor with clay soils.

#### **5.5.1 Soil flow rate**

The displacement of the piston, change of sample height, and the sample pressure measured during test 1 with the screw rotating at 5 rpm are shown in Figure 5.7. The 200 kPa pressure applied to the sample remained stable during the conveyor operation. With the screw rotating at a constant speed, the piston lowered into the container at a constant rate as the sample height reduced from the initial height at the start of the test.

The average rate of change of sample height in the container during the conveyor operation calculated from the measurements shown in Figure 5.7 is 0.25 mm/s. From the container dimensions, the measured rate of change of sample volume in the container is  $34.6 \times 10^3 \text{ mm}^3/\text{s}$ , or 124.6 L/hr. This should be equal to the volumetric flow rate of the screw conveyor, assuming that the conveyor is completely full of clay, and that the clay does not change in volume.

The maximum volumetric flow rate of the conveyor can be calculated from the volume of the screw channel over a length of one pitch, and the rotational speed of the screw. Assuming the conveyor is completely full of soil, and that the soil advances along the screw axis by a length equal to the screw pitch with each rotation, the maximum volumetric flow rate is given by:

$$Q_{\max} = \pi/4(D_c^2 - D_s^2) \times (t - e) \times (N \times 60) \quad \text{Eqn. 5.10}$$

where  $Q_{\max}$  is the maximum volumetric flow rate ( $\text{m}^3/\text{hr}$ )  
 $D_c$  is the internal diameter of the conveyor casing (m)  
 $D_s$  is the screw shaft diameter (m)  
 $t$  is the screw pitch (m)  
 $e$  is the screw flight thickness (m)  
 $N$  is rotational speed of screw (rpm)

From the dimensions of the conveyor and screw (1) shown in Tables 4.2 and 4.3, the maximum flow rate with a screw speed of 5 rpm is  $Q_{\max} = 173.4 \text{ L/hr}$ . The flow rate measured from the piston displacement is lower than the maximum calculated from equation 5.10. This indicates that the soil advances along the screw by a length less than the screw pitch for each rotation, due to the soil slipping on the screw surfaces. As a result of the relative movement between the soil and the screw, shear stresses act at the interfaces of the soil and the screw shaft and flight surfaces, and the flow rate is reduced below the maximum. Similar observations of the flow rates and the conveyor discharge efficiency were made in the other tests, as discussed later.

The flow rate of the soil along the conveyor is variable, depending on the forces acting on the soil as the screw rotates. The flow rate also influences the pressure gradient and the screw torque. This is discussed further for the theoretical model of the screw conveyor operation in Chapter 7.

### 5.5.2 Total normal stresses

The average total normal stress measured at each instrumented section during test 1 is shown in Figure 5.8. The conveyor is empty at the start of the test, and the load cells at each section respond as the soil moves along the conveyor. The stresses increase as the conveyor fills with soil, reaching approximately stable values once steady state operation is achieved when the conveyor is full and discharging soil at a constant rate. The increase in pressure at  $t = 175$  s corresponds to the time at which soil was first discharged, and is due to the pressure required to extrude the soil through the restricted discharge outlet. Stable pressures were then measured at all sections and the further increase in pressure at  $t = 275$  s was due to a small adjustment of the screw speed. The total normal stresses on the casing remained approximately constant during steady state operation with the screw rotating at a constant speed. The total pressure gradients obtained from these measurements are discussed in Section 5.5.6.

During operation, the ratio of the sample undrained shear strength to the total stress in the conveyor,  $S_u/p$ , is small. The clay is therefore fluid, and the total stress does not depend on the plane of measurement. At the steady state, the total normal stress on the casing at section 1, closest to the start of the conveyor, was slightly higher than 200 kPa. The total stress reduced along the conveyor to approximately 130 kPa at section 4, closest to the discharge outlet. The high pressure close to the end of the conveyor is required to extrude the soil through the restricted discharge outlet. Effects of the discharge outlet condition on the conveyor operation are discussed in Section 5.6.2.

The small fluctuations in the total normal stress measured by the load cells at each section are due to the flights of the screw passing the active face of the instruments on the surface of the conveyor casing. The period of the cyclic fluctuations shown in Figure 5.8 corresponds to the rotational speed of the screw.

### 5.5.3 Pore water pressures

The pore water pressures measured at the interface of the soil and the conveyor casing at each section during test 1 are shown in Figure 5.9. These measurements show similar trends as observed for the total normal stresses. The instruments respond as the soil moves along the conveyor, and the pore water pressures increase to approximately constant values once steady state operation is established. The pore water pressure reduced along the length of the conveyor, and was lower than the total normal stress at each section, indicating a positive effective stress in

the soil. The constant total stress and pore water pressure at each section results in the effective stress also reaching a constant value during steady state operation. The pore water pressure gradients along the conveyor obtained from these measurements are discussed in Section 5.5.6.

#### 5.5.4 Casing shear stresses

The shear stresses measured on the surface of the conveyor casing during test 1 are shown in Figure 5.10. The components of the shear stress parallel and perpendicular to the screw axis measured by the load cells at each section are shown in Figures 5.10(a) and (b). The resultant shear stresses calculated from equation 5.9 are shown in Figure 5.10(c). The shear stress components reached approximately constant values after 300 s, once steady state operation was established and the total normal stresses on the casing were stable. The shear stress measurements also show cyclic fluctuations due to the flights of the screw passing the active face of the load cells. The magnitude of the shear stress components measured at the different sections varied. Consistent trends in the shear stress components at the different sections were not observed between the screw conveyor tests performed, and these variations are thought to result from differences in the local direction of the soil flow in the screw channel at the different instrumented sections.

Although the parallel and perpendicular shear stress components varied between the instrumented sections, Figure 5.10(c) shows that during steady state operation the resultant shear stress at each section was approximately equal. This was observed consistently in all tests, and indicates that the resultant shear stress acting on casing was approximately constant along the conveyor. As shown later in Figure 5.17, the average resultant shear stress measured at each section during steady state operation in test 1 ranged from 9.3 to 10.1 kPa. As shown in Table 5.1, the vane shear strengths for this sample ranged from 10 to 12 kPa, and the undrained shear strength calculated from the moisture content was 10 kPa. These measurements indicate that the resultant shear stress acting on the casing surface is approximately equal to the undrained strength of the soil. This was also observed in the other screw conveyor tests with samples of varying strength.

Following the tests, it was observed that a layer of clay was adhered to, and completely covered, the surface of the conveyor casing. The thickness of the clay layer was approximately equal to the 3 mm radial clearance between the screw flights and the casing. The layer of clay on the casing surface indicates that shearing occurred on a surface formed within the soil, and involves a soil-

on-soil shearing mechanism rather than soil-steel shearing at casing interface. The screw shaft and flight surfaces did not have a layer of clay adhering to them, indicating that shearing on the screw surfaces involves a soil-steel interface shearing mechanism.

Similar observations have been reported from direct shear box tests performed with kaolin sheared against a mild steel interface, with a residual strength equivalent to the soil-on-soil value measured (Lemos and Vaughan, 2000). Other observations of the shear surface between clays and steel from shear box tests have shown that the majority of the shearing area involves clay on clay shearing, rather than direct shearing at the soil-steel interface (Littleton, 1976). Tsubakihara and Kishida (1993) report direct shear tests between clay and mild steel, and suggested that when the roughness of the steel surface exceeded a critical value, shearing occurred within the clay sample, with the maximum frictional resistance equal to the shear strength of the clay. For steel surfaces smoother than the critical roughness, shearing of the clay occurred by sliding at the interface. The roughness of the screw conveyor casing surface exceeds the suggested critical roughness, consistent with the shear surface observed forming within the clay. As discussed by Chow (1996), similar observations have been made in many studies of piles in various clay soils, with a layer of clay adhering to the surface of steel piles and shearing occurring in the soil away from the interface. The clay-steel interface shearing mechanisms and measurements in the screw conveyor tests are discussed in Section 5.7.

### **5.5.5 Screw torque**

The torque to rotate the screw during test 1 measured by the instrumented drive shaft is shown in Figure 5.11. The average torque measurement during the test is also shown. The torque increased linearly over time from the start of the test as the conveyor filled with soil, and reached a constant average value once steady state operation was established. The initial linear increase and the constant average torque result from the uniform resultant shear stresses acting on the casing surface along the conveyor, as shown by the load cell measurements. The torque required to rotate the screw is proportional to the shear stress acting over the surface area of the conveyor casing. The torque measurements from other tests with kaolin samples of varying strength and with different conveyor operating conditions are discussed in Section 5.6.

The screw torque measured by the instrumented drive shaft showed cyclic fluctuations in all of the tests. The period of the torque cycles is equal to the rotational frequency of the screw, and the amplitude was approximately constant. The amplitude did not depend on the magnitude of

the torque, and was similar in tests with different sample properties and conveyor operating conditions. The torque cycles are believed to result from mechanical effects of the eccentricity in the screw shaft created by the radial clearance between the screw flights and the conveyor casing. As the amplitude of the torque cycles is constant, the average torque during steady state operation is also constant, and is used for comparison of the torque for different tests. The stable period of the torque cycles allows an accurate direct measurement of the rotational speed of the screw during operation.

### 5.5.6 Pressure gradients

Once steady state operation was established, the total normal stress, pore water pressure and effective stress at each instrumented section reached approximately constant values. This is illustrated in Figure 5.12, showing the stresses measured at one of the sections during steady state operation in test 1. From these measurements at each section, the pressure gradients along the conveyor are determined as described in Section 5.4.2.7. The measurements from which the pressure gradients are calculated for test 1 are shown in Figures 5.13(a) and (b). The gradients of the total normal stress, pore water pressure, and effective stress calculated from the average measurements during steady state operation are shown in Figure 5.14. The total stress and pore water pressure decrease linearly along the conveyor at similar rates, resulting in the effective stress remaining approximately constant along the conveyor.

The resultant shear stresses acting on the casing are constant during steady state operation, and approximately equal along the conveyor, as shown by the measurements at each section during test 1 in Figure 5.15. The values of the resultant shear stress normalised by the effective stress, representing the friction coefficient  $\tau/\sigma_n'$ , are also calculated from the measurements. The values of  $\tau/\sigma_n'$  at each section are shown in Figure 5.16. The relatively large fluctuations are due to the fluctuations in the five measured parameters from which the values of  $\tau/\sigma_n'$  are calculated; however the average values are approximately constant. Figure 5.17 shows the constant average resultant shear stresses and friction coefficients along the conveyor. The average resultant shear stresses ranged from 9.3 to 10.1 kPa, approximately equal to the undrained shear strength of the clay, as discussed above. The average friction coefficients in this test ranged from 0.225 to 0.325, corresponding to friction angles of 12.7° to 18.0°. These values are similar to residual friction coefficients measured in ring shear tests with kaolin samples at high shear rates, reported by Tika *et al.* (1996). The friction coefficients measured in the conveyor tests with kaolin samples are discussed further in Section 5.7.

### **5.5.7 Mechanical operation of the model screw conveyor with clay soils**

The results of test 1 presented above are summarised here to describe the mechanics of the model screw conveyor observed during operation with clay soils.

Once the conveyor was completely filled and discharging soil with stable operating conditions, a steady state was established. The soil flow rate through the conveyor was constant, and the parameters measured at the instrumented sections were stable during the steady state operation. The resultant shear stresses acting on the casing were approximately equal at each instrumented section, indicating that the shear stresses were constant along the conveyor. The resultant shear stress was approximately equal to the undrained shear strength of the soil. The constant shear stresses result in a constant total pressure gradient along the conveyor. The changes in pore water pressure along the conveyor were approximately equal to the changes in total stress, which is associated with the undrained conditions of the screw conveyor operation, and results in similar total and pore water pressure gradients. The similar changes in total pressure and pore water pressure result in the effective stress remaining approximately constant along the conveyor, corresponding to the constant shear stresses. The torque to rotate the screw is also constant due to the uniform shear stresses acting on the casing along the conveyor.

The general mechanical behaviour of the screw conveyor operating with clay soils seen in test 1 was observed in a wide range of tests. The total pressure gradients along the conveyor are influenced by various operating conditions, including the soil strength, the discharge outlet condition, the pressure applied to the sample, and the screw pitch. Effects of these variables were investigated in the tests performed with kaolin samples, as discussed in Section 5.6.

The constant total pressure gradient measured is consistent with other studies of model scale and full scale EPB machine screw conveyors, described in Section 2.6.2. As discussed in Section 2.6.3, theoretical models of screw conveyors assuming constant shear stresses along the conveyor predict constant pressure gradients. The measurements from the model screw conveyor tests reported here confirm the assumptions and predictions of these theoretical models.

## 5.6 Effects of screw conveyor operating conditions

The tests with kaolin samples were performed with varying conveyor operating conditions, summarised in Table 5.3. The samples were prepared with different undrained strengths, and the conveyor discharge condition, applied test pressure, and screw pitch were varied. Measurements from the tests are summarised in Table 5.4, and the following sections discuss the results illustrating effects of the operating variables on the conveyor performance.

### 5.6.1 Sample strength

The samples for tests 1, 2 and 3 were consolidated to maximum piston pressures of  $\sigma_p'_{max} = 100$ , 200 and 50 kPa respectively, to achieve different undrained shear strengths. The vane shear strengths are shown in Table 5.3, which agreed with the strengths calculated from the moisture contents. For these tests the conveyor was operated with the same conditions, with a nominal screw speed of 5 rpm, piston pressure of 200 kPa, and the discharge outlet restricted.

The mechanical operation of the model screw conveyor observed in test 1 was discussed above and presented in Figures 5.7 to 5.17. Similar mechanics were observed in tests 2 and 3, although with variations in the pressure gradients, shear stresses and screw torque due to the different sample strengths, as summarised in Table 5.4.

The average total stress measurements from test 2 are shown in Figure 5.18. As the conveyor filled with soil during the first 200 seconds, the total stress decreased along the conveyor. The soil was first discharged at  $t = 225$  s, corresponding to the increase in total stress at all sections as the conveyor generated the pressure required to discharge the soil through the restricted outlet. The increase in total stress was greater towards the end of the conveyor, with the pressure gradient increasing along the length. A small adjustment of the motor speed was made at  $t = 350$  s, causing the increases in the total stress observed at this time. After  $t = 400$  s, steady state operation was established with the total stress constant at each section, and increasing along the conveyor. The gradients of the total stress, pore water pressure and effective stress during steady state operation are shown in Figure 5.19. The total stress increased approximately linearly along the conveyor, with a similar pore water pressure gradient, resulting in constant effective stresses.

The total pressure gradients during tests 1, 2 and 3 are compared in Figure 5.20. The total stress decreased along the conveyor in tests 1 and 3, while for test 2 with the higher strength sample,

the total pressure increased. The dissipation or generation of pressure along the conveyor depends on the pressure required to extrude the soil through the restricted discharge outlet. The total pressure measured at section 4 closest to the outlet increased with the sample strength. Inferred values of the discharge pressure, representing the total pressure in the conveyor at the outlet, are estimated from linear regression lines fitted to the total pressure gradients and extrapolated to a conveyor length of 950 mm (the mid point of the outlet). Table 5.4 includes the values of the inferred discharge pressure for these tests, showing the increase with the sample strength. This data is shown later in Figure 5.25 and discussed in Section 5.6.2.

Figure 5.21 shows the average resultant shear stresses at the casing surface during tests 1, 2 and 3. The shear stresses were constant along the conveyor, resulting in the constant total pressure gradients. For each test, the resultant shear stress acting on the casing was approximately equal to the undrained strength measured for the spoil samples after being remoulded during the passage through the conveyor, shown in Table 5.1. These values are slightly lower than the undrained strengths measured in the sample container and calculated from the moisture content. These measurements indicate that the shear stress acting on the casing corresponds to the undrained strength of the remoulded soil, due to the shearing of the soil as it flows along the conveyor.

The screw torque increased with the strength of the samples. Figure 5.22(a) shows the average torque from all tests with kaolin samples, plotted against the undrained shear strength. The undrained strength is approximately equal to the resultant shear stress acting on the casing, and Figure 5.22(b) shows the screw torque increasing with the average casing shear stress. The analysis of the conveyor operation presented in Chapter 7 shows that the screw torque is proportional to the shear stress acting on the casing, as observed in these tests.

The results from these tests with kaolin samples show effects of the soil strength on the pressure gradient, casing shear stress, discharge pressure, and screw torque during the conveyor operation. Further measurements showing the influence of the soil strength on the conveyor operation from tests with conditioned clay samples are presented in Chapter 6.

### 5.6.2 Discharge condition

Tests were performed with the discharge condition varied to investigate the effects on the conveyor operation. As described in Section 4.4.3, a restricted discharge condition was created by connecting the reduction valve to the unrestricted outlet. This modelled the variable opening of the outlet on a full scale EPB machine screw conveyor, usually controlled with a gate valve.

The results from tests 1, 2 and 3 discussed above showed that with the outlet restricted, the discharge pressure, and the dissipation or generation of pressure along the conveyor, are influenced by the strength of the soil. The total pressure gradients measured in these tests are shown in Figure 5.20, and the increase of the inferred discharge pressure with sample strength is shown in Figure 5.25. The inferred values of the discharge pressure are obtained from regression lines fitted to the total pressure gradients, extrapolated to the mid-point of the discharge outlet.

Test 3 was performed in two stages with the discharge condition varied. The total pressure gradients for the different discharge conditions are shown in Figure 5.23. The measured total pressure changes and gradients are shown in Table 5.4. When the reduction valve was removed from the outlet, the total pressure at section 4 dropped by about 70 kPa, with an increase in the pressure gradient. The inferred discharge pressures for both stages of this test are shown in Table 5.4 and in Figure 5.25. With the restricted discharge condition, the total pressure dissipated along the conveyor to approximately 92 kPa at the outlet. For the unrestricted condition, the pressure dissipated to approximately 11 kPa at the outlet.

For both discharge conditions in test 3, the average resultant casing shear stresses were equal, similar to the undrained strength of the soil. As shown in Table 5.4, the soil flow rate was higher and the screw torque was lower in the second stage of the test with the outlet unrestricted and the screw speed constant. The analysis of the screw conveyor operation in Chapter 7 shows that the total pressure gradient and the screw torque depend on the casing shear stress and the soil flow rate. The changes in the pressure gradient and torque observed when the discharge condition and the required discharge pressure were varied are related to the change in the soil flow rate, as discussed in Chapter 7.

Test 6 was performed with varied discharge conditions as in test 3, but using screw (2) with a longer pitch. Similar effects of the discharge condition on the conveyor operation were observed,

as discussed in Section 5.6.4. The inferred discharge pressures for this test are also shown in Figure 5.25.

The outlet of the screw conveyor can be modelled as an extrusion die, in which the soil flows from a barrel and through a die of reduced cross-sectional area. The outlet tube of the conveyor casing is considered as the barrel, and the reduction valve as the die. The geometry and dimensions of the discharge outlet are shown in Figure 4.4. Upper bound solutions for the axisymmetric extrusion of a Tresca material through a smooth square die are given by Calladine (1985). For a flow mechanism based on a ‘dead zone’ of material forming behind the entrance of the die as shown in Figure 5.24, an upper bound for the extrusion pressure,  $P$ , can be calculated approximately from the die area reduction,  $r_a$ , and the undrained shear strength of the soil,  $S_u$ , according to:

$$P = 2S_u \left[ 0.5 + 1.5 \ln \left( \frac{1}{1 - r_a} \right) \right] \quad \text{Eqn 5.11}$$

This calculation does not include the pressure from shear stresses acting on the walls of the die and the barrel. Following the analysis of paste extrusion through dies presented by Benbow and Bridgwater (1993), the additional pressure from the wall shear stresses can be combined with equation 5.11 to give an expression for the total extrusion pressure:

$$P = 2S_u \left[ 0.5 + 1.5 \ln \left( \frac{1}{1 - r_a} \right) \right] + 4\tau(L_d/D_d) + 4\tau(L_o/D_o) \quad \text{Eqn 5.12}$$

- where:
- $P$  is the extrusion pressure (kPa)
  - $S_u$  is the undrained shear strength of the soil (kPa)
  - $\tau$  is the wall shear stress (kPa)
  - $D_d$  is the die diameter (m)
  - $D_o$  is the barrel diameter (m)
  - $L_d$  is the length of the die (m)
  - $L_o$  is the barrel length (m)
  - $r_a$  is the die area reduction ( $r_a = 1 - (D_d/D_o)^2$ )

Equation 5.12 can be used to estimate the total pressure required in the conveyor at the discharge point to extrude the soil through the restricted outlet. Using the dimensions of the outlet shown in Figure 4.4, and assuming the wall shear stresses are equal to the undrained shear strength of the soil, the theoretical discharge pressure calculated for the restricted outlet is shown in Figure 5.25 with data from the kaolin tests.

The theoretical discharge pressure for the restricted outlet increases with the undrained strength of the soil, as observed in the tests. The theoretical calculation agrees reasonably well with the inferred discharge pressures from the tests, but under-estimates the data. As the soil flows from the screw into the outlet, the direction of flow changes, and the soil cross-section changes due to the different dimensions of the outlet relative to the casing and the screw channel. This flow causes internal shearing of the soil which is not included in the flow mechanism assumed for the theoretical die extrusion model, resulting in the discharge pressure in the tests with the restricted outlet being higher than predicted by the theory. The internal shearing as the soil flows from the screw into the outlet also accounts for the discharge pressures in the tests with the unrestricted outlet, as shown in Figure 5.25.

The theory based on the die extrusion model allows reasonably accurate estimates of the discharge pressure for the restricted outlet condition. This particular outlet condition is specific to the model screw conveyor. However, the effects of the discharge condition on the conveyor operation discussed here are expected to be similar for other screw conveyors where the outlet can be restricted, for example by the gate valve typically used on EPB machine screw conveyors.

### 5.6.3 Test pressure

Test 4 was performed in two stages with applied piston pressures of 100 and 200 kPa, with the test conditions summarised in Table 5.3. The screw was stopped to adjust the pressure, as shown in the record of the piston pressure, screw speed and sample height for this test in Figure 5.26.

Figure 5.27 shows the total normal stress measurements from test 4. The total pressure dissipated along the conveyor for both piston pressures with the outlet unrestricted. After the first stage, the piston pressure was increased from 100 to 200 kPa at  $t = 700$  s, causing an increase in the total stress at the start of the conveyor. The screw started rotating for the second stage at  $t = 840$  s with the conveyor full of soil, and steady state operation was quickly established with the total stress at all sections increasing to stable values. As shown in Figure 5.28, the total pressure

decreased linearly along the conveyor for both of the piston pressures applied. A larger pressure drop and gradient was measured with the higher piston pressure applied, with the values shown in Table 5.4. The inferred discharge pressures with the outlet unrestricted were equal for both piston pressures, as shown in Figure 5.25.

The average resultant shear stress on the casing was similar for both stages of test 4 with different piston pressures, as shown in Figure 5.29. As in other tests, the shear stresses were constant along the conveyor and approximately equal to the undrained strength of the sample. The measurements from test 4 summarised in Table 5.4 show that the soil flow rate increased and the average screw torque decreased slightly in stage 2 with the higher piston pressure. The changes in the total pressure gradient and screw torque when the different piston pressures were applied result from the change in the soil flow rate. As shown by the theoretical model of the screw conveyor presented in Chapter 7, the influence of the soil flow rate allows different pressure gradients and screw torques with similar shear stresses acting on the casing.

#### **5.6.4 Screw pitch**

The screw pitch influences the soil flow rate and pressure gradient along the conveyor. Model conveyor tests were performed with screw (2), of similar geometry to screw (1) but with a longer pitch of 133 mm. Two tests were performed with kaolin samples using screw (2), with the test conditions summarised in Table 5.3. Test 5 was performed with different piston pressures, and test 6 with different discharge conditions. These tests were performed to investigate effects of the screw pitch on the conveyor operation under different conditions.

The total pressure gradients measured in test 5 with piston pressures of 100 and 200 kPa are shown in Figure 5.30. A larger pressure gradient occurred when the higher piston pressure was applied, as observed in test 4 with screw (1). Comparison of the results from tests 4 and 5 performed with similar strength samples and operating conditions shows that a smaller pressure gradient was measured for screw (2) with the longer pitch.

Figure 5.31 shows the total pressure gradients measured during test 6 with varied discharge conditions. With the outlet restricted, the total pressure increased slightly along the conveyor due to the pressure required to extrude the soil through the reduction valve. With the outlet unrestricted, the pressure required to discharge the soil was reduced, and the total pressure dissipated along the conveyor. These results show a similar influence of the outlet condition on

the discharge pressure and pressure gradients as observed in test 3 with screw (1). Comparison of the measurements from stage 2 of test 6 with those from tests 3 and 4 with similar operating conditions again shows a smaller pressure gradient was measured for screw (2) of longer pitch.

The inferred discharge pressures with the different operating conditions in tests 5 and 6 are shown in Figure 5.25. With the outlet restricted and unrestricted, the discharge pressures in the tests with screw (2) were higher than those with screw (1) for similar operating conditions. Screw (2) with the longer pitch discharges a larger volume of soil with every rotation than screw (1). The discharge of soil from screw (2) therefore involves a greater amount of internal shearing as the soil flows from the screw into the outlet, resulting in the higher discharge pressures.

The average casing shear stress, screw torque, and soil flow rates measured in tests 5 and 6 are summarised in Table 5.4. The resultant shear stresses were constant along the conveyor, and approximately equal to the undrained strength of the samples. The torque measurements from tests 5 and 6 are plotted against the sample strength and the casing shear stress in Figures 5.22(a) and (b), with the data from the tests with kaolin samples using screw (1). The torque was similar for screws (1) and (2) with samples of similar strength, as the torque is related to the shear stress acting over the surface area of the conveyor casing and is not affected by the screw pitch.

The soil flow rates measured in tests 5 and 6 were higher than those for screw (1) with the same screw speed. The longer pitch and larger helix angle of screw (2) increases the component of the soil flow in the direction of the screw axis. This causes the soil to move along the conveyor by a greater amount with every screw rotation, increasing the flow rate. The flow of soil along the conveyor is discussed further in the analysis of the screw conveyor presented in Chapter 7.

The soil flow rates in the tests with screw (2) increased when the piston pressure was increased in test 5, and when the discharge outlet was unrestricted in test 6. Similar effects of the operating conditions on the flow rate were observed in tests 3 and 4 with screw (1). The changes in the pressure gradient and screw torque observed when the operating conditions were varied in tests 5 and 6 result from the changes in the flow rate. The theoretical model of the screw conveyor presented in Chapter 7 demonstrates that the pressure gradient and torque vary with the soil flow rate when the casing shear stress is constant, as observed in these tests. The theoretical model also predicts the smaller pressure gradients observed for a screw of longer pitch, resulting from the influence of the screw helix angle on the direction of soil flow along the conveyor.

## 5.7 Interface shearing mechanisms in the model screw conveyor

As discussed in Section 5.5.4, shearing of the soil on the conveyor casing occurred on a surface within the clay close to the interface, and involves soil-on-soil shearing. The test results show that the resultant shear stresses acting on the casing are approximately equal to the undrained shear strength of the soil. Due to the large shear displacements as the soil flows along the conveyor, the clay at the shear surface is sheared to a residual state. Assuming that the shear surface forms at a radius of 51 mm, corresponding to the edge of the screw flight, the shear rate with the screw rotating at 5 rpm is approximately 1600 mm/min, indicating a very fast shear rate during the conveyor operation.

As discussed in Section 5.5.6 and shown in Figure 5.17 for test 1, the average resultant shear stresses and friction coefficients are approximately constant along the conveyor. The average friction coefficients measured at each instrumented section in tests 1 to 6 with the kaolin samples of varying strength are shown in Figure 5.32, and the average values are shown in Table 5.4. Most of these values are within the range  $\tau/\sigma'_n = 0.25 - 0.30$ , corresponding to friction angles of  $14.0^\circ$  to  $16.7^\circ$ . These values represent the residual friction coefficients and friction angles measured for the kaolin samples under fast, undrained shearing conditions.

Results from ring shear tests performed on various soils at a range of shear rates are reported by Tika *et. al* (1996). Tests with kaolin samples at slow, drained rates of shear showed that shearing at the residual condition occurred in a sliding mode, in which the particles orientate in the direction of shearing and deform by sliding on a thin, polished, continuous shear surface. Tests performed at different shear rates showed a positive rate effect for kaolin, with the residual friction coefficient at fast shear rates higher than the slow, drained residual value. For kaolin samples with a plasticity index of 33%, residual friction coefficients of 0.229 and 0.238 were measured for slow, drained shear rates with normal stresses of 500 and 250 kPa. At various faster shear rates up to 5400 mm/min, fast residual friction coefficients in the range 0.234 to 0.365 were measured, increasing with the rate of shear.

Interface shear tests performed in the ring shear apparatus with clay soils at various shear rates are discussed by Tika (1989) and Lemos and Vaughan (2000). For a rough interface, the shear surface was observed to form within the soil away from the soil-interface boundary, and a residual state was reached at much smaller shear displacements than for soil-on-soil shearing. For

clays such as kaolin in which the residual soil-on-soil shearing occurs in the sliding mode, the residual interface shearing resistance approximated the soil-on-soil residual strength, and similar shear rate effects were observed.

The mechanisms of interface shearing observed for kaolin in ring shear and shear box tests is similar to that observed at the casing surface in the model screw conveyor tests. The shear surface formed within the clay, resulting in soil-on-soil shearing by the sliding mechanism. The residual friction coefficients measured at the casing surface compare well with those reported from ring shear tests for soil-on-soil shearing of kaolin at fast shear rates.

## 5.8 Summary

This chapter has reported a series of model screw conveyor tests performed with consolidated kaolin samples. The key results and conclusions from these tests are summarised below.

The consolidation and undrained strength properties of the E-grade kaolin samples were discussed. The one-dimensional compression curves for the large scale samples consolidated to maximum vertical effective stresses of approximately 30 to 120 kPa were presented. Wall friction effects in the container reduced the vertical effective stresses acting on the samples during consolidation to approximately 60% of the applied piston pressure. The consolidated samples had average vane shear strength in the range 7 to 20 kPa, which compared well with theoretical undrained strengths based on the sample moisture contents and the Cam-clay parameters reported for E-grade kaolin. An average value of  $S_u/\sigma'_v = 0.20$  was determined for the consolidated E-grade kaolin samples, which agrees well with typical values for normally consolidated clays.

Six model screw conveyor tests were performed with kaolin samples to investigate the operation of the conveyor with uniform soft clay samples. The tests were performed with varying sample strengths and conveyor operating conditions.

Detailed results from test 1 were presented to illustrate the mechanics of the model screw conveyor operation with clay soils. During steady state operation of the conveyor, the soil flow rate is constant. The shear stress acting on the casing is constant along the conveyor, and approximately equal to the undrained strength of the soil. The constant shear stress results in a

constant total pressure gradient along the conveyor, with a similar pore water pressure gradient. The effective stresses measured at the soil-casing interface were approximately constant. The screw torque is also constant during steady state operation. These mechanics were observed in all screw conveyor tests performed with clay soils. In all of the tests, controlled operation of the conveyor was achieved, with uniform pressure gradients and discharge rates. Results from further tests were presented to illustrate effects of the sample strength and varied operating conditions on the performance of the screw conveyor.

The total pressure gradient is influenced by the sample strength, the discharge outlet condition, and the piston pressure. With the outlet restricted, total pressure was either dissipated or generated along the conveyor, depending on the strength of the soil and the pressure required to extrude the soil through the outlet. With the outlet unrestricted, the total pressure dissipated along the conveyor. The discharge pressure with the outlet restricted can be calculated reasonably accurately using a theoretical model based on die extrusion. Larger pressure gradients were measured with higher applied piston pressures. The different conveyor operating conditions influenced the soil flow rate, resulting in the different pressure gradients.

The screw torque increased with the undrained strength of the samples and the resultant shear stress acting on the casing. The torque is related to the shear stress acting over the surface area of the conveyor casing, causing the increase in torque with the strength of the soil. The torque is also influenced by the soil flow rate which varied with the conveyor operating conditions.

The tests performed with screws of different pitch showed that the total pressure gradients decreased with a longer screw pitch, and the soil flow rates increased. The screw torque for a given soil strength was not influenced by the pitch of the screw.

The mechanism of shearing at the casing surface in the screw conveyor tests was similar to that observed in interface shear tests in ring shear and shear box apparatus. A shear surface formed within the clay close to the interface, resulting in soil-on-soil shearing. The average friction coefficients measured in the screw conveyor tests were similar for varying sample strengths. The values compare well with residual friction coefficients measured for soil-on-soil shearing of kaolin in ring shear tests performed at similar shear rates.

Test	$\sigma_p^{\max}$ (kPa)	$\sigma_v^{\max}$ (kPa)	Slurry $w_o$ (%)	Slurry $e_o$	Sample $w_r$ (%)	$e_r$	$H_r/H_o$	$\lambda^*$ (final increment)	Sample $S_u$ (kPa)	Sample $S_u/\sigma_v^*$	Spoil $S_u$ (kPa)	Spoil $S_u/\sigma_v^*$	Calculated $S_u$ (kPa)
1	100	59.7	106.1	2.769	45.4	1.185	0.59	0.156	10 - 12	0.18	6 - 8	0.12	10.0
4	200	120.6	105.6	2.756	42.4	1.106	0.56	0.127	19 - 21	0.17	14 - 15.5	0.12	18.8
5	50	28.8	105.6	2.756	48.4	1.263	0.60	0.282	7 - 8	0.24	4.5 - 5	0.17	5.3
6	100	60.3	110.4	2.881	46.0	1.198	0.56	0.137	11 - 13	0.20	7 - 8.5	0.13	9.0
12	100	59.6	110.4	2.881	45.6	1.190	0.57	0.175	10 - 12	0.19	7 - 8.5	0.13	9.6
16	100	58.4	107.1	2.795	45.2	1.180	0.59	0.173	11 - 13	0.21	8 - 9	0.15	10.4

Table 5.1. Properties of consolidated kaolin samples.

$\lambda$	0.124
$\kappa$	0.02
$M$	1.05
$\phi'$	26.5°
$\Gamma_{iso}$	2.65
$\Gamma_{csl}$	2.55

Table 5.2. Cam-clay parameters for E-grade kaolin.

Test stage	$\sigma'_{p \max}$ (kPa)	Average sample vane $S_u$ (kPa)	Average spoil vane $S_u$ (kPa)	Sample pressure (kPa)	Screw (screw 1 pitch=80 mm) (screw 2 pitch=133 mm)	Nominal screw speed (rpm)	Discharge condition
Test 1	100	11	7	200	1	5	Restricted
Test 2	200	20	15	200	1	5	Restricted
Test 3, stage 1	50	7	5	200	1	5	Restricted
Test 3, stage 2							Unrestricted
Test 4, stage 1	100	12	8	100	1	5	Unrestricted
Test 4, stage 2				200			Unrestricted
Test 5, stage 1	100	11	8	100	2	5	Unrestricted
Test 5, stage 2				200			Unrestricted
Test 6, stage 1	100	12	8.5	200	2	5	Restricted
Test 6, stage 2							Unrestricted

Table 5.3. Model screw conveyor test conditions with consolidated kaolin samples.

Test stage	Total pressure change, $\Delta P$ (kPa)	Total pressure gradient, $\Delta P/L$ (kPa/m)	Inferred discharge pressure ( $L=950\text{mm}$ ) (kPa)	Average resultant shear stress, $\tau_z$ (kPa)	Average friction coefficient $\tau/\sigma_n'$	Average torque (Nm)	Soil flow rate (L/hr)
Test 1	-81.0	-120.0	119.7	9.6	0.284	91.9	121.5
Test 2	147.0	217.7	332.0	15.5	0.266	249.0	117.9
Test 3 stage 1	-72.1	-106.8	91.8	5.8	0.241	68.9	145.5
Test 3 stage 2	-122.0	-180.7	11.2	5.7	0.299	63.3	151.6
Test 4 stage 1	-35.9	-53.2	11.1	7.2	0.280	92.2	123.1
Test 4 stage 2	-110.4	-163.5	9.2	7.5	0.254	89.7	124.7
Test 5 stage 1	-7.1	-10.5	34.3	7.5	0.263	86.7	200.2
Test 5 stage 2	-64.3	-95.3	40.8	7.3	0.272	75.0	218.5
Test 6 stage 1	12.4	18.3	175.8	8.1	0.295	107.7	188.5
Test 6 stage 2	-78.1	-115.8	38.0	7.7	0.291	88.2	211.5

Table 5.4. Measurements from screw conveyor tests with kaolin samples.

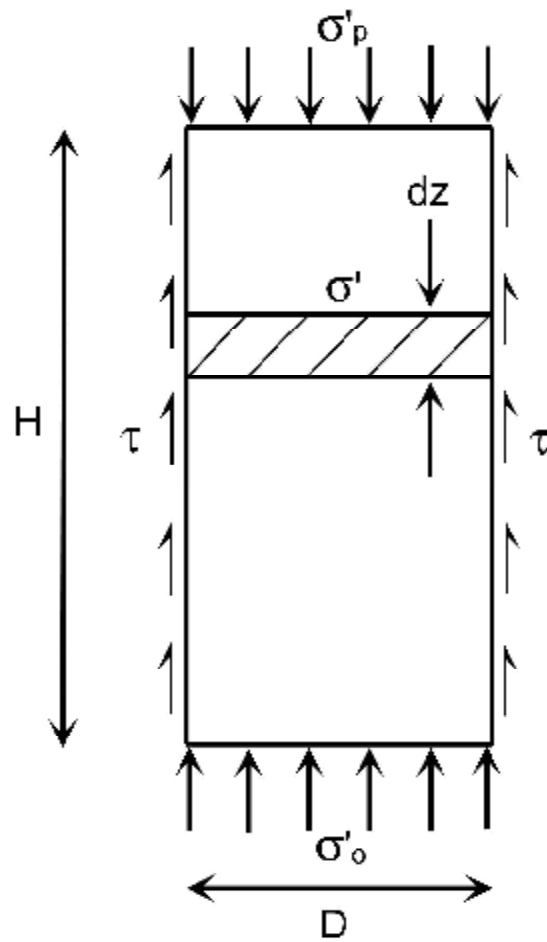


Figure 5.1. Forces acting on soil sample in container.

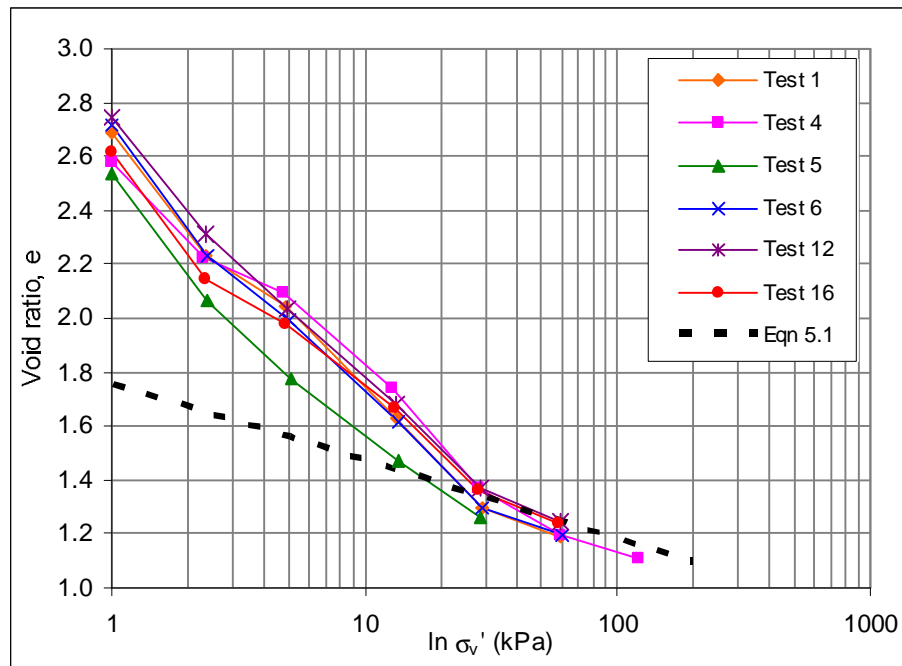


Figure 5.2. Consolidation of E-grade kaolin samples for screw conveyor tests.

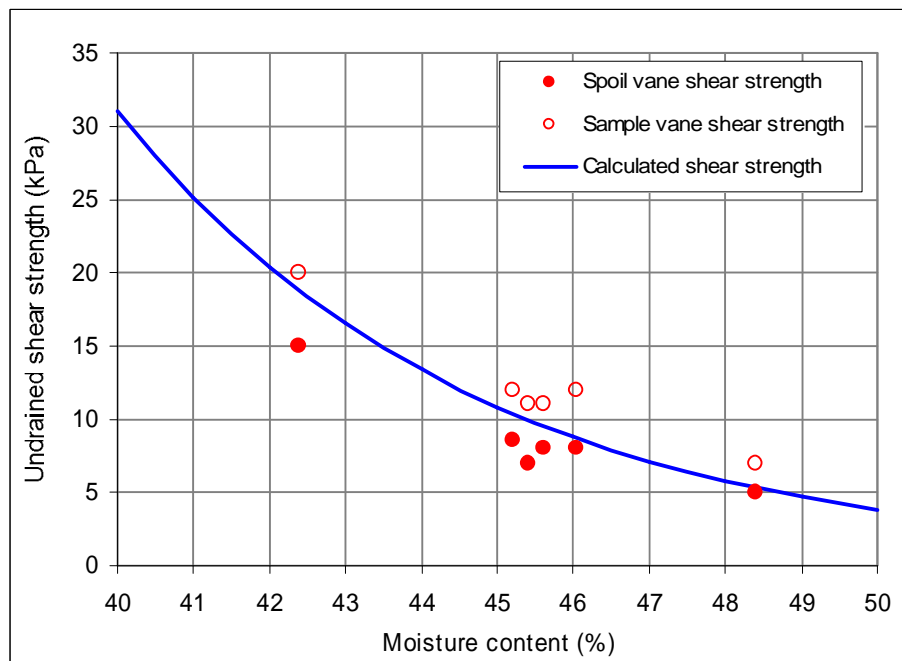


Figure 5.3(a). Measured and calculated undrained shear strength of E-grade kaolin samples at varying moisture contents.

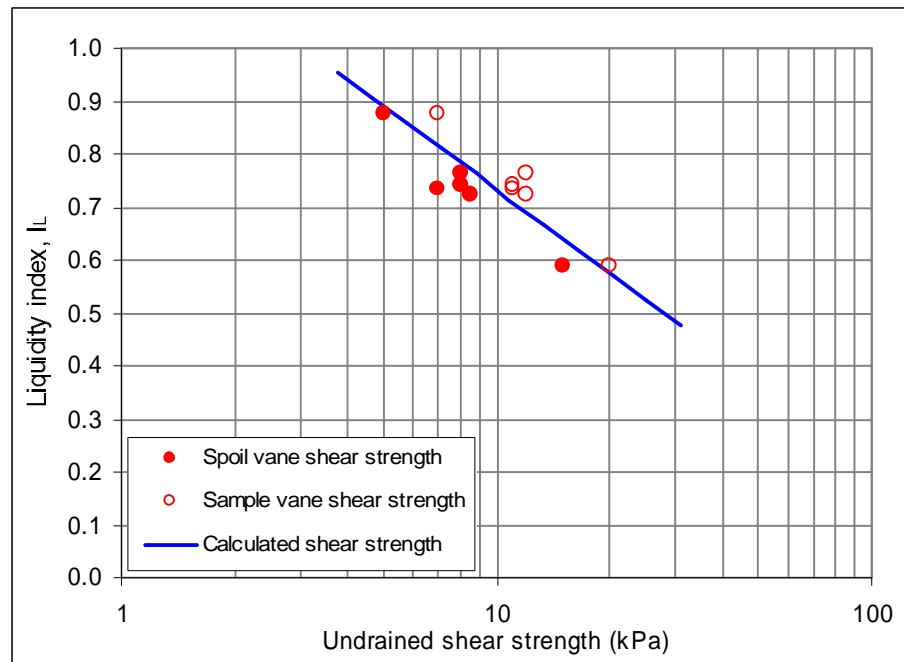


Figure 5.3(b). Measured and calculated undrained shear strength of E-grade kaolin samples at varying liquidity index.

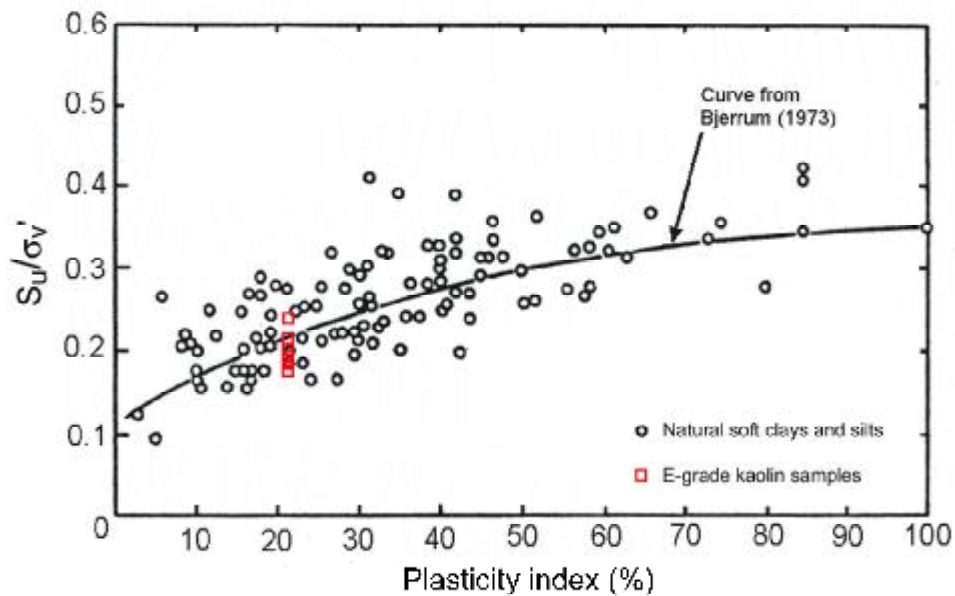


Figure 5.4. Undrained strength ratio of E-grade kaolin compared to values for various normally consolidated natural clays and silts (after Terzaghi *et. al.* 1996).

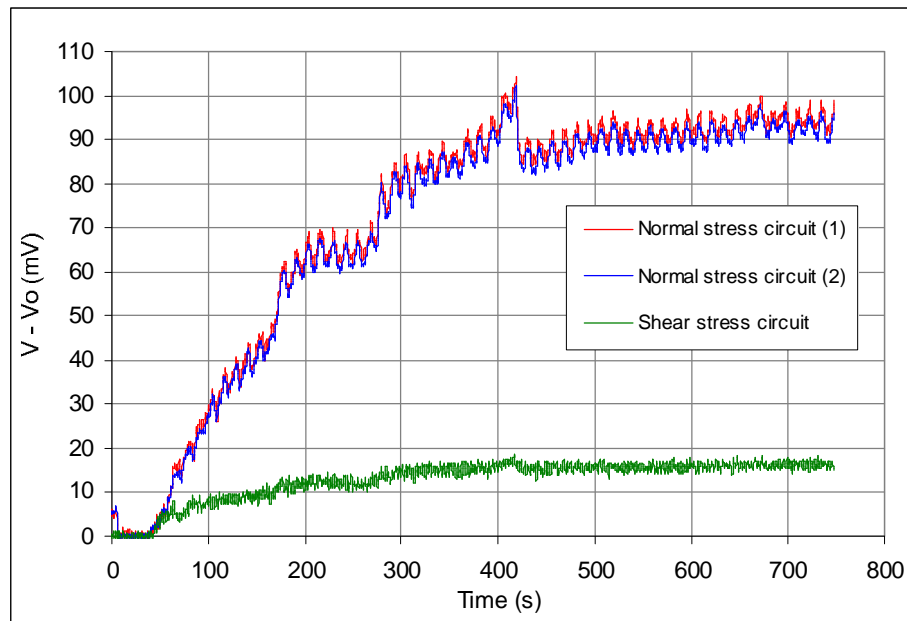


Figure 5.5. Typical load cell circuit outputs during screw conveyor operation.

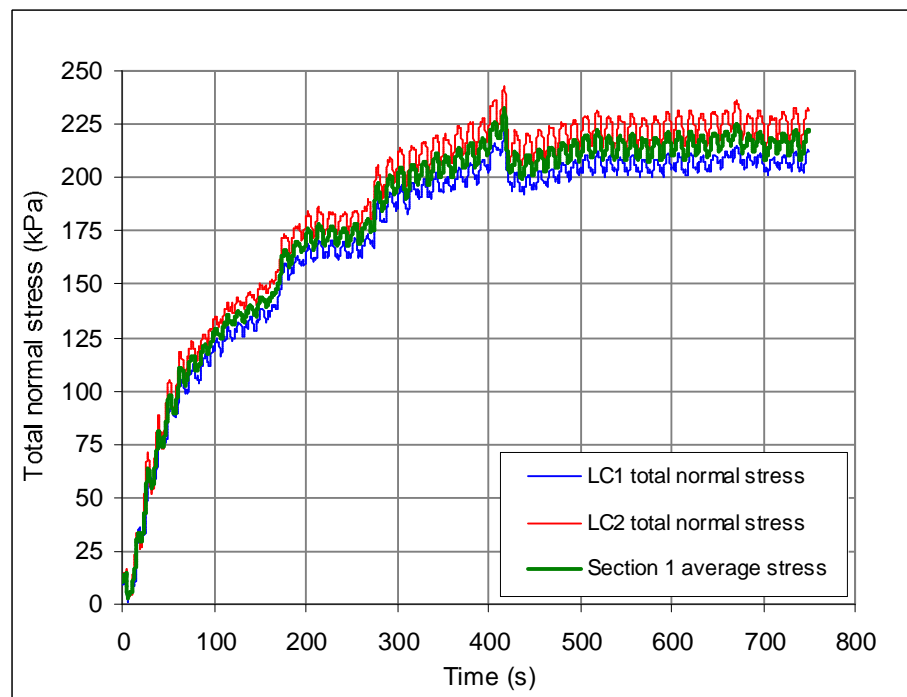


Figure 5.6. Total normal stress measured by loads cells at an instrumented section during conveyor operation.

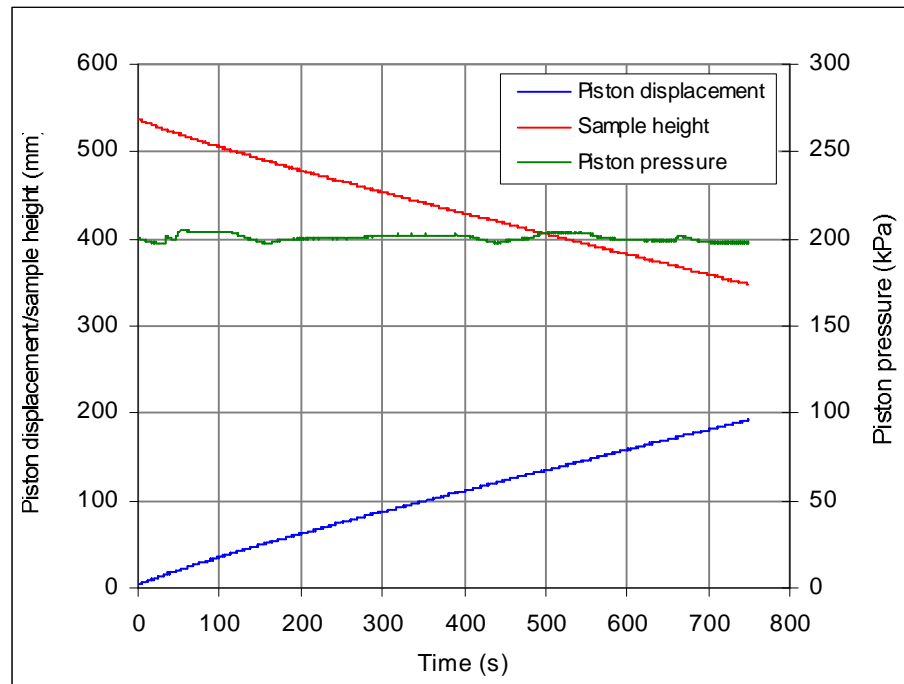


Figure 5.7. Piston pressure and sample height change during test 1.

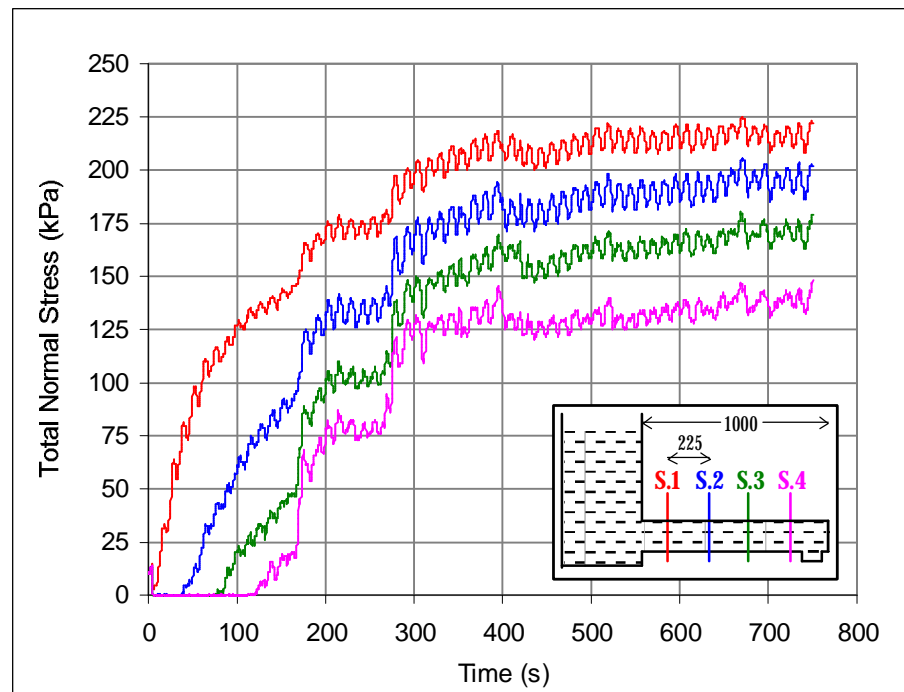


Figure 5.8. Average total normal stresses along conveyor during test 1.

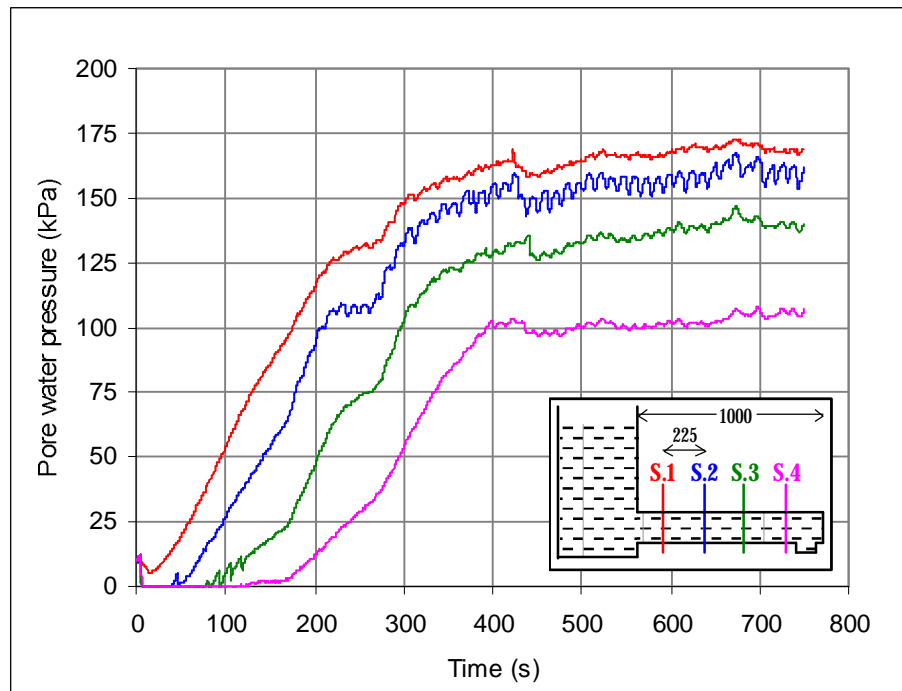


Figure 5.9. Pore water pressures along conveyor during test 1.

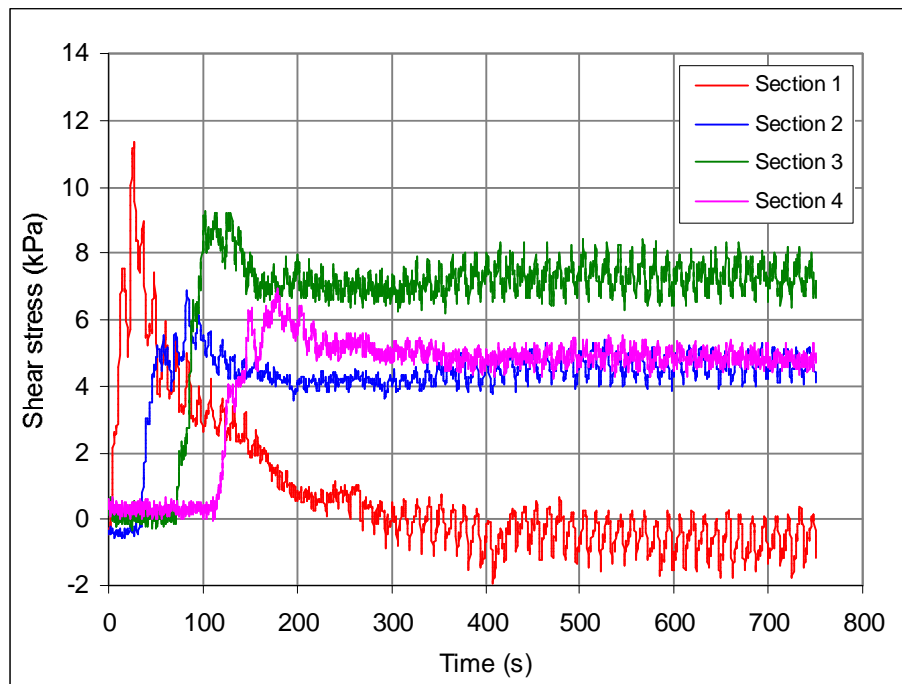


Figure 5.10(a). Casing shear stress components parallel to screw axis during test 1.

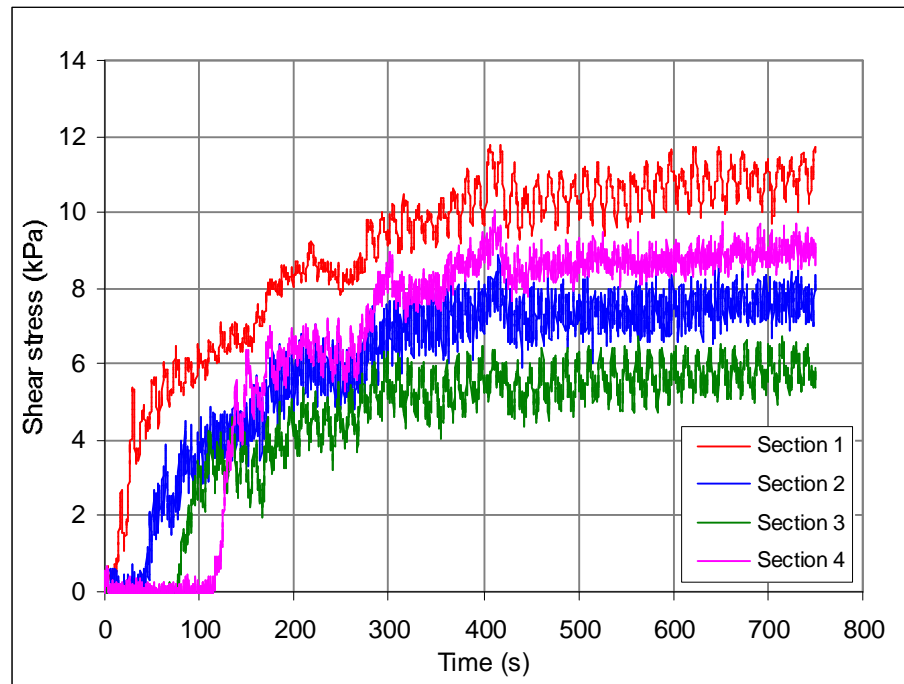


Figure 5.10(b). Casing shear stress components perpendicular to screw axis during test 1.

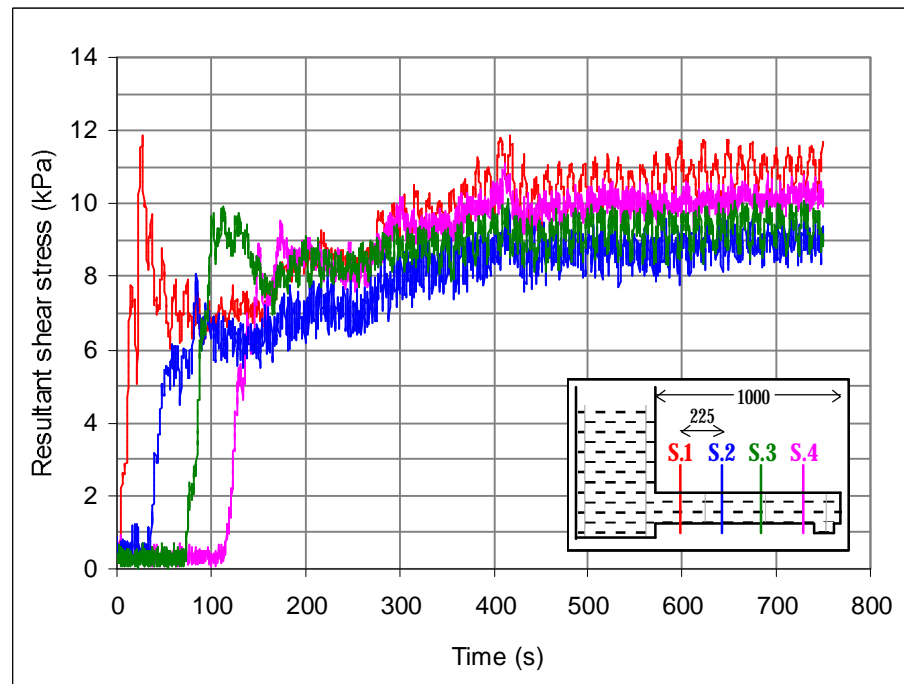


Figure 5.10(c). Resultant casing shear stresses during test 1.

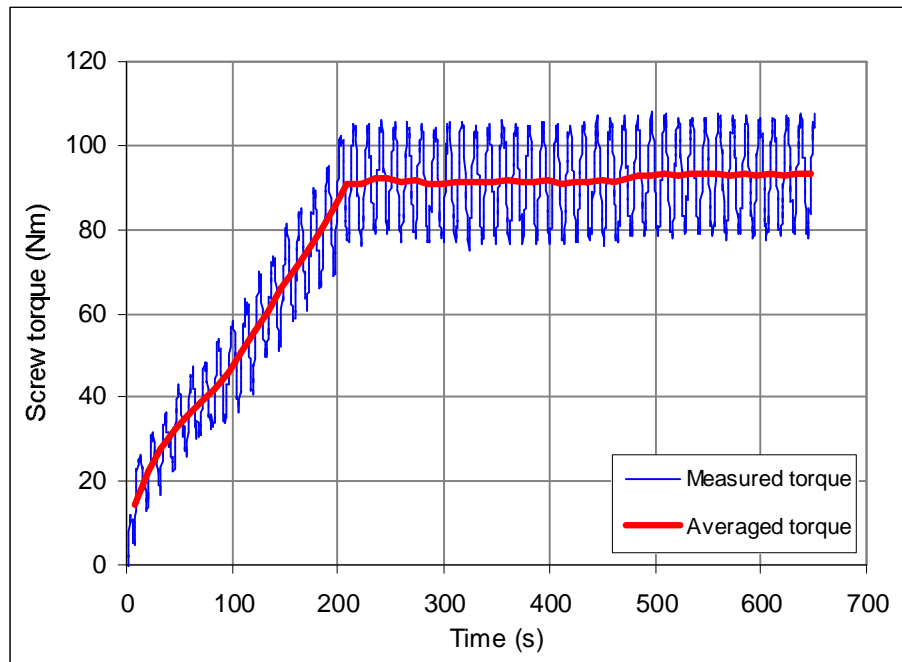


Figure 5.11. Screw torque measured during test 1.

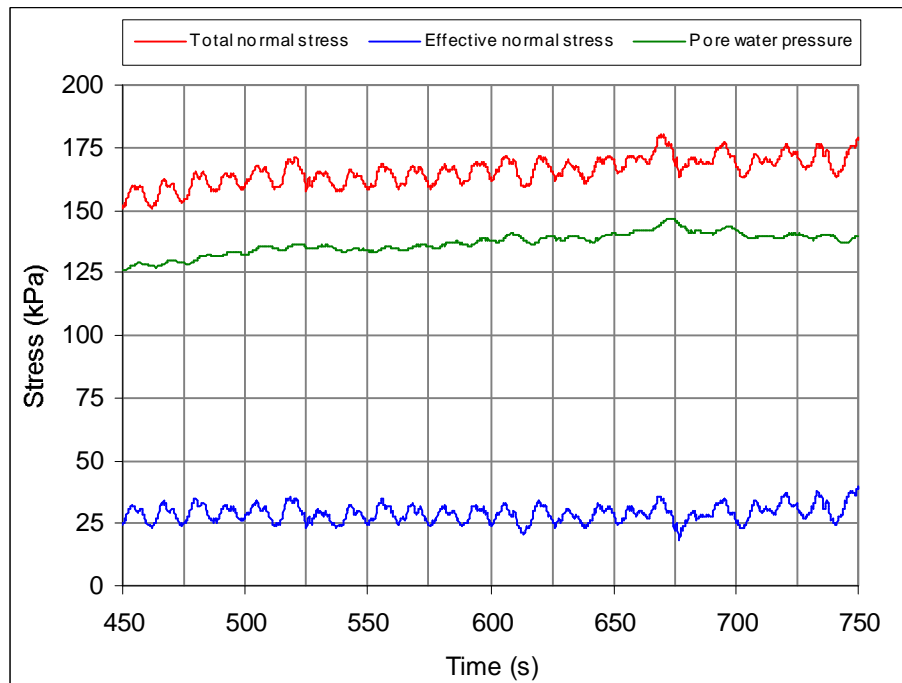


Figure 5.12. Pressures measured at Section 3 during steady state operation in test 1.

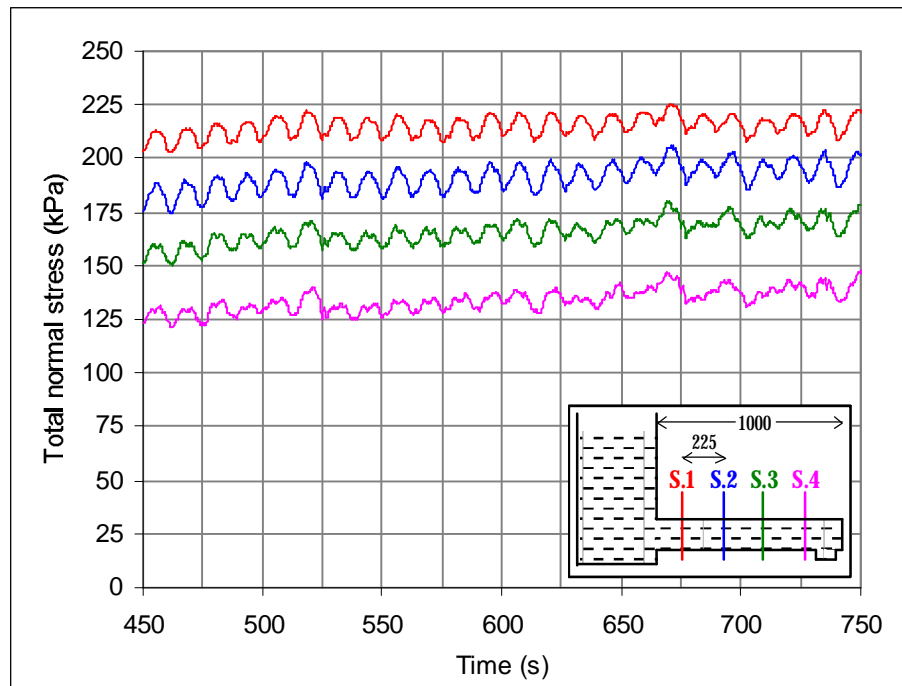


Figure 5.13(a). Total normal stresses at each section during steady state operation in test 1.

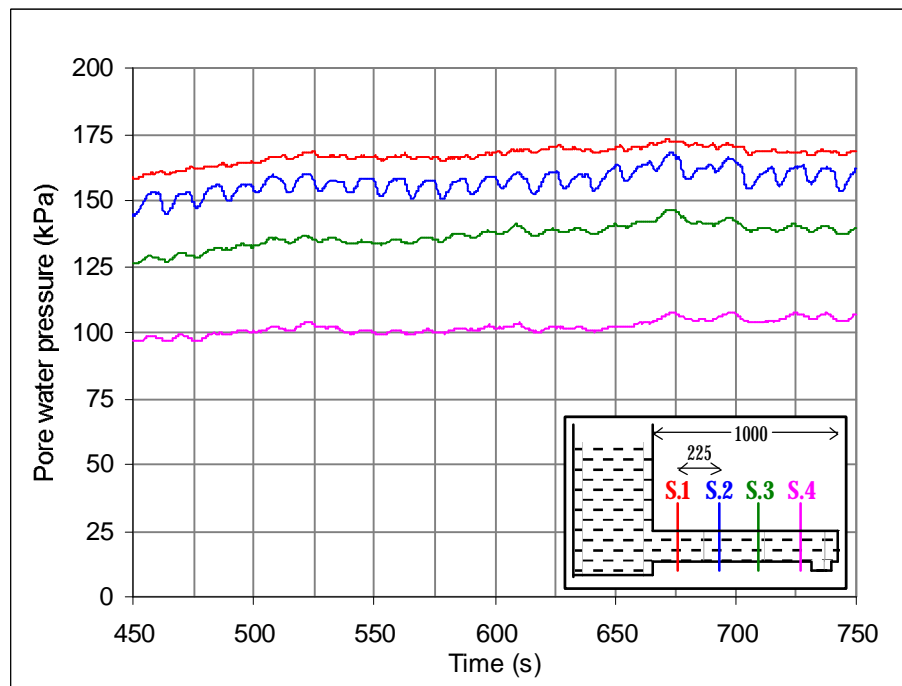


Figure 5.13(b). Pore water pressures at each section during steady state operation in test 1.

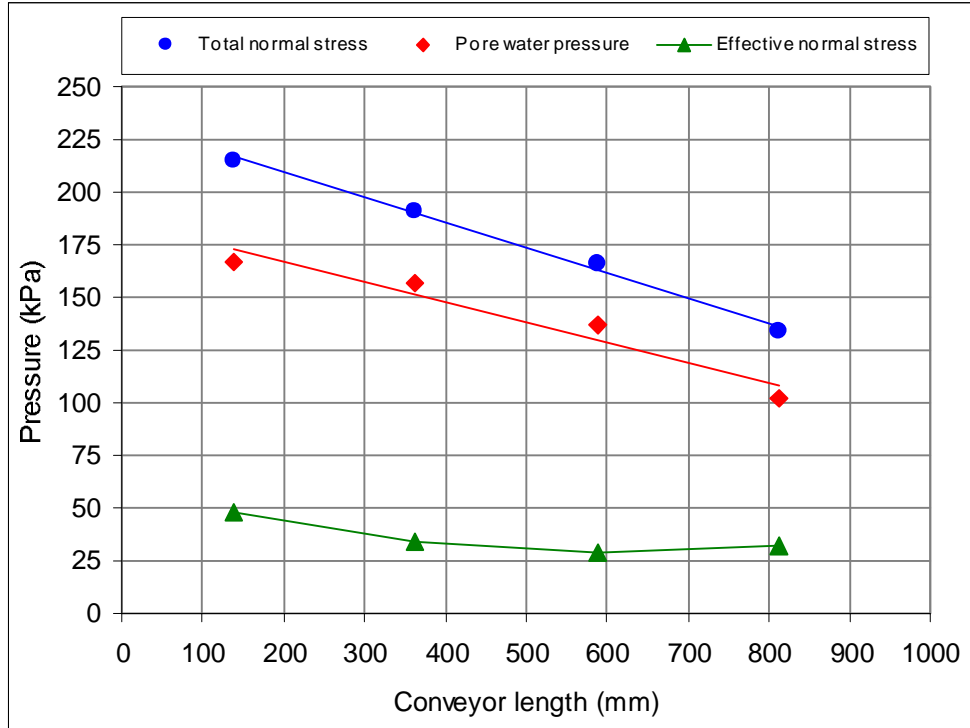
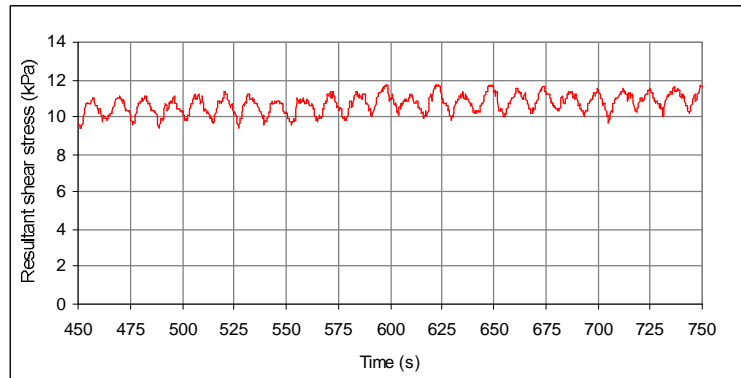
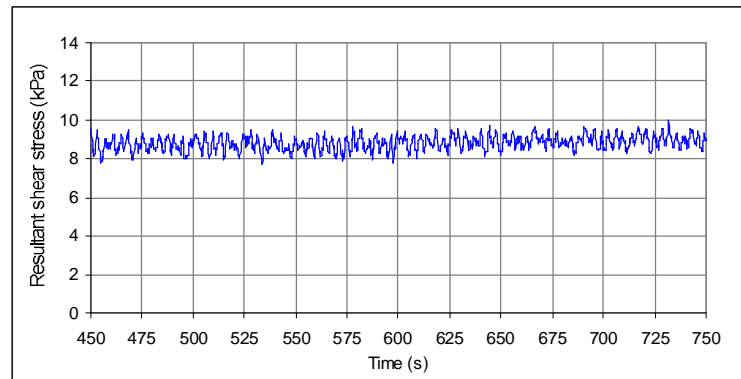


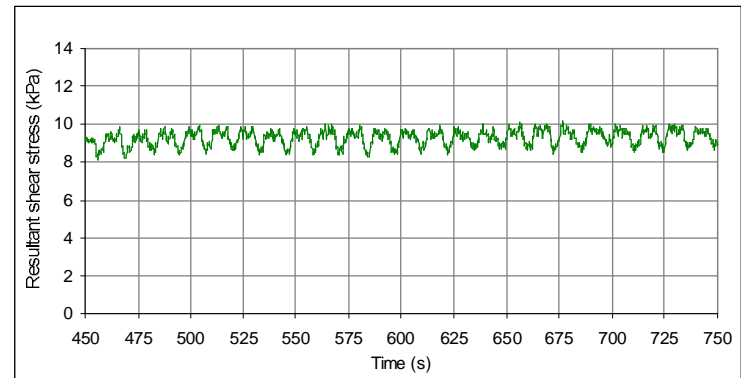
Figure 5.14. Pressure gradients along conveyor during steady state operation in test 1.



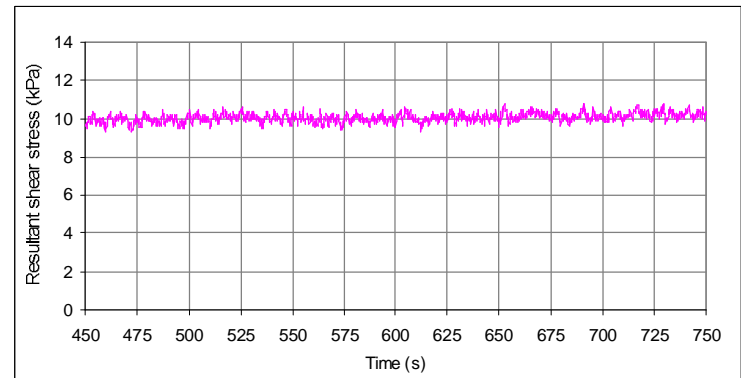
(a) Section 1.



(b) Section 2.

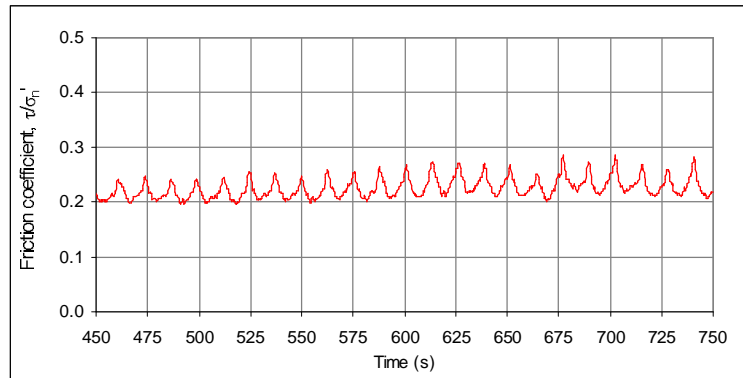


(c) Section 3.

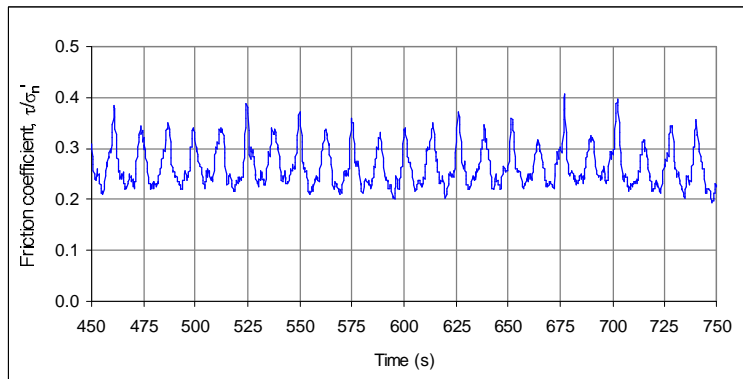


(d) Section 4.

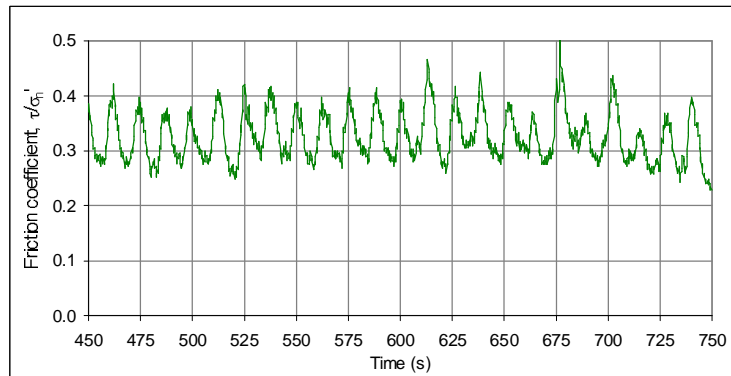
Figure 5.15. Resultant casing shear stresses during steady state operation in test 1.



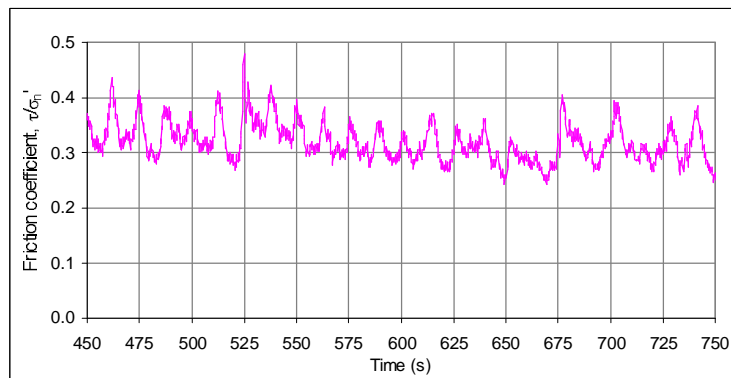
(a) Section 1.



(b) Section 2.



(c) Section 3.



(d) Section 4.

Figure 5.16. Friction coefficients during steady state operation in test 1.

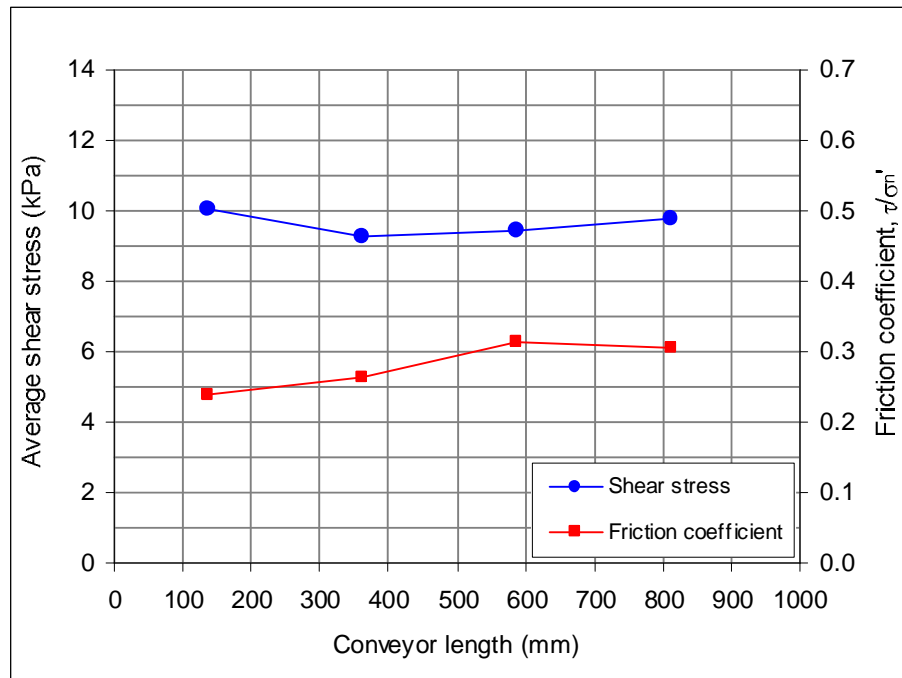


Figure 5.17. Average resultant casing shear stresses and friction coefficients along conveyor during steady state operation in test 1.

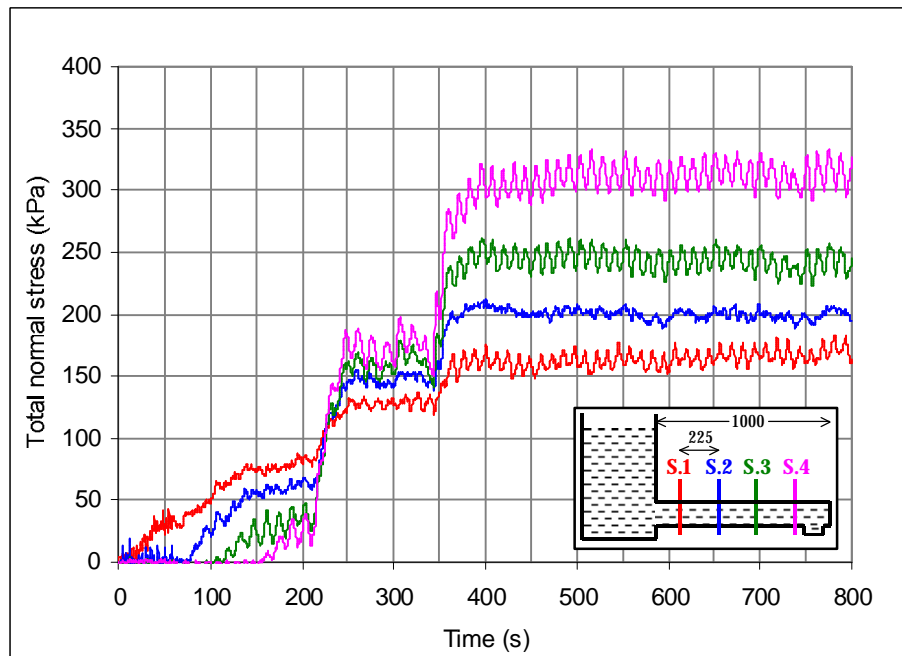


Figure 5.18. Average total normal stresses during test 2.

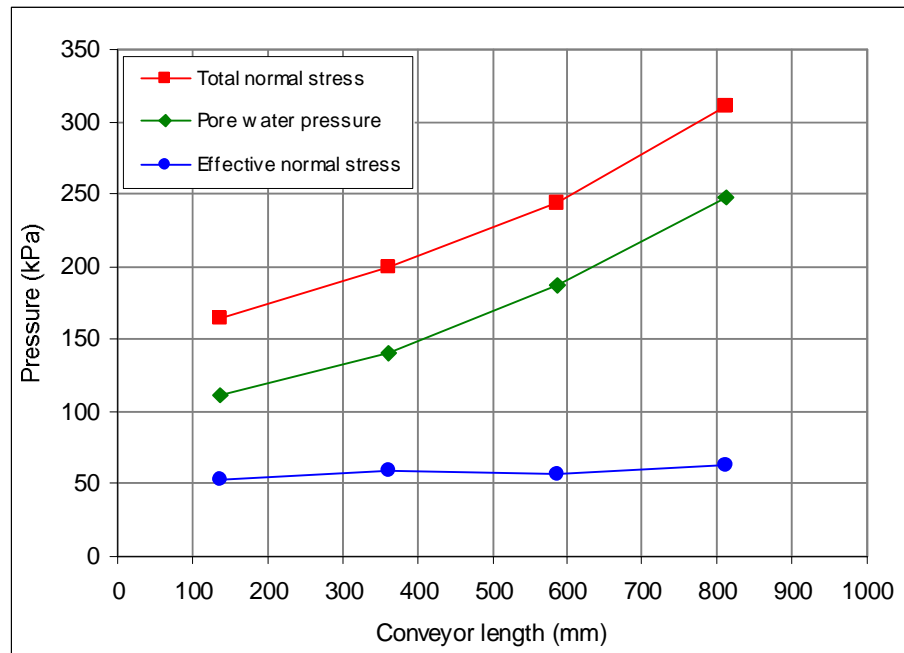


Figure 5.19. Pressure gradients during test 2.

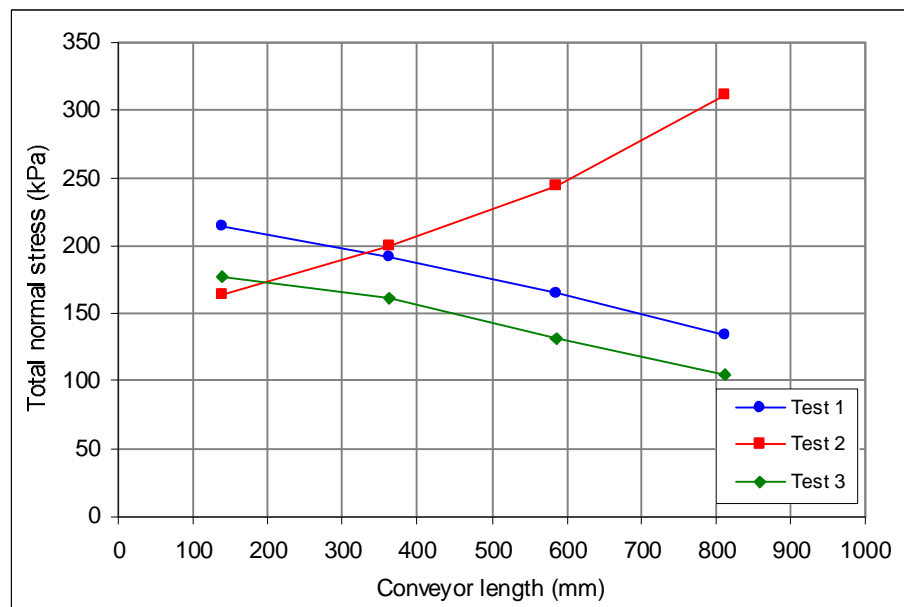


Figure 5.20. Total pressure gradients during tests 1, 2 and 3 with kaolin samples of varying strength.

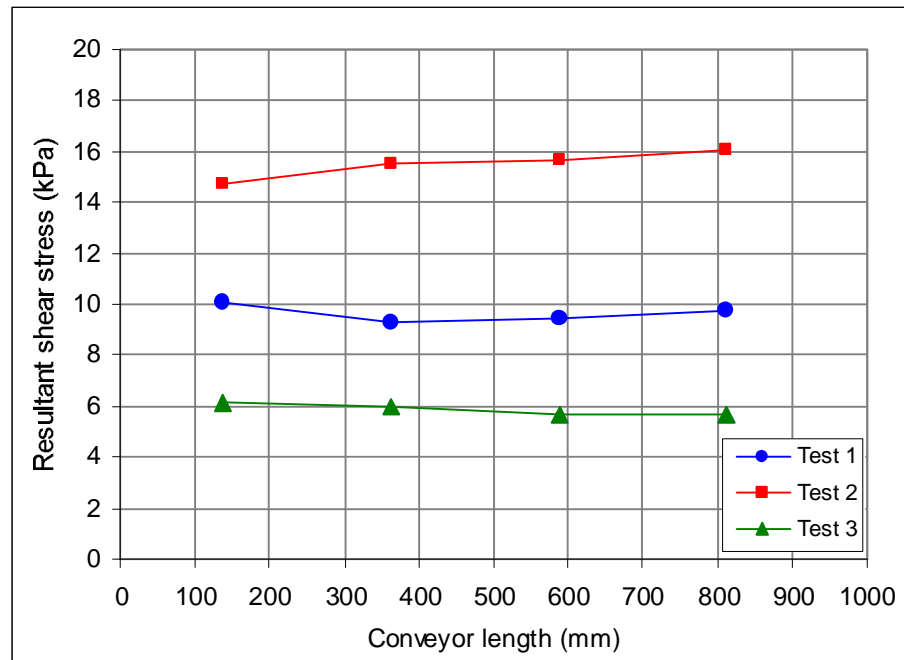


Figure 5.21. Resultant casing shear stresses along conveyor during tests 1, 2 and 3 with kaolin samples of varying strength.

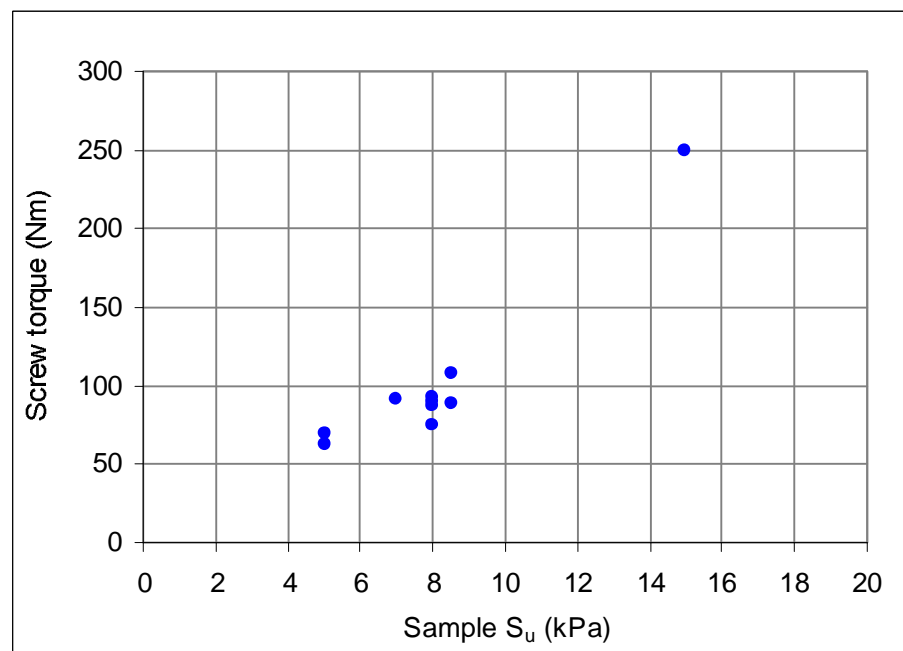


Figure 5.22(a). Increase of screw torque with undrained shear strength of kaolin samples.

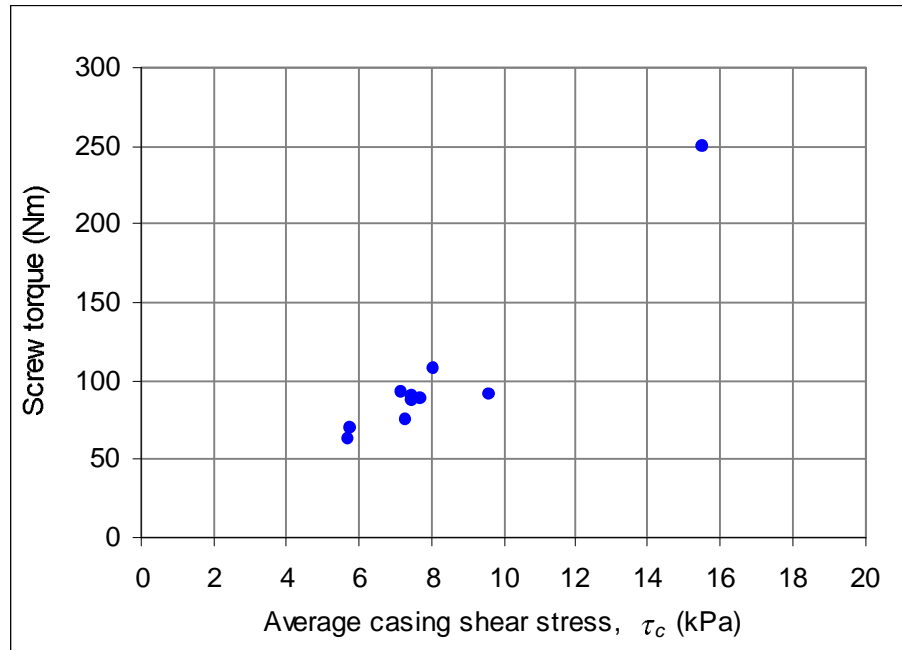


Figure 5.22(b). Increase of screw torque with casing shear stress for kaolin samples.

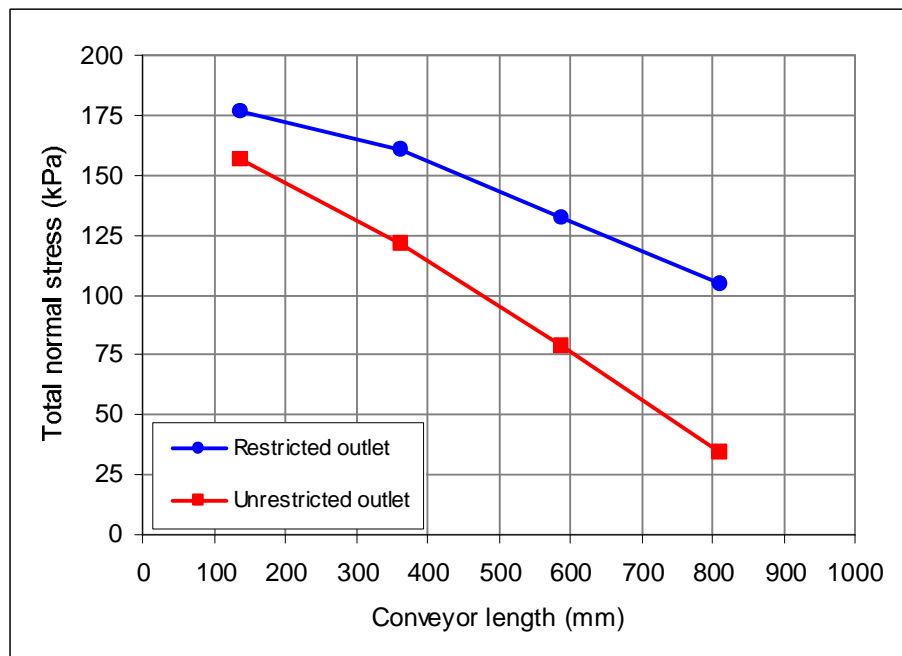


Figure 5.23. Total pressure gradients with varying discharge conditions in test 3.

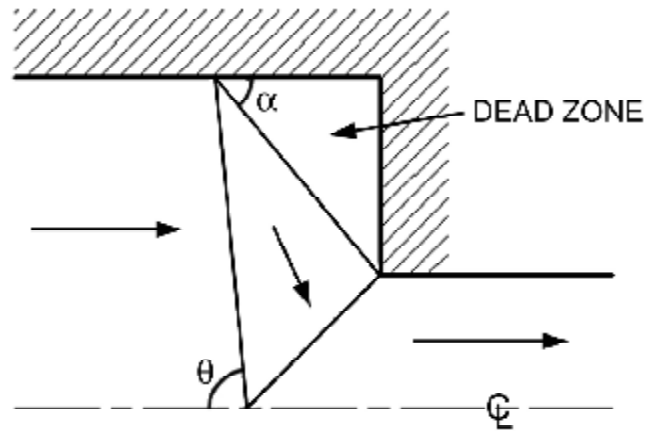


Figure 5.24. Plastic flow mechanism through square extrusion die with 'dead zone' of material.  
(after Calladine, 1985)

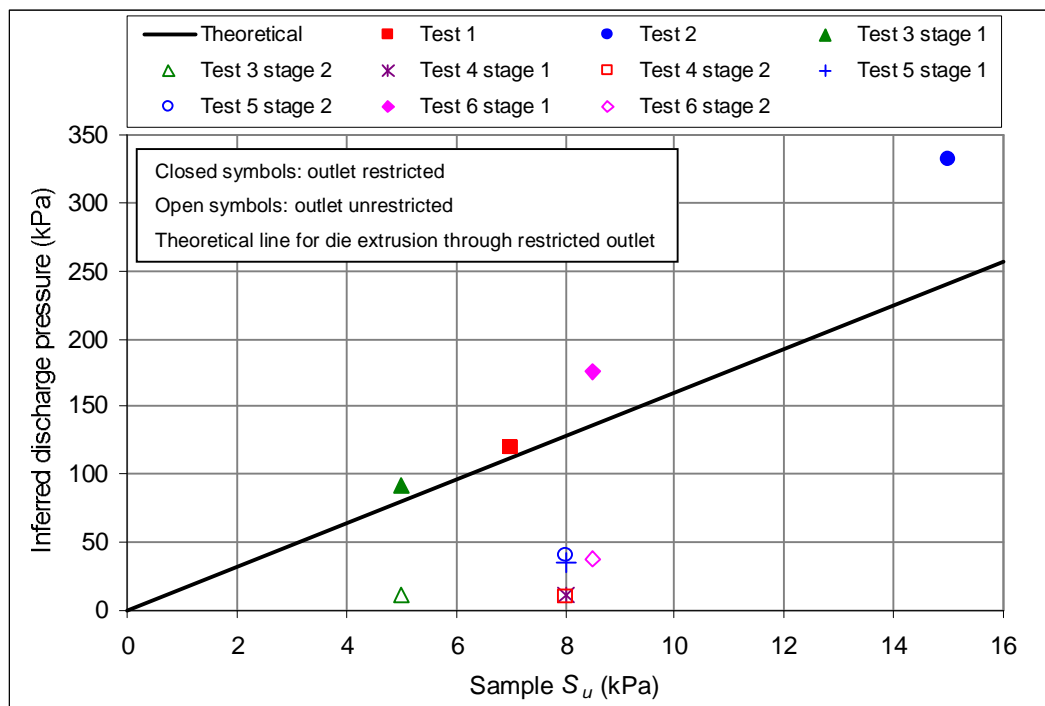


Figure 5.25. Inferred discharge pressures for kaolin tests with restricted and unrestricted outlet conditions.

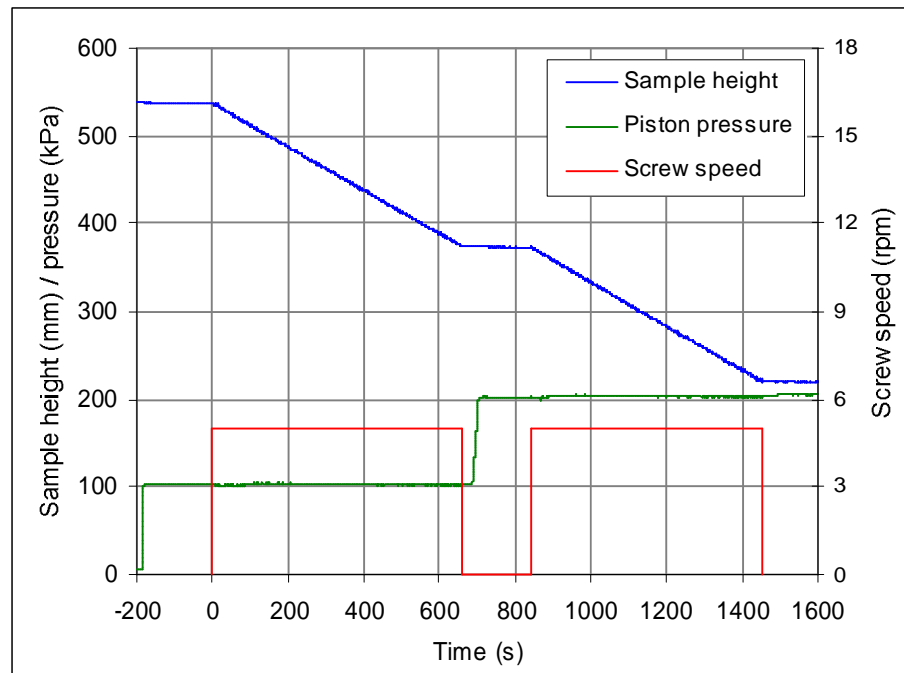


Figure 5.26. Monitoring of screw conveyor test 4.

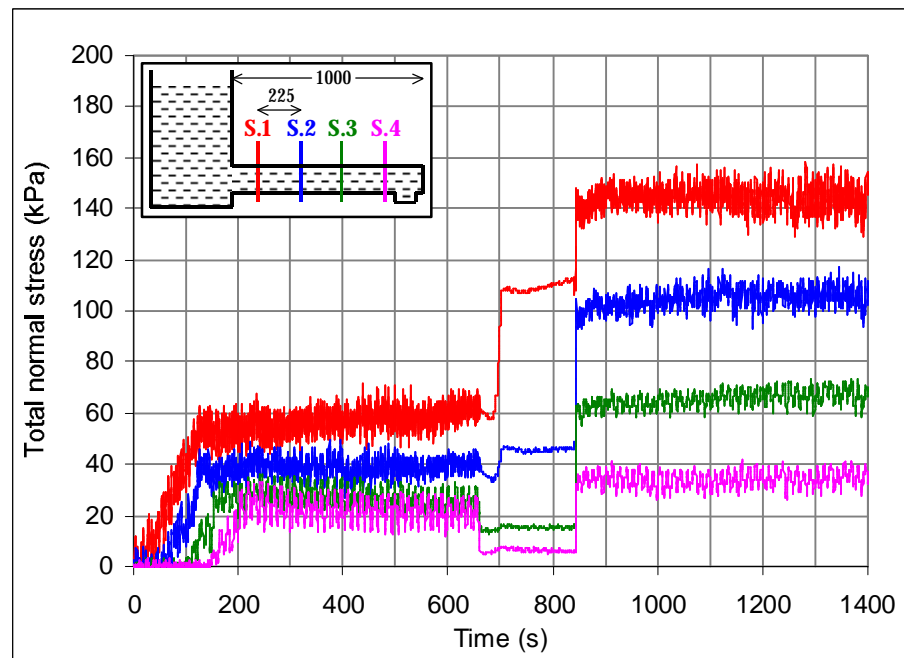


Figure 5.27. Total normal stresses during test 4.

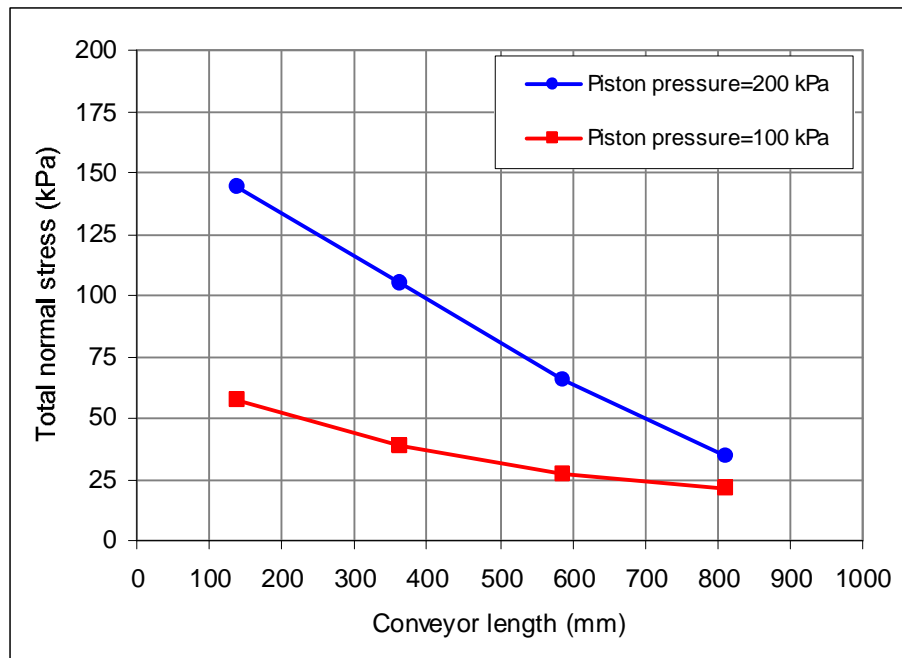


Figure 5.28. Total pressure gradients with different piston pressures in test 4.

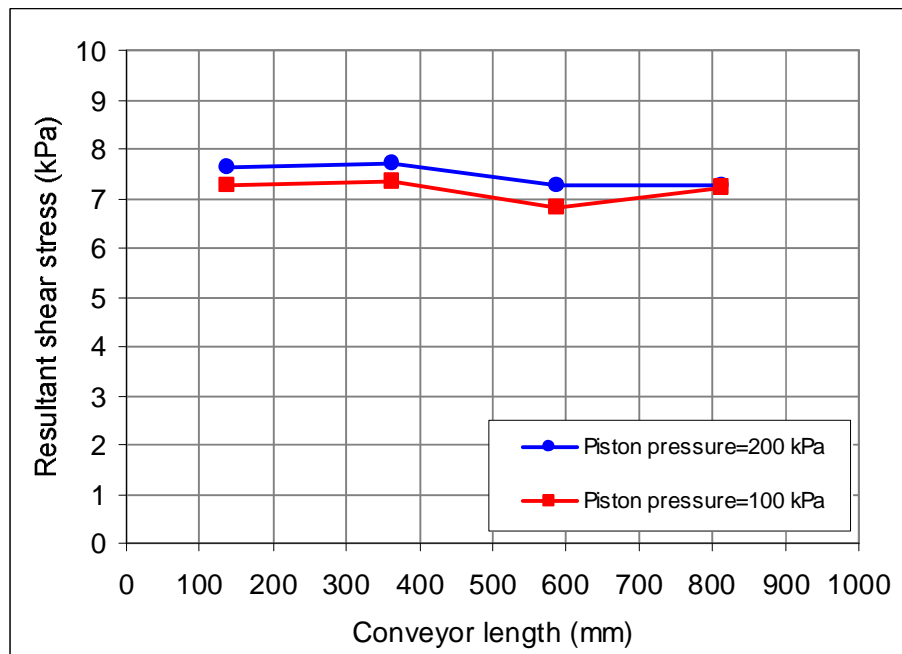


Figure 5.29. Average resultant casing shear stresses with different piston pressures in test 4.

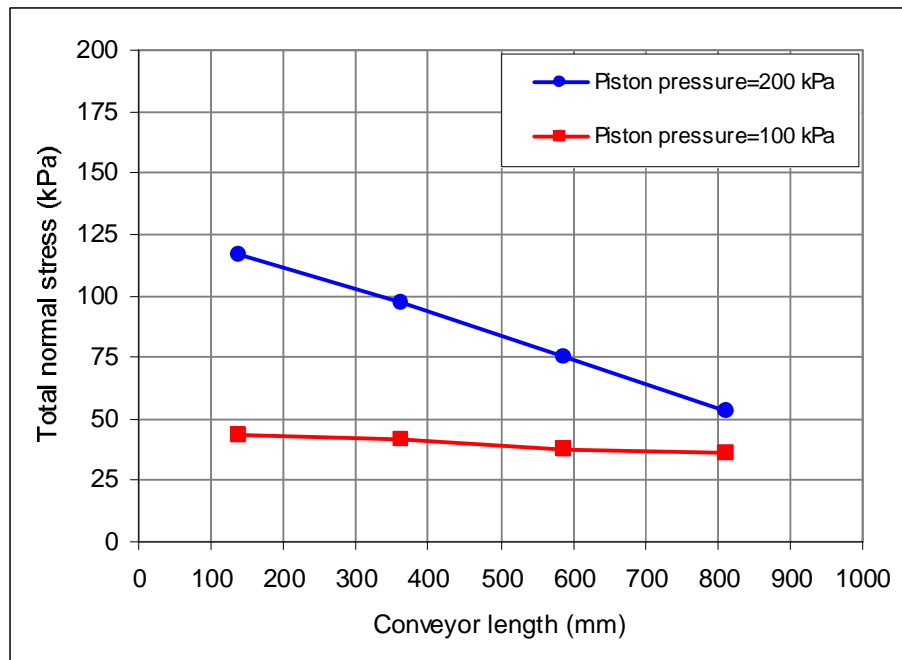


Figure 5.30. Total pressure gradients with different piston pressures in test 5.

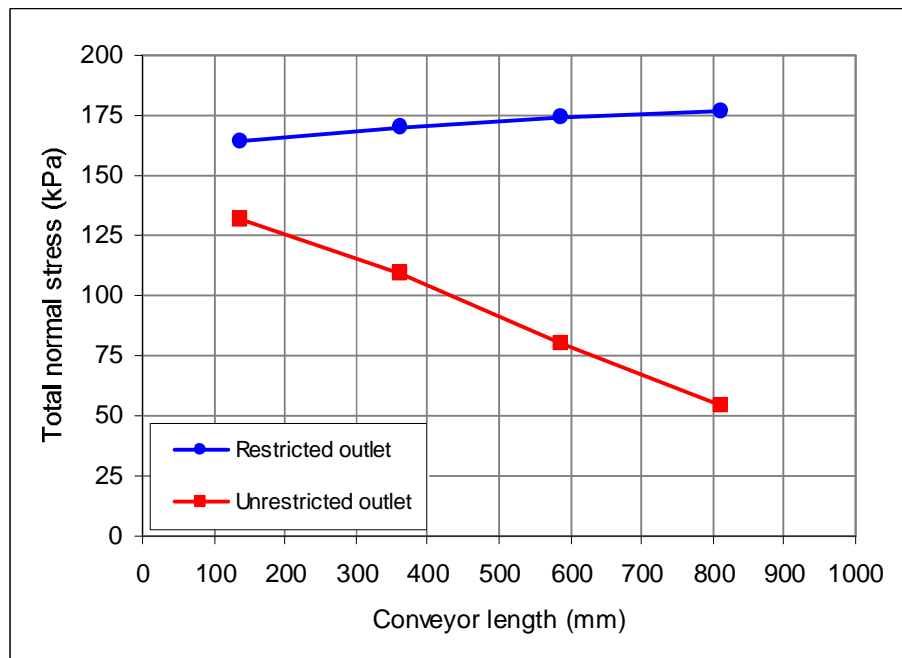


Figure 5.31. Total pressure gradients with varied discharge conditions in test 6.

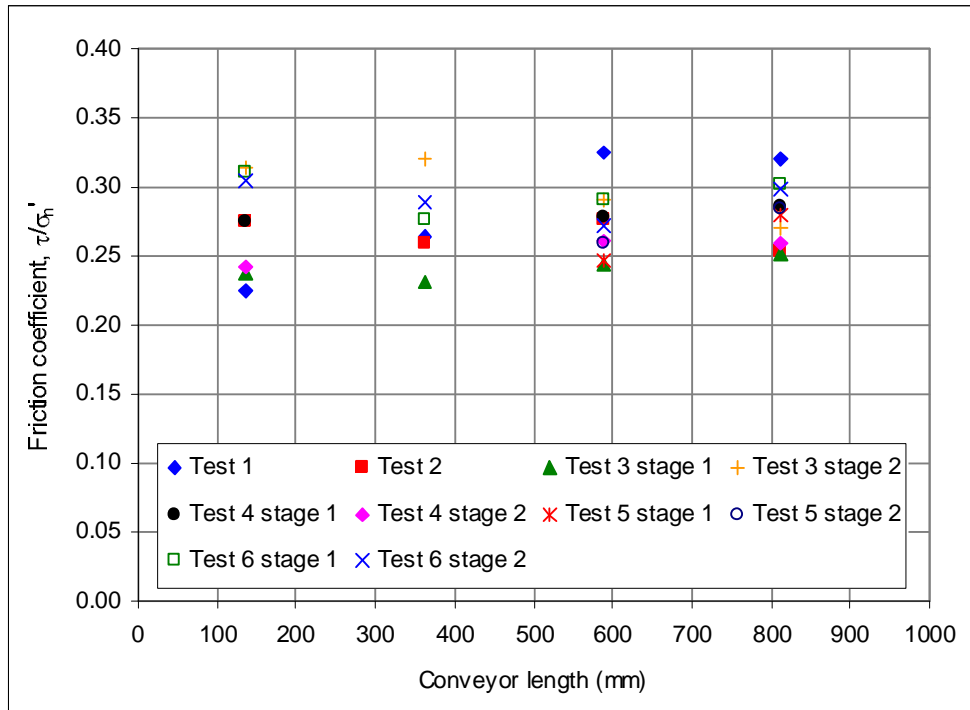


Figure 5.32. Average friction coefficients along conveyor in tests with kaolin samples.

# Chapter 6

## Model screw conveyor tests with conditioned clay soils

---

### 6.1 Introduction

This chapter reports a series of model screw conveyor tests performed with conditioned natural soil samples. The objectives of these tests were to investigate the operation of the conveyor with conditioned clay soils, and effects of different conditioning treatments on the performance. Ten tests were performed with soil samples conditioned with different foam and polymer treatments, and with varied conveyor operating conditions. Eight tests were performed with conditioned London Clay samples, and two with conditioned samples of mixed clay and sand soils. Some samples were conditioned to achieve varying strengths, and other samples were prepared with different conditioning treatments to achieve a similar target strength. This chapter describes the soils tested, and the preparation and properties of the conditioned soil samples. The tests were performed with similar conveyor operating conditions, with the screw speed varied in the different test stages. Results from the tests show that the mechanics of the screw conveyor operation with conditioned clay soils are similar to those observed in tests with kaolin samples. Effects of the different sample strengths, screw speeds and discharge conditions on the conveyor operation are discussed. The observed effects of the different soil conditioning treatments on the screw conveyor operation are also discussed.

## **6.2 Conditioned clay samples for screw conveyor tests**

The soils used for screw conveyor test samples are described below. The design of the conditioning treatments and preparation of the conditioned soil samples, and the measured sample properties are also described.

### **6.2.1 Soil samples**

#### **6.2.1.1 London Clay samples**

Eight tests were performed with London Clay samples conditioned with various polymer and foam treatments. These samples were prepared from the stiff, high plasticity London Clay cutting samples used for the index tests discussed in Chapter 3. The properties of the London Clay samples, and the sampling procedures, were described in Section 3.2.2. The particle size distributions and a plasticity chart for the London Clay at the sampling site are shown in Figures 3.2 and 3.3. Some properties of the London Clay sampled are summarised in Table 3.3.

For the model screw conveyor tests, clay cutting samples sieved to a maximum size of approximately 25 mm were required based on the dimensions of the screw conveyor, with the screw channel depth of 32.5 mm. Index tests performed to measure the undrained shear strength of London Clay cutting samples conditioned with foam and polymer treatments were discussed in Section 3.7. Results from these index tests are shown in Figures 3.21 to 3.24. The results of these index tests were used to design the conditioning treatments for preparation of the London Clay samples for the screw conveyor tests.

#### **6.2.1.2 WRB/UP samples**

Two screw conveyor test samples were prepared from a mixture of stiff, high plasticity clay (WRB) and silty sand (UP) from the Lambeth Group of soils in London. These soils samples were also obtained from the Corsica Street shaft excavation. For the test samples, the soils were mixed together and conditioned with combined foam and polymer treatments, representing the spoil produced by an EPB machine excavating a mixed face of these soils.

The Lambeth Group, containing the Woolwich and Reading Beds (WRB), are comprised of several units of variable soils, including stiff, high plasticity clays, silts, sands and gravels (Withers *et al.*, 2001). The WRB soil samples were obtained from the Upper Mottled Clay unit, located at depths between 33.2 and 38.4 m below ground level at the site of the Corsica Street shaft. This

soil is described as typically stiff to very stiff, intermediate to very high plasticity clay, with an undrained shear strength of at least 150 kPa. The plasticity index of samples from this site varied between 18 and 55% (CTRL, 1997). The natural moisture content is usually close to the plastic limit. Some index properties and design parameters for the Upper Mottled Clay are shown in Table 6.1, and a grading envelope for the soil is shown in Figure 6.1. The samples of WRB clay for the screw conveyor tests were obtained by a similar procedure as for the London Clay samples, with the excavated soil passed through the 25 mm mesh sieve and sealed to preserve the natural moisture content.

Upnor sand (UP) underlies the WRB soils in the Lambeth Group and is a variable material containing a range of soil types. The UP sand is generally described as a very dense clayey, very silty fine to medium sand (Withers *et. al.*, 2001). This soil also includes some gravel and pebble beds and some laminations of very stiff clay of low to intermediate plasticity. A grading envelope for UP sand is shown in Figure 6.2, and some properties are summarised in Table 6.2. The UP sand samples did not require sieving to control the particle size for the screw conveyor tests, and after sampling, the soil was sealed in bags to preserve the natural moisture content.

For the screw conveyor test samples, the WRB clay and UP sand were combined in equal proportions by mass to give a soil containing cuttings of very stiff, high plasticity clay mixed with clayey, very silty sand. Index tests measuring the undrained shear strength of conditioned WRB/UP samples were performed, as discussed below.

### **6.2.1.3 Index testing of conditioned WRB/UP soil**

Index tests to measure the strength of WRB/UP soil conditioned with various foam and polymer treatments were performed following the procedures used for the index testing of conditioned London Clay, described in Section 3.4.4. Samples of the WRB and UP soils at their natural moisture content were mixed in equal proportions by mass. Measured volumes of foam and polymer solutions were mixed with the soil to prepare conditioned soil samples with specific conditioner injection ratios. Vane shear tests were performed to measure the undrained strength of the conditioned WRB/UP samples.

Seven samples of conditioned WRB/UP soil were prepared for index tests. TR foam at a concentration of 1.5%, produced with the standard foam generator settings described in Section 3.5.1, was used. The foam had a FER of 16, and was mixed with the soil at FIRs of 0 to 125%.

MV polymer solutions at 0.2% concentration were mixed with the soil in combination with the foam, at PIRs of 0 to 20%. These injection ratios were used to achieve conditioned sample strengths of less than 25 kPa, as suitable for the model screw conveyor. The conditioned WRB/UP samples prepared, and the measured vane shear strengths are summarised in Table 6.3. The conditioner liquid injection ratios were calculated from the foam liquid and polymer injection ratios as described in Section 3.7.3.

The vane shear strength of the conditioned WRB/UP soil samples is shown plotted against the FIR for different PIRs in Figure 6.3. The results of these tests show similar trends as observed for the London Clay index tests discussed in Section 3.7. Foam injection ratios significantly higher than typically recommended were required to effectively condition the WRB/UP soil. For the combined foam-polymer solution treatments, a lower FIR was required with increasing PIR for a given sample strength, and the strength decreased with increasing conditioner liquid injection ratios. As for the London Clay samples, foam mixed with the WRB/UP soil tended to break down due to absorption of the foam liquid by the high plasticity clay present in the samples. The stability of the foam mixed with the WRB/UP soil was improved when used in combination with a polymer solution, which also allowed effective conditioning of the soil at significantly lower FIRs. Compared to the results of the London Clay index tests shown in Figure 3.21, lower ranges of FIR were required to condition the WRB/UP soil. This is due to the UP sand present in these samples, which reduced the amount of foam liquid absorbed by the soil and improved the stability of the foam compared to the London Clay samples.

Based on these index tests, ranges of foam and polymer injection ratios required to effectively condition the WRB/UP soil were determined. To achieve a strength of 5 to 20 kPa, conditioning with a FIR of 50 to 75% in combination with a PIR of 10 to 20% represent the optimum range of conditioning treatments. The conditioning treatments used for the screw conveyor test samples were chosen based on the strength measurements shown in Figure 6.3.

The results of these index tests were provided to Nishimatsu Construction Company as recommended soil conditioning treatments for EPB tunnelling on Contract 220 of the CTRL project in London, which passed through a mixed face of WRB clay and UP sand. The recommended conditioning treatments performed well in the field, and the vane shear strength of the conditioned spoil from the EPB machine was similar to that measured for index test samples prepared with similar conditioning treatments (Nishimatsu, 2002).

### 6.2.2 Preparation of screw conveyor test samples

The London Clay and WRB/UP soil samples for the screw conveyor tests were prepared with various foam and polymer conditioning treatments. The samples were prepared as pre-conditioned mixtures by mixing the soil and conditioning agents, and compacting the sample into the container. This method allowed preparation of samples conditioned to specific treatments, representing the state of excavated, conditioned soil in the head chamber of an EPB machine. For some of the samples, the conditioning treatments were varied to achieve different strengths. Other samples were prepared with different conditioning treatments resulting in similar strengths.

The conditioning treatments for the test samples were chosen to achieve target strengths, based on the results of the index tests of conditioned London Clay and WRB/UP soils. The screw conveyor test samples were prepared by a similar method as for the index test samples, described in Section 3.4.4.1. The samples were prepared for a target height in the container. This gives a total volume for the sample, and using the conditioner injection ratios defined by equations 6.1 and 6.2 below, the volume proportions of soil, polymer solution, and foam required for the sample are calculated. An in-situ bulk unit weight of  $20 \text{ kN/m}^3$  was assumed for all of the soils, used to calculate the mass of soil corresponding to the volume of soil in a sample.

$$PIR = (V_p / V_s) \times 100 \quad \text{Eqn 6.1}$$

$$FIR = (V_f / V_s) \times 100 \quad \text{Eqn 6.2}$$

where:  $V_p$  is the volume of polymer solution (L)  
 $V_f$  is the volume of foam at atmospheric pressure (L)  
 $V_s$  is the in-situ volume of excavated soil (L)

Details of the conditioned London Clay and WRB/UP soil samples prepared for the screw conveyor tests are shown in Table 6.4. The samples were prepared to a maximum height of 840 mm. For most of the samples, 160 to 200 kg of soil was mixed with the volumes of polymer solution and foam required for the specific injection ratios. The samples were conditioned with MV polymer solutions at 0.2% concentration, and at 0.5% concentration for one sample. Three samples were also conditioned with TR foam, produced at 1.5% concentration using the standard foam generator settings (see Section 3.5.1). One London Clay sample was conditioned with water only. The total mass of the conditioned soil samples compacted into the container and the

sample heights, volumes, and bulk densities are also shown. The bulk densities of the compacted, conditioned soil samples are within the typical range of 1.6 to 2.0 tonnes/m<sup>3</sup> for excavated material in an EPB machine head chamber (Herrenknecht and Rehm, 2003).

Due to the capacity of the mixer used, the samples were prepared in three or four batches. A weighed mass of soil was mixed with measured volumes of the conditioning agents, in proportion to the injection ratios. The batches of the samples were mixed for approximately 60 seconds to form a uniform conditioned soil mixture. The conditioned soil was then transferred to the sample containers, and compacted by hand to minimise air voids in the sample. Each batch of soil and conditioning agents were mixed and compacted into the containers to build the sample up to the initial height.

### **6.2.3 Properties of screw conveyor test samples**

Some properties of the conditioned soil samples were measured during preparation to characterise the screw conveyor test samples. For each batch of a sample mixed, several specimens were taken to measure the moisture content of the soil before and after mixing with the conditioning agents. For the samples conditioned with foam, the FER of the foam produced for each batch was measured to check that it was equal to the target value. After compaction of each batch of conditioned soil into the container, shear vane tests were performed to measure the strength throughout the depth of the samples. These properties of the conditioned soil samples are summarised in Table 6.5.

The moisture contents of the soil for the different samples were similar to the range of in-situ natural moisture contents. The conditioned soil moisture contents were close to those calculated based on the liquid injection ratios, and the vane shear strengths measured for each sample were within a narrow range, indicating uniform mixing of the conditioning agents with the soil. The average strength of the conditioned London Clay samples ranged from 4 to 27 kPa, and from 5 to 15 kPa for the two WRB/UP soil samples. The average vane shear strength of the conditioned London Clay samples are shown plotted against the moisture content in Figure 6.4, and compared to the strengths of samples prepared for the index tests discussed in Chapter 3. The large scale screw conveyor test samples were of similar strength to the index test samples conditioned with MV polymer solutions, and to the samples remoulded with water at similar moisture contents.

The methods described were successful for preparing uniform, conditioned soil samples from natural clay soils to represent the state of excavated, conditioned soil produced by an EPB machine. The samples were prepared to specific conditioning treatments and the properties relevant to the screw conveyor tests were characterised as described above.

### **6.3 Screw conveyor tests with conditioned soil samples**

The conditioned soil samples were prepared to investigate the operation of the model screw conveyor with natural clay soils, and the effects of different conditioning treatments on the performance. The test procedures and conveyor operating conditions for these tests are described below.

Following preparation of the samples, the containers were mounted in the load frame and a pressure of 100 kPa was applied to the piston for approximately five minutes. This compaction stage was performed to substantially remove any air voids and improve the uniformity of the samples. The compaction pressure was reduced to atmospheric, and the assembled screw conveyor was connected to the container. The test pressure was then applied to the piston for approximately three minutes before starting the screw conveyor.

The initial heights of the conditioned soil samples were in the range 680 to 840 mm, allowing the tests to be performed in two or three stages in which the screw speed was varied. The different stages were designed based on the sample height, as described in Section 4.5.2. The tests were performed with similar conveyor operating conditions, as summarised in Table 6.6.

Samples 7 to 10 were prepared from London Clay conditioned with MV polymer solutions at 0.2% concentration, with injections ratios of 20 to 50% to give undrained strengths ranging from 4 to 27 kPa with a similar conditioning agent. These tests were performed with a pressure of 200 kPa applied to the piston, the discharge outlet unrestricted, and the screw speed varied from 5 to 15 and 25 rpm for the different stages.

Sample 11 was prepared from London Clay with the same conditioning treatment as for sample 10, to give a similar undrained strength. This test was performed with the same conditions as for sample 10, but with screw (2) of longer pitch to investigate the effects on the conveyor operation.

Samples 12 to 14 were prepared from London Clay with different conditioning treatments based on the same liquid injection ratio to achieve similar sample strengths. These tests were performed under the same conditions as the earlier tests, in order to compare the conveyor operation with samples of similar strength prepared with different conditioning treatments.

Sample 12 was prepared with a combined polymer and foam conditioning treatment to give a 30% liquid injection ratio from the polymer solution and foam liquid. The index test sample prepared with this conditioning treatment had an undrained strength of 6.5 kPa (see Figure 3.21), with the clay cuttings dispersed by the foam. This conditioning treatment was chosen to attempt to prepare a screw conveyor test sample with the clay cuttings dispersed in foam, but most of the foam broke down during the time required to prepare the large scale sample. This resulted in a higher strength than for the index test sample, similar to the other samples prepared with a 30% liquid injection ratio. However, the concentration of polymer and surfactant present in the conditioning agent liquid phase for this sample was higher than for others. This test was performed in two stages with screw speeds of 5 and 15 rpm, due to the smaller sample volume.

Sample 13 was prepared using water only as the conditioning agent, with an injection ratio of 30%. The strength of this sample was similar to others prepared with this liquid injection ratio, to compare the conveyor operation with the samples conditioned with polymer and foam.

Sample 14 was conditioned with MV polymer solution at an injection ratio of 30%, but with a higher polymer concentration of 0.5%. The sample strength was slightly higher than for others prepared at the same liquid injection ratio with a lower polymer concentration. This conditioning treatment was used to investigate lubrication effects of the polymer on the conveyor operation, by comparison with the tests performed with samples prepared with water and a polymer concentration of 0.2%.

Samples 15 and 16 were prepared from the mixed WRB/UP soil conditioned with combined foam and polymer treatments. The conditioning treatments were chosen to achieve different sample strengths, based on the results of the index tests shown in Figure 6.3. The strength of sample 15 was higher than the index test sample prepared with a similar conditioning treatment, as some of the foam broke down during preparation of the large scale sample. For sample 16, the higher polymer injection ratio improved the stability of the foam mixed with the soil, resulting in a similar strength to that measured for the index test samples. Some of the foam air bubbles

remained in the samples during the screw conveyor tests. The tests with these two samples were performed under similar conditions, with the discharge outlet restricted and the screw speed varied for the different stages. Only two screw speeds were possible in test 16 due to a mechanical problem with the screw conveyor during the test.

This series of tests allowed investigation of the screw conveyor performance with conditioned natural clay soils. The tests provided measurements of the screw conveyor operation with different clay soils, and of the effects of variables including different conditioning treatments, sample strengths, screw speeds and discharge conditions.

## **6.4 Screw conveyor tests with conditioned London Clay**

The soil conditioning treatments and test conditions for the model screw conveyor tests with London Clay samples are summarised in Table 6.6. Results from these tests illustrating the conveyor performance with the different samples and operating conditions are presented here.

### **6.4.1 Soil flow rates**

The tests with conditioned soil samples were performed with the screw speed varied from approximately 5 to 15 and 25 rpm. The applied piston pressure, the sample height in the container, and the screw speed are monitored during the tests. Typical measurements from a test are shown in Figure 6.5. The sample compressed slightly when the 200 kPa pressure was applied prior to starting the screw conveyor, and the piston pressure remained stable throughout the test as the soil was extracted from the container. During each stage the sample height reduced at a constant rate, increasing with speed of the screw. Assuming undrained conditions and that the conveyor is full of clay, the volumetric soil flow rate through the conveyor is equal to the rate of change of sample volume in the container, measured from the change of sample height during each screw speed increment.

The soil flow rates at different screw speeds in tests 7 to 16 with the conditioned soil samples are shown in Figure 6.6 and summarised in Table 6.7. The screw speeds shown in this figure are the actual values during the conveyor operation, calculated from the period of the cycles in the torque measurements. As shown later in Figure 6.17, the period of the torque cycles corresponds to the rotational frequency of the screw. The measured screw speeds are close to the nominal values based on the motor speed setting, but are more accurate for comparison of the soil flow

rates. Figure 6.6 shows that the flow rates increased linearly with the screw speed, and the values varied for the different samples with similar conveyor operating conditions. The flow rates measured in test 11 with screw (2) are higher than those in the tests with screw (1), due to the larger helix angle of screw (2) causing the soil to move along the conveyor more rapidly. Also shown are the maximum flow rates for screws (1) and (2), calculated from equation 5.10. In all tests the measured flow rates were lower than the maximum values, due to the relative movement between the soil and the screw, which results in the soil advancing along the conveyor slower than the rotation of the screw.

The discharge efficiency of the screw conveyor can be defined as the flow rate during operation relative to the maximum flow rate based on the conveyor geometry. From equation 5.10, the ratio of the maximum flow rate of the conveyor ( $Q_{\max}$ ) to the screw speed (N) is given as:

$$\frac{Q_{\max}}{N} = \frac{\pi}{4} (D_c^2 - D_s^2) \times (t - e) \quad \text{Eqn 6.3}$$

The ratio  $Q_{\max}/N$  has a specific value for a given screw conveyor geometry, equal to the volume of the screw channel per pitch. From the measured flow rates, values of the ratio  $Q/N$  during conveyor operation can be calculated. The measured  $Q/N$  values relative to the maximum value,  $Q_{\max}/N$ , represents the discharge efficiency of the screw conveyor:

$$\eta = \left( \frac{Q/N}{Q_{\max}/N} \right) \times 100 \quad \text{Eqn 6.4}$$

where:  $\eta$  is the conveyor discharge efficiency (%)  
 $Q$  is the measured conveyor flow rate ( $\text{m}^3/\text{min}$ )

The discharge efficiency measured in the tests with conditioned soil samples is shown plotted against the screw speed in Figure 6.7. The measured soil flow rates correspond to approximately 60 to 80% of the maximum flow rate at the different screw speeds. For each test, the discharge efficiency reduced slightly with increasing screw speed. This indicates that at higher speeds, the soil moved along the screw channel by smaller amount with every screw rotation. Although the flow rate is higher in test 11 with screw (2), the discharge efficiency was similar to that in the tests using screw (1).

The discharge efficiencies from the tests with London Clay samples using screw (1) are shown plotted against the sample strength in Figure 6.8. This data shows an increase in the discharge efficiency with increasing sample strength. This results from the increase of the shear stress acting on the casing surface, causing the soil to move along the screw channel by a greater amount with every screw rotation.

The variations in the soil flow rates and discharge efficiencies observed for the different conditioned soil samples with similar conveyor operating conditions result from differences in the shear stresses acting on the soil in the screw channel. The different flow rates influence the total pressure gradients and the screw torque measured in these tests, as discussed in the analysis of the screw conveyor operation presented in Chapter 7.

#### **6.4.2 Pressure gradients**

The changes of total normal stress, pore water pressure and effective stress along the conveyor were determined from the measurements at the instrumented sections. Typical measurements of the total normal stress acting on the casing at different screw speeds during a test with a London Clay sample are shown in Figure 6.9. The total stress at each section increased as the conveyor filled with soil, reaching approximately stable values once steady state operation was established. At each section, the total stress was similar as the screw speed increased from 5 to 15 and 25 rpm. Some fluctuations in the total stresses are observed during the test, which result from the non-uniformity of the conditioned clay cutting sample. With the discharge outlet unrestricted, the total normal stress dissipated along the conveyor, with a similar pressure gradient at the different screw speeds in this test.

The gradients of the total normal stress, pore water pressure, and effective stress along the conveyor during test 9 with the screw rotating at 5 rpm are shown in Figure 6.10. This figure shows a similar response of the conditioned clay sample during the conveyor operation as observed for a consolidated kaolin sample. The total pressure dissipated linearly along the conveyor, with a similar pore water pressure gradient, associated with the undrained conditions of the test. The effective stress measured at the casing surface was approximately constant along the conveyor, corresponding to the constant resultant shear stresses measured along the conveyor casing, shown later in Figure 6.15. Pressure gradients similar to those shown in Figure 6.10 were measured with the screw rotating at different speeds in test 9. The similar results obtained from the various tests performed with consolidated kaolin and compacted conditioned

clay cutting samples demonstrate that the model screw conveyor operates by the same mechanics with different clay soils.

The total pressure gradients measured at different screw speeds in tests 9 and 7 are shown in Figures 6.11(a) and (b). These figures show typical measurements from the tests with conditioned London Clay samples performed with varying screw speeds and the discharge outlet unrestricted. The total pressure at the start of the conveyor was approximately 200 kPa, which dissipated linearly along the conveyor to a low pressure at the unrestricted discharge outlet. The total pressures measured at each section, and the pressure gradients, were similar at the different screw speeds in these tests.

Figure 6.12 shows total pressure gradients measured at different screw speeds during tests with conditioned London Clay samples of varying strength. The pressure at the start of the conveyor was approximately 200 kPa throughout the test, and dissipated linearly to pressures in the range 10 to 25 kPa at the unrestricted discharge outlet. Under these operating conditions, the total pressure gradients were similar for these samples with different undrained shear strengths in the range 4 to 13 kPa.

The total pressure gradients measured at different screw speeds during tests 13 and 11 are shown in Figure 6.13(a) and (b). These tests were performed with conditioned London Clay samples of similar strength and with the same test conditions, but using screw (1) for test 13 and screw (2) for test 11, to compare the conveyor operation with screws of different pitch. In each test, the total pressure gradients at the different screw speeds were similar. With the measured values shown in Table 6.7, the total pressure change and gradient was smaller in test 11 with screw (2) than in test 13 with screw (1). As observed in tests with kaolin samples, the screw pitch influences the total pressure gradient, with a smaller gradient measured for the screw of longer pitch with the same operating conditions.

A theoretical model of the total pressure gradient along the screw conveyor is proposed in Chapter 7. This model shows that the pressure gradient depends on the shear stresses acting on the casing and screw surfaces, the screw geometry, and the direction of soil flow along the conveyor (related to the soil flow rate at a given screw speed). These factors effect the pressure gradient in different ways, and the gradient for a particular sample and operating condition depends on their relative influences. In the tests discussed here, the shear stresses and the soil

flow rates vary depending on the sample properties and the conveyor operating conditions, resulting in the pressure gradients shown in Figures 6.11 to 6.13. The results from these tests with samples of varying strength, with different screw speeds, and with different screw geometries are discussed in relation to the proposed theoretical model in Section 7.3.

### 6.4.3 Casing shear stresses

Typical measurements of the resultant casing shear stress at each instrumented section during a test with a conditioned London Clay sample are shown in Figure 6.14. The measurements fluctuate over a range of 4 to 5 kPa due to non-uniformity of the sample, but the average shear stresses are approximately constant, and similar at each section along the conveyor. The measurements shown are from test 13, and average vane shear strength of this sample was 10 kPa. The range and average values of the resultant shear stress measured by the load cells correspond to the vane shear strength measurements, indicating that the casing shear stress was approximately equal to the undrained strength of the soil.

The average resultant casing shear stresses and friction coefficients measured along the conveyor at different screw speeds during some of the tests with conditioned London Clay samples are shown in Figures 6.15(a) to (d). The average values of these parameters from all of the tests with conditioned soil samples are summarised in Table 6.7. The average shear stresses were constant along the conveyor and varied slightly with the screw speed, which controls the rate of shear at the casing surface. The average casing shear stresses were approximately equal to the undrained strengths of the samples measured by vane shear tests. Figure 6.16 compares the average casing shear stresses at different screw speeds with the undrained strength of the conditioned London Clay samples, showing good agreement between the measurements.

As shown in Figure 6.15 and Table 6.7, the average values of the friction coefficient  $\tau/\sigma'_n$  for the London Clay samples were approximately constant along the conveyor, and did not vary significantly with the screw speed. Most of the values for the different samples and varying shear rates were in the range  $\tau/\sigma'_n = 0.14$  to  $0.24$ , corresponding to friction angles of  $8.0^\circ$  to  $13.5^\circ$ . As observed in the tests with kaolin samples, a layer of clay covered the surface of the conveyor casing, with the shear surface forming in the soil slightly away from the interface. The measured friction coefficients represent values for soil-on-soil shearing at a residual state under fast, undrained shearing conditions.

Residual friction coefficients measured for London Clay samples in ring shear tests at varying shear rates are reported by Tika *et. al.* (1996). London Clay was observed to shear by a sliding mechanism, with a thin polished shear surface of oriented clay particles forming at the residual state. For normal stresses of 200 to 400 kPa and shear rates of 0.001 to 6200 mm/min, the residual friction coefficients measured in several tests varied from  $\tau/\sigma'_n = 0.122$  to 0.220. A positive rate effect was observed as the friction coefficient increased with the rate of shear, but the effect was relatively small with variations of approximately 10% in the values measured for a sample at different shear rates. The average friction coefficients measured at shear rates of approximately 1600 to 8000 mm/min in the model screw conveyor tests with conditioned London Clay samples agree well with the fast residual values measured for similar soil under comparable conditions in ring shear tests.

#### 6.4.4 Screw torque

The tests with conditioned London Clay samples provided measurements of the screw torque at different speeds for samples of varying strength. Figure 6.17 shows a typical measurement of the torque at different screw speeds during these tests. The torque increased linearly as the conveyor filled with soil, reaching a stable average value when steady state operation was established. For this test, the average torque increased with each increase of the screw speed. Figures 6.17(b), (c) and (d) show that the period of the cycles in the torque measurements, due to the eccentricity of the screw shaft in the conveyor, corresponds to the rotational frequency of the screw at the different speeds.

The average torque measured at different screw speeds for the conditioned soil samples are shown plotted against the undrained strength in Figure 6.18. The screw torque generally increased with the undrained strength of the samples; however, there is significant scatter in the data. The torque increased with the screw speed for most tests, but the changes of the torque with the screw speed were not consistent in all of the tests.

The theoretical model of the screw conveyor operation presented in Chapter 7 shows that the screw torque is related to the casing shear stress and the direction of soil flow along the conveyor, which depends on the flow rate for a given screw speed. Figure 6.19 shows the screw torque plotted against the average casing shear stress at different screw speeds for the tests with conditioned soil samples. This figure shows an approximately linear increase of torque with the casing shear stress, as expected from the theoretical relationship. The scatter of this data results

partly from variations of the soil flow rate at the different screw speeds in the tests. This influences the direction of soil flow along the conveyor and the screw torque for a given casing shear stress, as discussed in Chapter 7.

## **6.5 Screw conveyor tests with conditioned WRB/UP soil**

Two tests were performed with WRB/UP soil samples conditioned with combined foam and polymer treatments for different strengths, to model an EPB machine excavation in a mixed face of clay and sand. The conditioning treatments and properties of these samples are summarised in Tables 6.4 and 6.5. As shown in Table 6.6, these tests were performed with the conveyor discharge outlet restricted and with different screw speeds. Results from these tests are summarised in Table 6.7 and discussed below.

### **6.5.1 Soil flow rates**

The soil flow rates measured in tests 15 and 16 with conditioned WRB/UP samples at different screw speeds are shown in Figure 6.6. The flow rates, and the increase with the screw speed, were similar to those measured in the tests with conditioned London Clay samples using screw (1).

The flow rates in tests 15 and 16 were less than the maximum values for the screw at the different speeds. The discharge efficiencies calculated from equation 6.4 are shown plotted against the screw speed in Figure 6.7. The discharge efficiency in these tests ranged from 57 to 66%, and reduced with increasing screw speed. As in the tests with other soils, these measurements indicate relative movement between the soil and the screw, resulting in interface shearing on the screw surfaces. The decrease of the discharge efficiency indicates that the soil moves along the screw channel by a smaller amount with every rotation at higher screw speeds, which influences the pressure gradient and torque at the different speeds.

### **6.5.2 Pressure gradients**

The total normal stress measured at each section along the conveyor during test 15 is shown in Figure 6.20. This sample had an average vane shear strength of 15.5 kPa, and the test was performed with the discharge outlet restricted and with nominal screw speeds of 5, 15 and 25 rpm. Although there are significant fluctuations in the measurements due to inhomogeneity of the sample, periods of steady state operation with the total normal stress approximately constant at each section were observed at each screw speed. With the screw rotating at 5 rpm, a steady

state was established with the pressure decreasing along the conveyor. A total pressure of 100 to 150 kPa was measured at Section 4, due to the pressure required at the end of the conveyor to discharge the soil through the restricted outlet. With the screw speed increased to 15 rpm, a higher pressure was required to discharge the soil at a faster rate, and the stresses along the conveyor increased during this stage of the test. The total pressure increased by a greater amount towards the end of the conveyor, resulting in a steady state operation with the pressure increasing along the conveyor. With the screw speed at 25 rpm, a higher pressure was again required to discharge the soil at a faster rate. The total pressure towards the end of the conveyor increased further as the conveyor generated the pressure required to discharge the soil.

The total pressure gradients at the different screw speeds during test 15 are shown in Figure 6.21(a). The pressure gradient at 5 rpm is from the period  $t = 700$  to  $800$  s, showing the dissipation of the total pressure along the conveyor during this stage of the test. The gradients shown for 15 and 25 rpm correspond to the periods  $t = 1100$  to  $1200$  s and  $t = 1225$  to  $1325$  s respectively, showing the increase of total pressure along the conveyor during these stages. At all speeds, the total pressure gradients were approximately constant, as observed in tests with other soils and varied operating conditions. With the outlet restricted, the pressure required at the end of the conveyor to discharge the soil increased with the screw speed and the soil flow rate. In this test, this resulted in the pressure gradient changing from dissipating pressure at low screw speeds, to generating pressure at higher speeds.

Figure 6.21(b) shows the total pressure gradients measured during test 16, performed with conditioned WRB/UP soil with an undrained strength of 5 kPa and with the discharge outlet restricted. With a lower strength sample than in test 15, the pressure required to discharge the soil was smaller. The total pressure at the end of the conveyor increased with the screw speed and the soil flow rate, although the pressure dissipated along the conveyor with the screw speeds of 5 and 15 rpm.

Figures 6.21(a) and (b) show that with the outlet restricted, the pressure required to discharge the WRB/UP soil increased with the screw speed, influencing the pressure gradients along the conveyor. The increase of the pressure to extrude the soil through the restricted outlet as the screw speed and soil flow rate increase is not expected from the theory of plastic flow through a die, discussed in Section 5.6.2. The reasons for the observations in these tests are not clear, but are possibly due to the properties of the conditioned WRB/UP soil and rate dependence of the

shear stresses acting in the extrusion process. As discussed in Section 6.5.3 and shown in Figure 6.22, the casing shear stresses measured in tests 15 and 16 increased with the screw speed and the shear rate, which could explain the higher extrusion pressures if the same shear stresses act in the discharge outlet.

The results of the tests performed with conditioned soil samples illustrate effects of the operating conditions on the total pressure gradients along the conveyor. In the London Clay tests performed with the discharge outlet unrestricted, the total pressure dissipated along the conveyor for a range of sample strengths and screw speeds. With the outlet restricted in the WRB/UP tests, higher pressures were required to discharge the soil, which increased with the sample strength and the screw speed. The dissipation or generation of total pressure along the conveyor depends on the required discharge pressure for a particular soil strength and flow rate. The different pressure gradients observed with the varied operating conditions result from the shear stresses acting on the soil in the screw channel and the direction of soil flow along the conveyor, as discussed in Section 7.3. It would be of interest to further investigate the effects of varying operating conditions on the conveyor performance, as observed in these tests.

### 6.5.3 Casing shear stresses

The average resultant casing shear stresses measured along the conveyor during tests 15 and 16 at the different screw speeds are shown in Figures 6.22(a) and (b). The values shown are the average shear stresses measured for the same periods of the tests for which the total pressure gradients in Figure 6.21 were measured. The pore water pressure measurements were unstable at some sections during different periods of these tests, so values of the friction coefficient are only shown at some sections in Figure 6.22. Average values of the resultant casing shear stress and friction coefficient for the different stages of these tests are shown in Table 6.7.

The shear stresses were approximately constant along the conveyor at the different screw speeds, corresponding to the constant total pressure gradients. For both tests, the resultant shear stresses increased with the screw speed, and varied significantly from the undrained shear strength of the samples. During test 15 with the screw speed at 5 rpm, the average casing shear stress was 8.3 kPa, lower than the undrained strength of the sample. At the higher screw speeds, the casing shear stresses were higher than the undrained strength. The total stress, effective stress and shear stress along the conveyor increased with the screw speed, with similar values of the friction coefficient at the different speeds. The average values ranged from  $\tau/\sigma'_n = 0.087$  to 0.103,

representing friction angles of approximately  $5.0^\circ$  to  $6.0^\circ$ . In test 16, the casing shear stress was higher than the undrained strength of the sample at both screw speeds. The total stress, effective stress and shear stress also increased with the screw speed in this test. The measured friction coefficients represent friction angles of approximately  $8.5^\circ$  for this sample.

The casing shear stresses measured in tests 15 and 16 were different to the behaviour observed in the tests with other soils, with the shear stresses differing from the undrained strength of the samples and varying with the screw speed, indicating some rate dependence of the casing shear stress. This unusual behaviour is thought to be due to the different properties of these samples of mixed clay, sand, polymer and foam.

#### **6.5.4 Screw torque**

The average torque measured at the different screw speeds during tests 15 and 16 are shown plotted against the undrained strength of the samples and the average casing shear stresses in Figures 6.18 and 6.19. These measurements are compared with those from the tests with London Clay samples, and show similar increases of the torque with the sample strength and the casing shear stress.

The torque increased with the screw speed for the WRB/UP samples, due to the higher casing shear stresses at the higher screw speeds as discussed above. The torque measured in the tests with WRB/UP samples is similar to that for the London Clay samples with a similar casing shear stress, indicating that the torque is similar for the different soils and conditioning treatments. As discussed in Chapter 7, the torque is related to the casing shear stress and the soil flow rate at a given screw speed. The soil conditioning treatment can influence the screw torque by reducing the shear stress acting on the casing, either by reducing the sample strength or by providing lubrication at the interface.

### **6.6 Effects of soil conditioning treatments on screw conveyor operation**

The results of the tests with conditioned soil samples allow some comments regarding the effects of the conditioning treatments on the performance of the model screw conveyor. The foam and polymer conditioning treatments formed soft plastic pastes from the natural soil samples, representing the state of conditioned excavated soil in the head chamber of an EPB machine. The conditioned soil pastes allowed controlled operation of the screw conveyor, with constant

total pressure gradients along the conveyor and controlled soil flow rates. The mechanics of the conveyor operation with the compacted conditioned soil samples were similar to those observed for the consolidated kaolin samples. The casing shear stresses were constant along the conveyor, resulting in a constant total pressure gradient and screw torque.

The screw conveyor operation in the tests with conditioned London Clay was dominated by the undrained strength of the samples. Control of the soil flow rate and pressure dissipation along the conveyor was achieved in all of the tests, even with very low sample strengths. The resultant shear stresses were approximately equal to the undrained strength of the samples prepared with different conditioning treatments. The tests with samples conditioned with the same amount of water and varying polymer concentrations showed no influence of the polymer reducing the shear stress at the casing or the screw torque, as the shearing at this surface involves a soil-on-soil mechanism rather than soil-on-steel interface shearing. The sample conditioned with the combined foam and polymer solution treatment showed no significant influence of the foam, as most of the foam air bubbles broke down during the sample preparation. As discussed in Chapter 7, there is some indirect evidence that the conditioning treatments with higher polymer and surfactant concentrations in the liquid phase provided lubrication to reduce the shear stresses at the soil-steel interface on the screw surfaces, which influenced the pressure gradients in these tests. Conditioning treatments with higher liquid injection ratios to achieve lower undrained strengths reduce the shear stress acting on the casing, and so reduce the torque and power required to operate the screw conveyor.

The combined foam and polymer solution treatments used for the WRB/UP samples created a soft paste from the mixed high plasticity clay and silty sand soils. The performance of the foam was improved in these samples compared to the London Clay. The screw conveyor operation in these tests was influenced by the restricted discharge condition. The soil flow rate, total pressure gradient, casing shear stress and torque at the different screw speeds were influenced by the pressure required at the end of the conveyor to discharge the soil. The casing shear stresses and the screw torque measured during the first stage of test 15 were lower than expected based on the undrained strength of the sample. This sample was conditioned with a high foam injection ratio, and these measurements suggest some lubrication effects due to the significant amount of foam in the soil influencing the conveyor operation.

## 6.7 Summary

This chapter has reported a series of model EPB screw conveyor tests performed with conditioned natural soil samples. Tests were performed to investigate the operation of the conveyor under different conditions with London Clay and WRB/UP soil samples conditioned with various polymer and foam treatments.

Geotechnical properties of the London Clay, WRB clay and UP sand samples were described. The conditioning treatments for the test samples were chosen based on the results of index tests measuring the undrained strength of conditioned soil samples. Index tests of conditioned London Clay were described in Chapter 3, and similar tests performed to determine effective conditioning treatments for WRB/UP samples were reported in this chapter.

The methods for preparation of natural soil samples, uniformly conditioned with specific polymer and foam treatments, for the screw conveyor tests were described. The conditioned soil samples were characterised by vane shear tests and the sample moisture contents. Some London Clay samples were prepared with different polymer injection ratios to give varying strengths. Further samples were prepared for similar strengths with different polymer concentrations and with combined foam-polymer treatments to investigate effects of different conditioning treatments on the conveyor operation. The WRB/UP samples were conditioned with combined foam-polymer treatments for different strengths. The screw conveyor tests with the conditioned soil samples were performed with varied conditions to observe the operation with different screw speeds, discharge conditions, and screw pitches.

The conditioning treatments turned the London Clay cuttings into soft pastes, allowing controlled operation of the model screw conveyor with uniform pressure gradients and soil flow rates, even with very low sample strengths. The mechanics of the screw conveyor operation with compacted conditioned natural soil samples were similar to those observed for the consolidated kaolin samples. The casing shear stress was constant along the conveyor, and approximately equal to the undrained shear strength of the samples. The constant shear stresses resulted in constant total pressure gradients along the conveyor, and a constant screw torque during steady state operation. The residual friction coefficients at fast shear rates in the screw conveyor tests were similar to those reported from ring shear tests on London Clay samples under comparable conditions. With the discharge outlet unrestricted in these tests, the total stress dissipated linearly

along the conveyor, and the pressure gradient was similar at different screw speeds and for different sample strengths. A smaller pressure gradient was measured in the test performed with the screw of longer pitch. The soil flow rate increased with the screw speed, although the discharge efficiency varied slightly between the tests with different samples strengths and screw speeds. The screw torque increased with the undrained strength of the samples, and was proportional to the shear stress acting on the casing. The total pressure gradients and screw torques measured in the tests with different sample properties and conveyor operating conditions are related to the soil flow rates and the shear stresses acting on the casing and screw surfaces, as discussed in Chapter 7.

The conditioning treatments formed soft pastes from the mixed WRB clay and UP sand samples, allowing controlled operation of the model screw conveyor. The conveyor mechanics were similar to those with other soils, but the restricted discharge condition influenced these tests. The pressure required at the end of the conveyor to discharge the soil increased with the soil strength and the screw speed, and influenced the soil flow rates and total pressure gradients. Depending on the specific operating conditions, the screw conveyor either dissipated or generated pressure along the length. The tests indicate that the mode of operation of an EPB screw conveyor can vary depending on the soil strength, the screw speed, and the opening of the discharge outlet.

These tests demonstrate that excavated natural clay soils can be effectively conditioned with foams and polymers to form materials suitable for controlled EPB machine operations with uniform pressure gradients and soil flow rates through the screw conveyor. For the London Clay tests, no significant influences of the different conditioning treatments on the model screw conveyor operation were observed directly. As discussed in Chapter 7, there is some indirect evidence from these tests that higher polymer and surfactant concentrations in the liquid phase of the conditioning agents can lubricate the soil-steel interfaces on the screw surfaces, leading to effects on the pressure gradient. For the WRB/UP tests, reduced casing shear stresses and screw torques were observed, which possibly resulted from lubrication provided by significant amounts of foam in the soil. Conditioning treatments giving lower sample strengths allowed controlled operation of the conveyor with reduced screw torque and power requirements.

<b>Index properties</b>	<b>Range (CTRL, 1997)</b>	<b>Range (Withers <i>et al.</i>, 2001)</b>
Bulk unit weight (kN/m <sup>3</sup> )	-	18 to 22.5
Natural moisture content (%)	-	9 to 58
Liquid limit (%)	30 to 78	20 to 84
Plastic limit (%)	12 to 25	11 to 53
Plasticity index (%)	18 to 55	11 to 39
<b>Design parameters values</b>		
Bulk unit weight (kN/m <sup>3</sup> )	20	19 to 21
Undrained shear strength (kPa)	300	100 to 400
Friction angle (°)	26	28 to 32
Permeability (m/s)	-	1 x 10 <sup>-8</sup> to 10 <sup>-6</sup>

Table 6.1. Index properties and design parameters of WRB soil (Upper mottled clay).  
(after CTRL, 1997; Withers *et al.*, 2001)

<b>Index properties</b>	<b>Range (CTRL, 1997)</b>	<b>Range (Withers <i>et al.</i>, 2001)</b>
Bulk unit weight (kN/m <sup>3</sup> )	-	20 to 22
Natural moisture content (%)	22	15 to 35
Liquid limit (%)	43	23 to 41
Plastic limit (%)	16	16 to 23
Plasticity index (%)	27	6 to 23
<b>Design parameters values</b>		
Bulk unit weight (kN/m <sup>3</sup> )	19	19 to 21
Undrained shear strength (kPa)	-	-
Friction angle (°)	33	33 to 40
Permeability (m/s)	5 x 10 <sup>-4</sup> to 5 x 10 <sup>-7</sup>	1 x 10 <sup>-3</sup> to 10 <sup>-6</sup>

Table 6.2. Index properties and design parameters of Upnor sand.  
(after CTRL, 1997; Withers *et al.*, 2001)

<b>Sample No.</b>	<b>Polymer injection ratio (%)</b>	<b>Foam injection ratio (%)</b>	<b>Conditioner liquid injection ratio (%)</b>	<b>Vane shear strength (kPa)</b>
1	0	125	7.8	21.5
2	10	50	13.1	21.0
3	10	100	16.3	14.0
4	15	50	18.1	14.0
5	15	70	19.4	8.0
6	20	0	20.0	10.5
7	20	50	23.1	4.5

Table 6.3. Index tests of conditioned WRB/UP soil.

(Foam: TR at 1.5% concentration, FER=16; Polymer: MV at 0.2% concentration)

Sample No.	Soil	Conditioning treatment	Liquid injection ratio (%)	Total soil mass (kg)	Total soil volume (L)	Polymer solution volume (L)	Foam volume (L)	Sample mass (kg)	Sample height (mm)	Sample volume (L)	Bulk unit weight (kN/m <sup>3</sup> )
7	London Clay	PIR=40% MV @ 0.2% conc.	40	165	82.5	33.0	-	193	810	112.2	16.9
8	London Clay	PIR=20% MV @ 0.2% conc.	20	167.5	83.75	16.5	-	184	750	103.9	17.4
9	London Clay	PIR=50% MV @ 0.2% conc.	50	160	80.0	40.0	-	191	815	112.9	16.6
10	London Clay	PIR=30% MV @ 0.2% conc.	30	181.5	90.75	27.0	-	196	840	116.4	16.5
11	London Clay	PIR=30% MV @ 0.2% conc.	30	182.5	91.25	27.0	-	195	830	115.0	16.6
12	London Clay	PIR=20% MV @ 0.2% conc. FIR=120% TR @ 1.5% FER=13.5	29	134.5	67.25	13.5	81	154	678	93.9	16.1
13	London Clay	Water Injection ratio=30%	30	167.5	83.75	26.0 (water only)	-	193.5	775	107.4	17.7
14	London Clay	PIR=30% MV @ 0.5% conc.	30	166.0	83.0	30.0	-	191.5	835	115.7	16.2
15	WRB/UP	PIR=15% MV @ 0.2% conc. FIR=70% TR @ 1.5% FER=14	20	200 (100 kg UP + 100 kg WRB)	100.0	15.0	70	215	840	116.4	18.1
16	WRB/UP	PIR=22% MV @ 0.2% conc. FIR=50% TR @ 1.5% FER=14	25.6	200 (100 kg UP + 100 kg WRB)	100.0	22.0	50	210	830	115.0	17.9

Table 6.4. Preparation of conditioned soil samples for screw conveyor tests.

Sample No.	Soil	Conditioning treatment	Liquid injection ratio (%)	Initial soil moisture content (%)	Conditioned soil moisture content (%)	Range vane shear strength (kPa)	Average vane shear strength (kPa)
7	London Clay	PIR=40% MV @ 0.2% conc.	40	23.7	48.5	6 - 8	7
8	London Clay	PIR=20% MV @ 0.2% conc.	20	24.2	36.3	23 - 29	26
9	London Clay	PIR=50% MV @ 0.2% conc.	50	23.7	54.5	3 - 5	4
10	London Clay	PIR=30% MV @ 0.2% conc.	30	26.6	44.4	9 - 12	10.5
11	London Clay	PIR=30% MV @ 0.2% conc.	30	27.0	44.4	10 - 13	11
12	London Clay	PIR=20% MV @ 0.2% conc. FIR=120% TR @ 1.5% FER=13.5	29	25.4	43.6	9 - 13	10.5
13	London Clay	Water Injection ratio=30%	30	25.3	44.3	8 - 12	10
14	London Clay	PIR=30% MV @ 0.5% conc.	30	24.9	43.4	11 - 15	13
15	WRB/UP	PIR=15% MV @ 0.2% conc. FIR=70% TR @ 1.5% FER=14	20	23.1	35.5	14 - 17	15.5
16	WRB/UP	PIR=22% MV @ 0.2% conc. FIR=50% TR @ 1.5% FER=14	25.6	18.3	33.8	4 - 6	5

Table 6.5. Properties of conditioned soil samples for screw conveyor tests.

Test No.	Soil	Conditioning treatment	Average $S_u$ (kPa)	Test pressure (kPa)	Screw*	Nominal screw speed (rpm)	Discharge condition
7	London Clay	PIR=40% MV @ 0.2% conc.	7	200	1	5, 15, 25	Unrestricted
8	London Clay	PIR=20% MV @ 0.2% conc.	26	200	1	5, 15, 25	Unrestricted
9	London Clay	PIR=50% MV @ 0.2% conc.	4	200	1	5, 15, 25	Unrestricted
10	London Clay	PIR=30% MV @ 0.2% conc.	10.5	200	1	5, 15, 25	Unrestricted
11	London Clay	PIR=30% MV @ 0.2% conc.	11	200	2	5, 15, 25	Unrestricted
12	London Clay	PIR=20% MV @ 0.2% conc. FIR=120% TR @ 1.5% FER=13.5	10.5	200	1	5, 15	Unrestricted
13	London Clay	Water Injection ratio=30%	10	200	1	5, 15, 25	Unrestricted
14	London Clay	PIR=30% MV @ 0.5% conc.	13	200	1	5, 15, 25	Unrestricted
15	WRB/ UP	PIR=15% MV @ 0.2% conc. FIR=70% TR @ 1.5% FER=14	15.5	200	1	5, 15, 25	Restricted
16	WRB/ UP	PIR=22% MV @ 0.2% conc. FIR=50% TR @ 1.5% FER=14	5	200	1	5, 15	Restricted

\*Screw (1) pitch = 80 mm; Screw (2) pitch = 133 mm

Table 6.6. Summary of model screw conveyor tests with conditioned soil samples.

Test No.	Average $S_u$ (kPa)	Screw speed, N (rpm)	Total pressure change, $\Delta P$ (kPa)	Total pressure gradient, $\Delta P/L$ (kPa/m)	Average casing shear stress $\tau_c$ (kPa)	Average friction coefficient $\tau/\sigma_n$	Average torque (Nm)	Soil flow rate, Q (L/hr)
7	7	4.9	-123.3	-182.6	7.3	0.188	113.9	109.7
		14.9	-118.8	-175.9	8.2	0.198	-	302.6
		24.0	-124.6	-184.6	8.3	0.216	-	519.2
8	26	4.8	-37.7	<i>Not uniform</i>	24.2	0.286	380.6	122.2
		13.6	-12.9	<i>Not uniform</i>	26.2	0.301	570.9	316.7
9	4	4.5	-136.2	-201.8	4.5	0.149	89.5	104.2
		13.8	-145.3	-215.3	4.6	0.142	93.8	311.2
		24.1	-143.9	-213.2	4.9	0.160	99.2	525.2
10	10.5	5.2	-95.5	-141.5	9.3	0.175	157.9	125.7
		14.3	-104.4	-154.7	10.8	0.189	198.1	333.7
		24.0	-102.4	-151.7	11.7	0.210	223.9	540.7
11	11	4.9	-64.4	-95.4	10.9	0.167	165.9	179.1
		14.3	-68.5	-101.5	12.5	0.190	203.2	505.7
		24.3	-75.0	-111.1	11.5	0.193	181.7	845.9

Table 6.7. Measurements from screw conveyor tests with conditioned soil samples.

Test No.	Average $S_u$ (kPa)	Screw speed, N (rpm)	Total pressure change, $\Delta P$ (kPa)	Total pressure gradient, $\Delta P/L$ (kPa/m)	Average casing shear stress $\tau_c$ (kPa)	Average friction coefficient $\tau/\sigma'_n$	Average torque (Nm)	Soil flow rate, Q (L/hr)
12	10.5	4.8	-85.5	-126.7	9.8	0.250	166.7	119.7
		14.0	-83.7	-124.0	12.9	0.257	-	351.6
13	10	4.9	-134.6	-199.4	10.5	0.208	151.4	113.4
		14.3	-136.4	-202.1	9.9	0.219	147.6	318.7
		24.0	-129.5	-191.8	8.4	0.197	119.7	522.7
14	13	4.6	-131.7	-195.1	12.0	0.239	167.5	122.7
		14.3	-88.9	-131.7	12.3	0.241	194.5	373.3
		24.0	-114.8	-170.1	12.6	0.239	203.2	606.0
15	15.5	3.8	-81.5	-120.7	8.3	0.087	99.1	83.8
		13.5	120.7	178.8	24.2	0.089	334.8	286.3
		23.2	171.2	253.6	29.0	0.103	420.2	458.4
16	5	4.5	-97.2	-144.0	8.0	0.147	128.0	103.0
		14.0	-41.6	-61.6	10.3	0.150	176.9	297.4

Table 6.7. Measurements from screw conveyor tests with conditioned soil samples.

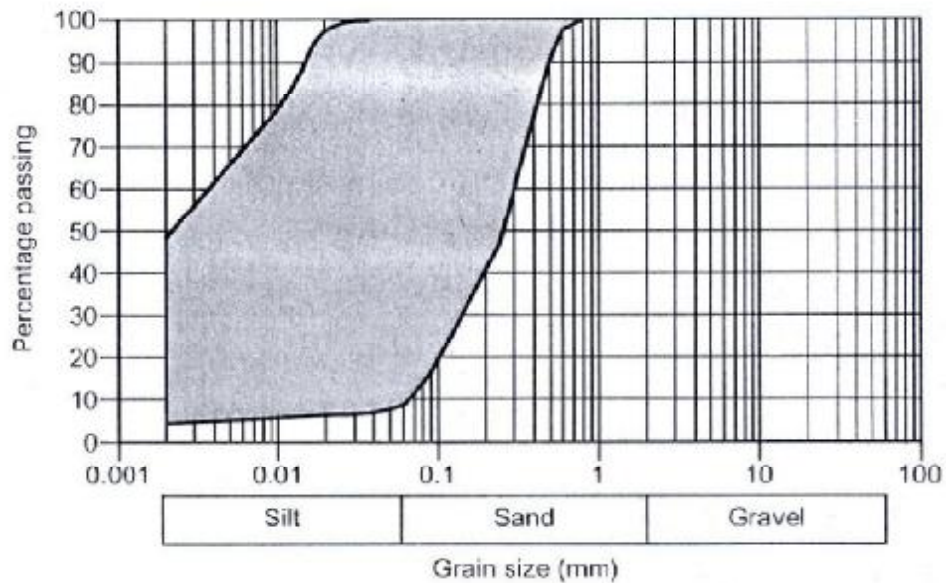


Figure 6.1. Envelope of particle size distributions for WRB soil (Upper Mottled Clay).  
(after Withers *et al.*, 2001).

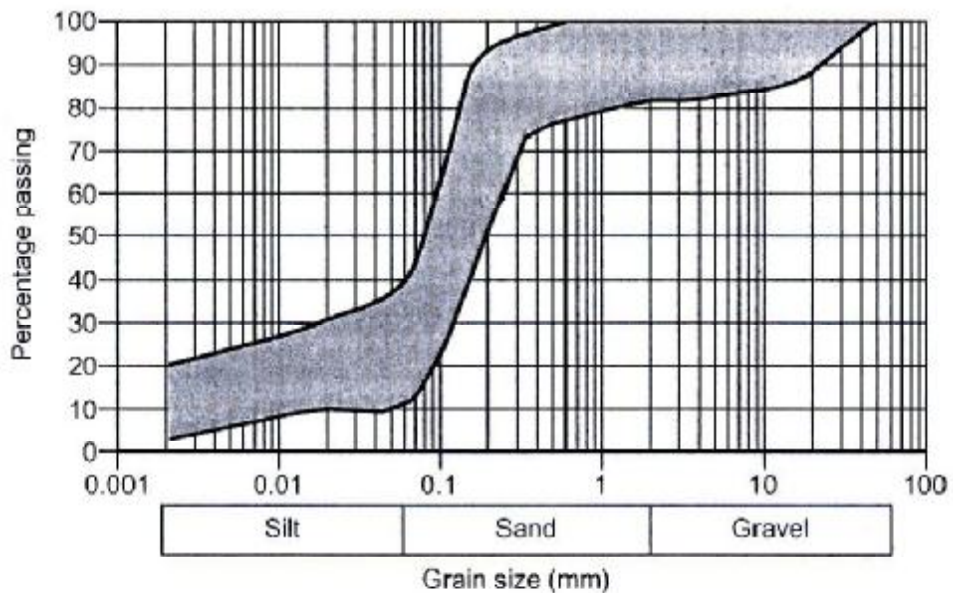


Figure 6.2. Envelope of particle size distributions for Upnor (UP) sand.  
(after Withers *et al.*, 2001).

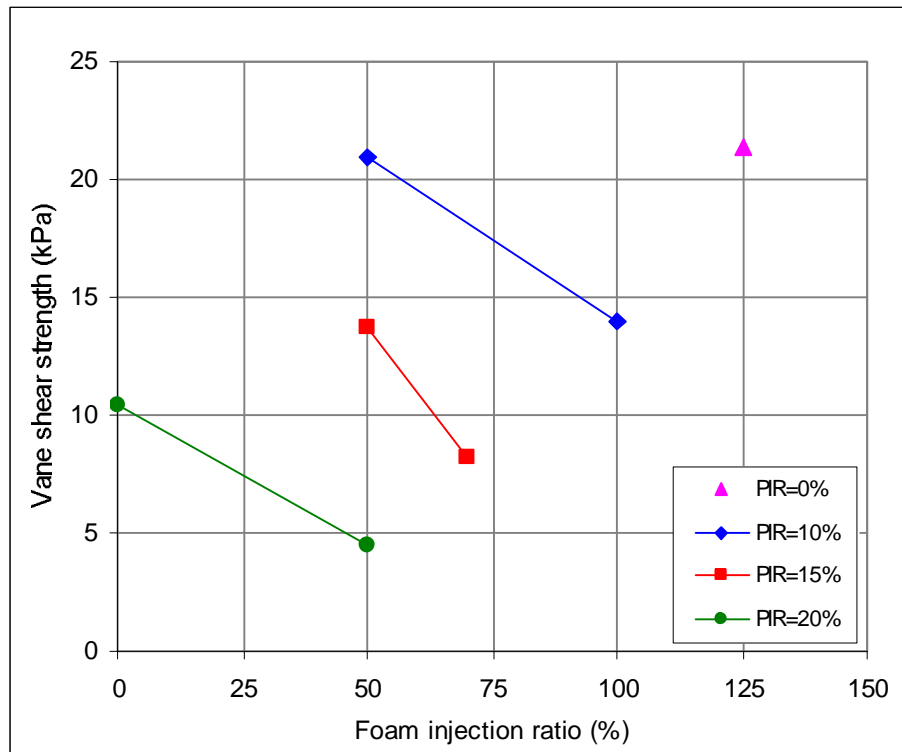


Figure 6.3. Vane shear strength of WRB/UP soil conditioned with foam and polymer treatments.

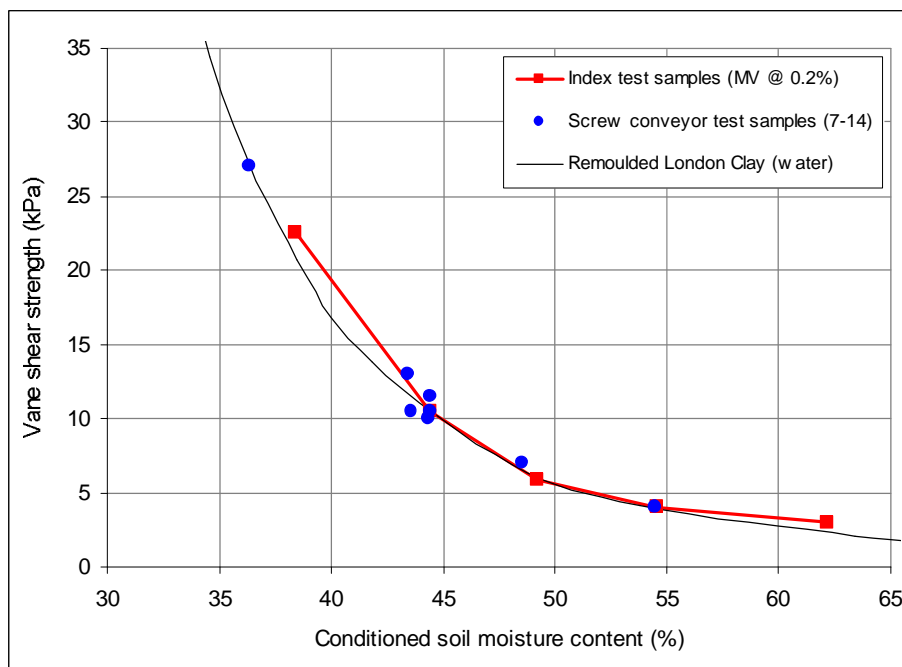


Figure 6.4. Vane shear strength of conditioned London Clay at varying moisture contents for screw conveyor and index test samples.

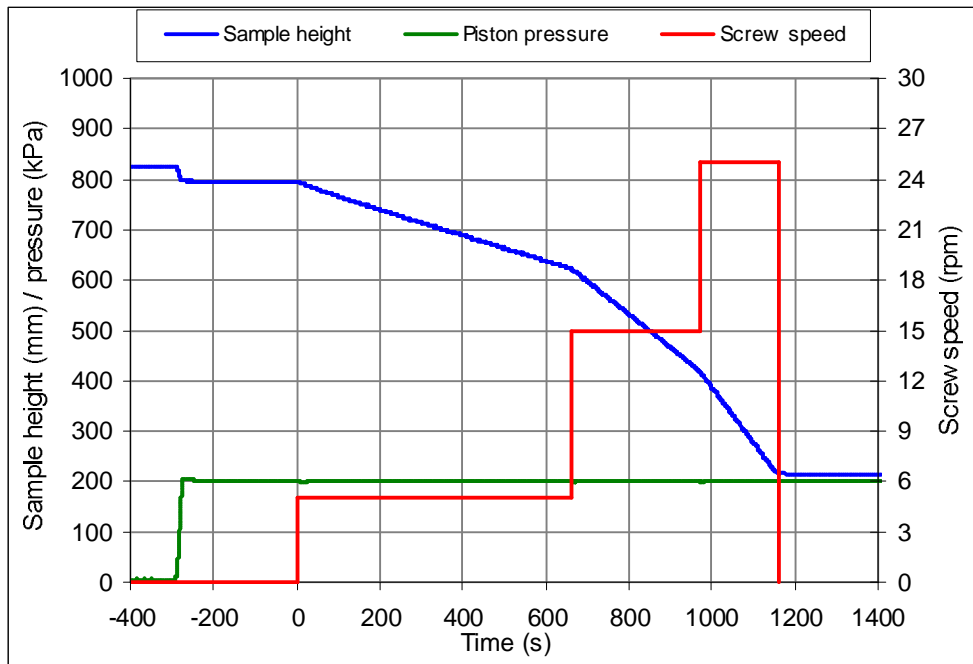


Figure 6.5. Sample height and pressure during test 10 with varied screw speeds.

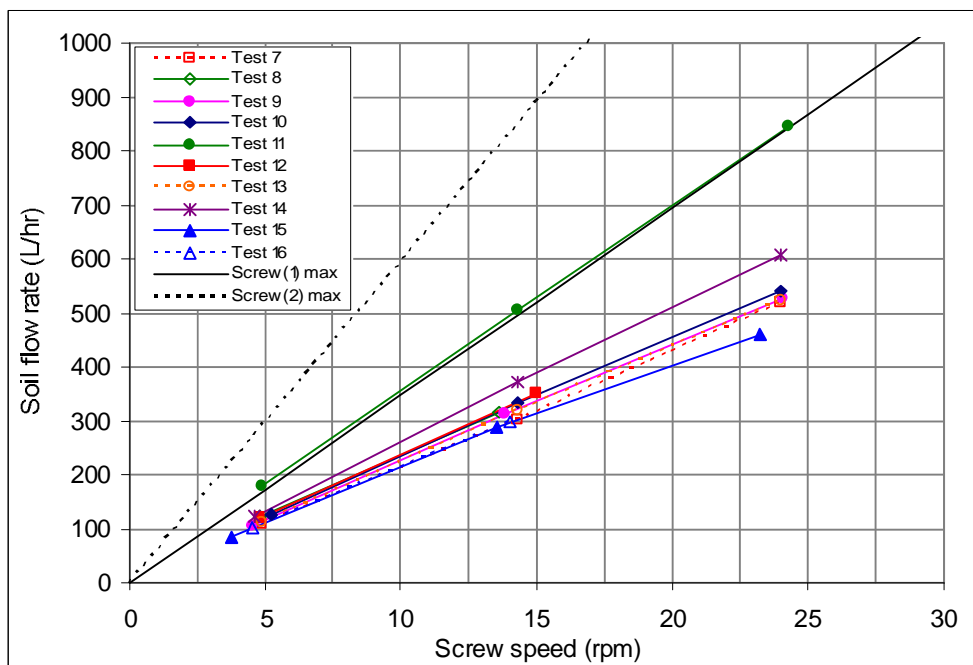


Figure 6.6. Soil flow rates at different screw speeds in tests with conditioned soil samples.

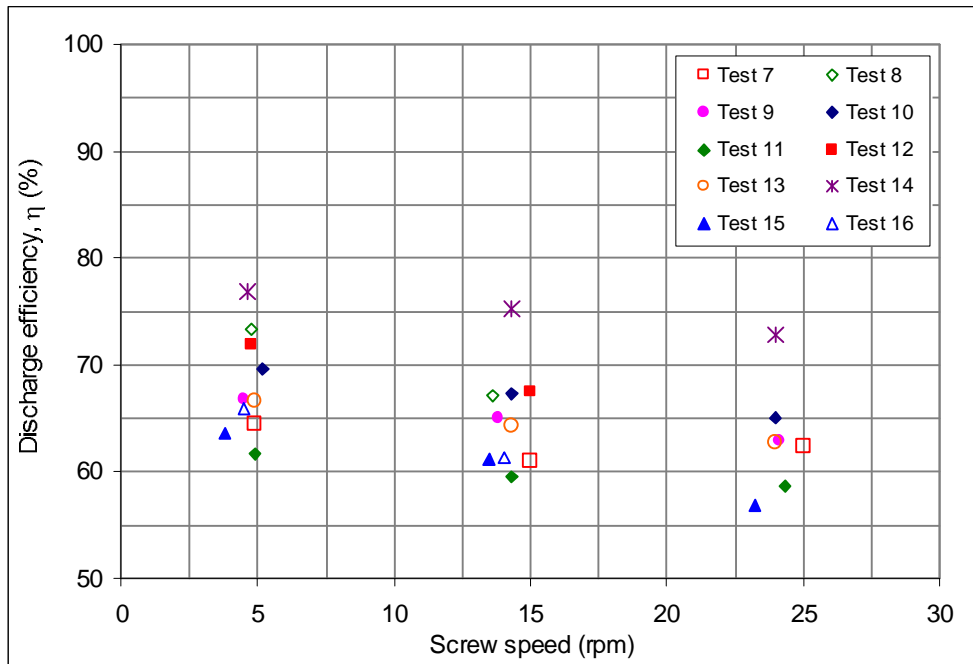


Figure 6.7. Conveyor discharge efficiency at different screw speeds in tests with conditioned soil samples.

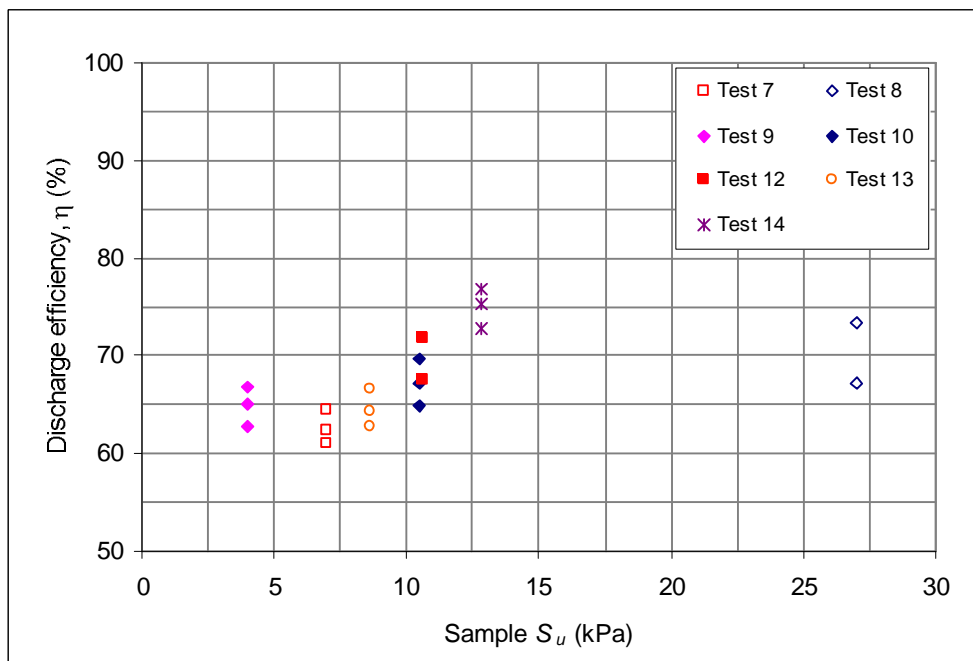


Figure 6.8. Conveyor discharge efficiency for conditioned London Clay samples of varying strength.

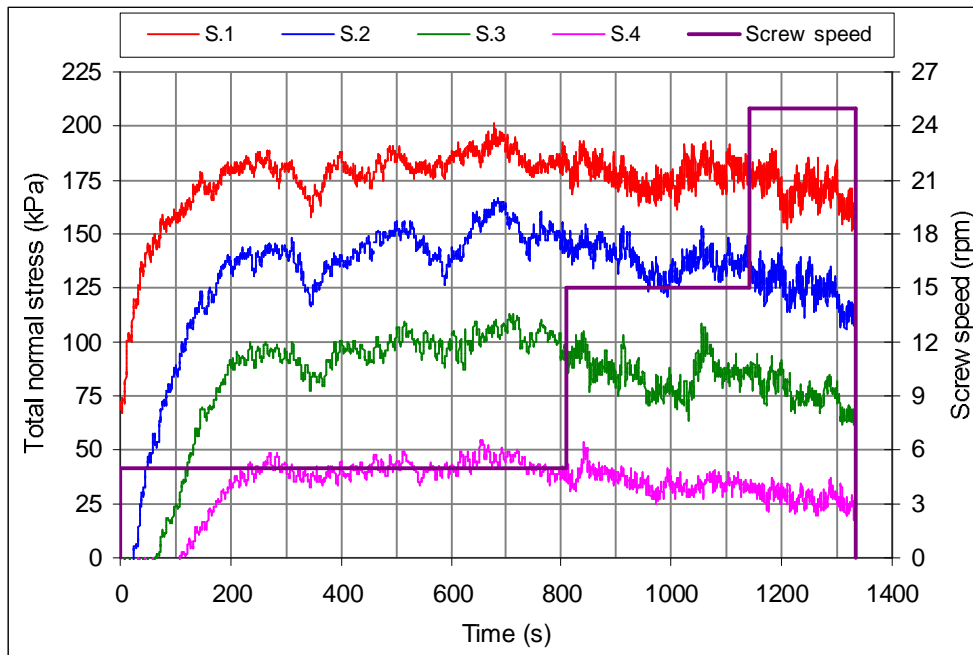


Figure 6.9. Total normal stresses during test 9 at varying screw speeds.

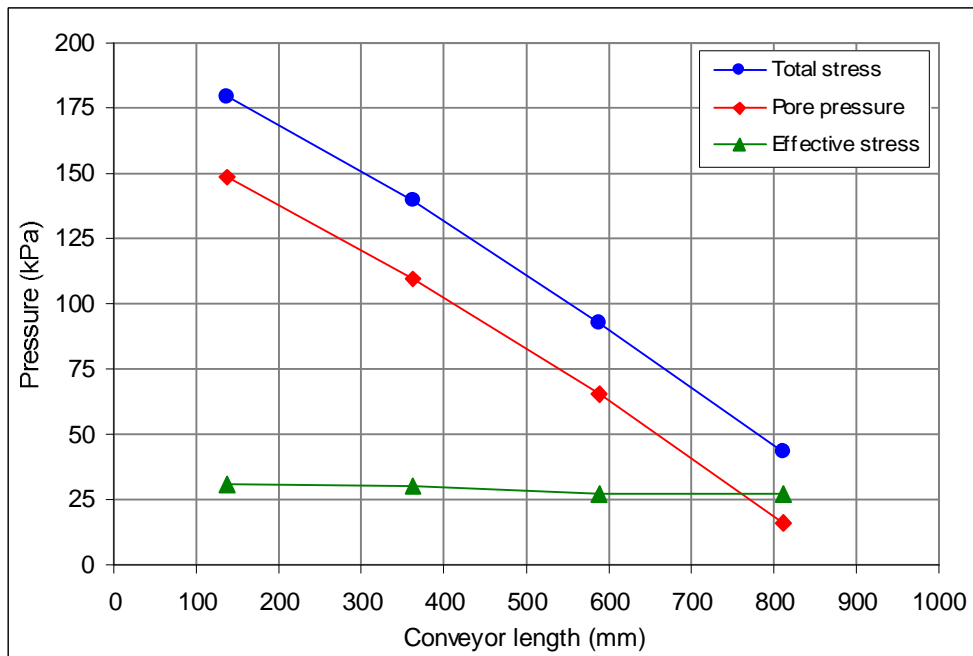


Figure 6.10. Pressure gradients during test 9 with screw rotating at 5 rpm.

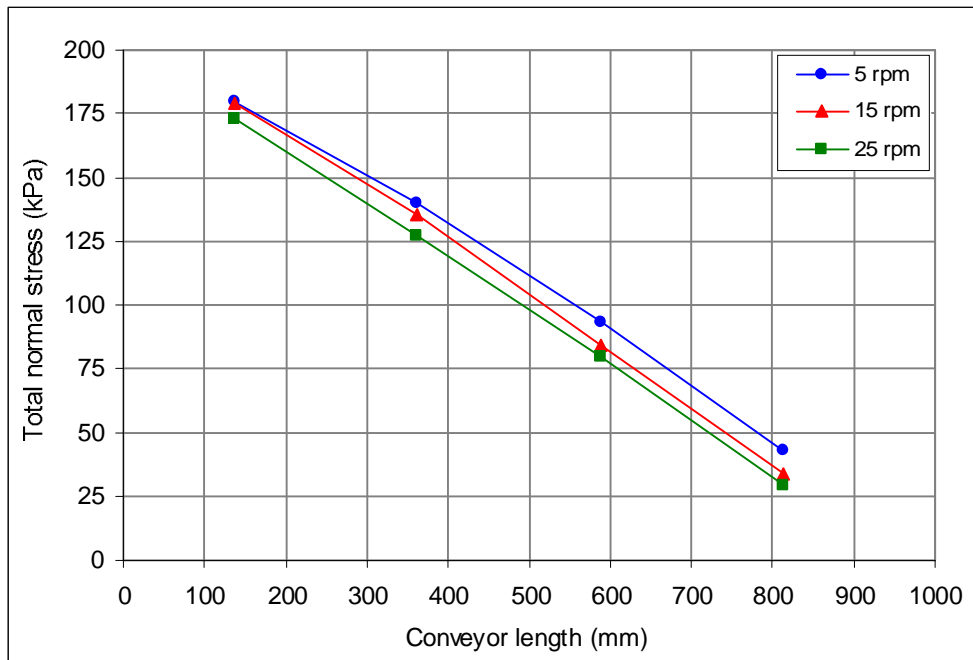


Figure 6.11(a). Total pressure gradients during test 9 with different screw speeds.

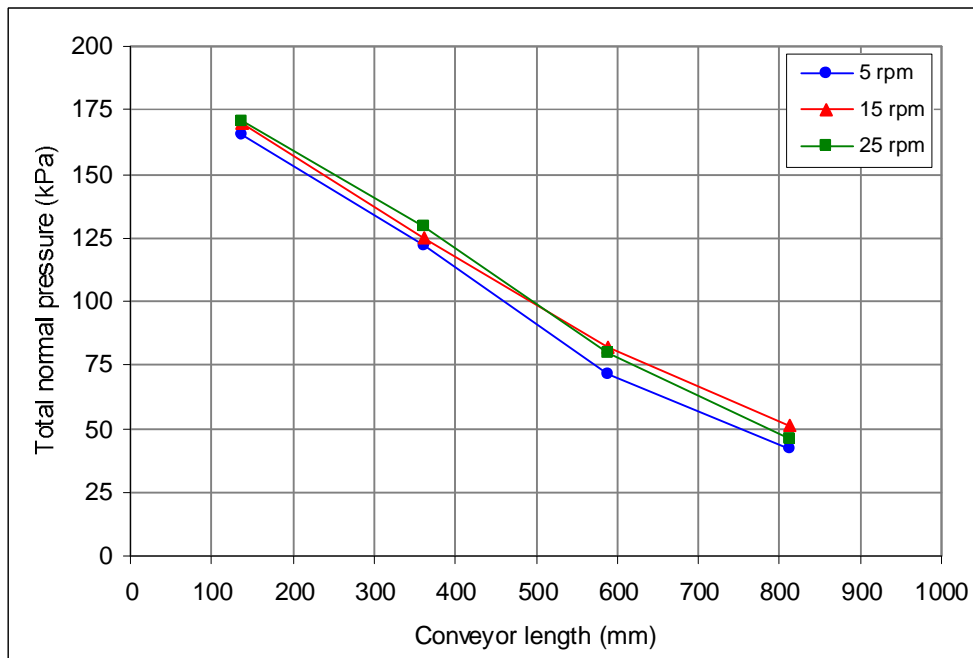


Figure 6.11(b). Total pressure gradients during test 7 with different screw speeds.

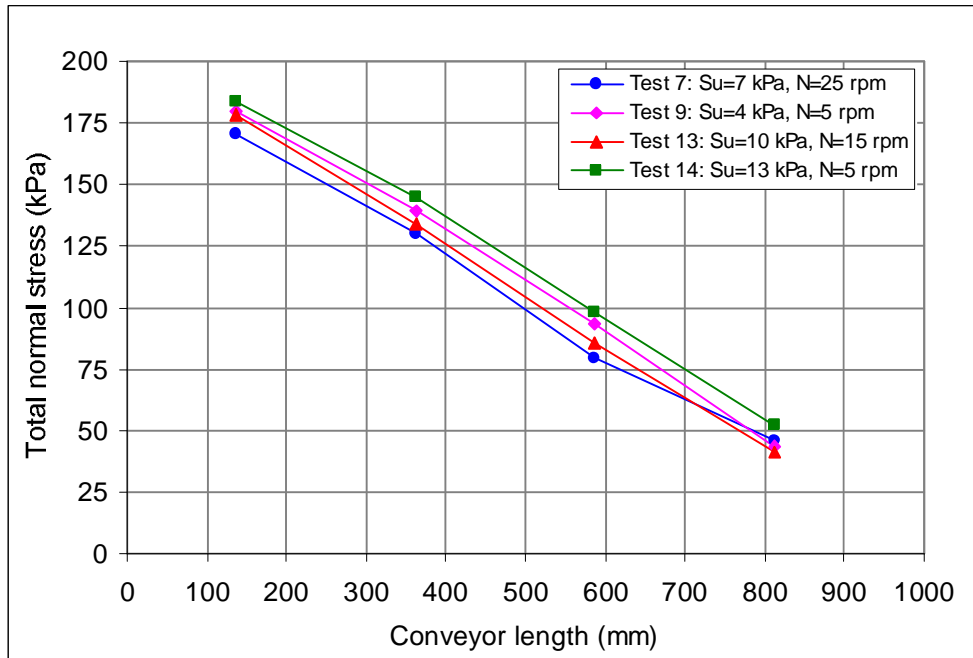


Figure 6.12. Total pressure gradients during tests with conditioned London Clay samples of varying strength.

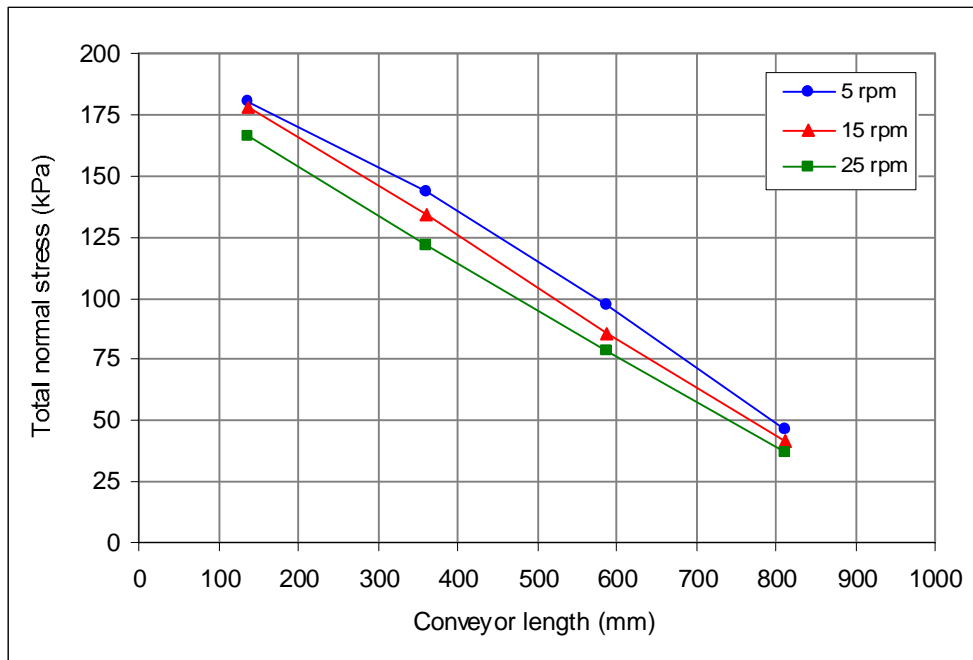


Figure 6.13(a). Total pressure gradients during test 13 with screw (1) at different speeds.

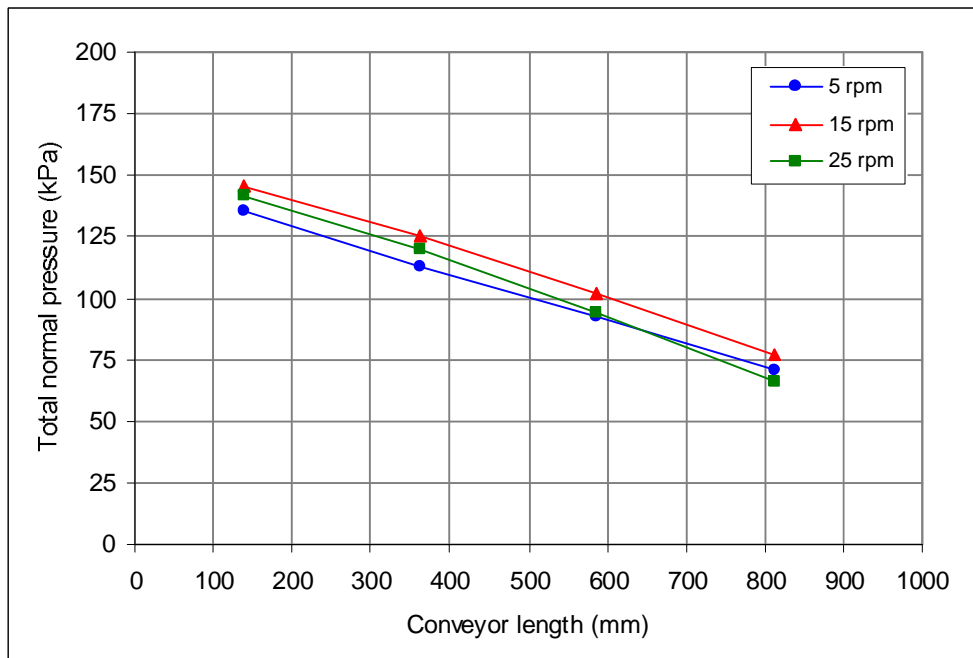
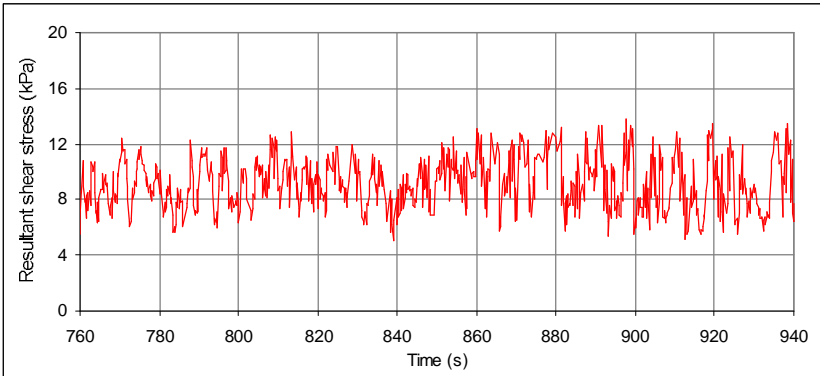
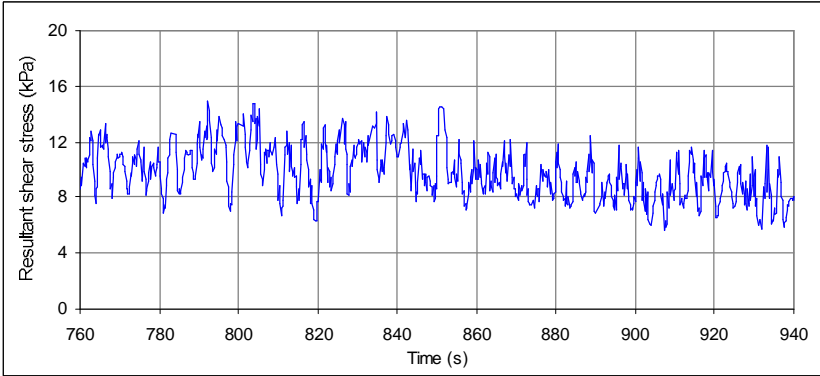


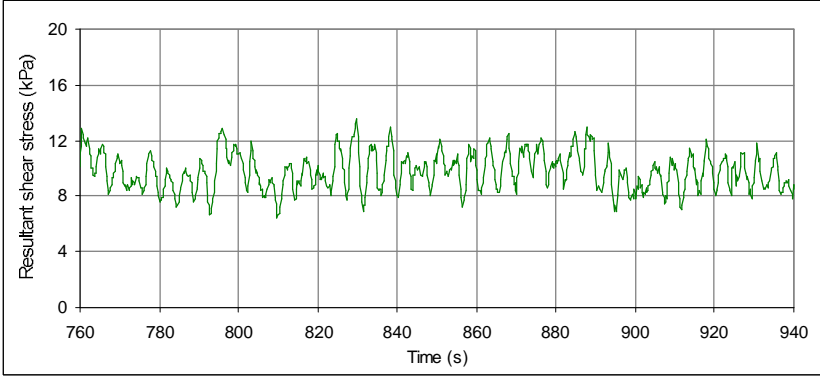
Figure 6.13(b). Total pressure gradients during test 11 with screw (2) at different speeds.



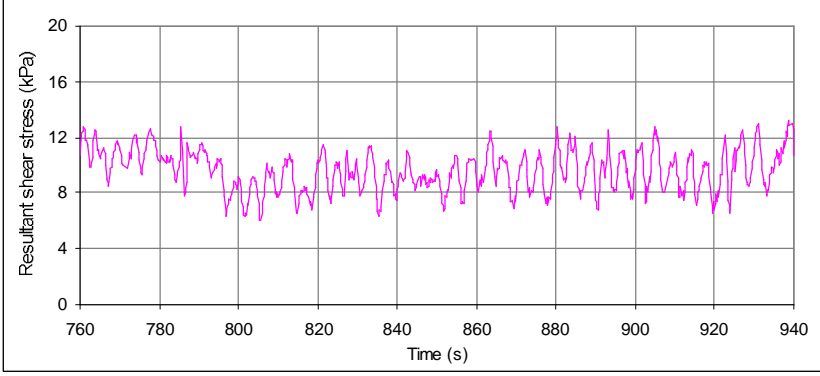
(a) Section 1.



(b) Section 2.

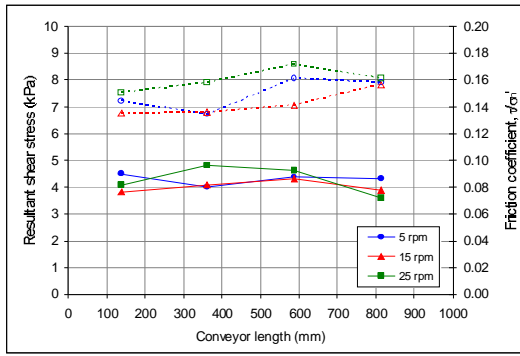


(c) Section 3.

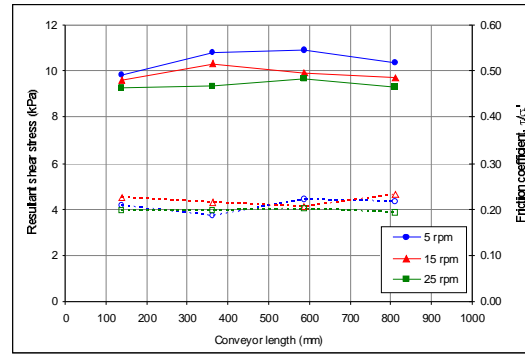


(d) Section 4.

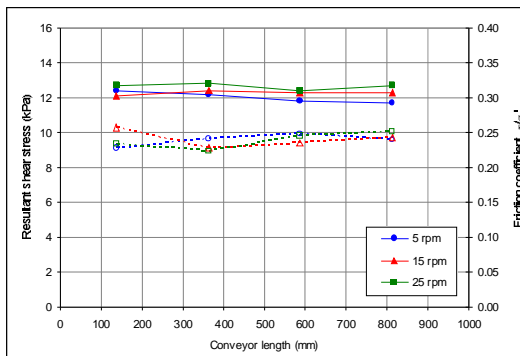
Figure 6.14. Resultant casing shear stresses during test 13 ( $S_u = 10$  kPa)



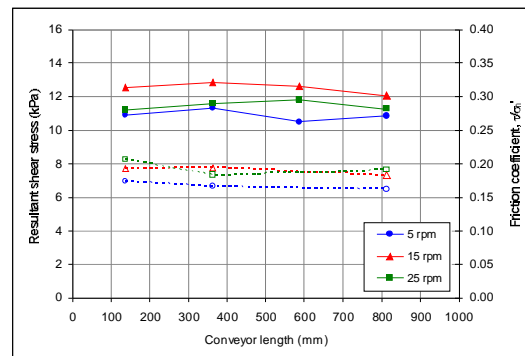
(a) Test 9 ( $S_u = 4$  kPa)



(b) Test 13 ( $S_u = 10$  kPa)



(c) Test 14 ( $S_u = 13$  kPa)



(d) Test 11 ( $S_u = 11$  kPa)

Figure 6.15. Average resultant shear stresses (solid lines) and friction coefficients (dashed lines) along conveyor from tests with conditioned London Clay samples of varying strength.

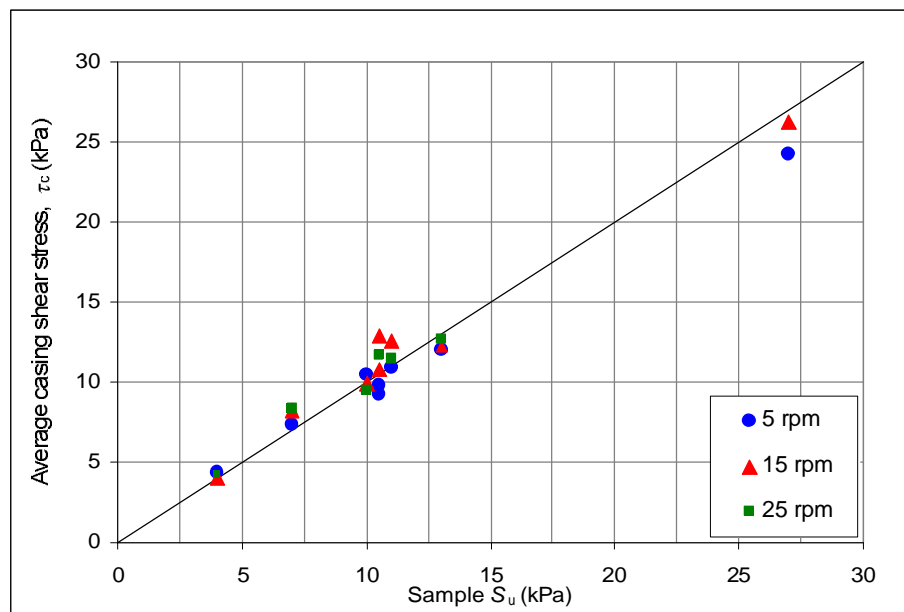
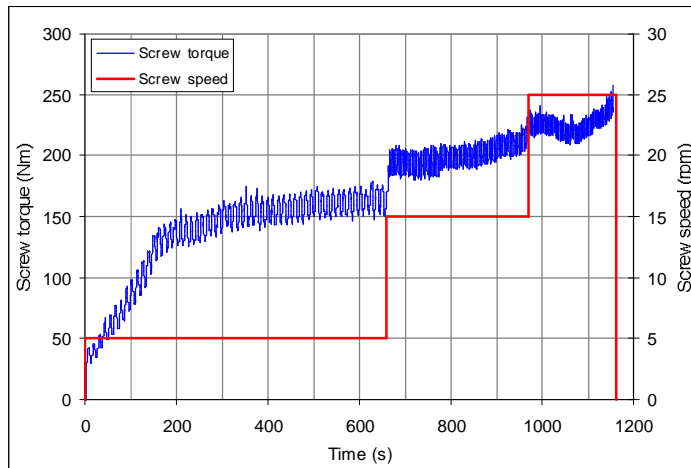
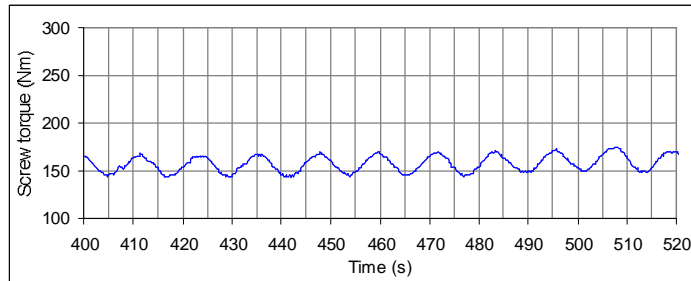


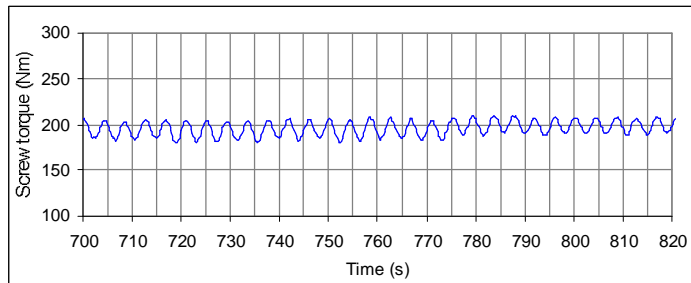
Figure 6.16. Comparison of casing shear stresses with undrained shear strength of conditioned London Clay samples.



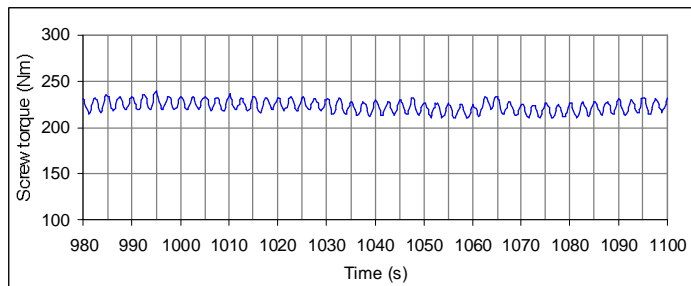
(a) Torque measurement throughout test.



(b) Torque measurement at 5 rpm.



(c) Torque measurement at 15 rpm.



(d) Torque measurement at 25 rpm.

Figure 6.17. Screw torque measurements during test 10 with different screw speeds.

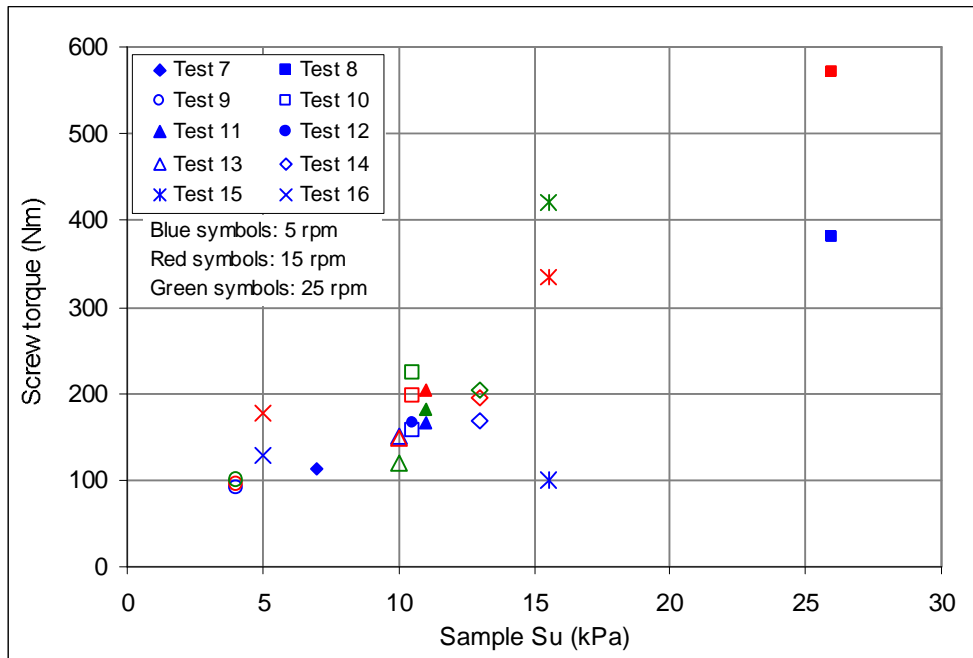


Figure 6.18. Torque for varying sample strengths and screw speeds with conditioned soils.

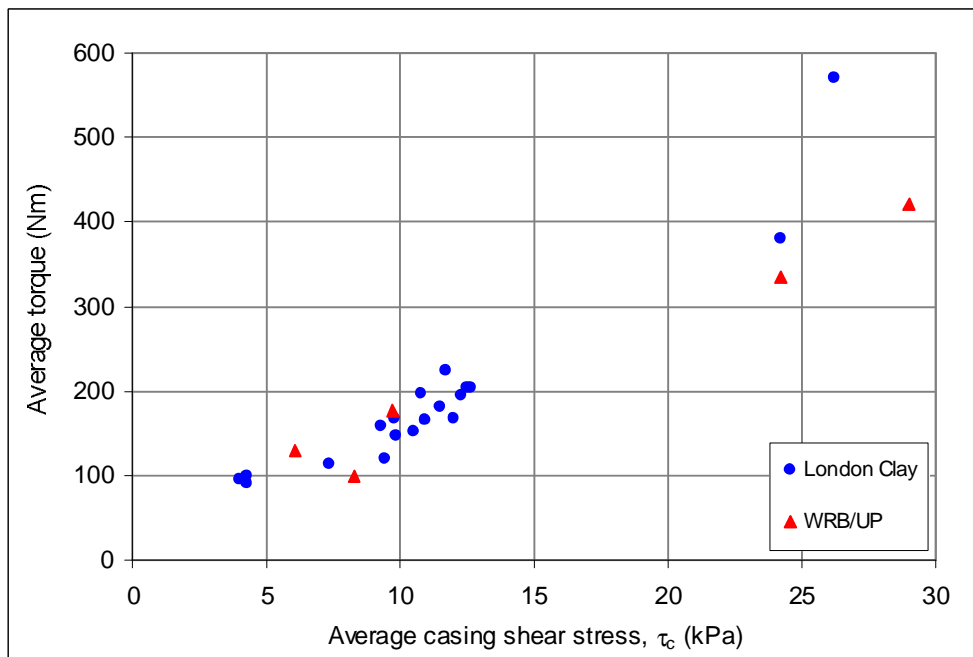


Figure 6.19. Increase of torque with casing shear stress for conditioned soil samples.

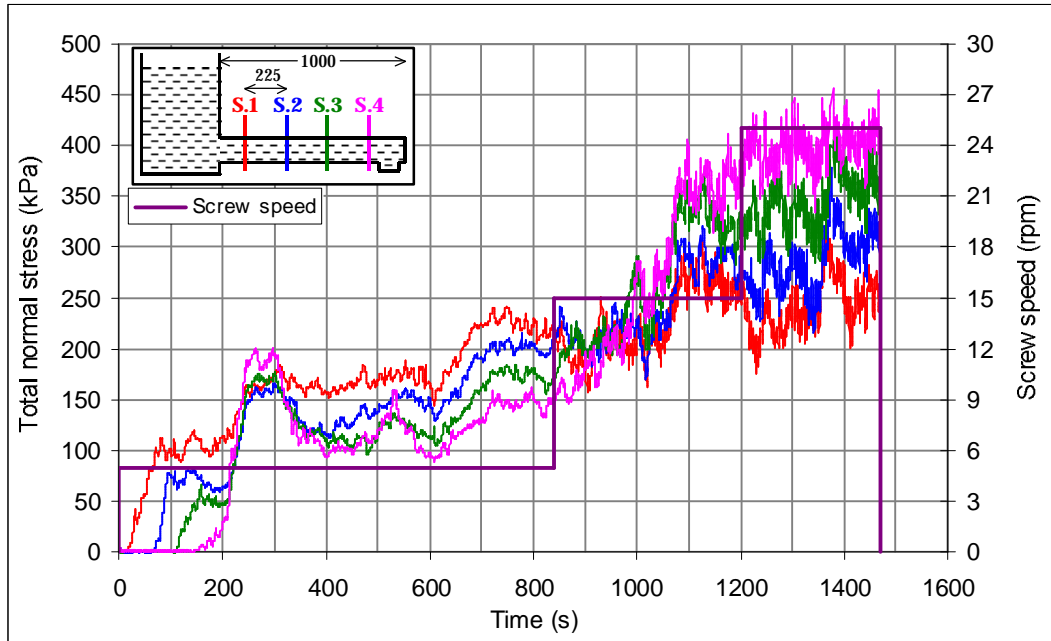
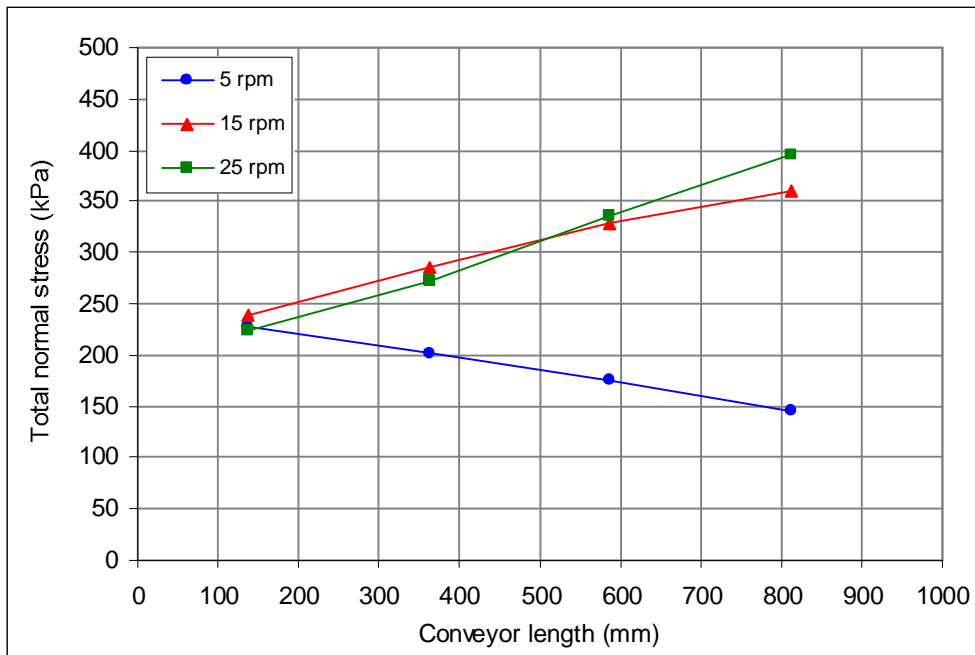
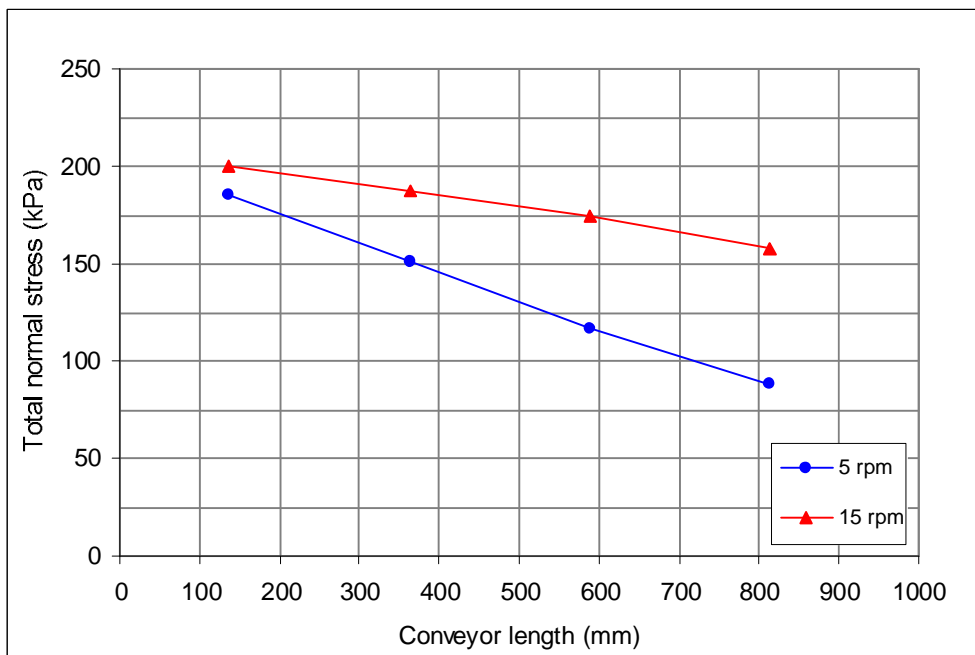


Figure 6.20. Total normal stresses along conveyor during test 15 with conditioned WRB/UP soil.

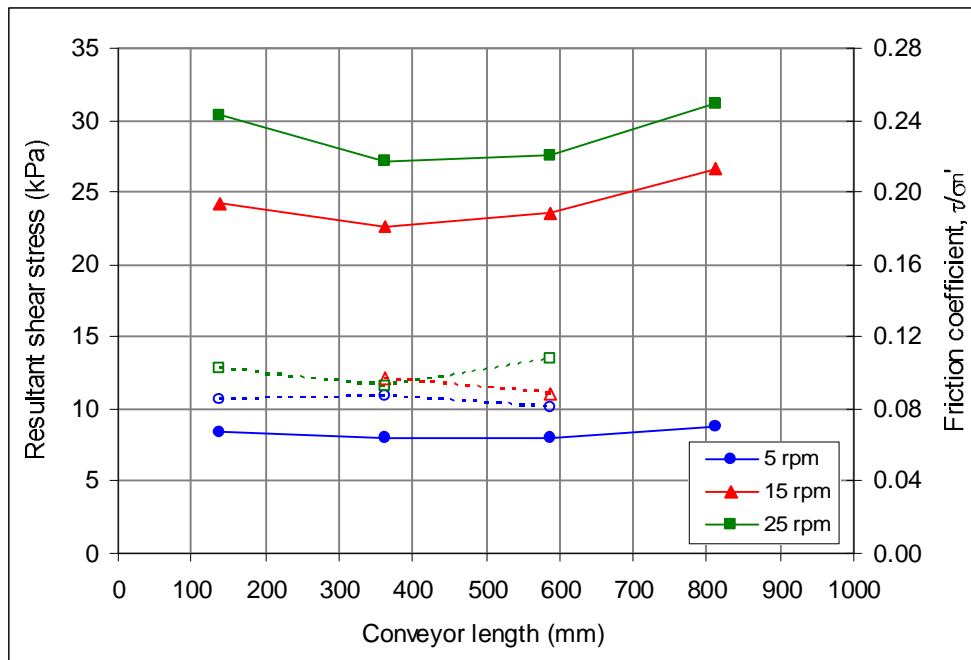


(a) Test 15.

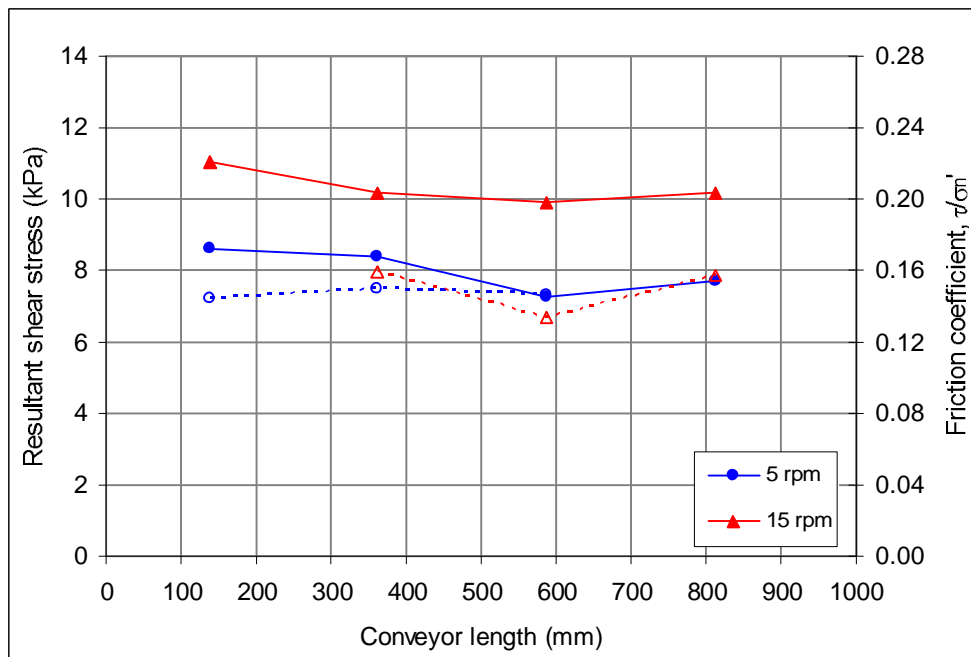


(b) Test 16.

Figure 6.21. Total pressure gradients at different screw speeds during tests 15 and 16 with conditioned WRB/UP samples.



(a) Test 15 ( $S_u = 15.5$  kPa)



(b) Test 16 ( $S_u = 5$  kPa)

Figure 6.22. Average casing shear stresses (solid lines) and friction coefficients (dashed lines) along conveyor during tests with conditioned WRB/UP samples.

# Chapter 7

## Theoretical model of screw conveyor operation

---

### 7.1 Introduction

The key parameters to control during the operation of an EPB machine screw conveyor are the soil flow rate, the total pressure gradient, and the screw torque. The control of these parameters depends on the soil properties and the conveyor operating conditions. Controlled flow of soil through the screw conveyor allows control of the EPB machine excavation process. Results from model screw conveyor tests performed to investigate the operation with clays soils were presented in Chapters 5 and 6. Effects of different sample properties and operating conditions on the soil flow rates, pressure gradients, and screw torque were illustrated in these tests. This chapter presents an analysis of the screw conveyor operation. A theoretical model is proposed to calculate the total pressure gradient and the screw torque based on the soil flow rate, the shear stresses acting in the conveyor, and the screw conveyor geometry. The theoretical equations are expressed in dimensionless form to allow their use with screw conveyors of different scales. Effects of varying soil flow rates, shear stresses, and screw geometry on the pressure gradients and torque are investigated. Measurements from the model conveyor tests are compared with the theoretical model. Good agreement was found between the test measurements and the theory, indicating the proposed theoretical model accurately describes the screw conveyor operation.

## 7.2 Theoretical model of screw conveyor operation

The analysis of the screw conveyor operation presented below follows a similar approach to that of Darnell and Mol (1956), Chung (1970), Burbidge and Bridgwater (1995), and Yoshikawa (1996a), discussed in Section 2.6.3. These analyses are based on similar models of the screw extruder or conveyor, and predict constant total pressure gradients when constant shear stresses are assumed to act along the conveyor. This was observed in the model tests, indicating these previous analyses are suitable for describing the conveyor operation. The motion of, and the forces acting on, an element of soil in the screw conveyor are analysed to develop a theoretical model describing the soil flow rate, the total pressure gradient, and the screw torque during the conveyor operation.

### 7.2.1 Screw conveyor geometry

The mechanics of the conveyor operation are influenced by the screw geometry. The parameters used in the analysis are defined here. The theoretical model is developed for a single flighted screw of constant pitch and channel depth, assumed to fit closely inside the conveyor so the radial clearance between the screw flight and the casing is neglected. The geometry of the screw conveyor is defined in Figure 7.1, and the parameters for the two screws used in the model tests are shown in Table 7.1. The axes systems used in the analysis are also defined in Figure 7.1. The  $(x, y)$  axes refer to the directions parallel and perpendicular to the screw axis. The  $(l, w)$  axes refer to the directions parallel and perpendicular to the screw flight.

Some dimensionless groups are defined to describe the screw geometry as follows:

- $\frac{D_s}{D_f}$  represents the ratio of the screw shaft and flight diameters
- $\frac{t}{D_f}$  represents the ratio of the screw pitch and flight diameter
- $\frac{e}{D_f}$  represents the ratio of the screw flight thickness and diameter
- $\frac{D_f}{L}$  represents the ratio of the screw flight diameter and screw length

The helix angle of the screw represents the angle of the flight with respect to the perpendicular to the screw axis, as shown in Figure 7.1(b). The helix angle varies with distance from the screw axis, and is defined at the flight diameter ( $\phi_f$ ), the shaft diameter ( $\phi_s$ ), and at the average flight diameter ( $\phi_a$ ) in terms of the screw pitch and diameter using the dimensionless groups above as:

$$\tan \phi_f = \frac{t}{\pi D_f} \quad \text{Eqn 7.1(a)}$$

$$\tan \phi_s = \frac{t}{\pi D_s} = \frac{t}{\pi D_f (D_s/D_f)} \quad \text{Eqn 7.1(b)}$$

$$\tan \phi_a = \frac{t}{\pi (D_f - h)} = \frac{t}{\pi D_f (1 + (D_s/D_f))} \quad \text{Eqn 7.1(c)}$$

The length along the screw channel in the  $l$  direction is related to the length along the screw axis in the  $x$  direction through the helix angle,  $\phi$ , as follows:

$$l = \frac{x}{\sin \phi} \quad \text{Eqn 7.2}$$

Due to the change of the helix angle with distance from the screw axis, the length in the  $l$  direction also varies, and is calculated at a specific radius using the corresponding helix angle.

### 7.2.2 Flow of soil in the screw conveyor

The development of the theoretical model begins by considering the motion of an element of soil in the channel of the screw conveyor. It is assumed that the screw channel is completely filled, with the soil in contact with the casing surface, the screw shaft, and the two flight surfaces. The radial clearance between the screw flight and the casing is neglected. The soil is assumed to flow along the screw channel as a plug. The clay soil is modelled as a homogeneous, isotropic Tresca material with a maximum shear stress equal to the undrained shear strength. The weight of the soil is neglected in the analysis. The relative movements between the soil plug and the casing and the screw shaft and flight surfaces generate shear stresses acting on the surfaces of the soil plug. These shear stresses are assumed to be uniformly distributed over shear surfaces formed at the interfaces of the soil and the screw channel surfaces. The shear stresses are assumed to be constant along the length of the conveyor casing. Undrained shearing conditions are assumed as

the clay soil is sheared rapidly as it flows along the screw channel, and no drainage boundaries are present in the conveyor so the soil volume remains constant.

The flow along the conveyor results from the forces acting on the soil plug in the screw channel as the screw rotates. The forces acting on a soil element in the screw channel considered in the analysis are shown later in Figure 7.4 and discussed in Section 7.2.3. A passive pressure is applied normal to the flight surface pushing on the soil, and the relative movement between the soil and the screw channel generates shear stresses acting on the surfaces of the soil plug. The shear stresses between the soil and the screw surfaces resist the movement along the screw channel. The shear stress between the soil and the casing surface provides a force component that causes the soil to flow along the screw channel, and generates a pressure gradient along the conveyor. The direction of soil movement along the conveyor is variable, depending on the shear stresses acting on the soil plug and the conveyor operating conditions.

Following the approaches of Chung (1970) and Burbidge and Bridgwater (1995), a relationship defining the direction of soil movement along the conveyor is first developed. As the screw rotates, the soil plug flows along the screw channel, moving relative to the casing and the screw. Figure 7.2 illustrates the motion of the screw and an element of the soil plug, viewed in plan at the top of the screw channel. As the screw rotates, point 'A' at the top of a flight moves tangentially relative to the casing in the direction perpendicular to the screw axis, represented by the velocity vector  $V_{sr}$ . Point 'A' also moves relative to the soil plug in the direction parallel to the screw flight, represented by the vector  $V_{st}$ . The soil plug moves relative to the casing at an angle  $\theta$  to the direction of the tangential screw flight velocity, represented by the vector  $V_{pc}$ . The soil also has a velocity component in the direction parallel to the screw axis, represented by the vector  $V_{px}$ .

The angle  $\theta$  represents the direction of soil flow relative to the tangential velocity of the screw flight at the casing surface. The angle of soil flow is variable, depending on the movement of the soil along the channel as the screw rotates, as determined by the shear stresses acting on the soil plug. The movement of soil in the axial direction is controlled by the angle  $\theta$ , determining the flow rate along the conveyor. The minimum value of  $\theta$  is zero, when the soil does not flow along the conveyor and is jammed in the screw channel. The maximum value of  $\theta$  for controlled flow is  $(90 - \phi)$ , when the soil moves perpendicular to the screw flight. Values of  $\theta$  greater than  $(90 - \phi)$

imply that the velocity of the soil along the screw channel,  $V_{st}$ , is greater than the velocity of the screw relative to the casing,  $V_{sy}$ . In this case the soil flows along the screw channel faster than the rotation of the screw.

From the velocity vector triangle shown in Figure 7.2 defining the motion of the soil plug, a relationship between the flow rate and the angle of soil flow,  $\theta$ , is derived. The magnitude of the vector  $V_{sy}$  at the top of the screw flight is known from the rotational speed of the screw,  $N$ , in rotations per second (i.e. rpm/60):

$$|V_{sy}| = \pi D_f N \quad \text{Eqn 7.3}$$

The magnitude of  $V_{pc}$  is related to  $V_{sy}$  by geometry:

$$|V_{pc}| = \frac{|V_{sy}| \sin \phi_f}{\sin(\theta + \phi_f)} = \frac{\pi D_f N \sin \phi_f}{\sin(\theta + \phi_f)} \quad \text{Eqn 7.4}$$

The velocity of the soil plug along the screw axis is then given by:

$$|V_{px}| = |V_{pc}| \sin \theta = \frac{\pi D_f N \sin \phi_f \sin \theta}{\sin(\theta + \phi_f)} \quad \text{Eqn 7.5}$$

Equation 7.5 simplifies to:

$$|V_{px}| = \frac{\pi D_f N \tan \phi_f \tan \theta}{\tan \theta + \tan \phi_f} \quad \text{Eqn 7.6}$$

The volumetric flow rate,  $Q$ , is given by the area of the screw channel perpendicular to the  $x$ -axis,  $A_x$ , multiplied by the velocity of the soil plug along the screw axis:

$$Q = A_x |V_{px}| = \frac{\pi}{4} (D_f^2 - D_s^2) \frac{\pi D_f N \tan \phi_f \tan \theta}{\tan \theta + \tan \phi_f} \quad \text{Eqn 7.7}$$

A dimensionless group representing the flow rate,  $\underline{Q}$ , is defined from equation 7.7:

$$\underline{Q} = \frac{Q}{A_x(\pi D_f N)} = \frac{\tan \phi_f \tan \theta}{\tan \theta + \tan \phi_f} \quad \text{Eqn 7.8}$$

If the volumetric flow rate at a given screw speed is known, the soil flow angle,  $\theta$ , can be calculated from equation 7.8:

$$\tan \theta = \frac{\underline{Q} \tan \phi_f}{\tan \phi_f - \underline{Q}} \quad \text{Eqn 7.9}$$

This analysis leads to a relationship between the volumetric flow rate and the direction of soil flow. The angle  $\theta$  defines the direction of the shear stress acting between the soil and the casing, which influences the pressure gradient along the conveyor and the torque to rotate the screw.

### 7.2.3 Forces acting on the soil

As the screw rotates, the forces acting on the soil plug cause it to flow down the screw channel, and generate a pressure gradient along the conveyor and a torque to rotate the screw. Figure 7.3 shows the geometry and dimensions of an element of soil in the screw channel. A free body diagram showing the forces acting on the surfaces of the soil plug is shown in Figure 7.4(a). These forces are defined with reference to this figure as follows:

- $F_{cs}$  is the force due to the shear stress on the casing, acting on the surface *adef*. This force opposes the motion of the soil at an angle  $\theta$  relative to the  $y$ -axis, and acts with a moment arm about the screw axis equal to  $(D_f/2)$ , neglecting the radial clearance between the screw flight and the casing, so  $D_f=D_c$ .
- $F_{cn}$  is the normal force acting on the surface *adef*, due to the total pressure acting on the conveyor casing.
- $F_{ss}$  is the force due to the shear stress on the screw shaft, acting on the surface *abgh*. This force opposes the motion of the soil relative to the screw shaft, and acts parallel to the  $l$ -axis as the soil moves along the screw channel. This force acts with a moment arm about the screw axis equal to  $(D_s/2)$ .
- $F_{sn}$  is the normal force acting on the surface *abgh*, due to the total pressure acting on the screw shaft.

- $F_{ps}$  is the force due to the shear stress on the screw flight pushing on the soil, acting on the surface  $abcd$ . This force opposes the motion of the soil relative to the screw, acting parallel to the  $l$ -axis with a moment arm about the screw axis equal to  $(D_f/2-h/2)$ .
- $F_{pn}$  is the force due to the passive pressure applied by the screw flight pushing on the soil. This force acts normal to the surface  $abcd$  in the direction of the  $w$ -axis, with a moment arm about the screw axis equal to  $(D_f/2-h/2)$ .
- $F_{ts}$  is the force due to the shear stress on the trailing screw flight, acting on the surface  $efgh$ . This force opposes the motion of the soil relative to the screw, acting parallel to the  $l$ -axis with a moment arm about the screw axis equal to  $(D_f/2-h/2)$ .
- $F_{tn}$  is the force due to the active pressure acting on the surface  $efgh$  in contact with the trailing screw flight. This force acts normal to the flight surface in the direction of the  $w$ -axis, with a moment arm about the screw axis equal to  $(D_f/2-h/2)$ .
- $F_{pl}$  is the resultant of the forces  $F_p$  and  $F_p + dP$  acting normal to the surfaces  $adeh$  and  $bcfg$  respectively.  $F_{pl}$  ( $= dP$ ) represents the force due to the change of total pressure over the length of the element,  $dL$ . This force acts parallel to the  $l$ -axis and can be in either direction, depending if the total pressure increases ( $dP > 0$ ) or decreases ( $dP < 0$ ) along the screw channel. The moment arm about the screw axis is equal to  $(D_f/2-h/2)$ .

Forces due to the self-weight of the soil are neglected. The centripetal force created by the radial acceleration of the soil rotating about the screw axis is proportional to the square of the angular velocity. In tests performed with nominal screw speeds ranging from 5 to 25 rpm, the centripetal force increases by a factor of about 25. However, the total normal stresses measured on the casing surface, as shown in Figures 6.9, 6.11, and 6.13, did not show an increase with the screw speed, indicating that the centripetal force is not significant and can be neglected in the analysis.

The free body diagram shown in Figure 7.4(a) illustrates the complex state of stresses acting on the soil element in the screw channel. In the model tests, the normal and shear stresses acting on the casing surface are measured, but the stresses acting on the screw surfaces are unknown. To simplify the analysis, some assumptions regarding the geometry and forces acting on the soil element are made. Assuming the effect of curvature of the screw channel is small, the channel is unrolled and considered as a long rectangular channel. The forces in the  $(l - w)$  plane of the channel then act in parallel planes. There is a total pressure gradient along the screw channel, expressed as  $dP/dL$  in Figure 7.4, where  $dL$  is the average length of the element along the

channel. This pressure gradient arises from the shear stresses acting on the surfaces of the moving soil plug. Because the ratio of the undrained shear strength to the total pressure,  $S_u/p$ , is small, the clay is fluid and the total normal stress does not depend on the plane of measurement. Therefore, the pressure gradient  $dP/dL$  along the screw channel is assumed to be equal to the change in total normal stress measured in the perpendicular plane by the load cells. This is recognised as an idealisation of the complex state of the stresses acting on the soil element; however, with these assumptions to simplify the analysis, the resulting theoretical model accurately describes the conveyor operation observed in the tests.

A simplified free body diagram of the soil element used in the analysis is shown in Figure 7.4(b). This figure shows the soil element in plan view, with the forces acting in the ( $l - w$ ) plane of the screw channel considered in the analysis. During steady state operation of the conveyor with the soil flowing along the screw channel at a constant velocity, the forces acting on the soil element and their moments about the screw axis are in equilibrium in any direction. By considering the balance of the forces and moments in the equilibrium condition, relationships defining the total pressure gradient along the conveyor and the screw torque are developed, as presented below.

#### 7.2.4 Theoretical model of total pressure gradient

The equilibrium of the forces acting on the soil element in the direction parallel to the screw channel is used to develop the proposed theoretical model of the total pressure gradient along the conveyor.

From the free body diagram of the soil plug element shown in Figure 7.4(b), the force balance equation in the direction of the  $l$ -axis is:

$$\sum F_l = F_{cs} \cos(\theta + \phi_f) - F_{ss} - F_{ps} - F_{ts} - F_{pl} = 0 \quad \text{Eqn 7.10}$$

The shear stresses acting on the surfaces of the soil element in contact with the screw channel are assumed to be uniformly distributed, and the shear stresses on the pushing and trailing flight surfaces are assumed to be equal. Representing the forces with the shear stresses and the dimensions of the soil plug element, with  $D_f = D_o$  equation 7.10 becomes:

$$(\tau_c w_f dL_f) \cos(\theta + \phi_f) - \tau_s w_s dL_s - 2\tau_f h dL_a - w_a h dP = 0 \quad \text{Eqn 7.11}$$

where:  $\tau_c$  is the shear stress acting on the casing surface (kPa)  
 $\tau_s$  is the shear stress acting on the screw shaft surface (kPa)  
 $\tau_f$  is the shear stress acting the surface of both screw flights (kPa)  
 $dP$  is the change of total pressure over the soil element (kPa)  
 $w_f, w_s, w_a$  are the widths of the screw channel perpendicular to the flight at the flight diameter, shaft diameter, and the average flight diameter (m)  
 $dL_f, dL_s, dL_a$  are the lengths of the soil plug element parallel to the screw channel at the flight diameter, shaft diameter and the average flight diameter (m)  
 $h$  is the screw channel depth (m)

The terms in equation 7.11 representing the length of the soil element along the screw channel,  $dL$ , can be transformed into the length along the screw axis,  $dx$ , using equation 7.2 with the appropriate helix angle, leading to:

$$\left( \tau_c w_f \frac{dx}{\sin \phi_f} \right) \cos(\theta + \phi_f) - \tau_s w_s \frac{dx}{\sin \phi_s} - 2\tau_f h \frac{dx}{\sin \phi_a} - w_a h dP = 0 \quad \text{Eqn 7.12}$$

From the geometry of the screw shown in Figure 7.1, the channel width perpendicular to the screw flight at a given radius,  $w$ , can be expressed in terms of the screw pitch and helix angle, including the flight thickness,  $e$  as follows:

$$w = (t - e) \cos \phi \quad \text{Eqn 7.13}$$

Substituting for the terms  $w_f$ ,  $w_s$ , and  $w_a$ , equation 7.12 becomes:

$$\frac{\tau_c ((t - e) \cos \phi_f) \cos(\theta + \phi_f) dx}{\sin \phi_f} - \frac{\tau_s ((t - e) \cos \phi_s) dx}{\sin \phi_s} - \frac{2\tau_f h dx}{\sin \phi_a} - ((t - e) \cos \phi_a) h dP = 0 \quad \text{Eqn 7.14}$$

Equation 7.14 can then be rearranged and simplified to give an expression for the total pressure gradient along the screw conveyor:

$$\frac{dP}{dx} = \frac{\tau_c \cos(\theta + \phi_f)}{h \cos \phi_a \tan \phi_f} - \frac{2\tau_f}{(t - e) \cos \phi_a \sin \phi_a} - \frac{\tau_s}{h \cos \phi_a \tan \phi_s} \quad \text{Eqn 7.15}$$

Assuming that the shear stresses on the screw shaft and flight surfaces are equal, they can be expressed as a proportion of the casing shear stress using a factor,  $\alpha$ :

$$\alpha = \frac{\tau_f}{\tau_c} = \frac{\tau_s}{\tau_c} \quad \text{Eqn 7.16}$$

Equation 7.15 can then be written as follows:

$$\frac{dP}{dx} = \tau_c \left( \frac{\cos(\theta + \phi_f)}{h \cos \phi_a \tan \phi_f} \right) - \alpha \tau_c \left( \frac{2}{(t-e) \cos \phi_a \sin \phi_a} + \frac{1}{h \cos \phi_a \tan \phi_s} \right) \quad \text{Eqn 7.17}$$

Equations 7.15 and 7.17 relate the total pressure gradient along the conveyor to the shear stresses acting on the soil in the screw channel, the screw geometry, and the direction of soil flow. The three terms of the equations represent the influence of the shear stresses on the casing surface, the screw flight surfaces, and the screw shaft surface on the pressure gradient. For a specific screw geometry, shear stress condition and flow rate (or angle  $\theta$ ), the theoretical pressure gradient is constant, resulting in a linear change of pressure along the conveyor. Depending on the relative magnitudes of the three terms, the pressure gradient can be either positive or negative, corresponding to generation or dissipation of pressure along the conveyor. The equations are derived for a horizontal screw conveyor, and do not include the static pressure drop resulting from the weight of the soil rising up an inclined conveyor.

The equations defining the total pressure gradient can be integrated with respect to the conveyor length variable,  $dx$ , to give an expression for the change of pressure over a length of the conveyor. Integrating equation 7.17 between the limits  $P = P_0$  at  $x = x_0$  and  $P = P_1$  at  $x = x_1$ ,

$$\int_{P_0}^{P_1} dP = \left( \frac{\tau_c \cos(\theta + \phi_f)}{h \cos \phi_a \tan \phi_f} - \alpha \tau_c \left( \frac{2}{(t-e) \cos \phi_a \sin \phi_a} + \frac{1}{h \cos \phi_a \tan \phi_s} \right) \right) \int_{x_0}^{x_1} dx \quad \text{Eqn 7.18}$$

leads to:

$$(P_1 - P_0) = \left( \frac{\tau_c \cos(\theta + \phi_f)}{h \cos \phi_a \tan \phi_f} - \alpha \tau_c \left( \frac{2}{(t - e) \cos \phi_a \sin \phi_a} + \frac{1}{h \cos \phi_a \tan \phi_s} \right) \right) (x_1 - x_0) \quad \text{Eqn 7.19}$$

For the case of  $x_0 = 0$  and  $x_1 = L$ , where  $L$  is the length of the screw conveyor, equation 7.19 allows calculation of the total pressure at the end of the conveyor ( $P_L$ ) from the pressure at the start of the conveyor ( $P_0$ ):

$$P_L = P_0 + \left( \frac{\tau_c \cos(\theta + \phi_f)}{h \cos \phi_a \tan \phi_f} - \alpha \tau_c \left( \frac{2}{(t - e) \cos \phi_a \sin \phi_a} + \frac{1}{h \cos \phi_a \tan \phi_s} \right) \right) L \quad \text{Eqn 7.20}$$

To allow application of these equations to screw conveyors of different scale, operating with soils of varying strength, equation 7.20 can be expressed in dimensionless form. A dimensionless group representing the total pressure gradient along a conveyor is formed by normalising the pressure change ( $\Delta P$ ) by the casing shear stress ( $\tau_c$ ) and the conveyor length ( $L$ ) and diameter ( $D$ ):

$$\underline{P} = \frac{\Delta P D_f}{2 \tau_c L} \quad \text{Eqn 7.21}$$

The screw channel depth, pitch and flight thickness can be expressed as follows:

$$h = \frac{D_f - D_s}{2} = \frac{D_f (1 - D_s / D_f)}{2} \quad \text{Eqn 7.22}$$

$$(t - e) = D_f (\pi \tan \phi_f - (e / D_f)) \quad \text{Eqn 7.23}$$

By substituting equations 7.22 and 7.23, equation 7.20 can be rearranged to give an expression for the dimensionless pressure gradient,  $\underline{P}$ , over a screw conveyor:

$$\underline{P} = \frac{\Delta P D_f}{2\tau_c L} = \left[ \begin{array}{l} \left( \frac{\cos(\theta + \phi_f)}{(1 - (D_s/D_f)) \cos \phi_a \tan \phi_f} \right) \\ -\alpha \left( \frac{1}{(\pi \tan \phi_f - (e/D_f)) \cos \phi_a \sin \phi_a} + \frac{1}{(1 - (D_s/D_f)) \cos \phi_a \tan \phi_s} \right) \end{array} \right]$$

Eqn 7.24

As discussed in Section 7.2.1, the screw geometry can be defined by the dimensionless groups  $(t/D)$ ,  $(D_s/D)$ ,  $(e/D)$ , and  $(D_f/L)$ . Using equations 7.1(a), (b) and (c), the helix angles  $\phi_f$ ,  $\phi_s$ , and  $\phi_a$  can be calculated from these ratios. The angle of soil flow,  $\theta$ , is defined by equation 7.9 in terms of the dimensionless flow rate,  $\underline{Q}$ . As defined by equation 7.16, the factor  $\alpha$  represents the ratio of shear stresses acting on the casing and screw surfaces.

With these parameters defined, equation 7.24 allows calculation of the dimensionless pressure gradient over a screw conveyor,  $\underline{P}$ . This equation can be applied to conveyors of any scale defined by the dimensionless geometric ratios, operating with any shear stress on the casing surface. For a given screw geometry, values of  $\underline{P}$  can be calculated for varying flow rates and shear stress ratios by varying the parameters  $\theta$  and  $\alpha$ . The screw flight thickness can be neglected from the calculation by omitting the term  $(e/D)$  from equation 7.24.

The results of the model screw conveyor tests showed that the resultant casing shear stress,  $\tau_c$ , can be well approximated by the undrained shear strength of the soil,  $S_u$ . The undrained strength of a soil is more easily measured or estimated than the shear stress acting on the casing of a screw conveyor. The equations derived here can be used to calculate total pressure gradients by substituting terms based on the undrained strength,  $S_u$  and  $\alpha S_u$  for the  $\tau_c$  and  $\alpha \tau_c$  terms to represent the shear stresses acting on the surfaces of the screw conveyor.

The effects of the screw geometry, flow rate, and shear stress ratio on the total pressure gradient predicted by the proposed theoretical model are discussed in Section 7.3. The measurements from the model screw conveyor tests are also compared with the theoretical pressure gradients.

### 7.2.5 Theoretical model of screw torque

The torque required to rotate the screw results from the moment about the screw axis in the direction of rotation created by the forces acting on the soil. These forces are defined in Section 7.2.3, and shown on the free body diagram of the soil element shown in Figure 7.4(b). During steady state operation, the soil plug is in an equilibrium condition and the resultant of the moments acting about the screw axis is zero. A theoretical model of the screw torque is proposed below, derived from the balance of moments about the screw axis due to the force components acting perpendicular to the axis. With reference to Figure 7.4(b), the moment balance equation in the direction perpendicular to the screw axis is as follows:

$$\sum M_x = F_{ss} \cos \phi_s \left( \frac{D_s}{2} \right) + F_{ts} \cos \phi_a \left( \frac{D_f}{2} - \frac{h}{2} \right) + F_{ps} \cos \phi_a \left( \frac{D_f}{2} - \frac{h}{2} \right) + \left( F_{pn} \sin \phi_a \left( \frac{D_f}{2} - \frac{h}{2} \right) - F_{tn} \sin \phi_a \left( \frac{D_f}{2} - \frac{h}{2} \right) \right) + F_{pl} \cos \phi_a \left( \frac{D_f}{2} - \frac{h}{2} \right) - F_{cs} \cos \theta \left( \frac{D_f}{2} \right) = 0$$

Eqn 7.25

In the equilibrium condition, the total moment acting in each direction about the screw axis is equal. The torque to rotate the screw is therefore equal to the total moment acting either direction. From Figure 7.4(b), the moments from the components of the forces due to the casing shear stress,  $F_{cs}$ , and the normal pressure on the trailing flight surface,  $F_{tn}$ , act in the direction opposite to the screw rotation. The moments created by the other force components act in the direction of the screw rotation. The forces  $F_{pn}$  and  $F_{tn}$  acting normal to the pushing and trailing flight surfaces have components perpendicular to the screw axis acting in opposite directions. The magnitudes of these forces are not known, but because  $F_{pn}$  originates from a passive pressure acting on the pushing flight surface, it is greater than  $F_{tn}$ , which is from an active pressure on the trailing flight surface. Therefore, the resultant of the perpendicular components of these two forces acts in the direction of the screw rotation. Then, only the force component from the casing shear stress creates a moment about the screw axis opposite to the direction of rotation. The torque to rotate the screw can therefore be related to the moment due to the force component from the casing shear stress acting perpendicular to the screw axis:

$$dT = F_{cs} \cos \theta \left( \frac{D_f}{2} \right) \quad \text{Eqn 7.26}$$

where  $dT$  is the torque required to rotate the screw containing the soil element in the channel. The radial clearance between the casing and the screw flight is neglected, so  $D_f = D_c$ . Expressing the force  $F_{cs}$  in terms of the casing shear stress,  $\tau_c$  and the soil element dimensions, equation 7.26 becomes:

$$dT = \tau_c w_f dL_f \cos \theta \left( \frac{D_f}{2} \right) \quad \text{Eqn 7.27}$$

The term  $w_f$  can be expressed in terms of the screw pitch and helix angle, neglecting the screw flight thickness, using equation 7.13. The length of the soil element along the screw channel at the casing surface,  $dL_f$  can be transformed into a length along the screw axis,  $dx$ , using the helix angle,  $\phi_f$ , as defined by equation 7.2. Making these substitutions, equation 7.27 becomes:

$$dT = \tau_c (t \cos \phi_f) \left( \frac{dx}{\sin \phi_f} \right) \cos \theta \left( \frac{D_f}{2} \right) = \left( \frac{\tau_c t \cos \theta D_f}{2 \tan \phi_f} \right) dx \quad \text{Eqn 7.28}$$

Using equation 7.1(a) to substitute for the term  $(\tan \phi_f)$ , and assuming the casing and flight diameters are equal, so  $D_f = D_c$ , equation 7.28 becomes:

$$dT = \frac{1}{2} \pi D_c^2 \tau_c \cos \theta dx \quad \text{Eqn 7.29}$$

To give an expression for the torque,  $T$ , required to rotate the screw during steady state operation when the conveyor is completely filled with soil, equation 7.29 can be integrated between the limits  $T_0 = 0$  for  $x_0 = 0$ , and  $T_1 = T$  for  $x_1 = L$ , leading to:

$$T = \frac{1}{2} \pi D_c^2 L \tau_c \cos \theta \quad \text{Eqn 7.30}$$

Equation 7.30 shows that the screw torque is equal to the moment about the screw axis due to the perpendicular component of the shear stress acting over the surface area of the conveyor casing. The torque is proportional to the casing shear stress, the conveyor length, and the square of the conveyor diameter. It is also related to the angle of soil movement,  $\theta$ , which depends on the soil flow rate at a given screw speed, and influences the magnitude of the perpendicular component of the casing shear stress. For a conveyor of any length and diameter, equation 7.30 allows calculation of the screw torque for varying casing shear stresses and flow rates. The undrained shear strength of the soil,  $S_u$  can be substituted for  $\tau_c$  in equation 7.30 to calculate the screw torque based on the soil strength.

A dimensionless group,  $\underline{T}$ , representing the screw torque normalised by the conveyor dimensions and the casing shear stress can be formed by rearranging equation 7.30 into dimensionless form:

$$\underline{T} = \frac{2T}{\pi D_c^2 L \tau_c} = \cos \theta \quad \text{Eqn 7.31}$$

This equation predicts that a unique relationship exists between  $\underline{T}$  and the angle of soil flow  $\theta$ , independent of the screw conveyor scale, the screw geometry, and the casing shear stress. Using this relationship, the theoretical screw torque can be calculated for a conveyor of any scale, operating with soils of varying strength and with different flow rates.

The theoretical relationships for the screw torque proposed here are discussed further and compared with measurements from the model screw conveyor tests in Section 7.4.

### 7.3 Total pressure gradients

The influences of different parameters and operating conditions on the pressure gradient along the screw conveyor based on the theoretical model proposed in Section 7.2.4 are discussed here. The measurements from the model screw conveyor tests are also compared with the theory.

#### 7.3.1 Theoretical pressure gradients

Equations 7.17 and 7.24 relate the total pressure gradient,  $dP/dx$ , and the dimensionless pressure gradient,  $\underline{P}$  to the screw geometry, the direction of soil flow, and the shear stresses acting on the

casing and screw surfaces. The effects of these parameters on the theoretical pressure gradient are discussed below.

### 7.3.1.1 Effect of shear stress ratio

The relationship between  $\underline{P}$  and the angle of soil flow,  $\theta$ , predicted by equation 7.24 for varying shear stress ratios,  $\alpha$ , is shown in Figure 7.5(a). The values of  $\alpha = 0 - 2.0$  cover the cases with no shear stresses acting on the screw surfaces ( $\alpha = 0$ ), equal shear stresses on the casing and screw surfaces ( $\alpha = 1$ ), and screw shear stresses greater than the casing shear stress ( $\alpha > 1$ ). The curves shown are calculated using the values of  $t/D_f$ ,  $D_s/D_f$  and  $e/D_f$  specified in Table 7.1 for the geometry of screw (1). The dimensionless flow rate,  $\underline{Q}$ , is related to  $\theta$  through equation 7.8. The relationship between  $\underline{P}$  and  $\underline{Q}$  for screw (1) with varying  $\alpha$  values is shown in Figure 7.5(b). The curves in Figure 7.5 are specific to the geometric ratios used, but similar relationships can be determined for any particular screw geometry. These curves are independent of the magnitude of the casing shear stress and the undrained strength of the soil (assuming  $\tau_c = S_u$ ), since the pressure gradient is normalised by  $\tau_c$  in the dimensionless group  $\underline{P}$ .

Figure 7.5 shows that the total pressure can increase ( $\underline{P} > 0$ ) or decrease ( $\underline{P} < 0$ ) along the conveyor, depending on the flow rate and the shear stress ratio. For a given value of  $\alpha$ ,  $\underline{P}$  varies with  $\theta$  and  $\underline{Q}$  as the direction of soil flow influences the component of the casing shear stress acting parallel to the screw channel which contributes to the pressure change. Depending on the magnitude of the term  $(\theta + \phi)$ , the shear stress acting on the casing can either generate or dissipate pressure along the conveyor. The shear stresses on the screw surfaces act parallel to the screw channel and are not influenced by the direction of soil flow at the casing. The shear stress ratio influences  $\underline{P}$  by varying the magnitude of the pressure change resulting from the stresses on the screw surfaces. These shear stresses dissipate the total pressure along the conveyor, with increasing values of  $\alpha$  causing  $\underline{P}$  to reduce for given value of  $\theta$  or  $\underline{Q}$ .

For clay soils, the shear stress ratio would usually have a maximum value of  $\alpha = 1$ , with equal shear stresses on the casing and screw surfaces. Values of  $\alpha$  greater than one could occur if conditioning agents are injected through the conveyor casing to provide lubrication and reduce the casing shear stress relative to the screw shear stresses. Figure 7.5 shows that such an increase in the shear stress ratio would increase the dissipation of pressure along the conveyor. For the

condition when the shear stress on the casing is zero, the theoretical model indicates that the pressure gradient due to shear stresses on the screw surfaces is constant for all angles of soil flow.

### 7.3.1.2 Effect of screw pitch

The theoretical relationships between  $\underline{P}$  and  $\theta$ , and  $\underline{P}$  and  $\underline{Q}$  for varying screw pitches, represented by different  $t/D_f$  ratios, are shown in Figures 7.6(a) and (b). These curves are calculated from equation 7.24 using the values of  $D_s/D_f$  and  $e/D_f$  shown in Table 7.1. The  $t/D_f$  values of 0.6 – 1.4 cover the typical range for screw conveyors, as discussed in Section 4.3.5. The helix angles for different screw pitches are calculated from the  $t/D_f$  and  $D_s/D_f$  ratios using equation 7.1. The values of  $\underline{Q}$  are calculated from the  $\theta$  values using the helix angle corresponding to the  $t/D_f$  ratio. A shear stress ratio of  $\alpha = 0.75$  was assumed for these curves, although similar trends result for different  $\alpha$  values.

Figure 7.6 shows that a smaller screw pitch (lower  $t/D_f$ ) results in a greater pressure gradient along the conveyor. The pitch has a greater influence on the pressure gradient for higher values of the angle  $\theta$  and flow rate  $\underline{Q}$ . For a given value of  $\theta$ , the pressure change  $\underline{P}$  varies non-linearly with the  $t/D_f$  ratio. Reducing the screw pitch increases the component of the casing shear stress acting parallel to the screw channel, and increases the magnitude of the pressure change due to the shear stresses on the screw surfaces. These effects increase the total pressure gradient along a conveyor with a smaller screw pitch. The effects of the screw pitch on the pressure gradient predicted by equation 7.24 are similar to those predicted by the theoretical model of Yoshikawa (1996c), shown in Figure 2.23.

### 7.3.1.3 Effect of soil strength

The influence of variations in the casing shear stress,  $\tau_c$ , on the total pressure gradient is not shown through the dimensionless group  $\underline{P}$ , as the pressure change is normalised by  $\tau_c$ . Assuming that the casing shear stress is equal to the undrained strength of the soil (i.e.  $\tau_c = S_u$ ), the effect of varying soil strengths on the total pressure gradient can be investigated using equation 7.17. Figures 7.7(a) and (b) show the theoretical total pressure gradient,  $dP/dx$ , plotted against  $\theta$  and  $\underline{Q}$  for soil strengths in the range  $S_u = 5 - 25$  kPa. These curves are based on the geometry of screw (1) from the model tests, assuming a shear stress ratio of  $\alpha = 0.75$ .

Figure 7.7 shows that for a specific screw geometry and shear stress ratio, the total pressure gradient is proportional to the casing shear stress or the soil strength. Higher shear stresses acting on the casing and screw surfaces result in a greater rate of pressure change along the conveyor. The pressure gradients vary with  $\theta$  and  $Q$ , as the component of the casing shear stress acting parallel to the screw channel varies with the direction of soil flow. For the conditions used in these calculations, the pressure gradient changes from positive to negative at different values of  $\theta$ , indicating that the screw will generate or dissipate total pressure depending on the flow rate.

The curves shown in Figure 7.7 are specific to the conditions assumed, however, they demonstrate that for a specific screw geometry and operating condition, the total pressure gradient varies depending on the strength of the soil flowing through the conveyor. For the case of a very low strength soil or a liquid flowing through the conveyor, the theoretical model indicates that there would be no pressure change along the conveyor when the shear stresses acting on the casing and screw surfaces are zero.

### **7.3.2 Effects of conveyor operating conditions**

The results of the screw conveyor tests presented in Chapters 5 and 6 show pressure gradients measured for samples of different strength with varying discharge conditions, sample pressures, and screw speeds. The effects of the sample properties and conveyor operating conditions on the pressure gradients can be related to the parameters in the theoretical model.

The tests performed with varying discharge conditions showed greater dissipation of pressure when the outlet was unrestricted, due to the lower pressure required to discharge the soil. The outlet condition influenced the angle of soil flow, resulting in different pressure gradients when similar shear stresses were acting on the casing and screw surfaces. With the outlet restricted, the flow of soil along the screw channel and the angle  $\theta$  was reduced as a high pressure was required to discharge the soil. The angle  $\theta$  increased when the outlet was unrestricted, resulting in greater dissipation of the pressure. Similar observations were made in the tests with WRB/UP samples with the outlet restricted. As the screw speed increased, the angle  $\theta$  reduced as higher pressures were generated along the conveyor to discharge the soil at faster rates. The theoretical model shows that the component of the pressure gradient due to the casing shear stress varies with the angle of soil flow. The effects of the outlet condition on the discharge pressure and the angle of soil flow result in the different pressure gradients observed in these tests.

In tests performed with varying sample pressures, different pressure gradients were observed with similar shear stresses acting on the casing and screw surfaces. When a higher sample pressure was applied, the soil flow rate and the angle of soil flow increased, and higher pressure gradients were observed. The different pressure gradients result from the different angles of soil flow, which influence the component of the pressure gradient due to the casing shear stress.

In tests with London Clay samples with the outlet unrestricted, the pressure gradients at different screw speeds were similar. Although the bulk soil flow rate increased with the screw speed, the dimensionless flow rate,  $\underline{Q}$ , and the angle of soil flow,  $\theta$ , only varied slightly. The pressure gradient depends on the angle  $\theta$ , so for a particular sample with similar casing and screw shear stresses acting, variations in the pressure gradient at different screw speeds resulted from changes in the soil flow angle.

As shown in Figure 6.12, similar pressure gradients were measured in tests with London Clay samples of varying strength and with different casing shear stresses. As shown in Figure 7.7, the influence of the casing shear stress on the pressure gradient varies with the angle  $\theta$ , and for values relevant to the tests the influence is relatively small. The effects of different parameters on the pressure gradient also vary. Increasing the angle  $\theta$  and the shear stresses on the screw increases the pressure dissipation, while increasing the casing shear stress reduces the pressure dissipation. The resulting pressure gradient depends on the relative influences of these factors. In the tests shown in Figure 6.12, the similar gradients with different casing shear stresses result from variations in the soil flow angles and shear stress ratios between the tests due to the different sample properties and conditioning treatments.

### **7.3.3 Comparison of experimental and theoretical pressure gradients**

#### **7.3.3.1 Dimensionless pressure gradients**

The measurements from the model screw conveyor tests allow comparison with the total pressure gradients predicted by the theoretical model. The test data is compared with the theory using the dimensionless group,  $\underline{P}$ , to allow comparison of pressure gradients measured during tests with different shear stresses acting on the casing. Values of  $\underline{P}$  are determined from the test measurements, and compared with theoretical values calculated from equation 7.24.

The dimensionless group,  $\underline{P}$ , representing the total pressure gradient, is defined by equation 7.21. The load cells measured the total normal stress and resultant shear stress acting on the casing at

four sections along the conveyor. From these measurements, the total pressure change,  $\Delta P$ , and the average resultant casing shear stress,  $\tau_c$ , over the length of the conveyor between the instrumented sections are known. Using equation 7.21, values of  $\underline{P}$  can be calculated from these measurements. The measurements from the different stages of the model tests and the experimental values of  $\underline{P}$  are summarised in Table 7.2.

Theoretical values of  $\underline{P}$  can be calculated from equation 7.24 for a given screw geometry, direction of soil flow,  $\theta$ , and shear stress ratio,  $\alpha$ . The geometry parameters for screws (1) and (2) are shown in Table 7.1. The angle of soil flow in the conveyor can be calculated through the flow rate and the rotational speed of the screw. In the model tests, the volumetric flow rate,  $Q$ , is measured through the rate of change of sample height in the container, and the rotational speed of the screw,  $N$ , is measured most accurately from the periodic cycles in the torque measurements. With the cross-sectional area of the screw channel given by the flight and shaft diameters, the dimensionless flow rate,  $\underline{Q}$ , can be calculated from equation 7.8. The value of  $\theta$  can then be calculated from equation 7.9, and the test values are shown in Table 7.2. The values of  $\theta$  from the test measurements are within the range of approximately  $20^\circ$  to  $60^\circ$ , smaller than the maximum value of  $(90 - \phi)$  for controlled flow of soil through the screw channel.

To calculate theoretical values of  $\underline{P}$  from equation 7.24, a value for the shear stress ratio,  $\alpha$ , must be assumed. As discussed in sections 5.5.4 and 6.4.3, a layer of clay adhered to the casing surface, resulting in clay-on-clay shearing at this interface with the resultant shear stress approximately equal to the undrained strength of the soil. The screw did not have a layer of clay adhering to the shaft or flight surfaces, indicating that shearing on the screw surfaces occurred by a soil-steel sliding mechanism. Therefore, the shear stresses on the screw are expected to be less than the undrained strength of the soil, and the values of  $\alpha$  less than one.

A large database of load tests of piles in clay soils exists, providing values of an  $\alpha$  ratio representing the skin friction from shear stresses acting on the pile shaft as a proportion of the undrained shear strength of the soil. Such data is discussed by many authors, including Fleming *et. al* (1985), Lehane (1992), and Chow (1996). Compilations of  $\alpha$  values from pile load tests show significant scatter, typically within a range  $\alpha = 0.4 - 1.2$ . It is often assumed  $\alpha = 1.0$  for the design of piles in soft clays of undrained strength less than about 30 kPa. However, significant scatter of  $\alpha$  values within the typical range still exists for such soft clays, as illustrated

in Figure 7.8 showing data from load tests of piles in clays of varying strength presented by Dennis and Olsen (1983).

The  $\alpha$  value from a pile load test can be considered to represent a similar phenomenon as the  $\alpha$  ratio used in the analysis of the screw conveyor, in that both parameters relate the shear stresses acting on a steel surface to the undrained strength of the soil. Based on the typical range of values from the extensive pile test data, it is reasonable to expect that the values of  $\alpha$  relevant to the screw conveyor operation should be within the approximate range  $\alpha = 0.5 - 1.0$ . Assuming values of  $\alpha$  within this range, equation 7.24 can be used to calculate theoretical values of  $\underline{P}$  for a specific screw geometry and a range of dimensionless flow rates,  $\underline{Q}$ , or soil flow angles,  $\theta$ .

Theoretical curves of  $\underline{P}$  versus  $\theta$  for screw (1) with  $\alpha = 0.5 - 1.0$  are shown in Figure 7.9(a). Data points from each stage of the model tests using screw (1) with different soils are also shown. Figure 7.9(b) also shows these theoretical curves and test data points with  $\underline{P}$  plotted against  $\underline{Q}$ . Theoretical curves of  $\underline{P}$  versus  $\theta$  and  $\underline{P}$  versus  $\underline{Q}$  for screw (2) with  $\alpha = 0.50 - 1.0$  are shown in Figures 7.10(a) and (b), with the data points from the tests with this screw. The theoretical curves show the smaller pressure gradients along the conveyor with screw (2) due to the longer pitch, as discussed above. The data points from the flow rates and pressure gradients measured during the tests with both screws fit within the expected range of theoretical pressure gradients, assuming values of  $\alpha$  in the range 0.5 to 1.0. Only the data points from the tests using screw (2) with kaolin samples are slightly outside this range. The pressure changes measured in these tests correspond to  $\alpha$  values slightly below 0.5, but these are still reasonable considering the typical range of  $\alpha$  values obtained from pile test data. The positive and negative pressure gradients measured in the tests are also successfully predicted by the theoretical model for the two screw geometries over the range of  $\alpha$  values and soil flow angles expected during the conveyor operation.

Based on the test measurements, exact values of  $\alpha$  can be calculated so the theoretical pressure gradient is equal to the measured gradient. These theoretical  $\alpha$  values are shown in Table 7.2. For most of the tests with conditioned London Clay samples, the theoretical  $\alpha$  values are within the range  $\alpha = 1.04 - 0.73$ . However, the values for tests 12 and 14 are significantly lower, ranging from  $\alpha = 0.54 - 0.66$ . The conditioning agents used for these tests differed from other samples. The test 12 sample was conditioned with a combined foam and polymer treatment, and the test 14 sample with a higher polymer concentration. The lower theoretical  $\alpha$  values for these tests

suggest that these conditioning treatments lubricated soil-steel interfaces at the screw surfaces, resulting in lower shear stresses on the screw and a smaller pressure gradient along the conveyor. The casing shear stress was not also reduced for these samples as shearing at this interface occurred by a soil-on-soil mechanism.

The theoretical  $\alpha$  values for the tests with kaolin samples are lower than those for the conditioned soil samples. The values range from  $\alpha = 0.54 - 0.59$  for the kaolin tests with screw (1), and from  $\alpha = 0.36 - 0.38$  for the tests with screw (2). The lower  $\alpha$  values for the kaolin tests are possibly due to the low plasticity of E-grade kaolin compared to the other soils tested, which might reduce the shear stresses at the soil-steel interfaces on the screw surfaces. A similar reduction of  $\alpha$  values with clay plasticity due to low shaft friction on piles in soft, low plasticity, silty clays was observed in pile load tests reported by Karlsrud *et. al.* (1993).

### 7.3.3.2 Calculated pressure gradients

The theoretical model can be used to calculate total pressure gradients for different operating conditions. Using equation 7.20, the pressure along the conveyor can be calculated for a specific screw geometry, angle of soil flow, shear stress condition, and initial pressure at the start of the conveyor.

The calculated pressure gradients are compared with the measurements from some of the model conveyor tests in Figures 7.11 and 7.12. These calculations are based on the average casing shear stresses and angles of soil flow measured in the tests, using the geometry of screw (1). The total pressure at the start of the conveyor was assumed equal to 200 kPa, and the shear stress ratios were based on the theoretical values shown in Table 7.2.

Figure 7.11 shows the measured and calculated pressure gradients from test 3 for different discharge conditions. A shear stress ratio of  $\alpha = 0.57$  was assumed for this kaolin sample. The calculated pressures decrease linearly along the conveyor, and agree well with the measurements. The different pressure gradients result from the measured change in the soil flow angle when the discharge condition was changed from restricted to unrestricted.

Figure 7.12 shows the measured and calculated pressure gradients at different screw speeds in test 7. A shear stress ratio of  $\alpha = 0.90$  was assumed for this London Clay sample. The calculated

pressure gradients agree closely with the measurements. The changes of the gradient at different screw speeds result from the measured changes in the soil flow angles and casing shear stresses.

These examples showing close agreement between the calculations and test measurements indicate that the theoretical model accurately predicts the total pressure gradient along the conveyor for different operating conditions.

## 7.4 Screw conveyor torque

A theoretical model of the screw torque was proposed in Section 7.2.5. The predictions of the theoretical model are discussed below, and measurements from the model conveyor tests are compared with the theory.

### 7.4.1 Theoretical screw torque

The theoretical analysis of the screw conveyor led to equation 7.30, relating the screw torque to the conveyor dimensions, the casing shear stress, and the angle of soil flow. This relationship is expressed in dimensionless form in equation 7.31, with the dimensionless group  $\underline{T}$  representing the normalised screw torque. The theoretical effects of varying soil flow rates, soil strengths, and screw geometry on the torque are discussed here.

Figure 7.13 shows the theoretical torque calculated from equation 7.30 for the model conveyor, with varying soil flow angles,  $\theta$ , and casing shear stresses,  $\tau_c$ . The calculations are based on the length and internal diameter of the conveyor casing, with the casing shear stresses covering the range of sample strengths from the tests. For a given angle of soil flow, the torque increases linearly with the casing shear stress, or with the undrained strength of the soil assuming  $\tau_c = S_u$ . As the angle of soil flow increases relative to the perpendicular to the screw axis, the torque decreases due to the perpendicular component of the casing shear stress reducing as the soil flow shifts towards the axial direction. The maximum screw torque occurs when the angle  $\theta$  is close to zero, with little flow along the conveyor and the soil jamming in the screw channel. For a specific conveyor length and diameter, equation 7.30 can be used to calculate the maximum torque required to rotate the screw for the soil strengths expected during operation.

Soil conditioning agents such as polymers or foam are often injected through the screw conveyor casing during EPB machine operations. This application of soil conditioning could form a

lubricating layer over the internal surface of the conveyor casing, causing reductions in the shear stress on the casing surface and so reduce the screw torque. As discussed in Section 7.3.1, reducing the casing shear stress relative to the screw shear stress also influences the pressure gradient along the conveyor.

Equation 7.31 defines a relationship between the dimensionless screw torque,  $\underline{T}$  and the angle of soil flow,  $\theta$ , shown in Figure 7.14. The dimensionless group  $\underline{T}$  represents the screw torque normalised by the conveyor length and diameter, and the casing shear stress. The curve in Figure 7.14 shows the theoretical variation of the dimensionless torque due to the change in the perpendicular component of the casing shear stress as the angle of soil flow varies. The minimum torque with controlled soil flow in the conveyor occurs with  $\theta = (90 - \phi_f)$ , and depends on the screw helix angle. This curve applies for conveyors of any scale, represented by the length and diameter, with any screw geometry, and with any casing shear stress or soil strength, assuming  $\tau_c = S_u$

Theoretical relationships between the dimensionless torque,  $\underline{T}$  and the dimensionless flow rate,  $\underline{Q}$ , for screws of different pitch can also be determined from equation 7.31. The flow rate  $\underline{Q}$  is related to the angle of soil flow,  $\theta$ , and the screw helix angle,  $\phi_f$  as defined by equation 7.8. The helix angle  $\phi_f$  is related to the screw pitch and flight diameter as defined in equation 7.1(a). Because  $\underline{Q}$  depends on  $\phi_f$  as well as  $\theta$ , the theoretical relationships between  $\underline{T}$  and  $\underline{Q}$  from equation 7.31 are specific to the value of  $\phi_f$  or the  $t/D_f$  ratio. These relationships for  $t/D_f$  values of 0.6 to 1.4 are shown in Figure 7.15. These curves express the same relationship as shown in Figure 7.14, but with the angle of soil flow,  $\theta$ , expressed as the corresponding dimensionless flow rate,  $\underline{Q}$ , for screws of varying pitch. Figure 7.15 shows that for values of  $\underline{Q}$  greater than about 0.15, the dimensionless torque  $\underline{T}$  varies significantly with the screw pitch. These curves can be applied to screw conveyors of any scale, with the screw pitch defined by the  $t/D_f$  ratio, operating with any casing shear stress or soil strength.

#### 7.4.2 Comparison of measured and theoretical screw torque

Measurements from the model conveyor tests are summarised in Table 7.2. The dimensionless flow rates,  $\underline{Q}$ , and soil flow angles,  $\theta$ , are calculated as described in Section 7.3.2. The screw torque measured in each test is shown, as well as the torque calculated from the theoretical model. The values of the dimensionless torque,  $\underline{T}$ , from the test measurements are also shown.

The test results presented in Chapters 5 and 6 showed that the screw torque increased with the sample strength and the casing shear stress. Figure 7.16(a) shows the screw torque measurements from all tests, plotted against the average resultant casing shear stress. The torque measurements are plotted against the undrained shear strength of the samples in Figure 7.16(b). These figures show the approximate linear increase of the torque with the casing shear stress and the sample strength, as observed in tests with different soils and varying conveyor operating conditions. The data in these figures has some scatter due to differences in the soil flow angles which influences the torque for a given casing shear stress, and also from the approximation of the casing shear stress by the undrained strength. However, the data shows that the trends between the parameters measured in the tests are as expected from the theoretical model.

The torque measurements are compared with theoretical values in Figure 7.17(a). The theoretical torque is calculated from equation 7.30 using the average casing shear stress  $\tau_c$ , the angle of soil flow  $\theta$ , and the length and internal diameter of the conveyor casing. The measured and calculated values of the torque shown in Figure 7.17(a) agree closely, indicating that the theoretical model accurately predicts the screw torque for the model conveyor. The torque can also be calculated assuming the casing shear stress is equal to the undrained strength of the soil. Figure 7.17(b) compares the test measurements with the theoretical torque calculated from the undrained strength of the samples. Although the agreement is not as close as in Figure 7.17(a), this comparison shows that the screw torque can be estimated accurately using equation 7.30 based on the undrained shear strength of the soil.

The torque measurements from the tests can also be compared with the theoretical model using the dimensionless relationship defined by equation 7.31 and shown in Figures 7.14 and 7.15. The dimensionless torque  $\underline{T}$ , calculated for each test from the measured torque and casing shear stress and the conveyor dimensions, is shown in Table 7.2. The measured values of  $\underline{T}$  and the angle of soil flow,  $\theta$ , are compared with the theoretical relationship between these parameters in Figure 7.18. This theoretical curve is independent of the screw geometry, so the data from tests with screws (1) and (2) of different pitch are shown together. The measurements from the tests with different soils and varying sample strengths and conveyor operating conditions agree with the theoretical curve reasonably well. The measured values of  $\underline{T}$  and the dimensionless flow rate,  $\underline{Q}$ , from the tests with screws (1) and (2) are compared with the theoretical relationships between these parameters for the different screw geometries in Figure 7.19. The measurements from the tests with each screw agree well with the theoretical curve for the specific screw geometry.

The comparisons of the results from the model tests with the proposed theoretical model for the screw torque show good agreement. The theoretical model allows calculation of the torque required for screw conveyors of any scale, with varying operating conditions and soil strengths.

## 7.5 Summary

This chapter has presented a proposed theoretical model describing the mechanics of a screw conveyor. From analysis of the soil flow, equations defining a dimensionless flow rate and the direction of soil flow in the conveyor are derived. The equilibrium of forces acting on the soil in the screw channel leads to equations relating the total pressure gradient and the screw torque to the shear stresses acting on the casing and screw surfaces, the direction of soil flow, and the geometry of the screw conveyor. The pressure gradient and torque equations are expressed in dimensionless form, with the conveyor geometry defined by some dimensionless groups, to allow application of the theoretical model to screw conveyors of varying scale.

The theoretical model predicts a constant total pressure gradient, resulting in a linear change of pressure along the conveyor. The effects of some variables and conveyor operating conditions on the pressure gradient were discussed. The dimensionless flow rate or the direction of soil flow influences the pressure gradient, as the component of the casing shear stress parallel to the screw channel changes. This allows the pressure to either increase or decrease along the conveyor. The ratio of shear stresses acting on the casing and screw surfaces also influences the pressure gradient. Increasing shear stresses on the screw causes greater dissipation of pressure along the conveyor. The screw geometry also influences the pressure gradient, with an increasing screw pitch resulting in a smaller pressure gradient. For a specific screw geometry and shear stress ratio, the pressure gradient is proportional to the casing shear stress. The effects of different conveyor operating conditions on the pressure gradients observed in the model tests were consistent with the theoretical model.

The pressure gradients measured in the model conveyor tests were compared with the theoretical model. Measured values of the dimensionless pressure gradient were compared with theoretical values calculated for the geometry of the model conveyor with varying soil flow angles and shear stress ratios. Good agreement between the measured and theoretical pressure gradients was obtained for the tests with different screw geometries, using values of the shear stress ratio within the expected range of  $\alpha = 0.5 - 1.0$ . The positive and negative pressure gradients measured in the

tests were also predicted theoretically for the model conveyor geometry over the range of soil flow angles and shear stress ratios relevant to the conveyor operation. Pressure gradients calculated from the theoretical model for different conveyor operating conditions agreed well with measurements from the model tests.

The theoretical model predicts a linear increase of the screw torque with the casing shear stress or soil strength, as observed in the model tests. The torque varies with the angle of soil flow at the casing, as the perpendicular component of the casing shear stress changes. The theory predicts a unique relationship between the dimensionless torque parameter and the direction of soil flow, valid for conveyors of different scale with any screw geometry, operating with any casing shear stress. The torque measurements from the model conveyor tests were accurately calculated by the theoretical model. The test data also compared well with the theoretical relationships between the dimensionless torque and the angle of soil flow, and the dimensionless flow rate.

The close agreement between the measurements from the model conveyor tests and the proposed theoretical model of the total pressure gradient and screw torque indicates that the theory accurately describes the screw conveyor operation. The theoretical equations can be used to predict the pressure gradient and torque for screw conveyors of varying scale, with different screw geometries and soil flow rates, and with different casing shear stresses. The casing shear stress can be approximated by the undrained strength of the soil, allowing calculations of the pressure gradient or screw torque using the theoretical model with the more commonly known soil strength properties.

<b>Geometry parameter</b>	<b>Screw 1</b>	<b>Screw 2</b>
Conveyor length, $L$ (mm)	1050	
Casing diameter, $D_c$ (mm)	108.0	
Flight diameter, $D_f$ (mm)	102.0	102.0
Shaft diameter, $D_s$ (mm)	43.0	43.0
Channel depth, $h$ (mm)	29.5	29.5
Screw pitch, $t$ (mm)	80.0	133.0
Flight thickness, $e$ (mm)	5.0	5.0
Flight helix angle, $\phi_f$ ( $^\circ$ )	14.0	22.5
Shaft helix angle, $\phi_s$ ( $^\circ$ )	30.6	44.5
Average helix angle, $\phi_a$ ( $^\circ$ )	19.3	30.3
$D_f/L$	0.097	0.097
$D_s/D_f$	0.422	0.422
$t/D_f$	0.784	1.304
$e/D_f$	0.049	0.049

Table 7.1. Geometry of model screws.

Test	Test stage	$S_u$ (kPa)	Screw speed (rpm)	Discharge rate, $Q$ ( $\text{mm}^3/\text{s}$ )	$Q$	$\theta$	Average casing shear stress $\tau_c$ (kPa)	Measured $\Delta P$ (kPa)	$\Delta P/L$ (kPa/m)	Measured $P$	Theoretical $\alpha$	Measured torque (Nm)	Measured $T$	Calculated torque (Nm)
1	1	7	4.7	33743	0.200	45.2	9.6	-81.0	-120.0	-0.638	0.590	91.9	0.498	130.1
	2	15	4.9	32762	0.186	36.3	15.5	147.0	217.7	0.716	0.533	249.0	0.835	240.3
3	1	5	5.5	40403	0.205	48.7	5.8	-72.1	-106.8	-0.939	0.579	68.9	0.617	73.7
	2		5.5	42109	0.213	55.7	5.7	-122.0	-180.7	-1.617	0.559	63.3	0.577	61.8
4	1	8	4.8	34220	0.199	44.2	7.2	-35.9	-53.2	-0.377	0.570	92.2	0.666	99.3
	2		4.6	34636	0.208	52.8	7.5	-110.4	-163.5	-1.112	0.538	89.7	0.662	87.3
5	1	8	5.0	55621	0.300	50.8	7.5	-7.1	-10.5	-0.071	0.377	86.7	0.601	91.3
	2		5.1	60682	0.332	58.8	7.3	-64.3	-95.3	-0.666	0.361	75.0	0.534	72.8
6	1	8.5	4.8	52370	0.304	48.7	8.1	12.4	18.3	0.115	0.372	107.7	0.691	102.9
	2		4.9	58743	0.334	59.7	7.7	-78.1	-115.8	-0.767	0.367	88.2	0.596	74.7

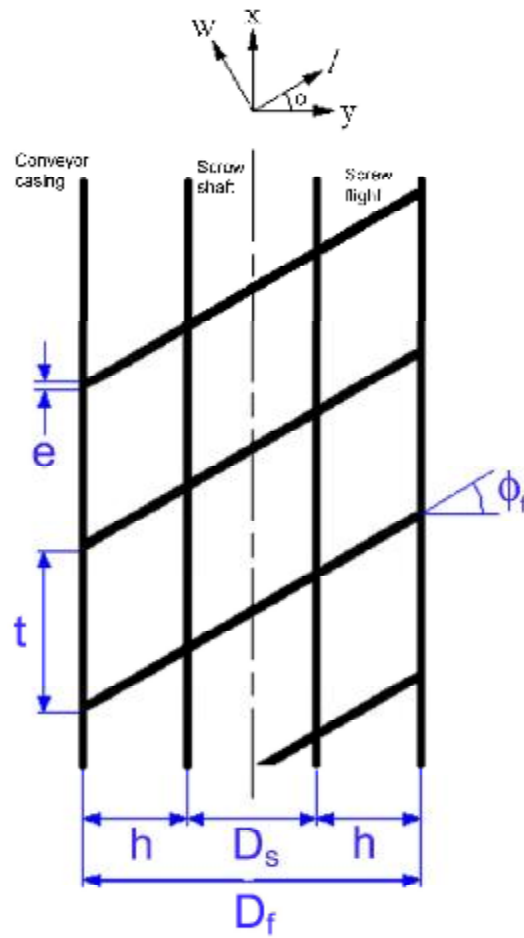
Table 7.2(a). Summary of screw conveyor test measurements for kaolin samples (Tests 1 – 6).

Test	Test stage	$S_{u1}$ (kPa)	Screw speed (rpm)	Discharge rate, $Q$ ( $\text{mm}^3/\text{s}$ )	$\Omega$	$\theta$	Average casing shear stress $\tau_c$ (kPa)	Measured $\Delta P$ (kPa)	$\Delta P/L$ (kPa/m)	Measured $P$	Theoretical $\alpha$	Measured torque (Nm)	Measured $I$	Calculated torque (Nm)
7	1	7	4.9	30480	0.173	29.6	7.3	-123.3	-182.6	-1.270	0.885	113.9	0.807	122.8
	2		14.3	84057	0.164	25.5	8.2	-118.8	-175.9	-1.098	0.908	-	-	142.0
	3		24.0	144228	0.167	27.0	8.3	-124.6	-184.6	-1.134	0.897	-	-	142.3
8	1	26	4.8	33943	0.197	43.1	24.2	-37.7	-	-0.118	-	380.6	0.818	340.0
	2		13.6	87976	0.180	33.0	26.2	-12.8	-	-0.037	-	570.9	1.133	422.9
9	1	4.5	4.5	28956	0.179	32.5	4.5	-136.2	-201.8	-2.287	0.999	89.5	1.034	73.0
	2		13.8	86452	0.175	30.1	4.6	-145.3	-215.3	-2.387	1.028	93.8	1.060	76.5
	3		24.1	145887	0.169	27.5	4.9	-143.9	-213.2	-2.219	1.037	99.2	1.052	83.6
10	1	10.5	5.2	34913	0.187	36.7	9.3	-95.5	-141.5	-0.778	0.728	157.9	0.885	143.0
	2		14.3	92686	0.180	33.1	10.8	-104.4	-154.6	-0.733	0.769	198.1	0.957	173.3
	3		24.0	150182	0.174	30.0	11.7	-102.4	-151.7	-0.662	0.798	223.9	0.997	194.5
11	1	11	4.9	49737	0.283	41.6	10.9	-64.4	-95.4	-0.447	0.660	165.9	0.792	156.7
	2		14.3	140484	0.274	38.8	12.5	-68.5	-101.5	-0.414	0.706	203.2	0.845	187.5
	3		24.3	234971	0.269	37.5	11.5	-75.0	-111.1	-0.494	0.751	181.7	0.823	175.2

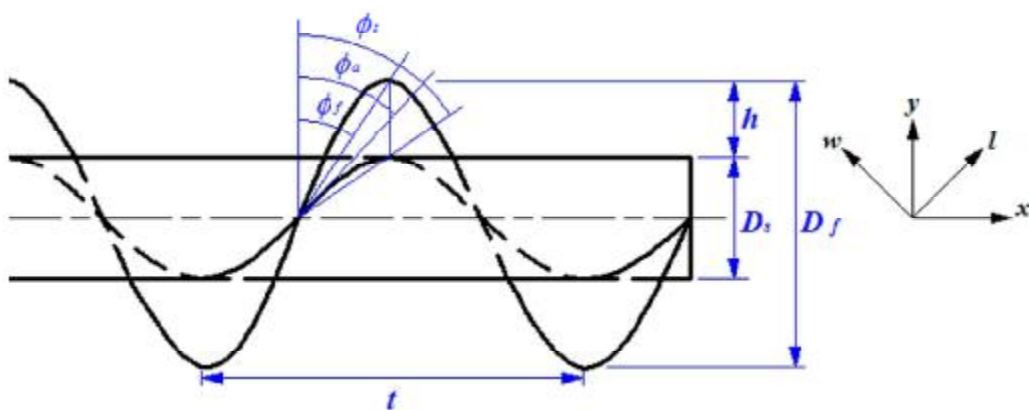
Table 7.2(b). Summary of screw conveyor test measurements for conditioned soil samples (Tests 7-11).

Test	Test stage	$S_{u1}$ (kPa)	Screw speed (rpm)	Discharge rate, $Q$ ( $\text{mm}^3/\text{s}$ )	$\Omega$	$\theta$	Average casing shear stress $\tau_c$ (kPa)	Measured $\Delta P$ (kPa)	$\Delta P/L$ (kPa/m)	Measured $P$	Theoretical $\alpha$	Measured torque (Nm)	Measured $I$	Calculated torque (Nm)
12	1	10.5	4.8	33251	0.193	40.4	9.8	-85.5	-126.7	-0.662	0.663	166.7	0.887	143.1
	2		14.0	97674	0.194	41.3	12.9	-83.7	-124.1	-0.492	0.627	-	-	183.7
13	1	10	4.9	31487	0.179	32.3	10.5	-134.6	-199.4	-0.971	0.811	151.4	0.751	170.2
	2		14.3	88530	0.172	29.2	9.9	-136.4	-202.1	-1.042	0.859	147.6	0.776	166.1
	3		24.0	145194	0.169	27.4	8.4	-129.5	-191.8	-1.165	0.895	119.7	0.741	143.4
14	1	13	4.6	34082	0.206	50.0	12.0	-131.7	-195.1	-0.827	0.542	167.5	0.724	148.6
	2		14.3	103696	0.202	46.7	12.3	-88.9	-131.7	-0.547	0.556	194.5	0.824	162.1
	3		24.0	168331	0.195	42.0	12.6	-114.8	-170.1	-0.686	0.643	203.2	0.835	180.8
15	1	15.5	3.8	23275	0.171	28.3	8.3	-81.5	-120.7	-0.743	0.828	99.1	0.622	140.2
	2		13.5	79524	0.164	25.6	24.2	120.7	178.8	0.376	0.709	334.8	0.718	420.6
16	3		23.2	127332	0.153	21.5	29.0	171.2	253.6	0.446	0.742	420.2	0.753	518.8
	1	5	4.5	28603	0.177	31.4	8.0	-97.2	-144.0	-0.918	0.816	128.0	0.823	131.4
	2		14.0	82613	0.164	25.7	10.3	-41.6	-61.6	-0.305	0.799	176.9	0.893	178.5

Table 7.2(b). Summary of screw conveyor test measurements for conditioned soil samples (Tests 12-16).



(a) Screw dimensions.



(b) Screw helix angles.

Figure 7.1. Definition of screw conveyor geometry.

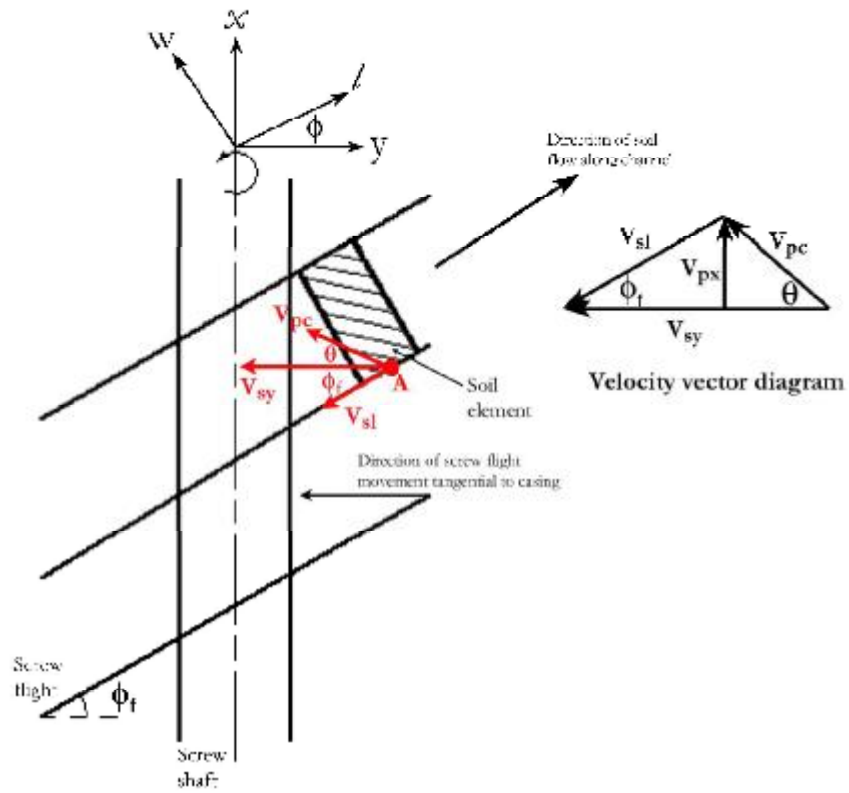


Figure 7.2. Movement of soil plug along screw channel.  
(plan view at top of screw channel)

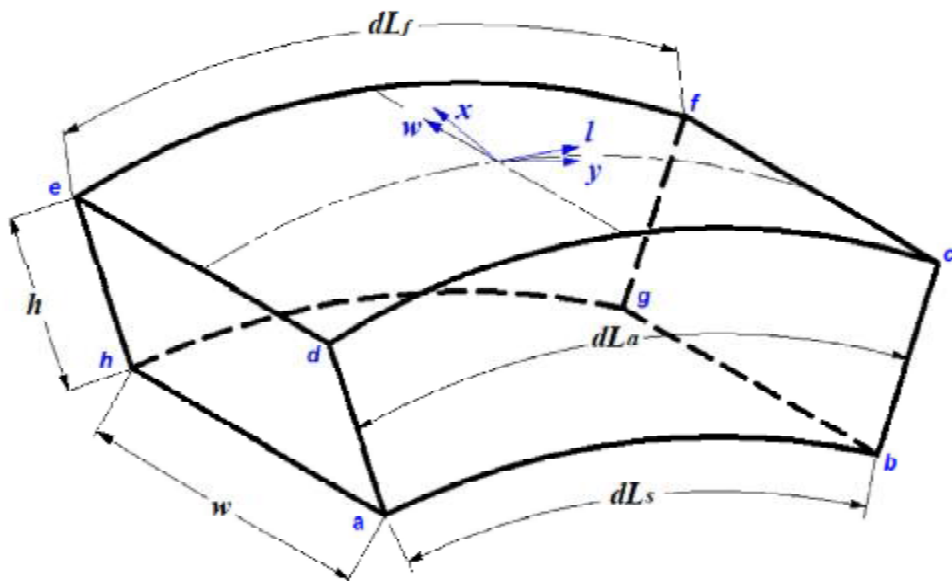


Figure 7.3. Element of soil in the screw channel.

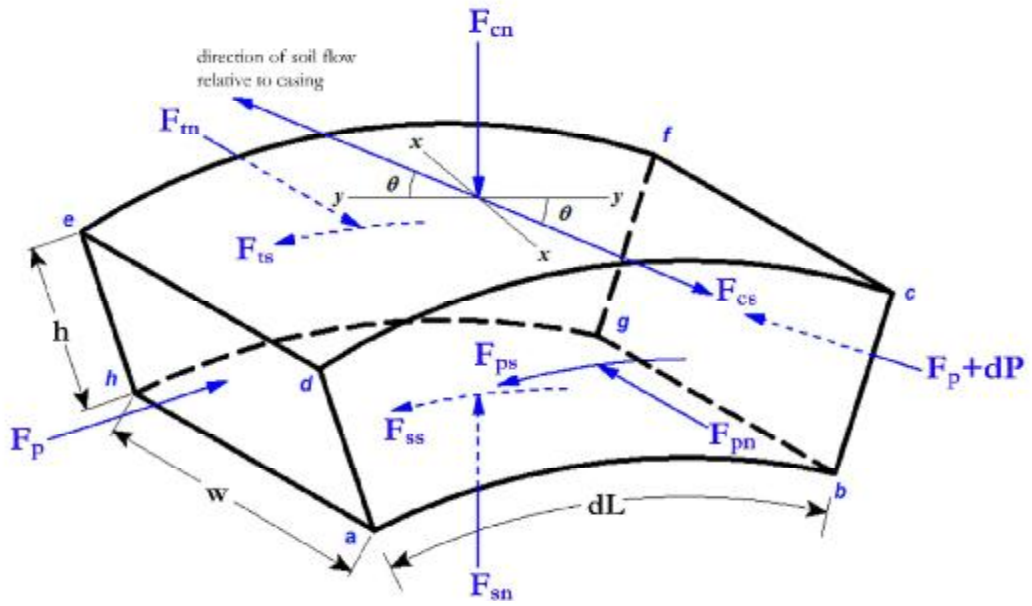


Figure 7.4(a). Free body diagram of soil element in screw channel.

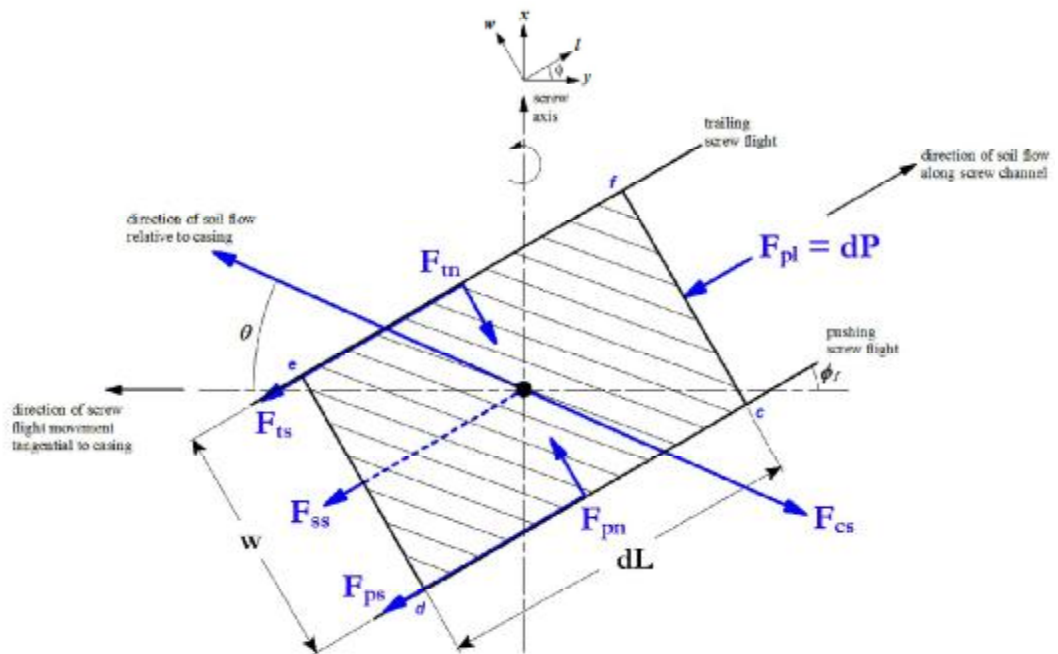


Figure 7.4(b). Simplified free body diagram of soil element in screw channel.  
(viewed in plan at top of channel)

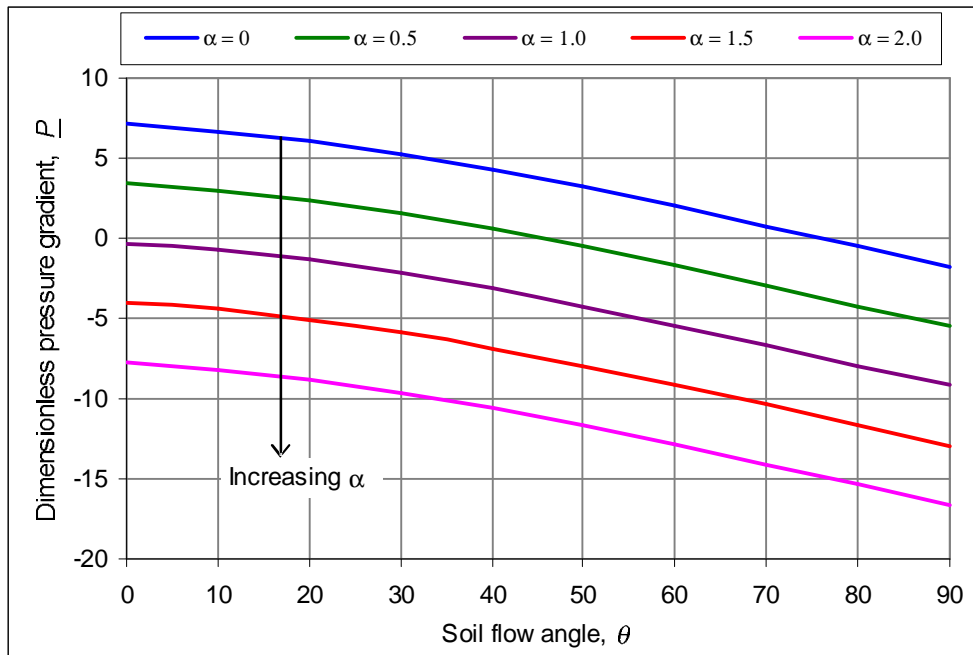


Figure 7.5(a). Effect of shear stress ratio and soil flow angle on dimensionless pressure gradient.

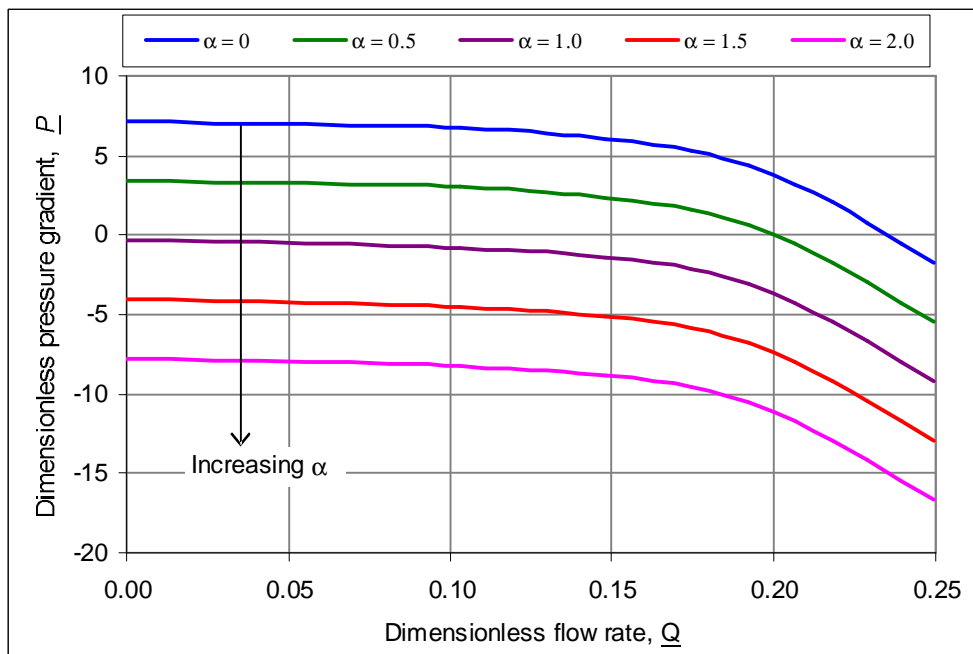


Figure 7.5(b). Effect of shear stress ratio and soil flow rate on dimensionless pressure gradient.

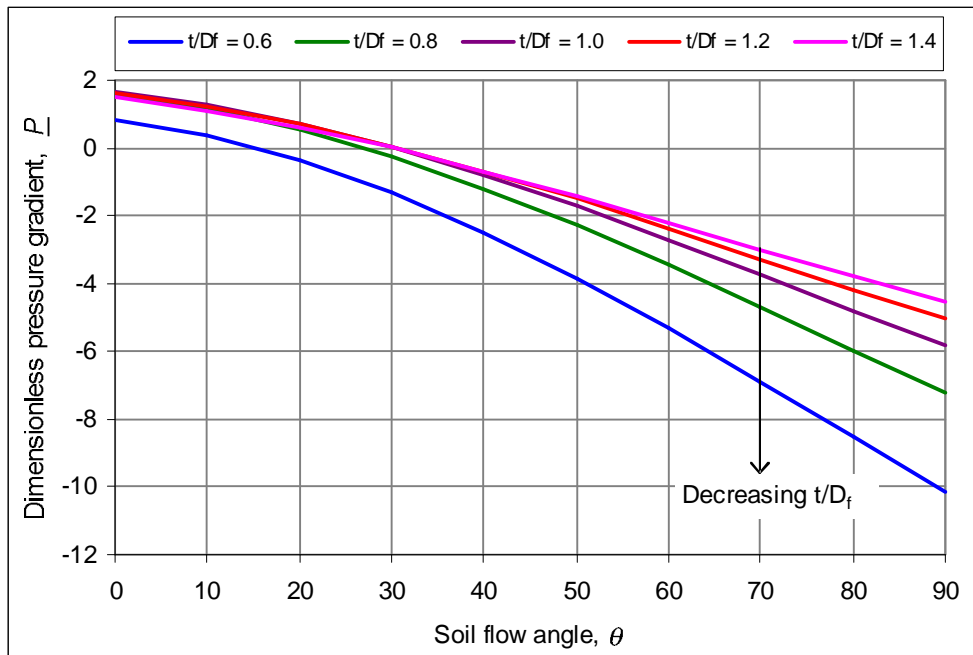


Figure 7.6(a). Effect of screw pitch and soil flow angle on dimensionless pressure gradient.

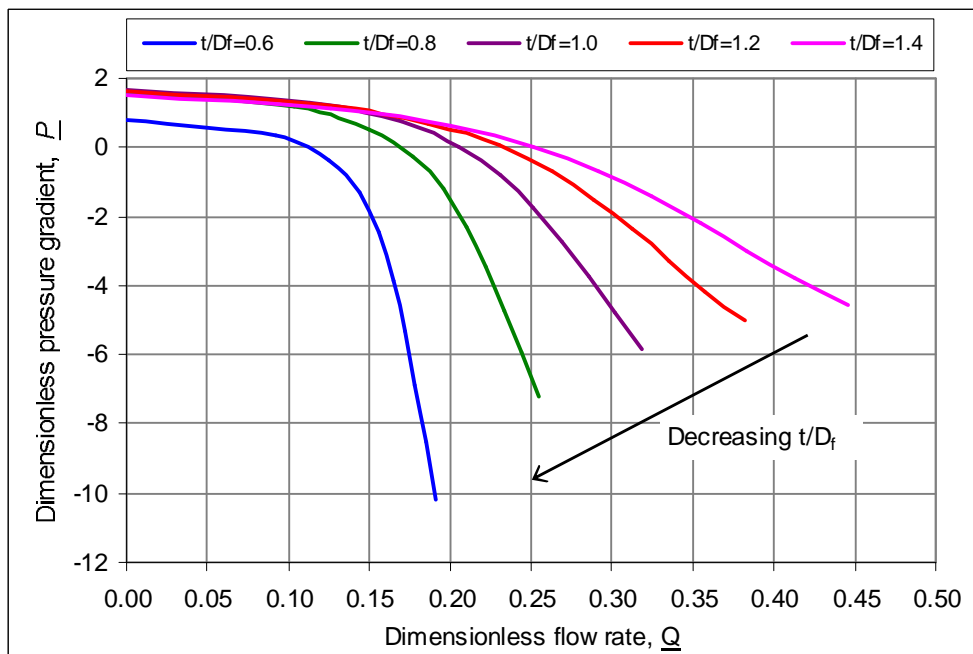


Figure 7.6(b). Effect of screw pitch and soil flow rate dimensionless pressure gradient.

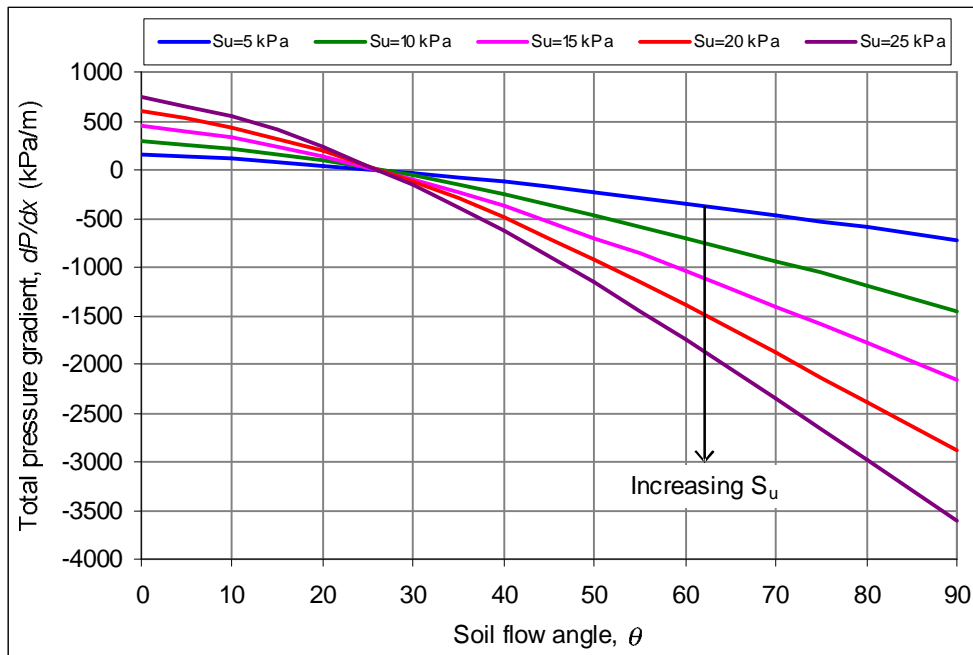


Figure 7.7(a). Effect of soil strength and flow angle on total pressure gradient.

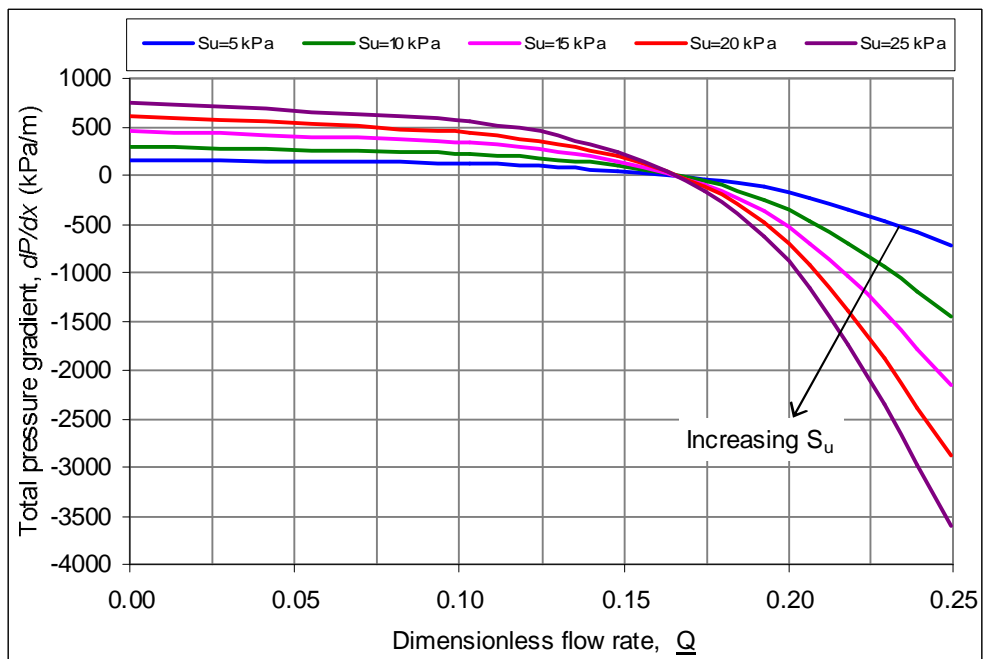


Figure 7.7(b). Effect of soil strength and flow rate on total pressure gradient.

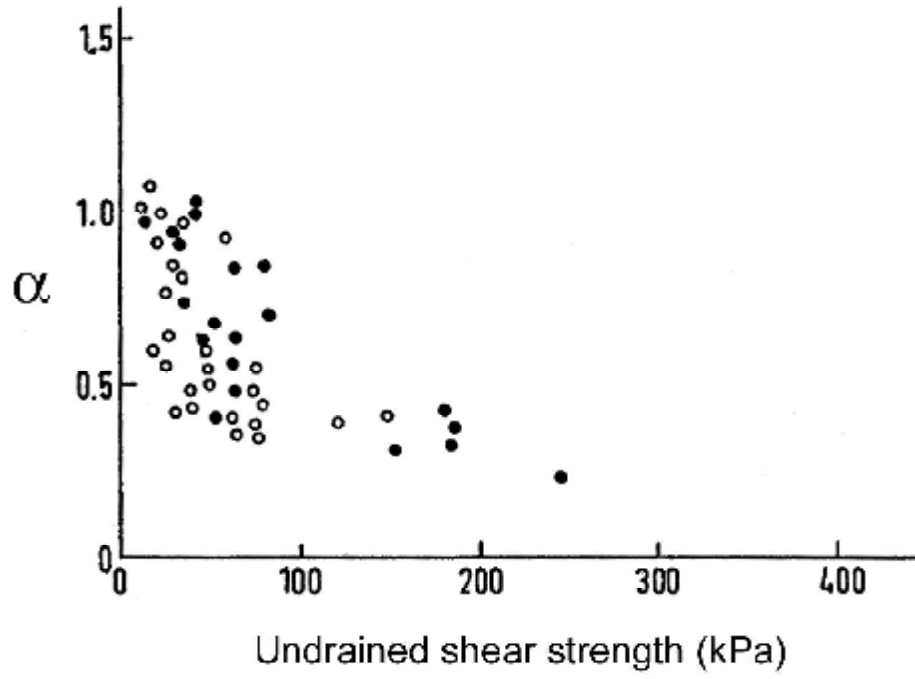


Figure 7.8. Variation of  $\alpha$  ratio with undrained shear strength of clay soils from pile load tests.  
(after Dennis and Olsen, 1983)

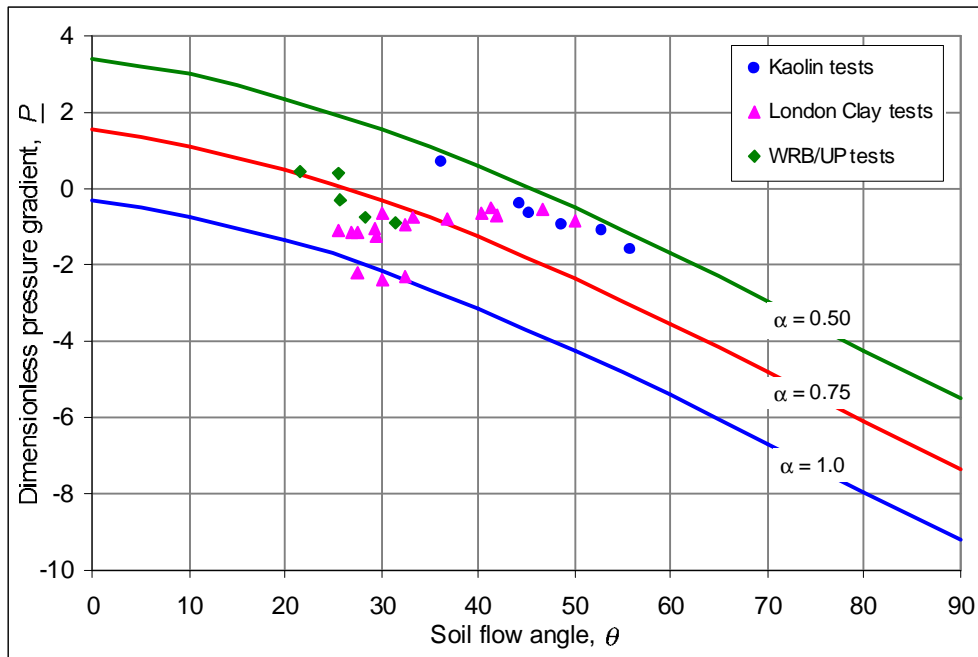


Figure 7.9(a). Measured and theoretical dimensionless pressure gradients and soil flow angles for screw (1) tests.

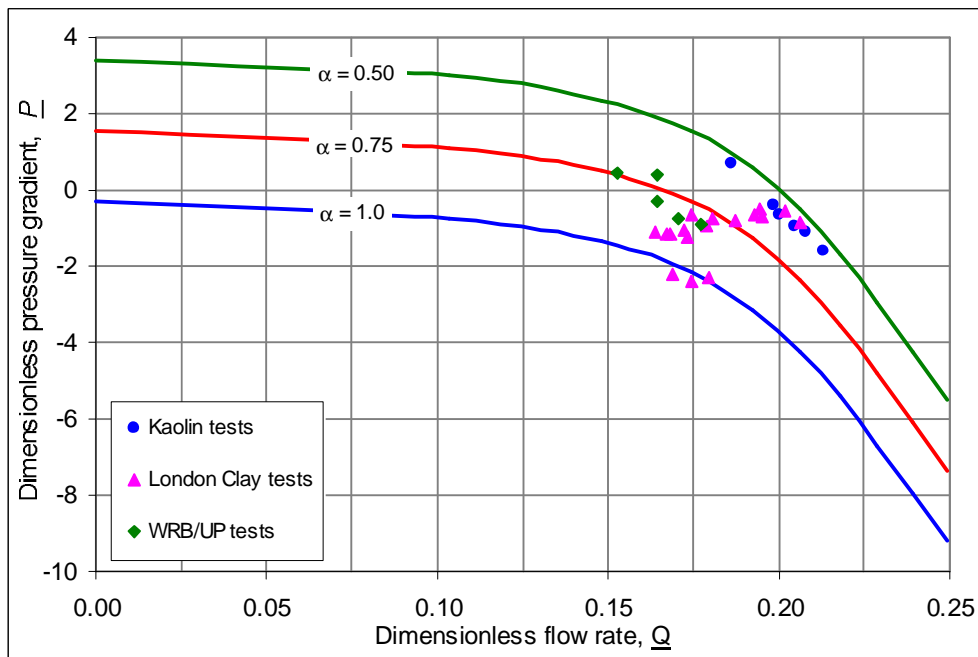


Figure 7.9(b). Measured and theoretical dimensionless pressure gradients and soil flow rates for screw (1) tests.

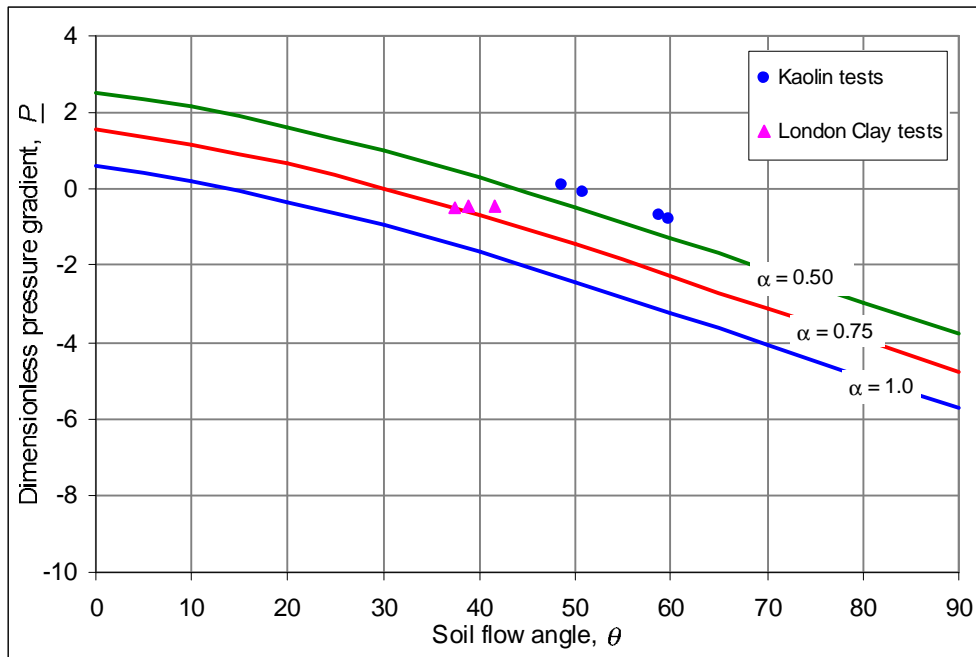


Figure 7.10(a). Measured and theoretical dimensionless pressure gradients and soil flow angles for screw (2) tests.

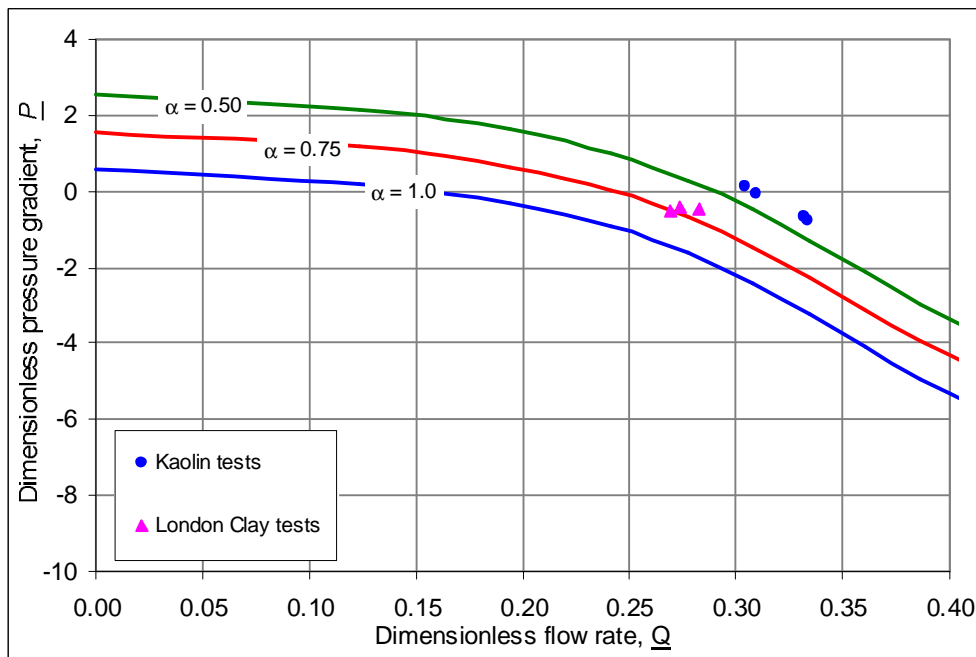


Figure 7.10(b). Measured and theoretical dimensionless pressure gradients and soil flow rates for screw (2) tests.

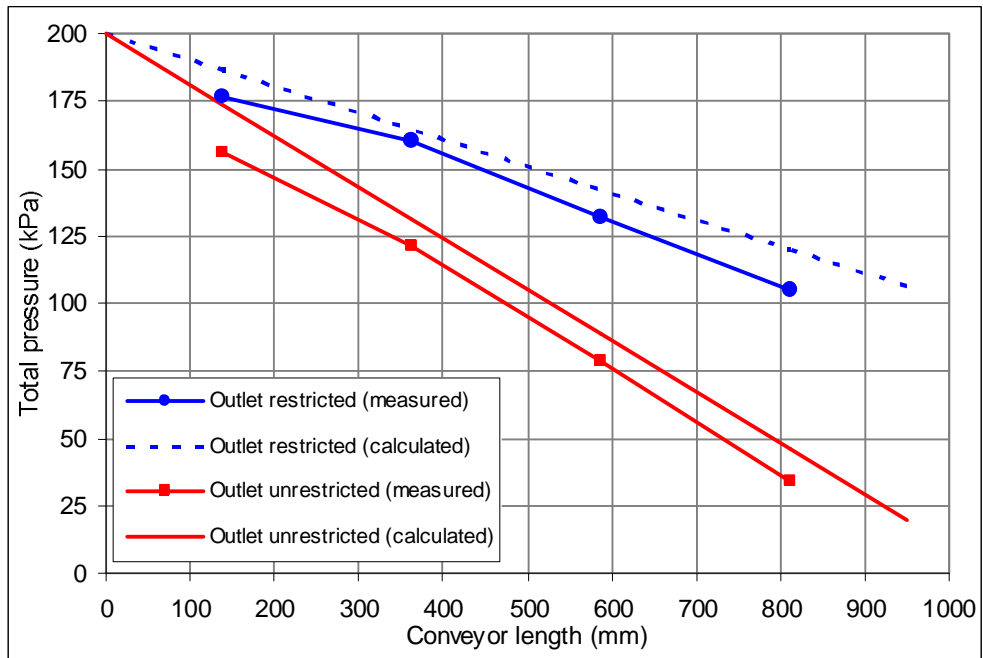


Figure 7.11. Measured and calculated total pressure gradients for test 3.

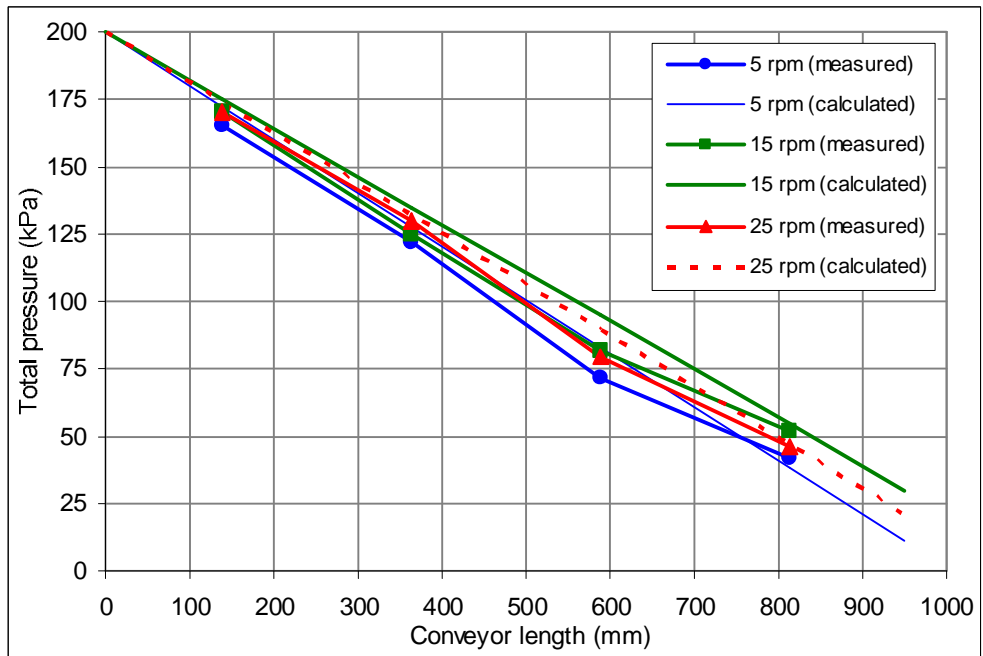


Figure 7.12. Measured and calculated total pressure gradients for test 7.

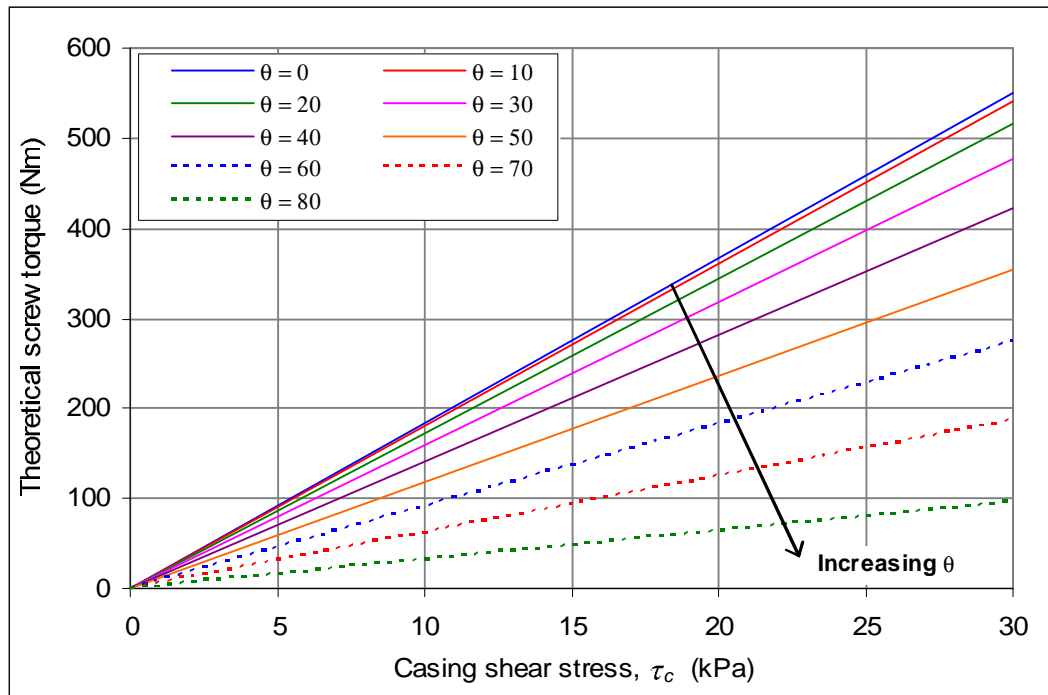


Figure 7.13. Theoretical screw torque for model conveyor with varying soil flow angles and casing shear stresses.

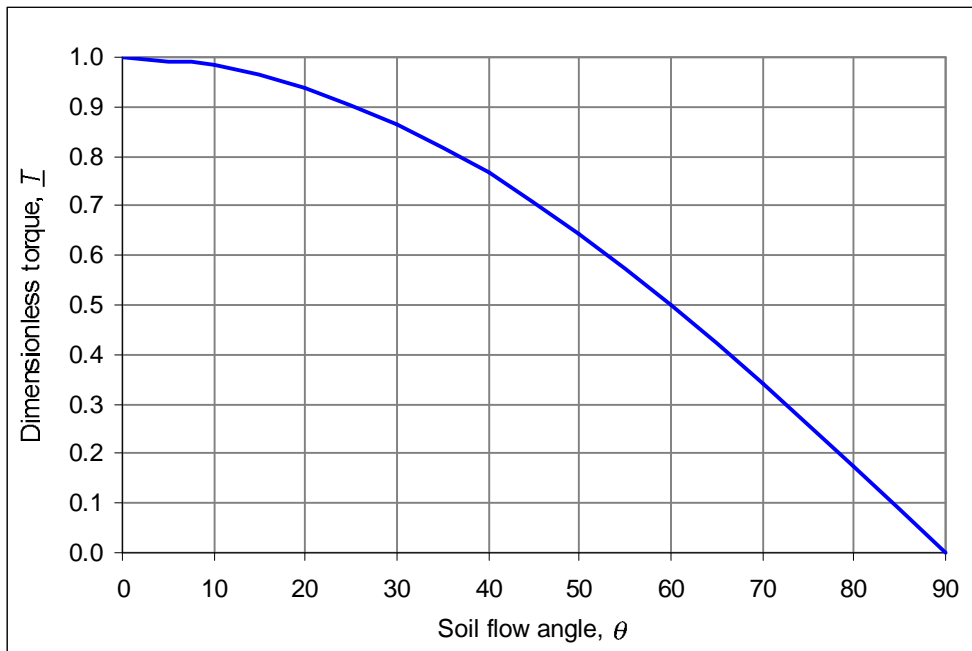


Figure 7.14. Theoretical dimensionless torque for varying soil flow angles.

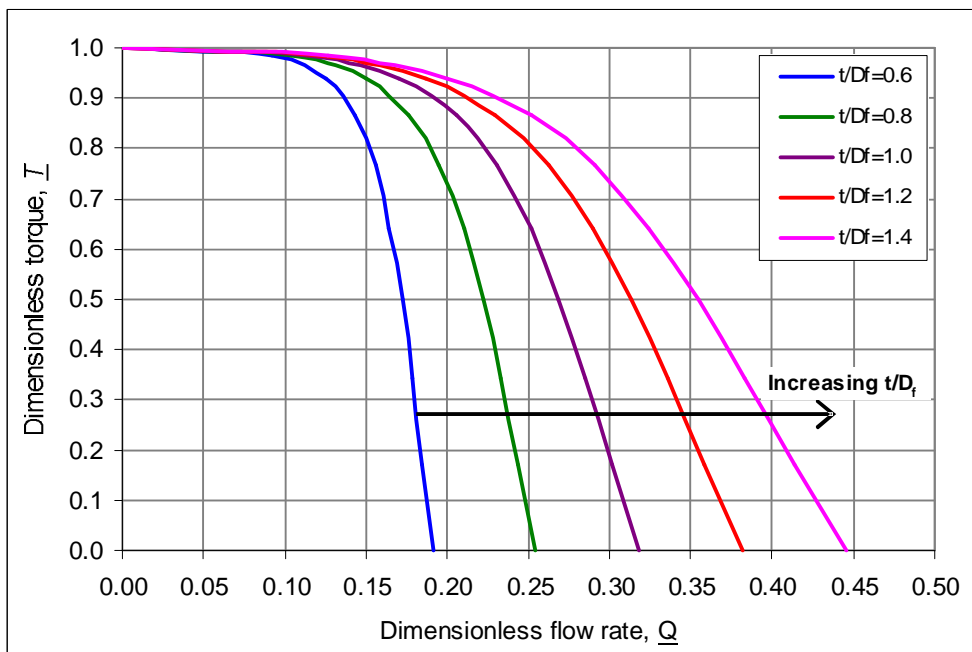


Figure 7.15. Theoretical dimensionless torque and flow rate for varying screw pitch.

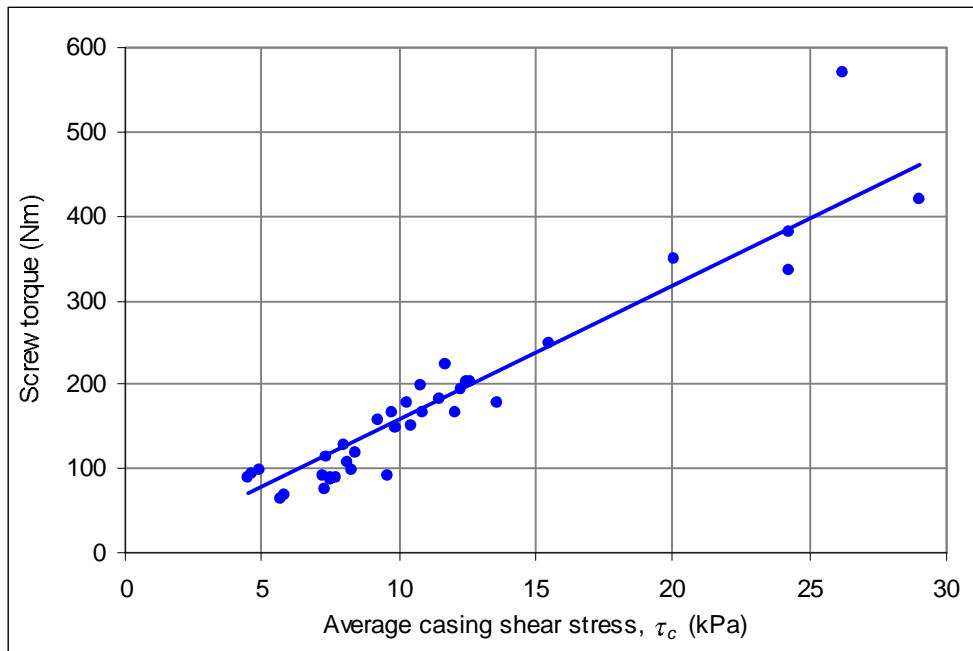


Figure 7.16(a). Measured screw torque and casing shear stresses from model conveyor tests.

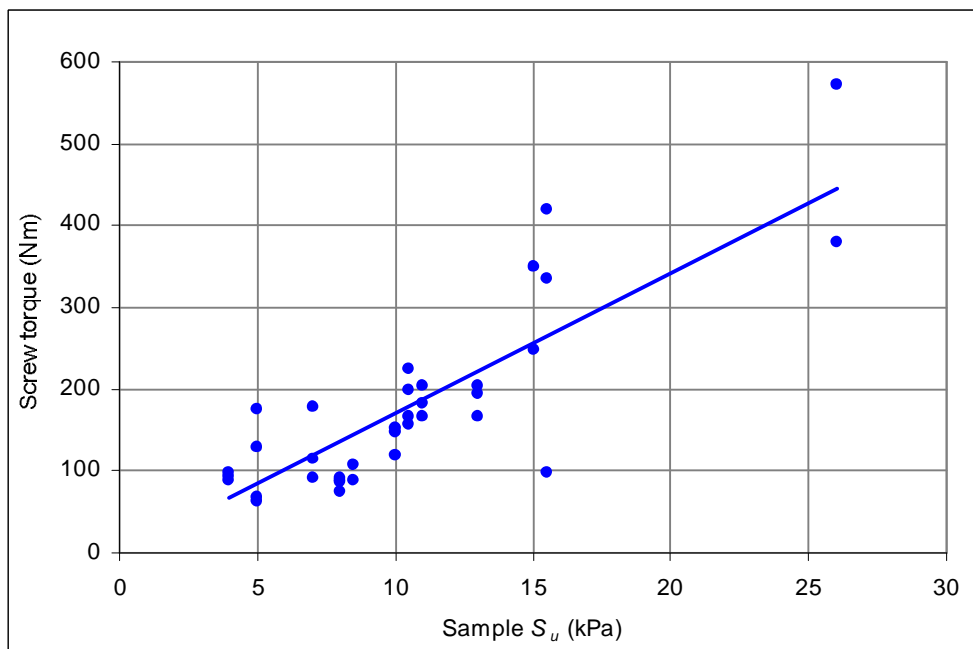


Figure 7.16(b). Measured screw torque and undrained sample strengths from model conveyor tests.

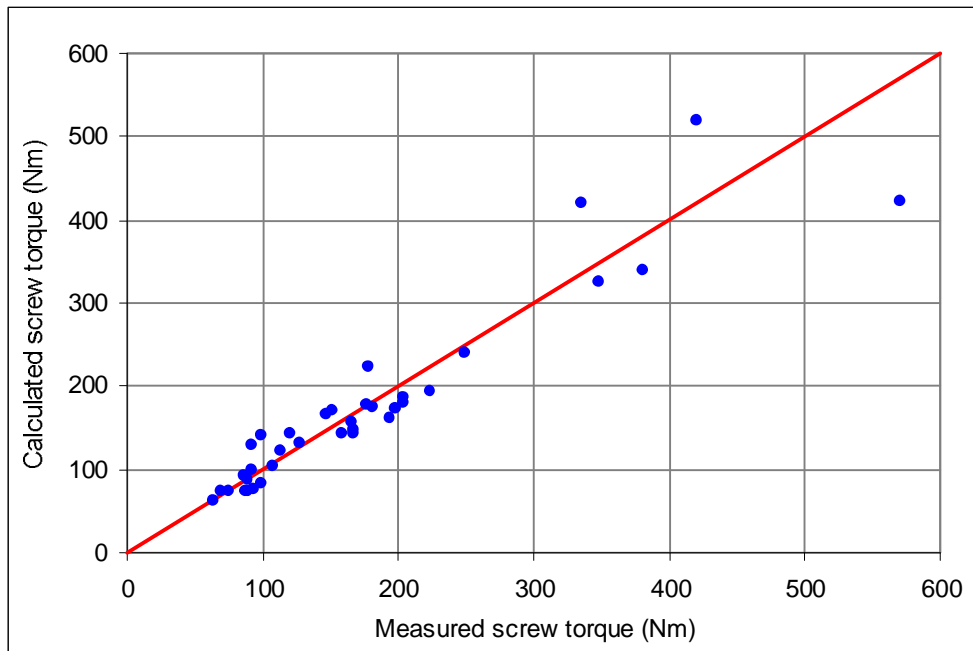


Figure 7.17(a). Comparison of measured and calculated torque based on casing shear stress.

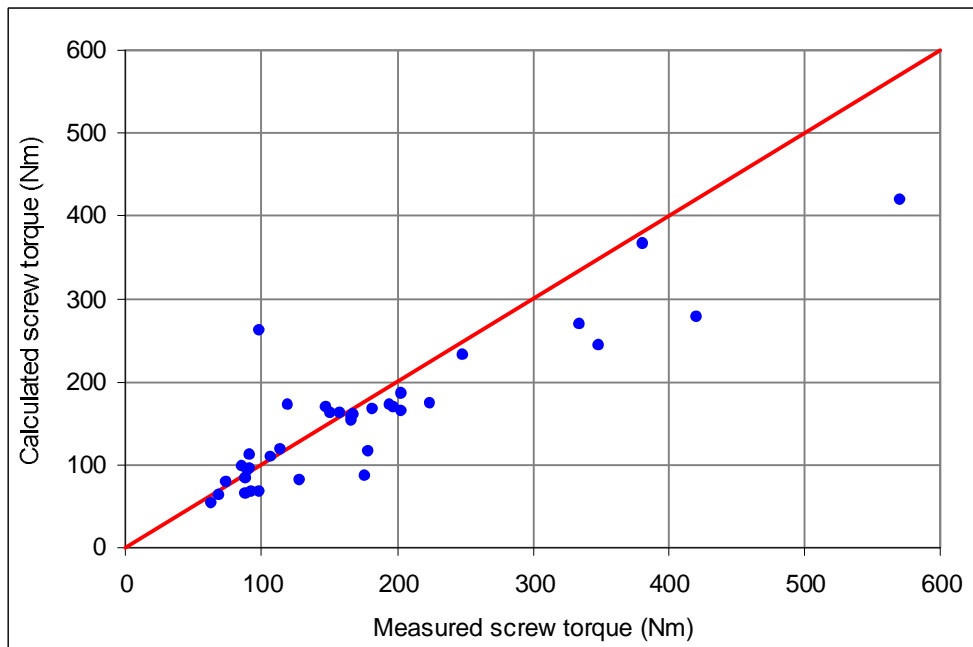


Figure 7.17(b). Comparison of measured and calculated torque based on undrained shear strength.

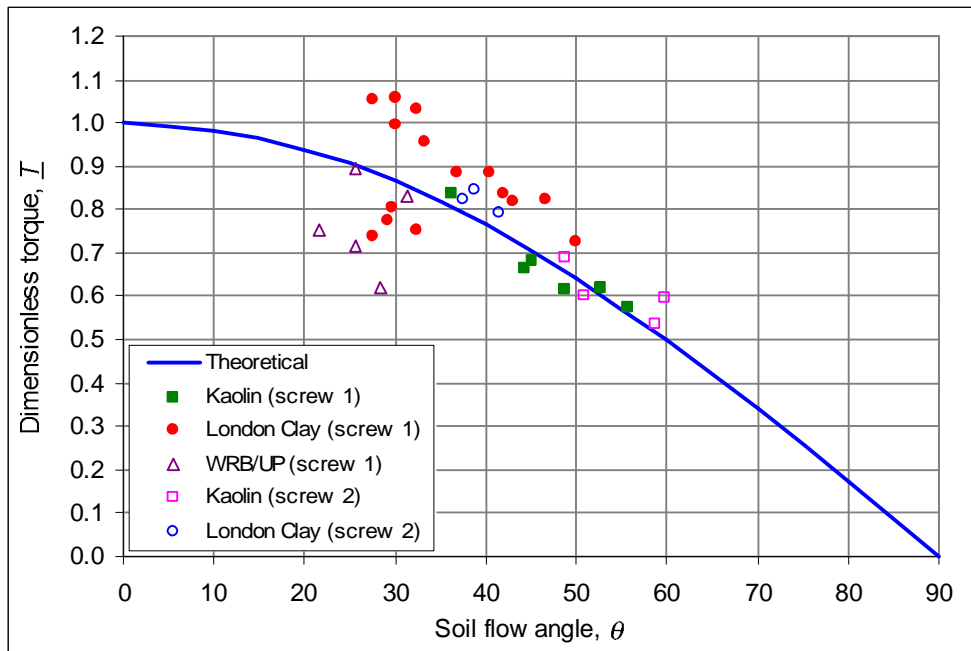


Figure 7.18. Comparison of measured and theoretical dimensionless torque and soil flow angles.

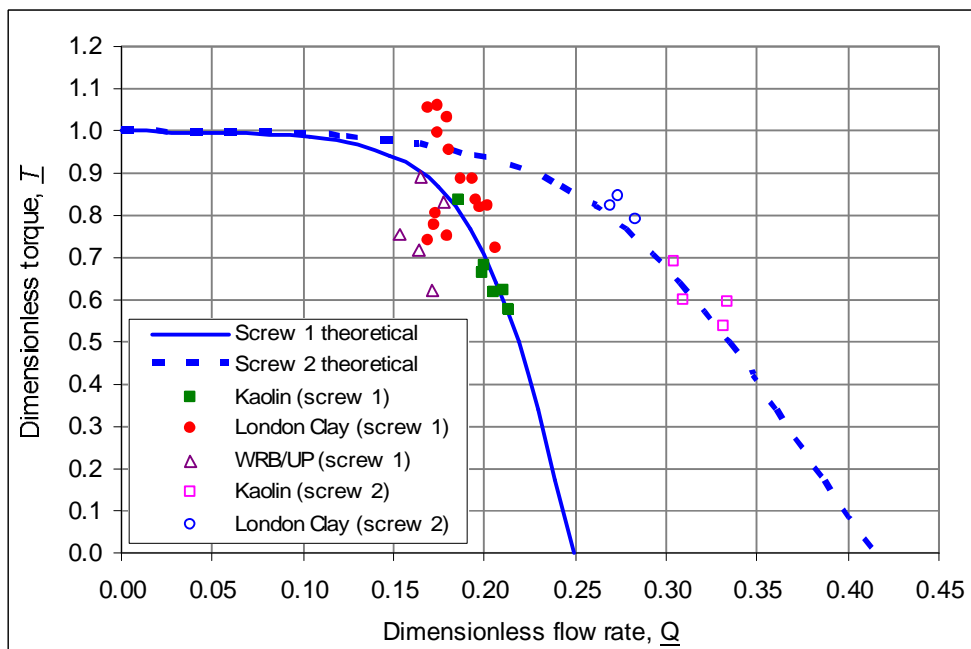


Figure 7.19. Comparison of measured and theoretical dimensionless torque and soil flow rates for different screw geometry.

# Chapter 8

## Conclusions

---

### 8.1 Introduction

This thesis has presented experimental investigations of soil conditioning for clays, and of the operation of a model EPB screw conveyor with clay soils. Interim conclusions from the research performed on these topics are given in the summary at the end of each chapter. This chapter summarises the key conclusions drawn from the research. Some suggestions for further research are given.

### 8.2 Conditioning treatments for clay soils

A series of index tests have been performed to investigate the properties of foams, and the effects of foam and polymer conditioning treatments on properties of clay soils. Conclusions from these tests are summarised here.

A number of generation variables influence the expansion ratio and stability of foams produced from various commercial foam agents. The properties of the different foams generated under the same conditions varied, due to differences in their chemical composition. The expansion ratio increased with the concentration of the foam agent, and with the air flow rate used to generate the foam. The properties of foam used to condition a soil can be varied by changing the generation parameters, but the specific properties depend on factors such as the foam agent chemistry, the chemistry of the water, and the generator design.

The effects of PHPA polymer on the plasticity and undrained strength of reconstituted clays were investigated. The liquid limit and plasticity index of E-grade kaolin and London Clay were increased significantly by small polymer concentrations in solution. This has the effect of increasing the undrained strength of the clay-polymer mixture compared with the undrained strength of the clay alone at the same moisture content. The increase of strength was greater for higher polymer concentrations, and was more pronounced at high moisture contents as more polymer was introduced to the clay.

An extensive series of index tests was performed to measure the undrained strength of London Clay cutting samples conditioned with various foam and polymer conditioning treatments. The simple tests methods allowed assessment of the performance of different conditioning treatments, and identification of ranges of optimum treatments for this soil.

London Clay cutting samples were conditioned with solutions of three different polymers, which bound the cuttings together to form a plastic paste. The undrained strength reduced with increasing polymer injection ratios (PIR) as the moisture content of the samples increased, but the polymers resulted in slightly higher sample strengths relative to those of London Clay with water. The effects of the three different polymer conditioning agents used were similar.

Conditioned London Clay cutting samples were prepared with foams at varying injection ratios (FIR) and expansion ratios (FER). At typically recommended FIRs of 30 to 60%, the foams rapidly broke down as the foam liquid was absorbed by the soil. Stable clay-foam mixtures were difficult to achieve with London Clay, and very high FIRs were required to reduce the sample strength to values suitable for EPB machines. With a FER of about 10, FIRs greater than 200% were required to achieve a strength less than 25 kPa. The sample strengths were controlled by the amount of foam liquid injected, determined by the combination of the FIR and FER. The performance of foam with clay was very different to that reported previously for sands. Further evidence from laboratory tests and field monitoring reported by others supports these results, showing that FIRs significantly higher than typically recommended are required to effectively condition clays with foam.

Conditioning with combined foam and polymer solution treatments improved the performance of the foam with London Clay. The stability of the foam was improved as the polymer solution reduced absorption of the foam liquid by the clay, and lower FIRs were required to effectively

condition the soil when used in combination with a polymer solution. The sample strength depends on the combination of the FIR and PIR, with an increase in the amount of one conditioning agent reducing the amount of the other required for a given strength. For some conditioning treatments, a mixture of discrete clay cuttings in foam was formed, as the foam prevented the cuttings from binding into a paste, as long as the foam remained stable. The strength of these samples was significantly lower than for others at similar conditioner liquid injection ratios and soil moisture contents.

Based on the results of these index tests, ranges of optimum conditioning treatments for London Clay have been suggested. Effective conditioning treatments for other stiff, high plasticity clays are expected to be similar. The index tests were also used to determine effective treatments for the WRB/UP soil samples. The conditioning treatments for model screw conveyor test samples were based on these index tests, and the samples prepared were all suitable for operation of the screw conveyor. The simple index test methods are suitable for identifying optimum conditioning treatments for clay soils, and could be used in the laboratory or on site for testing soils for a particular EPB tunnelling project.

### **8.3 Screw conveyor operation with clay soils**

A model EPB machine screw conveyor system has been designed and commissioned for investigations of the screw conveyor operation with clay soils. The system allows variation of the operating conditions, and is instrumented to measure the soil flow rate, the pressure gradients and casing shear stresses along the conveyor, and the screw torque. Series of tests were performed with consolidated kaolin samples and with compacted conditioned London Clay and WRB/UP samples, prepared with varying undrained strengths and conditioning treatments. The tests were performed with different sample pressures, discharge conditions, screw speeds, and screw geometries to investigate the effects on the conveyor operation.

The general mechanical operation of the model screw conveyor was similar in all of the tests performed. The conveyor reached a steady state operation with a constant soil flow rate, and with all of the measured parameters reaching stable values. The resultant shear stress acting on the casing was approximately constant along the conveyor, and approximately equal to the undrained shear strength of the soil. The total pressure gradient along the conveyor was constant, with a similar pore water pressure gradient. The effective stress measured in the soil at the casing was

approximately constant along the conveyor. The screw torque was also constant during steady state operation.

Following the tests, a thin layer of clay was observed adhering to the surface of the conveyor casing, indicating that shearing at this interface involved a soil-on-soil mechanism. The friction coefficients derived from the test measurements compare well with values of the soil-on-soil residual friction coefficients reported from ring shear tests performed on similar kaolin and London Clay soils at fast rates of shear.

The total pressure gradient along the screw conveyor was influenced by a number of factors related to the operating conditions and the sample properties. A higher sample pressure, representing a higher pressure in the head chamber of an EPB machine, increased the soil flow rate and resulted in a greater dissipation of pressure along the conveyor. A restricted outlet increased the pressure required at the end of the conveyor to discharge the soil, which influenced the soil flow rate and the total pressure gradient. The different outlet conditions on the model screw conveyor represent the variable outlet of a full-scale screw conveyor. The pitch of the screw influenced the soil flow rate and the total pressure gradient. A longer screw pitch increased the flow rate but reduced the pressure gradient. With the outlet unrestricted, the rotational speed of the screw and the soil flow rate did not significantly influence the pressure gradient.

The undrained strength of the soil influenced the total pressure gradient when the outlet was restricted. The required discharge pressure increased with the strength of the soil. When the discharge pressure was greater than the pressure at the start of the conveyor, the total pressure increased along the conveyor. Depending on the operating conditions and the sample properties, the total pressure can either reduce or increase along the conveyor.

The screw torque is proportional to the shear stress acting over the conveyor casing surface. This shear stress is approximately equal to the undrained strength of the soil, and the torque increased approximately linearly with the undrained strength and the casing shear stress.

The foam and polymer conditioning treatments used for the London Clay and WRB/UP samples formed soft plastic pastes from these soils suitable for the screw conveyor. These treatments can successfully condition these soils into materials suitable for EPB tunnelling machines. Controlled operation of the screw conveyor with uniform soil flow rates and pressure gradients was achieved

with the conditioned soil samples, even with very low undrained shear strengths. The same applies for the tests with kaolin samples consolidated to low undrained strengths.

Conditioning treatments resulting in low undrained strengths of the soil reduced the shear stress acting on the casing, and reduced the torque and power required to operate the screw conveyor. There is some evidence from the WRB/UP tests that the screw torque was reduced when significant amounts of foam were present in the soil. There is also some indirect evidence that the conditioning treatments for London Clay samples with high polymer and surfactant concentrations reduced the shear stresses acting at the soil-steel interface on the screw surfaces, which influenced the pressure gradients along the conveyor. These results suggest the conditioning treatments provided lubrication at soil-steel interfaces.

#### **8.4 Theoretical model of screw conveyor operation**

A theoretical model describing the screw conveyor operation was proposed. The model is based on equilibrium of the forces acting on the soil in the screw channel during steady state operation. The model allows calculation of the theoretical total pressure gradient and the screw torque, based on the shear stresses acting on the casing and screw surfaces, the angle of soil flow, and the screw conveyor geometry. The theoretical model is expressed in dimensionless form and can be applied to screw conveyors of any scale.

The theoretical model can be used if the soil flow rate at a given screw speed is known, the screw geometry is specified, and the shear stresses acting in the conveyor are known. The casing shear stress can be accurately approximated by the undrained shear strength of the soil. To calculate the theoretical pressure gradient, the ratio of the shear stresses acting on the screw and casing surfaces ( $\alpha$ ) must be specified, which can be reasonably assumed to be in the range  $\alpha = 0.5 - 1.0$ .

The theoretical model indicates the effects of variables on the total pressure gradient. The angle of soil flow, determined by the soil flow rate at a given screw speed, influences the pressure gradient by varying the direction of the shear stress acting on the casing surface. Increasing the ratio of the screw shear stress to the casing shear stress increases the dissipation of pressure along the conveyor. Increasing the screw pitch (or helix angle) reduces the pressure dissipation, due to the effect of the screw helix angle on the angle of soil flow. Depending on the angle of soil flow

and the shear stress ratio, the total pressure can either increase or decrease along the conveyor for a given screw geometry.

The total pressure gradients measured in the model screw conveyor tests compared well with the predictions of the theoretical model. The pressure gradients measured for different conveyor operating conditions and sample properties agreed with the theoretical gradients calculated for values of  $\alpha$  in the expected range of 0.5 to 1.0, over the range of soil flow angles measured in the tests. For the range of soil flow angles and shear stress ratios relevant to the tests, the theoretical model successfully predicted the positive and negative pressure gradients as observed in the tests.

The theoretical model for the screw torque predicts a linear relationship between the torque and the casing shear stress, as observed in the model conveyor tests. The angle of soil flow also influences the torque, due to the effect on the magnitude of the casing shear stress component acting perpendicular to the screw axis. Increasing the soil flow angle reduces the screw torque. A unique relationship between the dimensionless screw torque and the angle of soil flow is predicted, valid for conveyors of any scale and with any screw geometry, operating with soils of any strength.

The torque measurements from the model screw conveyor tests compared well with the theoretical torque calculated from the measured casing shear stress and soil flow angle. Good agreement between the measurements and theory was also obtained assuming that the casing shear stress was equal to the undrained strength of the soil. The test measurements also agreed well with the theoretical relationships between the dimensionless screw torque and the soil flow angle, or the dimensionless flow rate for the different screw geometries.

The close agreement obtained between the measurements from the model screw conveyor tests and the theoretical pressure gradients and screw torques indicate that the proposed theoretical model accurately describes the operation of the screw conveyor.

The theoretical model could be used in the design of EPB machine screw conveyors. The model can be applied based on the undrained shear strength of the soil, rather than the casing shear stress which usually unknown. For a conveyor of given length and diameter, the maximum torque required to rotate the screw can be estimated based on the maximum strength of soil expected during operation. The range of pressure gradients possible for a given screw geometry

can be calculated based on assumed soil flow rates and shear stress ratios. The effects of varying the screw geometry on the pressure gradient can be assessed using the theoretical model.

## **8.5 Further research**

Considerable scope remains for further research of soil conditioning for EPB machines and screw conveyor operations. Some suggestions to extend the research presented in this thesis are given below.

The index tests based on the undrained shear strength were useful for identifying effective conditioning treatments for the soils tested in this research. Similar tests could be performed with other clay soils, either in the laboratory or on site for specific tunnelling projects, to build up a data base of optimum conditioning treatments for different soils. The effects of parameters such as different surfactant properties, conditioning agent concentrations, and combinations of different agents on the properties of conditioned clays could also be investigated further. Slump tests have been found to be useful as index tests for assessing conditioning treatments in sands, and are also suitable for use on site (Pena, 2003). A data base and improved knowledge of effective conditioning treatments for different soils based on standard index tests would be of use for tunnelling practice.

Clay stickiness and adhesion to steel surfaces is a problem for EPB machines in clay soils. The mechanisms of clay stickiness and the effects of conditioning agents to reduce stickiness have not been clearly defined. Some tests for measuring adhesion of clays to steel were described in Section 2.4, but these have not been extensively used. Some research and development of test methods to investigate clay stickiness and effective conditioning treatments to reduce this problem would help improve EPB machine operations.

Some results from the model screw conveyor tests indicated that some conditioning treatments provided lubrication to reduce soil-steel interface shear stresses. Clay-steel interface shear tests could be performed in a shear box or ring shear apparatus with conditioned clay soils, or with conditioning agents introduced to the interface. Such tests would allow direct measurements of the effects of different conditioning treatments on soil-steel interface shearing behaviour.

Further research is possible with the model screw conveyor. Tests with higher sample pressures would be interesting to identify the maximum pressure that can be controlled by the screw conveyor. An upper bound might be found by keeping the screw stationary and increasing the sample pressure to force the soil to flow through the screw conveyor. Modification of the current system to allow application of higher sample pressures would be required.

Conditioning agents are often injected into the screw conveyor on EPB machines. Tests could be performed to investigate the effects of injecting conditioning agents into the conveyor at different points. This application of soil conditioning provides a lubricating layer around the casing surface, which can reduce the screw torque and also influence the pressure gradient. Some tests have been performed at Cambridge to investigate this, and the effects of varying the ratio of shear stresses on the screw and casing surfaces (Spencer-Allen, 2004).

Tests could be performed to further investigate effects of varying screw geometries. Different screw pitches could be used to compare with the results already obtained, and it would be interesting to perform tests using a screw with the pitch varying along the length. A shorter pitch could be used at the start of the screw, and increased towards the end to investigate the effects on the pressure gradient over different sections of the screw. Other geometric parameters such as the  $D_s/D_f$  and  $D_f/L$  ratios could be varied to investigate the effects on the conveyor operation. Some EPB machine screw conveyors have been designed with one flight left out towards the middle of the screw to improve the formation of a soil plug in the conveyor. Model tests with such a screw design could be performed to investigate the effects on the conveyor operation.

Model screw conveyor tests could be performed with other types of clay soils than those tested in this research. Tests could be performed with samples of higher strength than those already tested, and with clays of low plasticity which can be problematic in practice. Improvements to the conveyor operation resulting from conditioning treatments for low plasticity clays would be interesting to investigate. The screw conveyor operation with sands, and the effects of conditioning treatments for granular soils, can also be investigated. The improved stability of foam with sands should allow such tests to demonstrate effects of foam conditioning treatments on the conveyor operation more effectively than was achieved in the tests with clays, due to the poor foam stability. Some tests on conditioned sands using a similar model screw conveyor are being performed at Oxford University as part of the current research project.

Further model screw conveyor tests with different operating conditions, screw geometries, sample properties, and conditioning treatments would provide data to compare with the theoretical model proposed in this thesis. This would allow further assessment of the accuracy of the theoretical model to describe the screw conveyor operation.

Data obtained from EPB machines operating in the field is valuable to investigate effects of soil conditioning treatments on the machine performance. The conditioning treatments used in different soils, the conditioned soil properties, and data of the machine operating parameters such as the cutterhead and screw conveyor torque, and the head chamber pressure, provide information to assess effects of soil conditioning treatments in the field. The most effective conditioning treatments and conditioned soil properties found for an EPB machine in the field could be compared with results from index tests performed on conditioned soil samples. This would allow assessment of the index tests as methods for identifying effective conditioning treatments in advance of tunnelling.

Detailed monitoring of the operation of EPB machine screw conveyors would provide data to compare with the proposed theoretical model. The soil strength, flow rates, pressure gradients and torque data from screw conveyors of different scales and with different geometries could be compared with the theoretical behaviour to assess the validity of the theoretical model applied to screw conveyors of different scales.

Monitoring of EPB machines operating on the CTRL project in London is being performed as part of the current research project. Comparison of the observed machine performance and the conditioning treatments used in different soils with the results of the index tests, the model screw conveyor tests, and the theoretical model for the screw conveyor operation will be possible. This research will provide valuable information towards improving the understanding of effects of conditioning treatments for a range of soils in the field.

Together with further laboratory investigations, performing field monitoring and investigations of soil conditioning on various projects will lead to improvements in the practical application of soil conditioning in different ground conditions to improve the operation of EPB machines.

# References

- Al-Tabbaa, A. (1987). Permeability and stress-strain response of speswhite kaolin. PhD Thesis, University of Cambridge.
- Babendererde, L.H. (1998). Developments in polymer application for soil conditioning in EPB-TBMs. Tunnels and Metropolises, Negro Jr and Ferreira (eds), Balkema, Rotterdam, Vol. 2, pp 691-695.
- Bailar, J.C., Moeller, T., Kleinberg, J., Guss, C.O., Castellion, M.E., and Metz, C. (1989). Chemistry, 3<sup>rd</sup> Edition, Harcourt Brace Jovanovich, New York.
- Barker, H.R. (1998). Physical modelling of construction processes in the mini-drum centrifuge. PhD Thesis, University of Cambridge.
- Benbow, J. and Bridgwater, J. (1993). Paste flow and extrusion. Oxford University Press, UK.
- Bezuijen, A., Schaminee, P.E.L., and Kleinjan, J.A. (1999). Additive testing for earth pressure balance shields. Proc. 12<sup>th</sup> Euro. Conf. on Soil Mechanics and Geotechnical Engineering, Amsterdam, pp 1991-1996.
- Bezuijen, A. and Schaminee, P.E.L. (2000). Model experiments using foam simulating the drilling with an EPB shield. GeoDelft Report No. BF 51010, September 2000.
- Bezuijen, A., and Schaminee, P.E.L. (2001). Simulation of the EPB-shield TBM in model tests with foam as additive. Modern Tunnelling Science and Technology, Kyoto. Adachi, T., Tateyama, K. and Kimura, M. (eds) pp 935-940.
- Bjerrum, L. (1973). Problems of soil mechanics and construction on soft clays. Proc. 8<sup>th</sup> Int. Conf. on Soil Mechanics and Foundation Engineering, Moscow, vol. 3, pp 111-159.

- Bond, A.J. (1989). Behaviour of displacement piles in overconsolidated clays. PhD Thesis, Imperial College, London.
- Boone, S.J., McGaghan, S., Bouwer, G., and Leinala, T. (2002). Monitoring the performance of earth pressure balance tunnelling in Toronto. Proc. North American Tunnelling '02.
- Bransby, P.L. (1973). Cambridge contact stress transducers. Cambridge University Engineering Department Report CUED/C-SOILS/LN2.
- British Standard 1377 (1975). Methods of test for soils for civil engineering purposes. British Standards Institution.
- Burbidge, A.S. and Bridgwater, J. (1995). The single screw extrusion of pastes. Chemical Engineering Science, Vol. 50, No. 16, pp 2531-2543.
- Calladine, C.R. (1985). Plasticity for engineers. Ellis Horwood Ltd, Chichester, UK.
- Cash, T. and Vine-Lott, K.M. (1996). Foam as a tunnelling aid: its production and use. Tunnels and Tunnelling, Vol. 28, No. 4, pp 22-23.
- Chow, F.C. (1996). Investigations into the behaviour of displacement piles for offshore foundations. PhD Thesis, University of London.
- Condat (1998). Earth pressure balanced TBM CONDAT specific products. Commercial product information, CONDAT Lubrifiants.
- CTRL (1997). London Tunnels West Geotechnical Design Basis Report. Channel Tunnel Rail Link Technical Report No. 220-RUP-LCEEH-00025-AA, February 1997.
- Chung, C.I. (1970). New ideas about solids conveying in screw extruders. SPE Journal, Vol. 26, May 1970, pp 32-44.
- Darnell, W.H. and Mol, E.A.J. (1956). Solids conveying in extruders. SPE Journal, April 1956, pp 20-29.

- Dennis, N.D. and Olsen, R.R. (1983). Axial capacity of steel pipe piles in clay. Proc. Conf. on Geotech. Practice in Offshore Engineering, Austin, Texas, pp 370-388.
- Durian, D.J. (1994). Relaxation in aqueous foams. Bull. Materials Research Society, Vol. 19, pp 20-23.
- EFNARC (2001). Specification and guidelines for the use of specialist products for soft ground tunnelling. European Federation for Specialist Construction Chemicals and Concrete Systems.
- Elmes, D.R. (1985). Creep and viscosity in two kaolin clays. PhD Thesis, University of Cambridge.
- Evans, D.C. (1994). Contaminant migration through intact and damaged clay liners. PhD Thesis, University of Cambridge.
- Fleming, W.G.K., Weltman, A.J., Randolph, M.F., Elson, W.K. (1985). Piling engineering. Blackie and Sons Ltd, London.
- Goodson, F.J. (1959). Experiments in extrusion. Trans. British Ceramic Society, Vol. 58, pp 158-187.
- Herrenknecht, M. and Rehm, U. (2003). Earth pressure balanced shield technology. Soft ground and hard rock mechanical tunnelling technology seminar. Colorado School of Mines, March 2003. <http://www.mines.edu/academic/mining/research/emi/papers/seminar>
- Houlsby, G.T. and Psomas, S. (2001). Soil conditioning for pipejacking and tunnelling: properties of sand/foam mixtures. Proc. Underground Construction 2001, London, pp 128-138.
- Jancsecz, S., Krause, R. and Langmaack, L. (1999). Advantages of soil conditioning in shield tunnelling: Experiences of LRTS Izmir. Proc. ITA Conference, Oslo, pp 865-875.

- Jefferis, S.A. (1995). Water-soluble polymers in tunnelling and slurry supported excavations. In Cellulose and Cellulose Derivatives: Physico-chemical aspects and industrial applications, Kennedy, J.F., Phillips, G.O., and William, P.A. (eds), Woodhead Publishing Ltd, Cambridge, UK.
- Karlsrud, K., Kalsnes, B., and Nowacki, F. (1993). Response of piles in soft clay and silt deposits to static and cyclic axial loading based on recent instrumented pile load tests. Volume 28: Offshore Site Investigation and Foundation Behaviour, Society for Underwater Technology, pp 549-584.
- Koumoto, T. and Houlby, G.T. (2001). Theory and practice of the fall cone test. Geotechnique, Vol. 51, No. 8, pp 701-712.
- Kusakabe, O., Nomoto, T., and Imamura, S. (1997). Geotechnical criteria for selecting mechanised tunnel system and DMM for tunnelling. Panel discussion, Proc. 14<sup>th</sup> Int. Conf. on Soil Mechanics and Foundation Engineering, Hamburg, Vol. 4, pp 2439-2440.
- Lambe, T.W. (1953). The effect of polymers on soil properties. Proc. 3<sup>rd</sup> Int. Conf. on Soil Mechanics and Foundation Engineering, Zurich, Vol. 1, pp 253-257.
- Lamberti (2002). Earth pressure balance shield conditioning products. Commercial product information, <http://www.lamberti.com>.
- Langmaack, L. (2000). Advanced technology of soil conditioning in EPB shield tunnelling. Proc. North American Tunnelling '00, Balkema, Rotterdam, pp 525-542.
- Laquerbe, M. (2002). Sticky clays: General report on theme E. in Eupalinos 2000, General Report, AFTES, Paris, pp 49-56.
- Lee, L.T., Rahbari, R., Lecourtier, J., and Chauveteau, G. (1991). Adsorption of polyacrylamides on the different faces of kaolinites. J. Colloid and Interface Science, Vol. 147, No. 2, pp 351-357.

- Lehane, B. (1992). Experimental investigations of pile behaviour using instrumented field piles. PhD Thesis, University of London.
- Leinala, T., Delmar, R., Collins, J.R., Pennington, B.N., and Grabinsky, M. (1999). Soil conditioning for enhanced TBM performance in differing ground conditions. 52<sup>nd</sup> Canadian Geotechnical Conference, Regina, 1999. pp 537-544.
- Leinala, T., Grabinsky, M., Delmar, R. and Collins, J.R. (2000). Effects of foam soil conditioning on EPBM performance. Proc. North American Tunnelling '00, Balkema, Rotterdam, pp 514-524.
- Leinala, T., Grabinsky, M., and Klein, K. (2002). A review of soil conditioning agents for EPBM tunnelling. 17<sup>th</sup> Tunnelling Association of Canada Conference, Toronto, July 2002.
- Lemos, L.J.L. and Vaughan, P.R. (2000). Clay-interface shear resistance. *Geotechnique* 50, No. 1, pp 55-64.
- Littleton, I. (1976). An experimental study of the adhesion between clay and steel. *Journal of Terramechanics*, Vol. 13, No. 3, pp 141-152.
- Lyon, J. (1999a). Drilling fluids. *No-dig International*, Vol. 10, No. 2, Feb. 1999, pp 20-25.
- Lyon, J. (1999b). Fluids for tunnelling. *World Tunnelling*, Vol. 12, No. 4, May 1999, pp 177-182.
- Maidl, B., Herrenknecht, M., and Anheuser, L. (1996). *Mechanised shield tunnelling*. Ernst and Sohn, Berlin.
- Mair, R.J. (1979). Centrifugal modelling of tunnel construction in soft clay. PhD Thesis, University of Cambridge.
- Malik, M. and Letey, J. (1991). Adsorption of polyacrylamide and polysaccharide polymers on soil materials. *Soil Sci. Soc. Am. J.* 55, pp 380-383.

- MBT (2001). Environmental risk assessment – use of Meyco Fix SLF in tunnel constructions. <http://www.ugc.mbt.com/en/tbmfoam.htm>
- MBT (2001, 2002). Commercial product information. <http://www.ugc.mbt.com/>
- Merritt, A.S. and Mair, R.J. (2001a). Investigations of lubrication and soil conditioning for tunnelling and pipe jacking in clay soils. *Underground Construction 2001*, London, pp 117-127.
- Merritt, A.S. and Mair, R.J. (2001b). Lubrication and soil conditioning for pipejacking and tunnelling in clays. *Modern Tunnelling Science and Technology*, Kyoto, Adachi, T., Tateyama, K. and Kimura, M. (eds) pp 971-974.
- Milligan, G.W.E. (2000). Lubrication and soil conditioning in tunnelling, pipe jacking and micro-tunnelling; a state-of-the-art-review. Pipe Jacking Research Group, <http://www-civil.eng.ox.ac.uk>.
- Milligan, G.W.E. (2001). Soil conditioning and lubricating agents in tunnelling and pipe jacking. *Proc. Underground Construction 2001*, London, pp 105-116.
- Ministry of Defence Standard 42-40/Issue 1: Foam liquids, fire extinguishing. October 1998.
- Mitchell, J.K. (1993). *Fundamentals of soil behaviour*. 2<sup>nd</sup> Edition, John Wiley and Sons, New York.
- Moody, G. (1992). The use of polyacrylamides in mineral processing. *Minerals Engineering*, Vol. 5, No. 3-5, pp 479-492.
- Moody, G. M. (1995). Pre-treatment chemicals. *Filtration and separation*, April 1995, pp 329-336.
- Moss, N. (1978). Theory of flocculation. *Mine and Quarry Journal*, Vol. 7, No. 5, pp 57-61.
- Nishimatsu (2002). Personal communication.
- Pena, M. (2003). Soil conditioning for sands. *Tunnels and Tunnelling International*, July 2003.

- Potter, L.J. (1996). Contaminant migration through consolidating soils. PhD Thesis, University of Cambridge.
- Peron, J.Y. and Marcheselli, P. (1994). Construction of the 'Passante Ferroviario' link in Milan, Italy, lots 3P, 5P and 6P: excavation by large earth pressure balanced shield with chemical foam injection. Proc. Tunnelling '94, London, pp 679-707.
- Quebaud, S., Sibai, M., and Henry, J.P. (1998). Use of chemical foam for improvements in drilling by earth-pressure balanced shields in granular soils. Tunnelling and Underground Space Technology, Vol. 13, No. 2, pp 173-180.
- Schamp, N. and Huylebroeck, J. (1973). Adsorption of polymers on clays. J. Polymer Science Symposia, No. 42, pp 553-562.
- Shirlaw, J.N., Ong, J.C.W., Osborne, N.H., and Tan, C.G. (2002). The relationship between face pressure and immediate settlement due to tunnelling for the North East Line, Singapore. Proc. Geotechnical Aspects of Underground Construction in Soft Ground, Toulouse, 2002, pp 3/25-30.
- Skempton, A.W. (1957). 'Discussion: The planning and design of the new Honk Kong airport'. Proc. ICE 7, pp 305-307.
- Spencer-Allen, L. (2004). 'Soil conditioning for earth pressure balance tunnel boring machines'. MEng Report, Cambridge University Engineering Department.
- Springman, S. M. (1993). 'Centrifuge modelling in clay: Marine application'. Proc. 4<sup>th</sup> Canadian Conference on Marine Geotechnical Engineering, pp 853-895.
- Steiner, W (1996). Criteria for selecting mechanized tunnelling systems in soft ground. Proc. North American Tunnelling '96, Balkema, Rotterdam, pp 483-491.
- Talmon, A.M. and Bezuijen, A. (2002). Muck discharge by the screw conveyor of an EPB tunnel boring machine. Proc. Geotechnical Aspects of Underground Construction in Soft Ground, Toulouse, 2002, pp 1/89-94.

- Terzaghi, K., Peck, R.B, and Mesri, G. (1996). Soil mechanics in engineering practice. 3<sup>rd</sup> Edition, John Wiley & Sons, New York.
- Tika, T.E. (1989). The effect of rate of shear on the residual strength of soil. PhD Thesis, University of London.
- Tika, T.E., Vaughan, P.R. and Lemos, L.J.L.J. (1996). Fast shearing of pre-existing shear zones in soil. *Geotechnique* 46, No. 2, pp 197-233.
- Tsubakihara, Y. and Kishida, H. (1993). Frictional behaviour between normally consolidated clay and steel by two direct shear type apparatuses. *Soils and Foundations*, Vol. 33, No. 2, pp 1-13.
- Wallis, S. (1990). Screw conveyors will take the pressure. *Tunnels and Tunnelling*, April 1990, pp 31-34.
- Wallis, S. (1994). UK EPB machine conquers Bordeaux's karstic limestone. *Tunnels and Tunnelling*, July 1994, pp 43-46.
- Wallis, S. (1996). Jubilee Line Extension underground construction. *Supplement to World Tunnelling*, February 1996.
- Webb, R. and Breeds, C.D. (1997). Soft ground EPBM tunnelling – West Seattle, Alki Tunnel. *Proc. Tunnelling '97*, London, UK, pp 501-514.
- Williamson, G.E., Traylor, M.T., and Higuchi, M. (1999). Soil conditioning for EPB shield tunnelling on the South Bay Ocean Outfall. *Proc. Rapid Excavation and Tunnelling Conference*, Colorado, pp 897-925.
- Withers, A.D., Page, D.P., and Linney, L.F. (2001). Geology and geotechnical properties. *Building Response to tunnelling – Case studies from construction of the Jubilee Line Extension*, London. Vol. 1: Projects and Methods, Burland J.B., Standing J.R., and Jardine F.M. (eds), CIRIA SP200.

Wood, D.M. (1985). Some fall cone tests. *Geotechnique* 35, No. 1, pp 64-68.

Wood, D.M. (1990). *Soil behaviour and critical state soil mechanics*. Cambridge University Press, Cambridge UK.

Yoshikawa, T. (1996a). Soil pressure drop of screw conveyor for shield machines. *Trans. Japan Soc. of Mechanical Engineers, Part C*, vol. 62, no. 595, pp 1197-1203.

Yoshikawa, T. (1996b). Soil pressure drops of various screw conveyor structures for shield machines. *Trans. Japan Soc. of Mechanical Engineers, Part C*, vol. 62, no. 599, pp 2927-2930.

Yoshikawa, T. (1996c). Conditions on soil pressure drop of screw conveyor for shield machines. *Trans. Japan Soc. of Mechanical Engineers, Part C*, vol. 62, no. 599, pp 2931-2935.